Shuying Wang

Monotonic, Cyclic and Postcyclic Shear Behavior of Low-plasticity Silt

Science Press
Beijing

Springer

Monotonic, Cyclic and Postcyclic Shear Behavior of Low-plasticity Silt

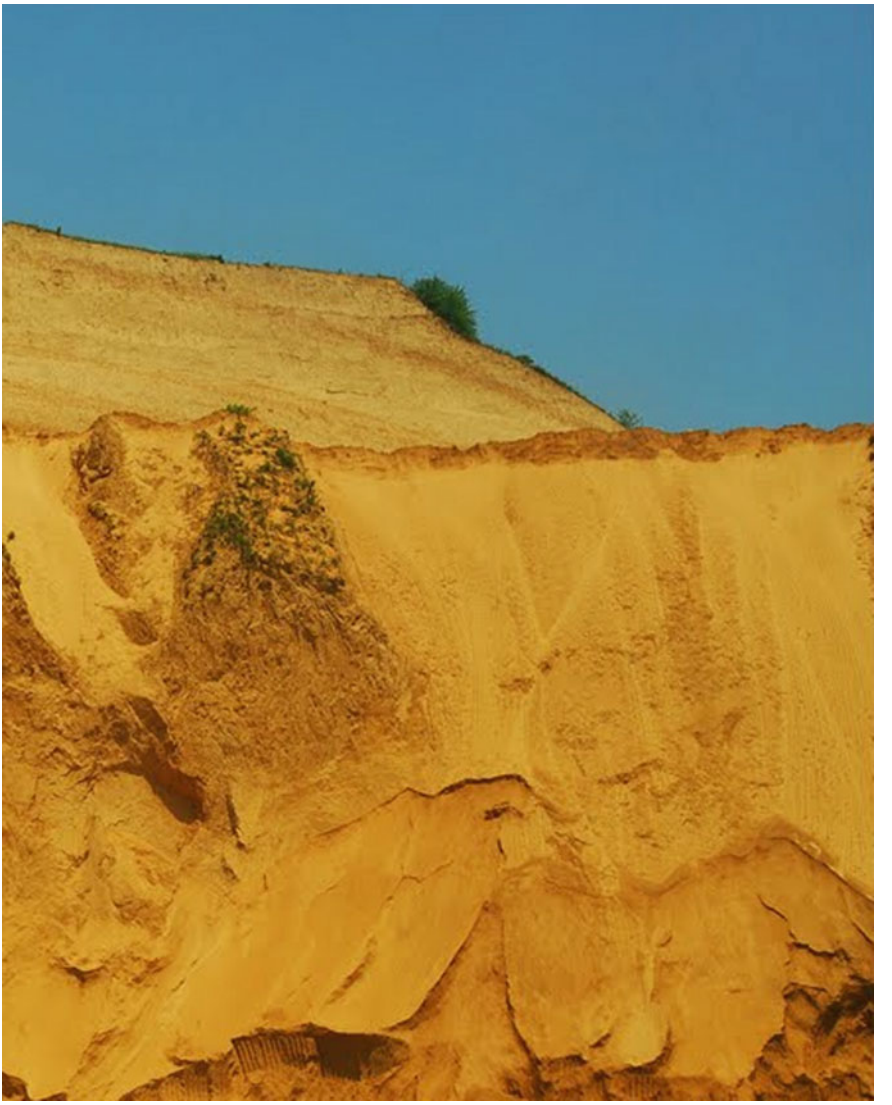

Shuying Wang

Monotonic, Cyclic and Postcyclic Shear Behavior of Low-plasticity Silt

Science Press
Beijing

Springer

Shuying Wang
School of Civil Engineering
Central South University
Changsha, Hunan
China

ISBN 978-981-10-7082-2 ISBN 978-981-10-7083-9 (eBook)
https://doi.org/10.1007/978-981-10-7083-9

Jointly published with Science Press

The print edition is not for sale in China Mainland. Customers from China Mainland please order the print book from: Science Press.
ISBN: 978-7-03-056125-1

Library of Congress Control Number: 2017960780

Printed on acid-free paper

This Springer imprint is published by Springer Nature
The registered company is Springer Nature Singapore Pte Ltd.
The registered company address is: 152 Beach Road, #21-01/04 Gateway East, Singapore 189721, Singapore

Preface

Low-plasticity silt with a plasticity index less than 10 is widespread throughout many countries, especially in countries located in large continents. For example, loess, as one typical low-plasticity silt, has an area of 1.3×10^7 km^2 (as 9.3% of total land area) in the world. Low-plasticity silt is a difficult material to characterize. Its particle size lies between those of sand and clay, and its unique composition determines its behavior differently from those of sand and clay. On one hand, it is difficult to prepare and handle specimens for laboratory tests because of its apparent lack of cohesion compared to clay. Undisturbed sampling of saturated silt is practically impossible with thin-walled tubes. On the other hand, vibration does not make silt as dense as it does sand, so the common moist tamping and water pluviation methods used for sand are not effective to prepare silt specimens. These difficulties in specimen preparation have discouraged research on shear behavior of low-plasticity silt, and so the work to investigate silt behavior in the laboratory is still limited.

Silts are usually thought to behave similar to clay or sand. However, some scholars pointed out that empirical correlations for strength and compressibility used for clays may be in error if applied to silt. The same study also noted that failure to recognize the difference between the shear characteristics of silts and clays on one hand and sands on the other hand could lead to overconservative designs of offshore structures. Particularly, liquefaction of low-plasticity silt happened due to dynamic loadings from earthquakes, trains, and ocean waves and induced big loss of properties in the previous events, especially in the 1976 Tangshan earthquake, the 1989 Loma Prieta earthquake, etc. Some civil infrastructures have failed not only due to cyclic loading during an earthquake, but also due to reduction of shear strength or stiffness after an earthquake. It is required to investigate the effect of cyclic loading on shear behavior of low-plasticity silt for the safety of civil infrastructures in silty ground.

The author has carried out continuous researches on monotonic and cyclic shear behavior of low-plasticity silt for several years. This book collects the main research findings, which can promote our understandings on silt behavior and its variation due to cyclic loading under different testing conditions. For example, differently

with the viewing points of classical critical state mechanics, it was found that the critical state line of low-plasticity silt can be changed due to liquefaction. The behavior of the low-plasticity silt changes from sand-like material to clay-like behavior at a PI of about 6 due to the addition of clay. It is encouraged that more related researches are carried out on low-plasticity silts.

The studies in this book are supported financially by the National Key R&D Program of China (No. 2017YFB1201204) and the National Natural Science Foundation of China (No. 51208516). In the early stages, the studies were critically reviewed by Prof. Ronaldo Luna in Saint Louis University, USA, and his comments are very helpful and appreciated strongly. The author also appreciates the favors from his colleagues and students in Central South University, China.

Changsha, China Shuying Wang
October 2017

Contents

Nomenclature

ASTM	American Society for Testing and Materials
AASHTO	American Association of State Highway Officials
USCS	Unified Soil Classification System
MOHURD	Ministry of Housing and Urban-Rural Development of the People's Republic of China
PI	Plasticity index
MT	Moist tamping
AP	Air pluviation
WP	Water pluviation
SP	Slurry deposition
MRV	Mississippi River Valley
UU	Unconsolidated undrained
CU	Consolidated undrained
OCR	Overconsolidation ratio
LMVD	Lower Mississippi Valley Division
e	Void ratio
σ'	Effective stress
M_w	Magnitude of earthquake
NMSZ	New Madrid Seismic Zone
C_c	Compression index
C_r	Recompression index
p'	Mean effective principal stress
w	Water content
σ'_c	Effective consolidation pressure
σ'_1	Maximum effective principal stress
σ'_2	Intermediate effective principal stress
σ'_3	Minimum effective principal stress
CSR	Cyclic stress ratio
N_{cyc}	Number of loading cycles
$\Delta\sigma$	Deviator stress

u_e	Excess pore (water) pressure
q	Deviator stress
ε_1	Axial strain
ϕ'	Effective friction angle
w_L	Liquid limit
w_P	Plastic limit
σ'_P	Preconsolidation pressure
σ'_{BP}	Back pressure
U	Pore water pressure
A_f	Ratio of excess pore water to deviator stress at the critical state
S_u	Undrained shear strength
σ_1	Maximum principal stress
σ_3	Minimum principal stress
M	Gradient of K_f line in the q-p′ space
NCL	Normal consolidation line
CSL	Critical state line
PTL	Phase transformation line
R_u	Excess pore pressure ratio
ε_{cyc}	Cyclic axial strain
k	Permeability
u_{rc}	Reconsolidation level after cyclic loading
e′	Void ratio after reconsolidation
CTX	Cyclic triaxial
CDSS	Cyclic direct simple shear
τ	Shear stress
σ'_{vo}	Effective overburden pressure for cyclic simple shear test
K_σ	A coefficient to adjust cyclic strength to that at effective confining pressure of 100kPa (1atm)
p_a	Atmospheric pressure
f	Frequency for cyclic loading
UP	Undisturbed sampling
SC	Slurry consolidation
D.A.ε	Double axial strain
S.A.ε	Simple axial strain
γ	Shear strain
R	Coefficient of variation
CRR	Cyclic resistance ratio
CRR_M	Cyclic resistance ratio at an earthquake with a moment magnitude of M
C_{2D}	Correction coefficient for two-dimensional versus one-dimensional cyclic loading
τ_{cyc}	Cyclic shear stress
MSF	Magnitude scaling factor to approximately account for the correlation between earthquake magnitude and number of equivalent uniform loading cycles

K_α	Correction factor for initial shear stress ratio
K_{PI}	Factor to correct CRR to that of soil with a PI of 18.5
a_v	Coefficient of compressibility
ρ_w	Density of water
g	Gravity acceleration
c_v	Coefficient of consolidation
e_0	Initial void ratio
k'	Permeability after liquefaction
ε_v	Volumetric strain
σ'_m	Mean effective stress
$C_{c'}$	Postcyclic compression index
Dr	Relative density
N_{liq}	Number of loading cycles required to liquefy soil specimen
D_r'	Relative density after reconsolidation
$S_{u,m}$	Measured undrained shear strength of liquefied silt
Ψ	State parameter computed based on CSL of postcyclic specimen
No_recon	Specimen which was not reconsolidated after cyclic loading
No_cyc	Specimen which was not previously subjected to cyclic loading
u_{rc}	Reconsolidation level
λ	Slope of normal consolidation line (compression line) in the e-logp′ space
κ	Slope of recompression line in the e-logp′ space
$S_{u,OC}$	Undrained monotonic shear strength of overconsolidation specimen
$S_{u,NC}$	Undrained monotonic shear strength of normally consolidated specimen
p_0'	Initial mean effective stress during postcyclic shearing
$S_{u,p}$	Predicted undrained shear strength
E_i	Initial stiffness
S_y	Yield shear strength
$E_{sec}(E_{s50})$	Secant modulus calculated at the intersection of 50% of the ultimate shear stress
OCR_{app}	Apparent overconsolidated ratio
$S_{u,post}$	Undrained shear strength of postcyclic soil
$S_{u,virgin}$	Undrained shear strength of virgin soil
$u_{e,cyc}$	Excess pore pressure induced by cyclic loading
$\varepsilon_{cyc,th}$	Threshold cyclic axial strain
γ_{th}	Threshold shear strain
N_c	Number of loading cycles
$N_{c,r}$	Number of loading cycles to liquefy the specimens with previous cyclic loading
$N_{c,v}$	Number of loading cyclic to liquefy the specimens without previous cyclic loading

Chapter 1
Introduction

1.1 Definition of Low-plasticity Silt

Silt is defined to have different grain size ranges according to different engineering soil classification systems. The ASTM and AASHTO standards classify the soil with a grain size of 0.005–0.075 mm as silt; In the British standard, the silt particle has a grain size of 0.002–0.06 mm. In the USCS standard, the soil with particle diameters in the range of 0.002–0.075 mm is classified as silt. It is well-known that majority of soils do not include only one type of soil. Maybe, they include clay, silt, sand and etc. For engineering purpose, engineering classification is required to identify the soil characteristics and mechanical behavior, such as permeability, compressibility, shear strength and etc. Based on the Unified Soil Classification System (USCS) standard, if the fraction smaller than 0.075 mm is more than 50%, Casagrande's plasticity chart will be used. In the Casagrande's plasticity chart, the soils with the data points below the A line belong to silty materials or organic clays. Organic clays have behavior similar to low plasticity soils. Differently, in some engineering codes, the soils with plasticity index (PI) less than 10 are simply classified as silts (MOHURD of China 2009). Boulanger and Idriss (2006) found that shear behavior of silt transforms from sandlike to claylike material when the PI increases from 2 to 9. Thus, in this book, silt with a PI less than 10 is defined to be low-plasticity one.

1.2 Distribution of Low-plasticity Silt

Low-plasticity silt is widespread throughout many countries, especially in countries located in large continents. For example, loess is one typical low-plasticity silt. Throughout the world, its area reaches 1.3×10^7 km^2, as 9.3% of total land area.

S. Wang, *Monotonic, Cyclic and Postcyclic Shear Behavior of Low-plasticity Silt*,
https://doi.org/10.1007/978-981-10-7083-9_1

Especially in China, the distribution of loess is wide, deep and continuous. The loess mainly locates in the northwest of China and along the middle reach of Yellow River. The loess normally has a thickness of up to 100 m, however, in Lanzhou, the loess is as thick as more than 300 m (Zhao and Yu 2011). The United State is also a country with widespread loess. As noted by Puri (1984), one type of low-plasticity silt, loess, occupies the uppermost stratigraphic layer over extensive areas of the central United States; it is found in other parts of the country as well. Usually, the thickest deposits occur adjacent to the Missouri and Mississippi Rivers to the leeward side of the prevailing westerly winds.

1.3 Research Significance

Low-plasticity silt is a difficult material to characterize. Its particle size lies between those of sand and clay, and its unique composition determines its behavior differently from those of sand and clay. These factors have two consequences: First, specimens for laboratory tests are difficult to prepare and handle. On one hand, because of its apparent lack of cohesion compared to clay, low-plasticity silt is very friable, so its fabric tends to break during sampling, trimming and preparation (Izadi 2008). Undisturbed sampling of saturated silt is practically impossible with thin-walled tubes. On the other hand, vibration does not make silt as dense as it does sand, so common moist tamping and water pluviation methods used for sand are not effective to prepare silt specimens. Second, because air is easily trapped among silt particles as it is among fine sand particles and cavitation easily occur due to negative excess pore pressure produced during shearing, saturation of silt specimens is more difficult than that of clay and coarse sand specimens (Izadi 2008; Duncan and Wright 2005). These difficulties have discouraged research on the shear and cyclic behavior of low-plasticity silt. Because of the previous reasons, Wang et al. (2011) proposed a new slurry consolidation approach to reconstitute low-plasticity silt specimens for laboratory triaxial testing, and Wang and Luna (2012) and Wang et al. (2017) investigated monotonic shear behavior of low-plasticity silt and its change with soil plasticity.

Silt liquefaction is a common phenomenon observed during earthquakes, such as, the 1976 Tangshan earthquake, the 1989 Loma Prieta earthquake, the 1994 Northridge earthquake, the 1999 Chi-Chi earthquake, the 1999 Kocaeli earthquake, and the 2010 Chile Earthquake, among others (e.g., Boulanger et al. 1998; Bray and Sancio 2006; Bray and Frost 2010). Many scholars studied liquefaction characteristics of low-plasticity silt. For example, Wang et al. (2016a, b) reexaminated effect of plasticity on liquefaction resistance of low-plasticity fine-grained soils and proposed its potential application. However, the damage to property and potentially loss of life does not occur only during earthquakes. Some dams or slopes have failed not only due to cyclic loading during an earthquake, but also due to reduction of shear strength or stiffness after an earthquake. Most failures of earth dams have occurred from just a few hours to up to 24 h after an earthquake (Soroush and

Soltani-Jigheh 2009). This phenomenon, called delayed failure or delayed response, has demonstrated the need to study postliquefaction characteristics of soils.

Some researchers have studied postliquefaction behavior of sand (e.g., Chern and Lin 1994; Vaid and Thomas 1995; Porcino and Caridi 2007; Amini and Trandafir 2008; Alba and Ballestero 2008; Ashour et al. 2009). In particular, a National Science Foundation workshop held in April, 1997, addressed postliquefaction shear strength of granular soils (Stark et al. 1997). Byrne and Beaty's keynote paper in this report articulated the requirement that direct tests should be carried out to determine postliquefaction strength under consolidated undrained conditions. This requirement may be reasonable for sand due to its high permeability; however, low-plasticity silt is less permeable than sand. Additionally, the reconsolidation rate depends on drainage boundary conditions in the field. If low-permeability layers are present around liquefied zone, reconsolidation may take a long time. The 2000 Tottoriken-Seibu earthquake in Japan experienced high levels of pore water pressure a long time after the earthquake. In the Takenouchi Industrial Park, the sand boiled for 7.5 h, much longer than previously observed in sandy deposit in Niigata, Japan. The ground at the industrial park consists of no-plastic silt (Towhata 2008). Before the ground can recover its stiffness and shear strength after liquefaction, the soil must reconsolidate, and it is during this period of instability that structures can undergo further damage. Wang and Luna (2014), Wang et al. (2014b, 2015a, 2016a) presented postliquefaction behavior of low-plasticity silt at various degrees of reconsolidation.

Full liquefaction (i.e., excess pore pressure ratio reaches one) does not necessarily occur during an earthquake. Its likelihood depends on the duration and magnitude of earthquake and the resistance to liquefaction of the soil. During a short-duration or low-magnitude of earthquake, liquefaction does not occur; however, soil properties are affected. Typically, shear strength and stiffness of soil are reduced without reconsolidation and increased after full reconsolidation. This book refers to the effect of limited cycles of dynamic loading on soil behavior as *limited liquefaction* (Ashour et al. 2009). Thus, Wang et al. (2013a, 2014a) investigates postcyclic behavior of low-plasticity silt at various levels of liquefaction (i.e., excess pore pressure ratios) and further with full and no reconsolidation. Additionally, they investigated effects of cyclic loading magnitude, plasticity and initial consolidation condition on shear behavior of low-plasticity silt and compressibility characteristics of low-plasticity silt before and after liquefaction (Wang et al. 2015b, Wang and Luna 2014).

The energy released during aftershocks or other earthquakes may induce repeated liquefaction (i.e., reliquefaction). For example, a number of high-magnitude aftershocks were recorded in Japan after the devastating 9.0-magnitude earthquake and the associated tsunami flattened the northeastern coast on the March 11, 2011. Aftershocks with a magnitude as high as 7.1 was recorded. Such high-magnitude aftershocks can release enough energy to induce liquefaction. Similar high magnitude aftershocks were also recorded after other earthquakes, such as the 2008 Wenchuan, the 2010 Chile and the 2011 New Zealand earthquakes. In the later two earthquakes, liquefaction in silt was reported. These earthquakes and aftershocks

can cause repeated liquefaction in soils. Finn et al. (1970) conducted a laboratory investigation into the effect of previous strain history on the repeated liquefaction characteristics of sand. They found that soil fabric can be changed by various factors, such as previous static or cyclic shearing, geological effects, and construction method (especially in backfilled deposits). During aftershocks or other seismic events, liquefied silt (liquefied during the major earthquake event) has the potential to liquefy again. This is mainly due to the change in the soil fabric induced by previous cyclic loading. Due to this change in soil fabric, the liquefaction resistance of silts during aftershocks is expected to be different from that of virgin silt. "Virgin" is used in the context of this study to mean silt that has not been loaded previously. Thus, Wang et al. (2013b) and Wang and Yang (2013) studied liquefaction characteristics of low-plasticity silt with previous cyclic shearing.

1.4 Research Background

The previous studies on monotonic and cyclic shear behaviors of low-plasticity silt are reported. Herein, because there are few researches on some behaviors of low-plasticity silt and comparison are made to show the behavior difference among different soils, monotonic and cyclic shear behaviors of other soils are also included.

1.4.1 Soil Specimen Preparation for Laboratory Testing

The common methods to reconstitute soil specimens include moist tamping, water pluviation, air pluviation, and slurry consolidation methods. These different methods can yield different soil properties for the same materials under the identical test conditions due to different fabric produced by the specimen preparation methods (Ladd 1977; Mulilis et al. 1977; Kuerbis and Vaid 1988). Soil specimens prepared by wet tamping could have a cyclic strength as much as 100% greater than those prepared by dry deposition (Ladd 1977). The specimens prepared by the moist tamping method have considerably higher undrained shear strength and a slightly smaller flow potential than those prepared by the slurry deposition method (Murthy et al. 2007). However, at large strain, these differences in fabric vanish, leading to a unique fabric at the critical state. Wood et al. (2008) reported that the effect of depositional method on the undrained response decreased with an increase in soil density, and this effect became more significant with increased silt content, particularly at lower densities. The effect of silt content on change of the microstructure due to depositional method was reported by Yamamuro et al. (2008). Dry funnel deposition yielded higher percentage of potential unstable grain contacts than water sedimentation (or pluviation), and this effect was pronounced as silt content increased.

The moist tamping (MT) method best models the soil fabric of compacted construction fills, for which the method was originally designed (Kuerbis and Vaid 1988). Water tension forces exist in the specimen and honeycomb structure easily forms (Guo and Wang 2009). Vaid (1994) stated that the MT technique neither simulates the fabric of alluvial soil deposits nor guarantees specimen uniformity. Bradshaw and Baxter (2007) presented a new modified moist tamping method and stated that the samples using this method could give comparable cyclic strengths to the slurry consolidation samples and the in situ block samples. They compared the new modified moist tamping method with the slurry consolidation method for the Wellington Ave. Silt and with the block sample method for the Olneyville Silt, respectively. Making a direct comparison with the same silt material would be preferred.

The Air pluviation (AP) method models the natural deposition process of wind-blown Aeolian deposits, which generally consist of either well-sorted sand or well-sorted silt (Kuerbis and Vaid 1988). Well-graded sand is not suitable for the air pluviation method. It is easily segregated, since the process of sample saturation may disrupt initial sand fabric and fines are washed out from the sample (Kuerbis and Vaid 1988; Carraro and Prezzi 2007).

The water pluviation (WP) method simulates the deposition of sand through water as occurs in many natural environments and mechanically placed hydraulic fills (Kuerbis and Vaid 1988). It produces uniform samples of poorly graded sand, but particle size segregation is a problem. Water pluviation of a well-graded soil results in a larger maximum void ratio comparable to that of a more poorly-graded soil. Vaid et al. (1999) carried out an experimental program to study the influence of reconstituted methods for sand. They concluded that water-deposited specimens were very uniform compared to the large non-uniformities that usually occur on moist tamping. Vaid et al. (1999) compared the shear resistance of undisturbed frozen sand with that of other sample preparation methods and presented that the water pluviation could closely simulate the fabric of the natural alluvial and hydraulic fill sands. Hoeg et al. (2000) finally stated that the method of water pluviation seems promising, although there are difficulties with segregation for sands with high fines content.

It is well known that a silt specimen is difficult to densify using vibration to achieve the desired density. Slurry deposition (SD) or slurry consolidation (SC) method is a common technique to prepare silt specimens, and even sandy silt and silty sand specimens, although the SD method only yields loose specimens compared to the silt deposit in the field. Using the SD method, specimens easily reach saturation under back pressure compared to the MT and AP methods because specimens are essentially prepared saturated (Carraro and Prezzi 2007). Ishihara et al. (1978) developed the SD technique for silty sand and sandy silt but their specimens were not very homogeneous when the fine content was between 30 and 80%. Kuerbis and Vaid (1988) presented a new slurry deposition method to prepare sand specimens. The specimens were exceptionally homogeneous with respect to void ratio and particle size distribution, regardless of gradation and fines content. This method simulated well the soil fabric found within a natural fluvial or hydraulic fill deposit, yet created homogenous samples that can be easily replicated

as required. Carraro and Prezzi (2007) reported another slurry method for silty sands. The homogeneous specimens of sand containing fines were prepared and the characteristic strain-softening response associated with the usually collapsible fabric obtained by AP and MT techniques was not observed. Yasuhara et al. (2003) used the silt SD method to prepare specimens and study the postcyclic degradation of strength and stiffness. Hyde et al. (2006) also prepared silt specimen using the SD method. The samples were not highly uniform due to the friction in the consolidation tubes and sample disturbance during preparation. They stated that this method of preparation did not produce samples that were representative of silt placed as a coastal fill material, which would often be pluviated under water and then consolidated by an overburden. Instead, they applied a simple sedimentation technique to consolidate the slurry under a negative head of water. Hyde et al. (2006) did not report the verification of uniformity within the specimen. In addition to the above-mentioned SD methods for silt, sandy silt and silty sand, Khalili and Wijewickreme (2008) presented a new slurry displacement method to reconstitute specimens of mixtures of waste rock and tailings and overcame the difficulties in preparation of highly gap-graded specimens.

It can be concluded from the recent published results that the SD method is the preferred method to reconstitute slit specimens. However, the problems shown by other researchers' work include the complexity and duration of specimen preparation. Wang et al. (2011) presented a new slurry consolidation approach to prepare low-plasticity silt specimens for triaxial testing.

1.4.2 Monotonic Shear Behavior of Low-plasticity Silt

Although the study of static behaviors of low-plasticity silt began about 60 years ago, work in this field is still limited, because the behavior of silt is much more complex than that of sand and clay. The published work on static behavior of low-plasticity silt is summarized below.

Early in 1953, Penman studied the static behavior of the Braehead silt under normally consolidated tests, both drained and undrained (Penman 1953). The silt specimens showed dilative behavior. Such dilative behavior was also found in Alaska silts (Wang et al. 1982; Fleming and Duncan 1990; Arulmoli et al. 1992). Wang et al. (1982) found in Alaska silts no unique undrained shear strength with various effective consolidation pressures. They determined that the ratio of undrained shear strength to effective consolidation pressure was higher than that for clay with an identical over consolidation ratio. Fleming and Duncan (1990) investigated the characteristics of undisturbed and reconstituted Alaskan silt specimens using a slurry deposition approach. In unconsolidated undrained (UU) tests, the reconstituted specimens reduced the undrained shear strength of undisturbed specimens by as much as 42%. On the other hand, consolidated undrained (CU) tests indicated that the undrained strength of reconstituted specimens was higher than that of undisturbed specimens. Fleming and Duncan concluded that the

silt was more likely to be seriously affected by disturbance. In general, the undrained strength of Alaskan silts could be normalized by effective consolidation pressure. As over consolidation ratio (OCR) increases, the normalized value of shear strength increases. Yasuhara et al. (2003) observed the same normalized behavior in the Keuper Marl silt, which has a plasticity index (PI) of 19.7.

Hoeg et al. (2000) investigated the effect of specimen preparation method on the static behavior of silt in Borlange, Swedan with a PI of 5. Using triaxial compression tests, they compared the strength of undisturbed specimens with that of reconstituted silt specimens at normally consolidated conditions. Most of specimens were prepared by moist tamping, but one was created using the slurry deposition approach. The undisturbed specimens showed dilative and ductile behavior, whereas almost all the reconstituted specimens showed contraction, brittle behavior.

Brandon et al. (2006) studied the drained and undrained strength of two silts, undisturbed gray silt (called Yazoo silt, no plastic) and disturbed tan silt (called LMVD silt, PI = 4) from Lower Mississippi Valley Division (LMVD). In undrained tests, both consolidated and unconsolidated, all specimens showed dilative behavior. That study demonstrated that the unconsolidated undrained tests did not provide useful information on the undrained strengths of the Yazoo silts. The authors suggested that the failure criterion that best determined ratio of undrained shear strength to effective consolidation stress was the constant Skempton pore pressure parameter A equal to zero.

Izadi (2006) investigated static behavior of Collinsville silt from the same region where the silt tested here was collected. Using the slurry deposition approach, he reconstituted specimens in a large consolidometer. The soil showed fairly high dilation behavior, even normally consolidated. Without high enough B values after saturation, cavitations easily developed due to negative excess pore water pressure, and specimens became unsaturated under large strain. Thus, the stress-strain behavior could not be determined well.

Boulanger and Idriss (2006) reviewed the behavior of three blended silt mixtures with normal consolidation, which was originally presented by Romero (1995). The specimen with a PI of 10.5 showed a plastic stress-strain response like that of normally consolidated clay. Its normal consolidation and critical state lines were almost parallel, and it exhibited no quasi-steady state behavior. Yasuhara et al. (2003) observed such plastic stress-strain behavior in the Keuper Marl silt. Boulanger and Idriss (2006), on the other hand, noted that throughout the test the silt specimen without plasticity exhibited strain hardening like that seen in loose sands, and its normal consolidation and critical state lines were not parallel. However, the silt with a PI of 4 exhibited behavior more like that of clay-like silt, but with a tendency toward some strain hardening and phase transformation behavior. Its normal consolidation and critical state lines were approximately parallel, but it had a quasi-steady state line. Boulanger and Idriss (2006), therefore, concluded that fine-grained soils with a PI greater than or equal to 7 can confidently be expected to exhibit clay-like behavior, and fine-grained soils with PI values ranging from 3 to 6 exhibit intermediate behavior. Nocilla et al. (2006) observed such transitional behavior in an Italian silt. For this Italian silt with clay content of

8% and PI of 3.5, no unique normal consolidation and critical state lines were found because specimens prepared with slurries of different water contents generated different fabric.

Low-plasticity silt can show strain-hardening behavior, strain-softening behavior, and even plastic stress-strain behavior, which depends primarily on the plasticity index, overconsolidation ratio, and specimen preparation technique. The overconsolidated silt is widespread in the shallow ground, because the ground water goes up and down. Wang and Luna (2012) investigated the static behavior of Mississippi River Valley (MRV) silt by conducting consolidated undrained tests with various OCRs and effective consolidation pressures.

1.4.3 Liquefaction of Low-plasticity Silt

Initially, the liquefaction potential was evaluated according to the Chinese criteria by Seed et al. (1983), in which clay content rather than plasticity index is used. As pointed out by Seed et al. (2003) and Bray and Sancio (2006), the condition about percentage of "clay-size" particles in the Chinese criteria is misleading and the importance is the percent of clay minerals present in the soil. Therefore, the plasticity index is used as one of key parameters in liquefaction criteria to evaluate the liquefaction potential instead. As presented by Boulanger and Idriss (2006), there is a transition zone for cyclic behavior of fine-grained soil, which transits from sand-like to clay-like with higher plasticity index. Boulanger and Idriss (2006, 2007) proposed that the soils with PI >7 can confidently be expected to exhibit clay-like behavior (i.e., cyclic softening, meaning that soil failure develops early before excess pore pressure ratio reaches or is close to 1.0). The soils with PI <7 has initial liquefaction (i.e., soil failure develops only after the excess pore pressure ratio reaches or is close to 1.0) under cyclic loading.

The variation of liquefaction resistance with plasticity index of soil has been studied by a few researchers. Puri (1984) found that the cyclic strength increased with an increase of plasticity index from 10 to 20 by conducting cyclic triaxial tests on the undisturbed and reconstituted silt from Memphis, TN. Conversely, Sandoval-Shannon (1989) observed that the silt from East Saint Louis, IL had a decrease in cyclic strength when the PI increased from 1.7 to 3.4; but with the PI of 12, the silt had higher cyclic strength than the silt with the PI of 3.4. Izadi (2008) added kaolinite to the silt from Collinsville, IL to form soil mixtures having 5% and 10% kaolinite. The tests indicated that the cyclic strength decreased with an increase in clay content, because of a decrease in hydraulic conductivity and no obvious increase in plasticity index. Guo and Prakash (1999) stated that the liquefaction resistance increases with a decrease in plasticity index in the low range, conversely, the opposite is true in the high range of plasticity index. They suggested that there be a need for further systematic study of the liquefaction behavior of silty and silty clay mixtures.

Beroya et al. (2009) studied the effect of mineralogy on the cyclic strength of silt-clay mixtures. Three different clays, including kaolinite, illite, and montmorillonite, were used to mix the nonplastic silt to form different silt-clay mixtures. It was concluded that the relationships of % clay fraction, % clay mineral and PI with cyclic strength are not unidirectional and they cannot be used to evaluate the susceptibility to cyclic failure, because the PI does not adequately encapsulate the effects of clay mineralogy on the cyclic strength of soils. The finding overturns the previous liquefaction criteria, in which the PI value is an important indicator to evaluate liquefaction resistance. As a comparison, the work of Gratchev et al. (2006) was also reviewed here, although the subject material for them was not fine-grained soil but clayey sand. They studied the liquefaction resistance of clayey sand, concluding that liquefaction resistance increased with an increase in plasticity of clayey sand with pure water. However, when the clayey sand has high ion concentration in pore water, questions are brought on the effectiveness of PI as a measure of liquefaction resistance.

So far, the effect of plasticity on liquefaction resistance of low-plasticity fine-grained soils is not monotonic. To reexamine the effect of PI on the liquefaction resistance of low-plasticity fine-grained soils, Wang et al. (2016a, b) collected existing cyclic experimental data and normalized them to reduce the effect of other relevant factors such as shear mode, density, effective confining stress and cyclic loading frequency. Then, a new correction factor K_{PI} to estimate the effect of plasticity index on CRR was proposed for design purposes.

1.4.4 Postcyclic Compressibility of Low-plasticity Silt

There is a paucity of research findings on the effect of cyclic loading on the compressibility of low-plasticity silt. Of the few published works, Thevanayagam et al. (2001) found the reconsolidation line in the e-logσ' (e—void ratio, σ'-effective stress) space nearly parallel to the compression line rather than the recompression line. For powdered limestone, Hyde et al. (2007) found that the slope of reconsolidation line was about 10 times steeper than that obtained from the precyclic recompression line and rather similar to that of the compression line. On the other hand, some researchers (Yasuhara and Andersen 1991; Hyodo et al. 1994; Hyde et al. 1997) reported opposite results for clays and plastic silts. Yasuhara and Andersen (1991) found that the slopes of the reconsolidation lines after cyclic loading were 1.5 times the recompression index for Drammen clay (PI = 27) and Ariake clays (PI = 69 and 72). Hyde et al. (1997) observed that the slope of reconsolidation line of Keuper Marl silt (PI = 19) after cyclic loading was almost identical to that of recompression line without previous cyclic loading.

To promote understanding on the effect of cyclic loading on compressibility of low-plasticity silt, Wang and Luna (2014) investigated compressibility of low-plasticity silt before and after cyclic loading and its change against plasticity.

1.4.5 Postcyclic Shear Behavior of Low-plasticity Silt

There is a paucity of works on the postcyclic behavior of silt; most published works are on sand and mixed clayey soils. Vaid and Thomas (1995) performed triaxial tests on Fraser River sand using water pluviation method to reconstitute specimens. They found that the liquefied sand deformed at virtually zero stiffness over a large range of axial strain (about 20%). With further straining, the sand always responded in a dilative manner under static loading, even though the initial sand was contractive under static loading. The postliquefaction response represented continuously stiffening behavior and an approach to any residual strength was not observed, regardless of density or effective consolidation pressure prior to cyclic loading, even after a postliquefaction strain of 32%. Amini and Trandafir (2008) also observed the dilation behavior in Bonneville silty sand. Ashour et al. (2009) found similar results for sand, as did Liu et al. (2007) for silt. Byrne et al. (1992) hypothesized that the steady state (or residual) strength of sand remains unaltered under monotonic loading following liquefaction induced by cyclic loading, if it is contractive under static loading.

Some work has also examined the effect of specific factors, including density, axial strain induced by cyclic loading, and fines content, on the postliquefaction behavior of silts and sands. Wijewickreme and Sanin (2010) reported that volumetric strain of low-plasticity Fraser River silt due to postcyclic reconsolidation generally increased with an increase in excess pore-water pressure or cyclic strain. Vaid and Thomas (1995) found that the recovery rate of postliquefaction stiffness increased as relative density increased. Liu et al. (2007), similar to Vaid and Thomas (1995), found that the threshold strain after which stiffness increases quickly decreased as dry unit weight increased and maximum double axial strain decreased. Ashour et al. (2009) presented equations to assess the undrained response of liquefied sand based on drained test behavior, indicating that the postcyclic excess pore pressure and associated residual effective confining pressure govern the postliquefaction undrained behavior of sand.

Following is a review of the few works on silt. Yasuhara et al. (2003) carried out triaxial tests to study postcyclic degradation of shear strength and stiffness of silt with a PI of 20. It was observed that postcyclic stiffness of over consolidated specimens correlated with the excess pore pressure ratio, R_u ($R_u = u_e/\sigma'_c$; u_e = excess pore pressure, σ'_c = mean effective consolidation pressure) generated during cyclic loading. However, compared to that for normally-consolidated specimens, this correlation was not strong. By conducting direct simple shear tests on nonplastic silt, Song et al. (2004) found that without postcyclic loading reconsolidation, the ratio of postcyclic maximum shear modulus to pre-cyclic maximum shear modulus decreased rapidly with an increase in excess pore pressure ratio. The rapid decrease in the stiffness ratio began at a lower R_u with a higher initial shear stress. Hyde et al. (2007) concluded that the ratio of undrained shear strength after cyclic loading to that before cyclic loading decreases with an increase in the initial sustained deviator stress ratio in both compression and extension tests for silt with a

PI of 6. On the other hand, the cyclic strength for second loading increased with an increasing initial sustained deviator stress ratio up to 0.75. Erken and Ulker (2007) conducted torsion tests in hollow specimens and determined yield cyclic shear strain, which was determined as 0.75% for reconstituted fine-grained soils with plasticity index (PI) of 2–33 and as 0.50% for undisturbed fine-grained soils with PIs of 5–13.

The effect of previous cyclic loading on monotonic shear behavior should be different for the soils with different PIs; however, few reports address the effect of PI on the changes in shear strength and stiffness due to cyclic loading. Song et al. (2004) found that the tendency of the stiffness of nonplastic silt to decrease with the excess pore pressure ratio is not as significant as that in plastic Arakawa clay with a PI of 17.3. However, case histories in Robertson (2010) indicate that very young, very loose, nonplastic or low-plastic soils tend to be more susceptible to significant and rapid strength loss than older, denser, or more plastic soils. Alba and Ballestero (2008) stated that increasing fines content decreases the undrained shear strength of soil after liquefaction, but they did not investigate the effect of PI on the change of undrained shear strength due to cyclic loading. Thus, according to existing reports, postcyclic shear strength decreases with an increase in PI, as static shear strength of low-plasticity soil varies as a function of PI. However, there was no consistent data reported on the effect of PI on reductions in shear strength and stiffness between Song et al. (2004) and Robertson (2010). Thus, there has not been definitive research result for evaluating the effect of clay on cyclic and postcyclic shear behavior of low-plasticity fine-grained soils until now.

The foregoing review indicates that the effect of initial consolidation condition on postcyclic undrained monotonic behavior of low-plasticity silt has not been studied extensively. Wang et al. (2015a, b) studied postcyclic shear strength of MRV silt, both reconsolidated and not reconsolidated. The variations of postcyclic shear behavior of the silt with plasticity and initial consolidation condition were addressed, and its postcyclic undrained monotonic shear strength was also investigated for engineering applications.

1.4.6 Effect of Cyclic Loading Magnitude on Static Behavior

(1) **Effect of excess pore pressure on soil behavior**

During cyclic loading, soil experiences a build-up of pore water pressure under undrained condition and a decrease in volume under drained condition. After undrained cyclic loading without reconsolidation, the shear strength of postcyclic soil is lower than that of virgin soil (i.e., reconstituted specimens without previous cyclic loading), while with reconsolidation the opposite result is true, except for sensitive clay (i.e., a clay that loses a very substantial proportion of its strength when disturbed) and peat (Yasuhara 1994).

Chern and Lin (1994) carried out cyclic loading and postcyclic consolidation tests on loose, clean sand and silty sand. They found that the reconsolidation volumetric strain is related to the maximum cyclic strain amplitude and excess pore pressure ratio developed during cyclic loading, regardless of the cyclic stress ratio or the number of stress cycles applied. For loose sand with accumulated, cyclic, single-amplitude axial strain of less than 1% or an excess pore pressure ratio of less than 1.0, the magnitude of postcyclic reconsolidation volumetric strain is relatively small compared to that in liquefied specimens. Sanin and Wijewickreme (2010) presented similar findings after they conducted cyclic direct simple shear testing on Fraser River Delta silt. Chern and Lin (1994) proposed that liquefaction ($R_u = 1.0$) is a prerequisite to significant volume change due to one-dimensional reconsolidation of loose deposits on level ground after an earthquake.

Ashour et al. (2009) studied the undrained postcyclic response of sand, which was not reconsolidated, following cyclic loading with an induced $R_u < 1.0$. With a $R_u < 1.0$, sand may exhibit initial (restrained) contractive behavior (inducing a little positive u_e to develop) followed by dilative behavior. Here, the excess pore pressure (more significant than initial density or confining pressure) governed the postcyclic undrained behavior (stress-strain relationship) of the sand. Vaid and Thomas (1995) found that the postcyclic shear behavior of sand with small R_u values approached the behavior of the soil under undrained conditions.

Less has been reported on the postcyclic behavior of silt, and most of the previous research has been on sand and mixed clayey soil. Yasuhara et al. (2003) carried out triaxial tests to study the postcyclic degradation of the strength and stiffness of "low-plasticity silt" (PI = 19.7). The silt was not reconsolidated after cyclic loading. With the same OCR, they found that postcyclic undrained shear strength without reconsolidation decreased with an increase in excess pore pressure ratio following cyclic testing. With increasing cyclic-induced excess pore pressure, stiffness at the beginning of postcyclic shearing decreased along with the peak deviator stress. That work demonstrated that postcyclic stiffness of over consolidated specimens correlates with excess pore pressure ratio generated during cyclic loading. However, compared to that for normally consolidated specimens, this correlation is not strong. By conducting direct simple shear tests on non-plastic silt, Song et al. (2004) found that the ratio of postcyclic maximum shear modulus to precyclic maximum shear modulus ($G_{max,cy}/G_{max,NCi}$) decreased rapidly with an increase in excess pore pressure ratio. This rapid decrease in the stiffness ratio ($G_{max,cy}/G_{max,NCi}$) began at a lower excess pore pressure ratio, for the series of tests with a higher initial shear stress (τ_s).

In summary, the volume change in sand due to the reconsolidation after cyclic loading with an induced $R_u < 1.0$ is much lower than that after liquefaction ($R_u = 1.0$). Excess pore pressure ratio after cyclic loading controls the postcyclic undrained shear behavior of sand and low-plasticity silt, irrespective of initial density or initial confining pressure. It was found that the higher the excess pore pressure ratio, the greater the reduction in undrained shear strength for soils without reconsolidation after cyclic loading. The reduction in shear strength and stiffness of

mixed clay soils is related to the axial strain induced by the cyclic loading. The reduction of stiffness is more marked than that of shear strength.

(2) **Effect of cyclic strain on soil behavior**

Soil characteristics (including microstructure, stiffness, shear strength) under cyclic strain can be divided into small-strain, medium-strain and large-strain regions (Diaz-Rodriguez and Santamarina 2001). In the small-strain region, the soil remains linear-elastic during cyclic loading. There is no change in the microstructure, and bonds at interparticle contacts are preserved. In the medium-strain region, the soil starts displaying nonlinear elastic behavior, while the reduction in strength is minor. In the large-strain region, the soil fabric is destroyed and interparticle interaction starts loosening. The reduction in strength in this case is substantial.

Adjacent regions are separated by a threshold strain. The small- and medium-strain regions are separated by an elastic threshold strain, and the medium- and large-strain regions are separated by a degradation threshold strain. Diaz-Rodriguez and Santamarina (2001) and Vucetic (1994) divided the medium-strain region into two regions, separated by a volumetric cyclic threshold strain. Below the volumetric cyclic threshold, nonlinear elastic behavior commences with no significant development of excess pore pressure in the undrained condition and no significant volume change in the drained condition (2008). The development of excess pore-water pressure and permanent volume change is attributed to microstructural changes in the soil (Vucetic 1994).

Vucetic (1994) presented a chart with a band to show the variation of volumetric threshold strain against plasticity index (PI). The volumetric threshold strain includes the strain, over which pore water pressure builds up substantially in undrained cyclic tests and volume decreases substantially in drained cyclic tests. However, Hsu and Vucetic (2004) stated that the magnitudes of the different types of cyclic threshold shear strains, including for pore water pressure, cyclic settlement, cyclic degradation, and cyclic stiffening, are not necessarily the same for the same soil. The two clayey soils with symbols of SC-222 and SC-666, tested by Hsu and Vucetic (2004, 2006) had threshold shear strains of 0.07–0.09% and 0.07–0.08% for volume change in drained cyclic condition, and threshold shear strains of 0.03–0.06% and 0.03–0.05% for pore pressure build-up in undrained cyclic condition, respectively. Thus, for these two clayey soils the threshold shear strains for volume change are larger than these corresponding values for the build-up of pore pressure. Hsu and Vucetic (2004, 2006) found that threshold shear strain is larger for cohesive soils than for non-cohesive soils and increases with PI for clay.

Several researchers (Diaz-Rodriguez and Santamarina 2001; Vucetic 1994; Hsu and Vucetic 2004, 2006; Silver and Seed 1971; Dobry et al. 1982; Dyvik et al. 1984) have studied the threshold shear strains for pore water pressure and volume change. Diaz-Rodriguez and Santamarina (2001) reported that Mexico City clay had a threshold shear strain of 3% for postcyclic strength reduction. The threshold shear strain based on postcyclic strength reduction was reported to be 2% (maximum) for seafloor soils by Houston and Herrmann (1980), and 0.5–0.9% for

sensitive clay with a PI of 12 from the Hudson Bay by Lefevbre et al. (1989). Erken and Ulker (2007) conducted torsion tests in hollow specimens and determined yield cyclic shear strains of 0.75% for reconstituted fine-grained soils with PI of 2–33 and 0.50% for undisturbed fine-grained soils with PI of 5–13. When soil specimen had a higher shear strain than yield cyclic shear strain, the postcyclic shear strength reduced substantially. Hyde et al. (2007) studied postcyclic behavior of a creamy powdered limestone (69.2% silt sized particles) with a PI of 6 using a servo pneumatic triaxial testing system. The volume changes of limestone specimens during postcyclic recompression were almost identical for all samples with identical axial strains induced by cyclic loading, irrespective of excess pore pressure, differently with postcyclic behavior of sands studied in Chern and Lin (1994). Soroush and Soltani-Jigheh (2009) carried out strain-controlled cyclic triaxial testing on mixed clayey soils (clay-sand and clay-gravel mixtures), and the postcyclic soils not reconsolidated after cyclic loading. They concluded that the ratio of postcyclic undrained shear strength to initial undrained shear strength ($S_{u(PC)}/S_{u(M)}$) and the ratio of postcyclic secant deformation modulus to initial secant deformation modulus ($E_{50(PC)}/E_{50(M)}$) generally decreased as axial strain induced by cyclic loading increased. Further, they found that the reduction in the deformation modulus was more pronounced than that in the undrained shear strength. Specimen behavior during postcyclic loading was similar to that of overconsolidated soils. Generally, the value of the apparent overconsolidation ratio (OCR_{app}) was proportional to the axial strain amplitude induced. Porcino et al. (2009) conducted a series of cyclic shear tests on un-cemented carbonate sands (Quiou sand) using the modified NGI cyclic simple shear device. Reconsolidation was allowed after cyclic loading. A limiting shear strain was defined based on the phase transformation line, where beyond this strain level the material's mechanical properties are impacted. They proposed a normalizing criterion, capable of providing a unified description of the pore-pressure build-up curves for different pre-shearing histories.

Comparatively, there are few studies on the determination of the threshold strain for postcyclic shear strength, especially for low-plasticity silt. Wang et al. (2014a, b) investigates cyclic loading induced threshold strain for postcyclic shear strength after reconsolidation using reconstituted silt from Mississippi River Valley (MRV).

1.4.7 Reliquefaction Characteristics

There is a paucity of published works on the effect of previous shearing on cyclic behavior. The few published works available are mainly on sand. Finn et al. (1970) found that the liquefaction resistance increased when the previous residual axial strain was as low as 0.2%. Finn et al. (1970) states that this benefit resulted from the interlocking of the particles in the original structure due to elimination of small local instabilities at the contact points without any general structural rearrangement taking place. They suggested the threshold of residual axial strain to be 0.5%. However, when the previous residual axial strain was greater than 0.5%, the

liquefaction resistance decreased. This decrease is probably due to the uniform structural arrangement, which was weak in resisting cyclic shear loads; alternatively, it is due to the nonuniform structure, which was induced by liquefaction and led to nonuniform deformation and reduction in reliquefaction resistance. The nonuniform structure was reported by Finn et al. (1969) and also by Emery et al. (1973). Emery et al. (1973) investigated the uniformity of saturated sand specimens after cyclic loading using the cyclic triaxial, simple shear, and shake table tests. Reporting that a loose layer of sand formed at the top of specimen, they further stated that such loose zone can result in a significant reduction in the liquefaction resistance, which can become more significant with an increase in the previous strain (greater than 0.5%). The reduction in the liquefaction resistance due to previous strain was also reported by Porcino and Caridi (2007), who conducted cyclic simple shear tests on loose and dense sands (relative density of 40 and 70%, respectively). While the loose sand showed a reduction in liquefaction resistance after single amplitude shear strain of 3.75%, the dense sand showed no reduction in liquefaction resistance due to the previous shear strain.

Ishihara and Okada (1978, 1982) conducted a study on the effect of preshearing on cyclic behavior of sand. Large and small preshearing were defined in Ishihara and Okada (1978). When the stress path passes through the line of phase transformation, the previous shearing is considered as large preshearing; otherwise, the previous shearing is thought to be small preshearing. When the specimens were subjected to small preshearing, they developed excess pore pressures and shear strains in both triaxial compression and extension. On the contrary, when the specimens were subjected to large preshearing on either sides of triaxial compression and extension, they became stiffer and developed less excess pore pressure on that side, but softer and more excess pore pressure on the opposite side. Similar results were reported by Suzuki and Toki (1984), which stated that the effect of preshearing was brought about mainly by microscopic fabric change and regardless of whether the preshear stress was applied in triaxial compression or extension. The threshold preshear strain at which the effect of the opposite direction preshearing begins to appear was 0.30%. Wichtmann et al. (2005) proposed a correlation of the liquefaction resistance with cyclic preloading, which induces a cyclic strain of less than 0.1%.

In Ishihara and Okada (1978), the cyclically induced axial strain was held constant, and the deviator stress was brought back to zero. However, in Ishihara and Okada (1982), both cyclically induced axial strain and deviator stress were set to zero after large prehearing. When the specimens were subjected to a large cyclically induced axial strain oriented to the triaxial compression under very low effective confining pressure, Ishihara and Okada (1982) found that the excess pore pressure response of presheared specimens was essentially the same with that of the virgin specimen during the cyclic loading. Ishihara and Okada (1982) thought that the newly formed cross anisotropic structure of the specimen due to liquefaction and reconsolidation had the same vertical axial symmetry as the virgin specimens so their specimens had almost the same excess pore pressure response. On the other hand, when the specimens were subjected to a large cyclically induced axial strain

oriented to the triaxial extension under very low effective confining pressure, the excess pore pressure of the presheared specimen was different from that of virgin specimens. As explained by Ishihara and Okada (1982), this difference was ascribed to the fact that the newly formed cross anisotropic structure has horizontal axial of symmetry instead of the vertical axial of symmetry, which was shown in the virgin specimens.

Porcino et al. (2009) presented the effect of cyclic shearing on cyclic behavior of carbonate sand tested with the modified NGI (Norwegian Geotechnical Institute) cyclic simple shear device. A limiting shear strain related to the phase transformation line was defined. Specimens subjected to strains below this limiting value benefit from cyclic loading. Conversely, specimens subjected to strains above this limiting value do not benefit from cyclic loading. They proposed a normalizing criterion capable of providing a unified description of the pore-pressure development curves for different pre-shearing histories.

In summary, liquefaction resistance of presheared soil depends on the magnitude of preshearing strain, direction of preshearing, soil density, and others. A search of literature has yielded no published work on the repeated liquefaction characteristics of low-plasticity silt. The undrained cyclic response of low-plasticity silts is more difficult to predict than that of sand since they are near the transition between "sand-like" and "clay-like" behavior. Due to different soil composition of silt from sand, research studies aimed at investigating the effect of previous cyclic shearing on liquefaction resistance of low-plasticity silt are warranted.

1.5 Soil Material Tested in This Study

The studied low-plasticity silt material in this book was collected from Collinsville, Illinois, USA. These soils are common in the New Madrid seismic zone (NMSZ) where a high risk of damage related to earthquakes (M >7.0) continues to exist (El Hosri et al. 1984). According to the grain size distribution of the MRV silt, determined by sieve and hydrometer analysis, the clay (< 5 μm) and silt contents of the materials were 18.8 and of 76.1%, respectively. The liquid and plasticity limits of the MRV silt were measured following the procedure with special provisions explained in Wang et al. (2011). The specific gravity of the material was measured to be 2.71. The maximum void ratio (1.604) and minimum void ratio (0.436) were obtained following the slurry deposition approach and modified compaction approach (Bradshaw and Baxter 2007; Polito and Martin 2001), respectively. The MRV silt was classified with a group name: "Silt" and symbol: ML, according to the Casagrande's plasticity chart. Consolidation tests were carried out in a triaxial chamber by applying an isotropic confining pressure to determine the compression and recompression indices (C_c and C_r, which were computed based on the Δe-$\Delta \log p'$ space), which are 0.090 and 0.009, respectively. Index and compressibility properties of MRV silt are presented in Table 1.1.

Table 1.1 Index properties and compressibility of MRV silt

Soil property	Value
Clay content (<5 μm)	18.8%
Liquid limit	28.1
Plastic limit	22.3
Plasticity index	5.8
Specific gravity	2.71
Compression index (C_c)	0.0896
Recompression index (C_r)	0.0090

1.6 Scope of This Book

The book includes eight chapters, and its main organization is shown as follows:

Chapter 1: Introduction
This chapter first discusses the definition, distribution and research significance of the low-plasticity silt, and then discusses state-of-the-art on specimen preparation, monotonic shear behavior, cyclic behavior, postcyclic shear behavior of low-plasticity silt, and etc.
Chapter 2: Specimen Preparation
A new slurry consolidation approach is reported step by step for reconstituting low-plasticity specimen in a split vacuum mold. The reliability of the specimen preparation is verified.
Chapter 3: Monotonic Shear Behavior of Low-plasticity Silt
The testing program for studying monotonic shear behavior of the MRV silt is presented. The testing results are reported, including stress-strain behavior, friction angle, critical state, and normalized behavior. Then, the effect of plasticity on shear behavior of low-plasticity silt is investigated.
Chapter 4: Liquefaction characteristics of Low-plasticity Silt
The cyclic shear behavior of the MRV silt is then presented. More importantly, laboratory data of previous researchers is reexamined, and then the change of liquefaction resistance with PI is reported.
Chapter 5: Postcyclic Compressibility of Low-plasticity Silt
The testing program for investigating postcyclic compressibility of the MRV silt is stated step by step. Finally, the effects of cyclic loading on permeability and compressibility are reported, following by investigation on change of compressibility due to cyclic loading against plasticity.
Chapter 6: Postcyclic Shear Behavior of Low-plasticity Silt
Following the presentation of testing program, postcyclic shear behavior of the MRV silt with and without reconsolidation is investigated. The change of critical state line due to cyclic loading is presented. The effects of plasticity index and reconsolidation level on postliquefaction shear behavior, including undrained shear strength and shear modulus of the MRV silt, are studied. The phenomenon of apparent OCR induced by reconsolidation after cyclic loading is finally presented.

Chapter 7: Effect of Cyclic Loading Magnitude on Shear Behavior of Low-plasticity Silt
The testing results of postcyclic shear behavior of the MRV silt, respectively with full reconsolidation and without reconsolidation, are reported for the MRV silt. The effect of excess pore pressure ratio on shear behavior of Low-plasticity silt is investigated. The findings on the MRV silt are compared with other laboratory data. Then, a simple method to determine threshold strain for postcyclic shear strength and its change against different influence factors is reported.
Chapter 8: Reliquefaction
After the testing program is explained, excess pore pressure response, axial strain and liquefaction resistance of low-plasticity silt are investigated after different levels of cyclic loading.

References

Alba, P. D., & Ballestero, T. P. (2008). Effect of fines on sand residual strength after liquefaction, *Geotechnical Earthquake Engineering and Soil Dynamics Congress IV*. USA: Geotechnical Special Publication.

Amini, Z. A., & Trandafir, A. C. (2008). *Post-liquefaction shear behavior of Bonneville Silty-Sand, Geotechnical earthquake engineering and soil dynamics* (p. 181). USA: Geotechnical Special Publication.

Arulmoli, K., Muraleetharan, K. K., Hossain, M. M., and Fruth, L. S. (1992). Verification of liquefaction analysis by centrifuge studies laboratory testing program. *The Earth Technology Corporation*. Irvine, CA, USA: Soil Data Report.

Ashour, M., Norris, G., & Nguyen, T. (2009). Assessment of the undrained response of sands under limited and complete liquefaction. *Journal of Geotechnical and Geoenvironmental Engineering, 135*(11), 1772–1776.

Beroya, M. A. A., Aydin, A., & Katzenbach, R. (2009). Insight into the effects of clay mineralogy on the cyclic behavior of Silt-clay mixtures. *Engineering Geology, 106,* 154–162.

Boulanger, R. W., & Idriss, I. M. (2006). Liquefaction susceptibility criteria for Silts and clays. *Journal of Geotechnical and Geoenvironmental Engineering, 132*(11), 1413–1426.

Boulanger, R. W., & Idriss, I. M. (2007). Evaluation of cyclic softening in Silts and clays. *Journal of Geotechnical and Geoenvironmental Engineering, 133*(6), 641–652.

Boulanger, R. W., Meyers, M. W., Mejia, L. H., & Idriss, I. M. (1998). Behavior of a fine-grained soil during the Loma Prieta earthquake. *Canadian Geotechnical Journal, 35,* 146–158.

Bradshaw, A. S., & Baxter, C. D. P. (2007). Sample preparation of Silts for liquefaction testing. *Geotechnical Testing Journal, 30*(4), 1–9.

Brandon, T. L., Rose, A. T., & Duncan, J. M. (2006). Drained and undrained strength interpretation for low-plasticity Silts. *Journal of Geotechnical and Geoenvironmental Engineering, 132*(2), 250–257.

Bray, J. D. & Frost, D. (2010). Geo-engineering Reconnaissance of the 2010 Maule, Chile Earthquake. Report No. Geer-022, Geo-Engineering Extreme Events Reconnaissance (Geer) Association.

Bray, J. D., & Sancio, R. B. (2006). Assessment of the liquefaction susceptibility of fine-grained soils. *Journal of Geotechnical and Geoenvironmental Engineering, 132*(9), 1165–1177.

Byrne, P.M., Jitno, H., & Jeremy, H. (1992). A Procedure for Predicting the Seismic Response of Tailings impoundments. In *Proceedings of Geotechnique and Natural Hazards: Geohazards 92*, (pp 281–289). Vancouver, Canada: Vancouver Geotechnical Society.

Carraro, J. A. H., & Prezzi, M. (2007). A new slurry-based method of preparation of specimen of sand containing fines. *Geotechnical Testing Journal, 31*(1), 1–11.

Chern, J. C., and Lin, C. C. (1994). Post–cyclic Consolidation Behavior of Loose Sands. In *Proceeding of Settlement 94*, Geotechnical Special Publication, ASCE, No. 40.

Diaz-Rodriguez, J. A., & Lopez-Molina, J. A. (2008). Strain Threshold in Soil Dynamics. In *Proceedings of the 14th World Conference on Earthquake Engineering*, Beijing, China, October 12–17 2008. Tokyo, Japan: International Association for Earthquake Engineering.

Diaz-Rodriguez, J.A. & Santamarina, J. C. (2001). Mexico city soil behavior at different strains: Observations and physical interpretation. *Journal of Geotechnical and Geoenvironmental Engineering*, *127*(9), 783–789.

Dobry, R., Ladd, R. S., Yokel, F. Y., Chung, R. M., & Powell, D. (1982). Prediction of pore-water pressure buildup and liquefaction of sands during earthquakes by the cyclic strain method. NBS Building Science Series No. 138, National Bureau of Standards, U.S. Dept. of Commerce, Washington, D.C. p. 150.

Duncan, J. M., & Wright, S. G. (2005). *Soil strength and slope stability*. Hoboken, N.J.: Wiley.

Dyvik, R., Dobry, R., Thomas, G. E., & Pierce, W. G. (1984). Influence of consolidation shear stresses and relative density on threshold strain and pore pressure during cyclic straining of saturated sands. Miscellaneous Paper, GL-84–15, Department. of the Army, U.S. Army Corps of Engineers, Washington, D.C., 1984, p. 74.

El Hosri, M. S., Biarez J., & Hicher P. Y. (1984). Liquefaction Characteristics of Silty Clay. In *Proceedings of the Eighth World Conference on Earthquake Engineering*. San Francisco, CA.

Emery, J. J., Finn, W. D., & LEE, K. W. (1973). Uniformity of saturated sand specimen. *Evaluation of Relative Density and Its Roll in Geotechnical Projects Involving Cohesionless Soils, STP, 53,* 182–194.

Erken, A., & Ulker, B. M. C. (2007). Effect of cyclic loading on monotonic shear strength of fine-grained soils. *Engineering Geology, 89,* 243–257.

Finn, W. D., Pickering, D. J., & Bransby, P. L. (1969). Sand Liquefaction in Triaxial and Simple Shear Tests. Soil Mechanics Research Report Series No. 11, University of British Columbia, Vancouver, Canada.

Finn, W. D., Bransby, P. L., & Pickering, D. J. (1970). Effect of strain history on liquefaction of sand. *Journal of Soil Mechanics and Foundations Division, 96*(SM6), 1917–1933.

Fleming, L. N., & Duncan, J. M. (1990). Stress-deformation characteristics of Alaskan Silt. *Journal of Geotechnical Engineering, 116*(3), 377–393.

Gratchev, I. B., Sassa, K., & Fukuoka, H. (2006). How reliable is the plasticity index for estimating the liquefaction potential of Clayey Sands? *Journal of Geotechnical and Geoenvironmental Engineering, 132*(1), 124–127.

Guo, T., & Prakash, S. (1999). Liquefaction of silts and Silt-Clay Mixtures. *Journal of Geotechnical and Geoenvironmental Engineering, 132*(6), 716–735.

Guo, Y., & Wang, Y. X. (2009). Experimental study about the influence of initial water content in wet tamping method on static triaxial test results of Silt. *Electronic Journal of Geotechnical Engineering, 14*.

Hoeg, K., Dyvik, R., & Sandbækken, G. (2000). Strength of undisturbed versus reconstituted silt and silty sand specimens. *Journal of Geotechnical and Geoenvironmental Engineering, 126*(7), 606–617.

Houston, W. N., & Herrmann, H. G. (1980). Undrained cyclic strength of marine soils. *Journal of Geotechnical Engineering Division, 106*(6), 691–712.

Hsu, C. C., & Vucetic, M. (2004). Volumetric threshold shear strain for cyclic settlement. *Journal of Geotechnical and Geoenvironmental Engineering, 130*(1), 58–70.

Hsu, C. C., & Vucetic, M. (2006). Threshold shear strain for cyclic pore-water pressure in cohesive soils. *Journal of Geotechnical and Geoenvironmental Engineering, 132*(10) 1325–1335.

Hyde, A. F. L., Marto, A., & Yasuhara, K. (1997). Volumetric compression of periodically loaded silt (pp. 629–634). Pergamon, London: *Proceeding of International Symposium on Deformation and Progressive Failure in Geomechanics*.

Hyde, A. F. L., Higuchi, T., & Yasuhara, K. (2006). Liquefaction, cyclic mobility, and failure of silt. *Journal of Geotechnical and Geoenvironmental Engineering, 132*(6), 716–735.

Hyde, A. F. L., Higuchi, T., & Yasuhara, T. (2007). Postcyclic recompression, stiffness, and consolidated cyclic strength of silt. *Journal of Geotechnical and Geoenvironmental Engineering, 133*(4), 416–423.

Hyodo, M., Yamamoto, Y., & Sugiyama, M. (1994). Undrained cyclic shear behavior of normally consolidated clay subjected to initial static shear stress. *Soils and Foundations, 34*(4), 1–11.

Ishihara, K., & Okada, S. (1978). Effects of stress history on cyclic behavior of sand. *Soils and Foundations, 8*(4), 31–45.

Ishihara, K., & Okada, S. (1982). Effects of large preshearing on cyclic behavior of sand. *Soils and Foundations, 22*(3), 99–125.

Ishihara, K., Sodekawa, M., & Tanaka, Y. (1978). Effects of overconsolidation on liquefaction characteristics of sands containing fines. ASTM, West Conshohocken, PA: Dynamic Geotechnical Testing, 246–264.

Izadi, A. (2006). Static Behavior of Silts. MS Thesis, University of Missouri-Rolla, Missouri, US.

Izadi, A. (2008). Liquefaction and Post-Liquefaction Behavior of Low Plasticity Silts using Cyclic Triaxial Tests. Ph.D. Dissertation, Missouri University of Science and Technology, Rolla, MO, US.

Khalili, A., & Wijewickreme, D. (2008). New Slurry displacement method for reconstitution of highly gap-graded specimens for laboratory element testing. *Geotechnical Testing Journal, 31*(5), 1–9.

Kuerbis, R. H., & Vaid, Y. P. (1988). Sand sample preparation—the slurry deposition method. *Soils and Foundation, 28*(4), 107–118.

Ladd, R. S. (1977). Specimen preparation and cyclic stability of sands. *Journal of Geotechnical Engineering Division, 103*(6), 535–547.

Lefebvre, G. S., Leboeuf, D., & Demers, B. (1989). Stability threshold for cyclic loading of saturated clay. *Canadian Geotechnical Journal, 26*(1), 122–131.

Liu, H. L., Zeng, C. N., & Zhou, Y. D. (2007). Test study on post-liquefaction deformation behavior of silt ground. *Chinese Journal of Rock and Soil Mechanics, 28*(9), 1866–1870. (in Chinese).

MOHURD of China. (2009). Code for investigation of Geotechnical Engineering. GB 50021-2001, Beijing, China.

Mulilis, J. P., Seed, H. B., Chan, C. K., Mitchell, J. K., & Arulanandan, K. (1977). Effects of sample preparation on sand liquefaction. *Journal of Geotechnical Engineering Division, 103*(2), 91–108.

Murthy, T. G., Loukidis, D., Carraro, J. A. H., et al. (2007). Undrained monotonic response of clean and silty sands. *Geotechnique, 57*(3), 273–288.

Nocilla, A., Coop, M. R., & Colleselli, F. (2006). The mechanics of an italian silt: An example of 'transitional' behavior. *Geotechnique, 56*(4), 261–271.

Penman, A. D. M. (1953). Shear characteristics of a saturated silt, measured in triaxial compression. *Geotechnique, 3,* 312–328.

Polito, C. P., & Martin, J. R. (2001). Effects of nonplastic fines on the liquefaction resistance of sands. *Journal of Geotechnical and Geoenvironmental Engineering, 127*(5), 408–415.

Porcino, D., & Caridi, G. (2007). Pre- and post-liquefaction response of sand in cyclic simple shear, Dynamic response and soil properties (p. 160). USA: Geotechnical Special Publication.

Porcino, D., Marciano, V., & Ghionna, V. N. (2009). Influence of cyclic pre-shearing on undrained behavior of carbonate sand in simple shear tests. *Geomechanics and Geoengineering, 4*(2), 151–161.

Puri, V. K. (1984). Liquefaction behavior and dynamic properties of loessial (Silty) Soils, Ph. D. Disseratation. Rolla, MO, USA: University of Missouri.

Robertson, P. K. (2010). Evaluation of flow liquefaction and liquefied strength using the cone penetration test. *Journal of Geotechnical and Geoenvironmental Engineering, 136*(6), 842–853.

Romero, S. (1995). The behavior of silt as clay content is increased. MS thesis, Davis, Calif: University of California.

Sandoval-Shannon, J. A. (1989). liquefaction and settlement characteristics of silt soils, Ph.D. Disseratation. Rolla, MO, US: University of Missouri.

Sanin, M. V., & Wijewickreme, D. (2006). Cyclic shear response of channel-fill Fraser River Delta Silt. *Soil Dynamics and Earthquake Engineering, 26*, 854–869.

Seed, H. B., Idriss, I. M., & Arango, I. (1983). Evaluation of liquefaction potential using field performance data. *Journal of Geotechnical Engineering, 109*(3), 458–482.

Seed, R. B., Cetin, K. O., Moss, R. E. S., Kammerer, A. M., Wu, J., Pestana, J. M., et al. (2003). Recent Advances in Soil Liquefaction Engineering: A unified and Consistent Framework. In *26th Annual ASCE Los Angeles Geotechnical Spring Seminar*, ASCE, Long Beach, CA, USA.

Silver, M. L., & Seed, H. B. (1971). Volume changes in sands during cyclic loading. *Journal of Soil Mechanics and Foundation Division, 97*(9), 1171–1182.

Song, B. W., Yasuhara, K., & Murakami, S. (2004). Direct simple shear testing for postcyclic degradation in stiffness of nonplastic silt. *Geotechnical Testing Journal, 27*(6), 1–7.

Soroush, A., & Soltani-Jigheh, H. (2009). Pre- and Postcyclic behavior of mixed clayey soils. *Canadian Geotechnical Journal, 46,* 115–128.

Stark, T. D., Kramer, S. L., & Youd, T. L. (1997). Post-liquefaction shear strength of granular soils. *National Science Foundation Workshop*. USA: University of Illinois-Urbana-Champaign.

Suzuki, T., & Toki, S. (1984). Effects of preshearing on liquefaction characteristics of saturated sand subjected to cyclic loading. *Soils and Foundations, 24*(2), 16–28.

Thevanayagam, S., Martin, G. R., Shenthan, T., & Liang, J. (2001). Post-liquefaction Pore Pressure Dissipation and Densification in Silty Soils. In *Proceedings of 4th International Conference on Recent Advances in Geotechnical Earthquake Engineering and Soil Dynamics*, San Diego, CA.

Towhata, I. (2008). *Geotechnical Earthquake Engineering*. Spring Series in Geomechanics and Geoengineering.

Vaid, Y. P. (1994). *Liquefaction of Silty Soils*. Ground Failures under Seismic Conditions, Atlanta, GA, New York, 1–16.

Vaid, Y. P., & Thomas, J. (1995). Liquefaction and postliquefaction behavior of sand. *Journal of Geotechnical Engineering, 121*(2), 163–173.

Vaid, Y. P., Sivathayalan, S., & Steaman, D. (1999). Influence of specimen reconstituting method on the undrained response of sand. *Geotechnical Testing Journal, 22*(3), 187–195.

Vucetic, M. (1994). Cyclic threshold shear strain in soils. *Journal of Geotechnical Engineering, 120*(12), 2208–2228.

Wang, J. L., Vivatrat, V., & Rusher, J. R. (1982). Geotechnical Properties of Alaska OCS Silt. In *4th Annual offshore Technology Conference*, Houston, Texas, US.

Wang, S., Luna, R., & Stephenson, R. W. (2011). A slurry consolidation approach to reconstitute low-plasticity silt specimens for laboratory triaxial testing. *Geotechnical Testing Journal, 34* (4), 288–296.

Wang, S., & Luna, R. (2012). Monotonic behavior of Mississippi River Valley silt in triaxial compression. *Journal of Geotechnical and Geoenvironmental Engineering, 138*(4), 516–525.

Wang, S., & Yang, J. (2013). The effect of previous cyclic loading on static and cyclic strength of low-plasticity silt. *Chinese Journal of Rock Mechanics and Engineering, 32*(2), 363–368. (in Chinese).

Wang, S., Luna, R., & Yang, J. (2013a). Postcyclic Behavior of low-plasticity silt with limited liquefaction. *Soil Dynamics and Earthquake Engineering, 54,* 39–46.

Wang, S., Yang, J., & Onyejekwe, J. (2013b). Effect of previous cyclic shearing on liquefaction resistance of Mississippi River Valley silt. *Journal of Materials in Civil Engineering, 25*(10), 1415–1423.

Wang S., & Luna, R. (2014). Compressibility characteristics of low-plasticity silt before and after liquefaction. *Journal of Materials in Civil Engineering*, *26*(6), 040140141-1–6.

Wang, S., Onyejekwe, S., & Yang, J. (2014a). Threshold strain for postcyclic shear strength change of Mississippi River Valley silt due to cyclic triaxial loading. *Journal of Testing and Evaluation, 42*(1), 69–77.

Wang, S., Yang, J., & Zhang, X. (2014b). Study on postliquefaction shear strength of low-plasticity silt with reconsolidation. *Rock and Soil Mechanics, 35*(7), 1849–1854. (in Chinese).

Wang, S., Luna, R., & Onyejekwe, S. (2015a). Postliquefaction behavior of low-plasticity silt at various degrees of reconsolidation. *Soil Dynamics and Earthquake Engineering, 75,* 259–264.

Wang, S., Luna, R., & Zhao, H. (2015b). Cyclic and postcyclic shear behavior of low-plasticity silt with varying clay content. *Soil Dynamics and Earthquake Engineering, 75,* 112–120.

Wang, S., Luna, R., & Onyejekwe, S. (2016a). Effect of initial consolidation condition on post-liquefaction undrained monotonic shear behavior of mississippi river valley silt. *Journal of Geotechnical and Geoenvironmental Engineering*, *142*(2) 04015075-1–11.

Wang, S., Onyejekwe, S., & Yang, J. (2016b). Reexamination of effect of plasticity on liquefaction resistance of low-plasticity fine-grained soils and its potential application. *Acta Geotechnica, 11*(5), 1209–1216.

Wang, S., Luna, R., & Yang, J. (2017). Effect of plasticity on shear behavior of low-plasticity fine-grained soil. *Journal of Materials in Civil Engineering, 29*(3), 1–7.

Wichtmann, T., Niemunis, A., Triantafyllidis., Th., & Poblete, M. (2005). Correlation of cyclic preloading with the liquefaction resistance. *Soil and Dynamics and Earthquake Engineering, 25,* 923–932.

Wijewickreme, D., & Sanin, M. (2010). Postcyclic reconsolidation strains in low-plastic fraser river silt due to dissipation of excess pore-water pressures. *Journal of Geotechnical and Geoenvironmental Engineering, 136*(10), 1347–1357.

Wood, F. M., Yamamuro, J. A., & Lade, P. V. (2008). Effect of depositional method on the undrained response of silty sand. *Canadian Geotechnical Journal, 45,* 1525–1537.

Yamamuro, J. A., Wood, F. M., & Lade, P. V. (2008). Effect of depositional method on the microstructure of silty sand. *Canadian Geotechnical Journal, 45,* 1538–1555.

Yasuhara, K. (1994). Postcyclic undrained strength for cohesive soils. *Journal of Geotechnical Engineering, 120*(11), 1961–1979.

Yasuhara, K., & Andersen, K. H. (1991). Recompression of normally consolidated clay after cyclic loading. *Soils and Foundations, 31*(1), 83–94.

Yasuhara, K., Murakami, S., Song, B. W., Yokokawa, S., & Hyde, A. F. L. (2003). Postcyclic degradation of strength and stiffness for low plasticity silt. *Journal of Geotechnical and Geoenvironmental Engineering, 129*(8), 756–769.

Zhao, Y., Li, G., & Yu, Y. (2011). *Tunnel Engineering in Loess*. Beijing: China Railway Publishing House. (in Chinese).

Chapter 2
Preparation Approach of Low-plasticity Silt Specimens for Triaxial Testing

This chapter presents a new approach of slurry consolidation to reconstitute low-plasticity silt specimens in a split mold without trimming. The technique can expedite testing process. The specimen uniformity was verified with measurements of water content and grain size distribution throughout specimens. This specimen preparation approach was developed within an experimental program to study the static and cyclic behavior of silts. The preparation of replicas was needed so that the effects of cyclic stress ratio and confining stress could be isolated from soil specimen variations. It was found early that the specimen preparation technique affected testing dramatically and the procedure presented herein is the one that produced superior results, according the replicas of static and cyclic triaxial tests (Wang et al. 2011).

2.1 Specimen Reconstitution

2.1.1 Reconstitution Procedures

The silt specimens were reconstituted using a slurry consolidation method in a 71.1 mm diameter split vacuum mold. The target dimensions of the specimen were 71.1 by 142.2 mm to accommodate static and dynamic triaxial testing. The silt slurry was consolidated under incremental dead weights and vacuum. The procedure to prepare specimens was presented as follows.

(1) Preparation of silt slurry

The portion of the silt that passed through the No. 40 sieve (0.425 mm) was selected for the slurry. One kilogram of dry silt was mixed with deaired water, resulting in a water content of 44%. The slurry was then covered with plastic wrap to prevent water from evaporating and left to soak overnight (for about 10 h) to

S. Wang, *Monotonic, Cyclic and Postcyclic Shear Behavior of Low-plasticity Silt*,
https://doi.org/10.1007/978-981-10-7083-9_2

ensure complete absorption of the water. Finally, the slurry was mixed thoroughly for 15 min using an industrial Hobart electric mixer (Model: N-50) with a flat paddle. To avoid air entrapment during mixing, the slurry was mixed at a low speed (60 rpm).

(2) Pouring of slurry into split vacuum mold

After the silt slurry was mixed, it was poured into a split vacuum mold. Because the volume of slurry was larger than the split vacuum mold, an extension tube with internal graduated marks was place on the top of split mold (Fig. 2.1a). The slurry was poured into the split vacuum mold through a funnel to the desired height so that the specimen target height (142.2 mm) was obtained after consolidation under weights and vacuum. The desired slurry height was determined through several trials. The excess slurry was collected in a bowl so that the mass of the soil specimen could be determined accurately.

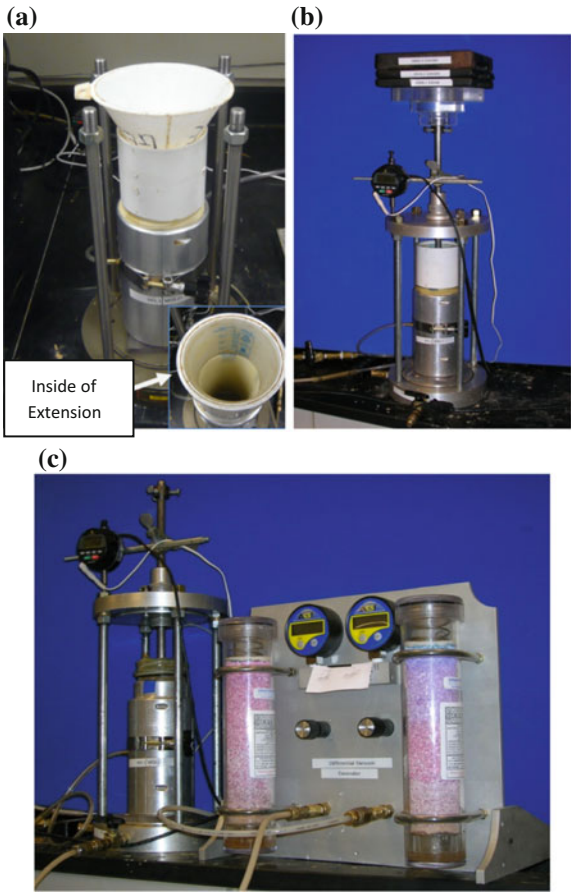

Fig. 2.1 Experimental setup used for reconstitute silt specimens: **a** slurry holder, **b** slurry consolidated under incremental dead weight, **c** specimen consolidated under the vacuum

(3) Consolidation of the silt slurry in the split mold

The slurry was left to settle under its own weight for 3 h to prevent slurry from squeezing out under the dead weights. A plastic cap was placed on the slurry for 2 h, and a loading rod was placed overnight. The loading times were determined based on several trials in order to avoid squeezing slurry out of mold during incremental weight placement. As shown in Fig. 2.1b, weights were then added, and primary consolidation was achieved under each load increment before the next weight was added. Consolidation progress was monitored using a digital dial gauge on the loading rod to monitor specimen deformation. The vertical stress (less than 32.3 kPa) imposed by all the weights added was less than the desired effective minimum consolidation pressure of 50 kPa.

(4) Use of vacuum to improve consolidation pressure

Due to the friction that develops between membrane liner and the consolidating soil in the mold, the effective vertical consolidation pressure tends to decrease from the top (loading) face of the specimen to the bottom of the specimen, resulting in a non-uniform void ratio. To improve the uniformity of the specimen, identical vacuum pressures (less than effective consolidation pressure) were applied simultaneously at the top and bottom of the specimen. The vacuum was applied using a unique differential vacuum control apparatus, which collects the water drained from the specimen and dries the air with a gas drying unit to avoid the drained water to be sucked into the vacuum regulator and pump when the slurry consolidates under vacuum (Stephenson, personal communication). In this way, the specimen consolidated under the same top and bottom pressures. Before applying the vacuum, the weights were removed, the top porous stone and filter paper were replaced with clean ones, the membrane was folded over the top cap, and o-rings were placed around the membrane. The consolidation process under the vacuum was also monitored using the digital dial gauge (Fig. 2.1c). The specimen was then ready for triaixal testing.

The soil adhering to the porous stone and filter paper was cleaned. After the soil particles settled out of suspension, the surface water was removed, and the excess soil was dried and weighed to obtain the total weight of the silt solids in the specimen. Each incremental pressure took about 8 h to consolidate. Preparation of one specimen under all loads took a total of about two days.

2.1.2 Specimen Uniformity

The uniformity of the silt specimen was verified by measuring the variation in water content (ω) and particle size distribution throughout the specimen. Assuming that the degree of saturation was identical throughout the specimen, water content is a measure of void ratio. The grain size distribution indicated whether particles had been segregated by size.

The silt specimens were cut into seven slices, and the water content of each slice was measured. Figure 2.2 shows the variation in water content versus height of the specimen. As expected, the water content was lower towards the top and bottom ends of the specimen where the vacuum was applied and the pressure gradients were the highest. The maximum difference in water content (Δw) throughout the specimen was just 1.20%.

To verify that the specimen preparation was not dependent on the fines content, two other silt specimens were prepared with 2.5 and 5% bentonite added. With the added bentonite, the variation in water content (Δω) was even smaller, as seen in Fig. 2.2. These results make it reasonable to conclude that the void ratio was essentially uniform throughout the specimen.

Once the water content was determined, 50 g were cut from each silt slice and placed in a 250 mL beaker mixed with 125 mL of sodium hexametaphosphate solution (40 g/L) for hydrometer analysis (Brandon et al. 2006). The dry silt slices were easily disaggregated into the solution. Figure 2.3 shows the particle size distributions, which were very consistent. Actually, the deposition of silt slurry is different from that of sand. For sand, the larger sand particles settle easily and quickly so that segregation may be more common. However, for a silt slurry, the water content is only about 1.6 times of the liquid limit. Voids among the silt particles are insufficient to allow the larger particles to pass and settle down to induce segregation.

The distribution of water content and particle size in the reconstituted specimens of natural silt and silt with bentonite indicated that the specimens were quite uniform and could be used to prepare relatively identical reconstituted silt specimen.

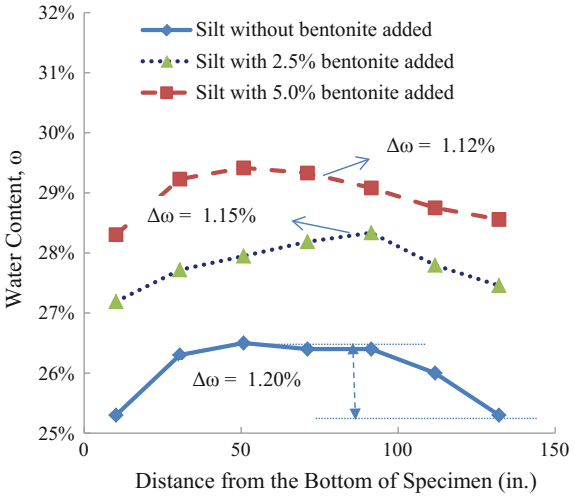

Fig. 2.2 Variation in water content from top to bottom of specimen

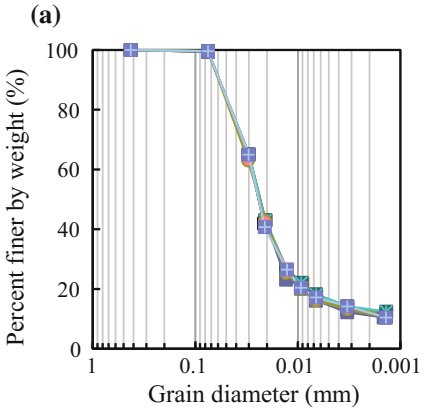

Average	
Diameter (mm)	% finer
0.425	100.00
0.075	99.51
0.030	64.72
0.021	42.48
0.013	25.76
0.009	20.88
0.007	17.15
0.003	13.61
0.001	11.04

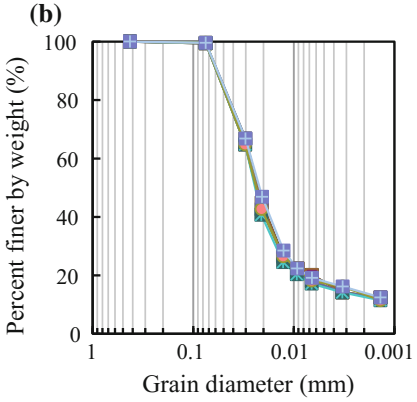

Average	
Diameter (mm)	% finer
0.425	100.00
0.075	99.51
0.030	65.37
0.021	43.62
0.013	26.49
0.009	21.77
0.007	18.70
0.003	14.74
0.001	12.15

Fig. 2.3 Variation in grain size distribution of silt specimen reconstituted by slurry deposition for each of the 7 slices: **a** natural silt; **b** silt with 2.5% Bentonite added

2.2 Specimen Preparation for Testing

2.2.1 Specimen Movement

Specimens can be prepared directly on the triaxial base platen. Saturation, consolidation, and shearing can then be completed with the specimen in the same position. This process, however, makes a complete test sequence time consuming. To expedite the testing process, this research developed a special procedure. The specimen was prepared on another base platen, which was then moved to the triaxial base platen. A key requirement of this process was that the specimen be moved with as little disturbance as possible. A following procedure was developed to accomplish this: (1) The split vacuum mold was removed while the vacuum was kept on the specimen. A split miter sample mold with diameter of 71.0 mm was used to hold the specimen. A clamp was used to hold the split mold together (Fig. 2.4a).

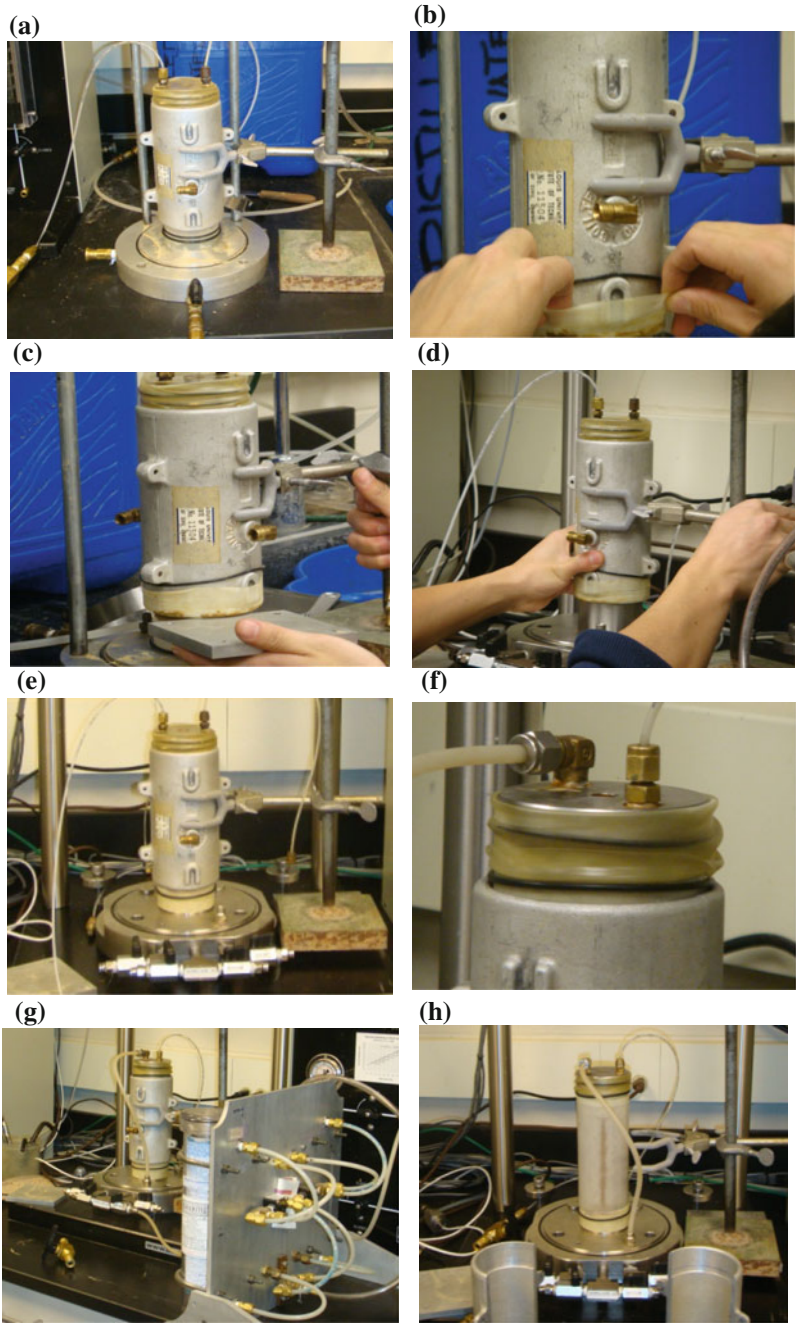
(a)
(b)
(c)
(d)
(e)
(f)
(g)
(h)

◂**Fig. 2.4** Specimen translation from preparation location to GCTS chamber on load frame pedestal: **a** remove the split vacuum mold and use a split miter box to hold the silt specimen; **b** move o-rings up and stretch the membrane upwards; **c** slide silt specimen onto a metal plate; **d** move silt specimen to a triaxial base platen and fix it with a clamp; **e** stretch membrane down and move o-rings down to the triaxial base; **f** set triaxial cap with screw; **g** place vacuum at top and bottom of specimen for 8 h to remove air in the specimen; **h** remove split miter mold

(2) The vacuum was then reduced to zero. After a waiting 30 min period to dissipate the vacuum and avoid entrapment of air in the specimen, the O-rings and the membrane were stretched around the bottom of the split miter sample mold (Fig. 2.4b). (3) The top porous stone and cap were left attached to the specimen, and the specimen with the bottom porous stone was slid onto a metal plate. Before this, the plate was placed next to the base so that the specimen could be moved onto the metal plate with the bottom porous stone level (Fig. 2.5c). (4) The specimen, with the porous stones and cap, was moved onto the triaxial base platen and fixed with another clamp (Fig. 2.4d). (5) The membrane and O-rings were stretched down to the triaxial base platens (Fig. 2.4e). (6) The plastic cap was removed, and the triaxial top cap was carefully placed. The membrane was folded over the triaxial top cap, and the o-rings were placed around the membrane (Fig. 2.4f). (7) A 45 kPa vacuum was applied at the ports connected to top and bottom ends of the specimen with tubing and left for 8 h to remove any air in the specimen, porous stones and lines. The vacuum system allowed the vacuum to be increased to as necessary to remove more air bubbles out of the specimen to achieve good saturation. However, the vacuum was always smaller than the effective consolidation pressure (Fig. 2.4g). (8) The split miter mold was removed and specimen dimensions were measured (Fig. 2.4h). The cell chamber was mounted and secured, and then deaired water was filled in the chamber. After a low cell pressure was applied to hold the specimen, vacuum was removed and the specimen was then connected with tubing to the top and bottom burettes on the pressure panel to allow access of deaired water into the specimen under back pressure (air bubbles in the tubing should be drained out with deaired water from burettes). At this time, the specimen was ready for triaxial testing.

While testing was conducted on the specimen in the triaxial chamber, another specimen was prepared on the special experimental setup simultaneously. Since the time to prepare a specimen was almost equal to that required for the saturation, consolidation, and shearing, this process reduced the time for the whole testing program by at least 50%.

2.2.2 Disturbance During Handling and Moving of the Specimen

Observations of the specimen indicated that there was very little disturbance during movement as long as the specimen remained vertical. This technique required no

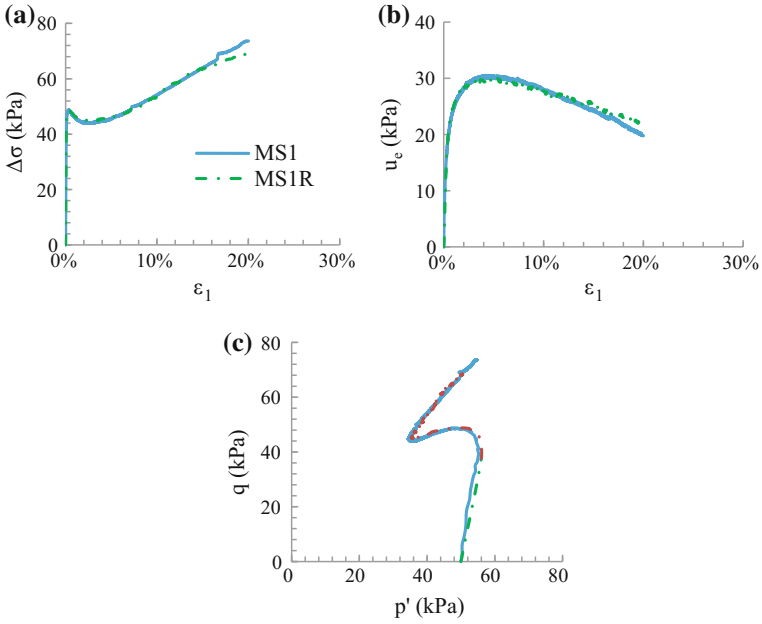

Fig. 2.5 Repeatability of static testing: **a** deviator stress versus axial strain; **b** excess pore water pressure versus axial strain; **c** stress path, $p' = (\sigma'_1 + \sigma'_2 + \sigma'_3)/3$, $q = \sigma_1 - \sigma_3$

any direct handling to trim of the specimen. Trimming is normally required if silt sedimentation occurs in a large-scale consolidometer, into which sampling tubes are pushed to sub-sample the silt specimen. In particular, the membrane was kept so that it helps hold the specimen during handling and moving of the specimen.

To verify that there was very little disturbance of the specimens during movement from the special experimental setup to the triaxial base platen, the resulting size of specimen under a 45 kPa vacuum was measured with a PI tape before and after movement (Table 2.1). This value was recorded as an initial diameter before the vacuum was removed. Removal of the vacuum unloads the specimen and can cause swelling. The vacuum of 45 kPa was left on the specimen for 8 h to remove the air out of the specimen after movement. This process behaved as a recompression and the size of specimen may recover. The diameter at this time was recorded at the same location and compared to the original measurement (Table 2.1). If handling and movement had disturbed the specimen, the two diameters before and after movement would have varied. The difference, however, was very small, confirming that handling and moving process created only minimal disturbance on the specimen.

Table 2.1 Change of diameter (mm) of specimen due to specimen translation

Location	Before translation	After translation	Difference
Top	70.45	70.40	−0.05
Middle	69.06	68.95	−0.11
Bottom	69.40	69.50	0.10

2.3 Replication

The ability to produce identical specimens was verified by conducting triaxial tests under identical conditions. The objective was to quantify the reproducibility of the testing protocols and assess their quality. For this purpose, two static triaxial compression tests and several cyclic triaxial tests were conducted.

2.3.1 Monotonic Triaxial Tests

Two normally consolidated undrained (CU) triaxial tests with an effective consolidation stress (σ'_c) of 50.0 kPa were conducted to verify the repeatability of monotonic triaxial testing under the same conditions. After the specimens were moved to the triaxial base platen from the specimen preparation location, vacuum and then back pressure were applied to saturate the specimens, resulting in a Skempton B-value higher than 0.98.

Figure 2.5 shows the testing results. The stress-strain curves are nearly identical in shape at the initial phase of shearing; they become dissimilar at large strains. The differences in deviator stress and excess pore pressure between the tests were insignificant under large strain. The percent differences are 5.9 and 10.4% of the average values of deviator stresses and excess pore pressures, respectively. Further, the reliability of stress and strain computations at large strain values (>10%) are inherently unreliable because of the area corrections at these levels. These small differences, however, are acceptable and can be attributable to unavoidable variations in testing and to human factors. These results confirm the repeatability of monotonic triaxial compression testing on specimens prepared as described here.

2.3.2 Cyclic Triaxial Test

Cyclic Triaxial tests were conducted at two cyclic stress ratios (CSR) of 0.18 and 0.35, normally consolidated to an effective confining stress of 90 kPa (Fig. 2.6). For a CSR of 0.18, the specimens MD2 and MD2R required 35.2 and 32.2 cycles of loading, respectively, to liquefy. The average number of cycles is 33.7. The difference between the average value and 35.2 or 32.2 is 1.5, which is only 4.5% of

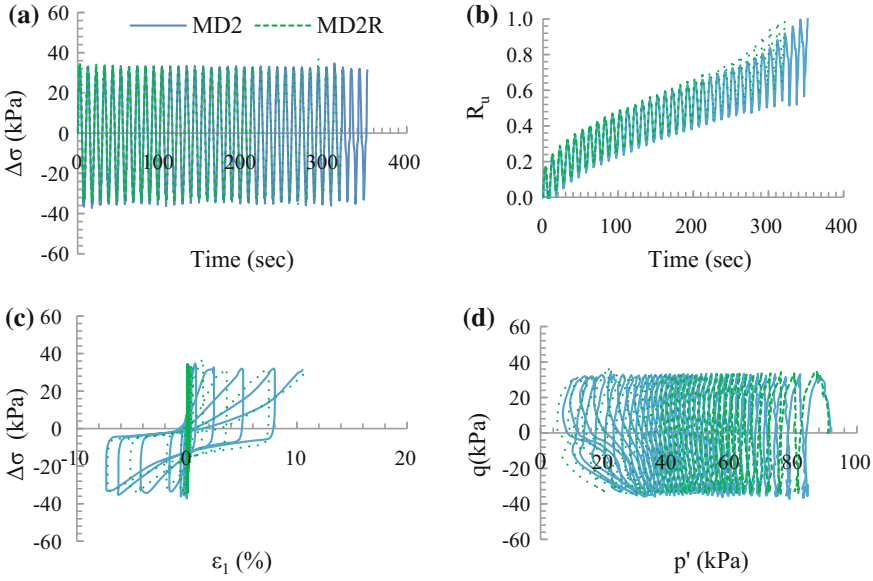

Fig. 2.6 Repeatability of cyclic testing with CSR of 0.18: **a** deviator stress versus time; **b** R_u versus time; **c** Deviator stress versus axial strain; **d** q versus p′

the average number 33.7. Thus, the difference of number of cycles between two tests is small. For the higher CSR = 0.35, the tests MD4 and MD4R yielded even smaller differences, as shown in Fig. 2.7. Both liquefied at only 1.2 cycles of loads. The excess pore water pressure and stress paths were nearly identical. Thus, the replicated reconstituted specimens produced near identical dynamic failure conditions of liquefaction.

In addition to the above testing program, this specimen preparation technique was used for studying postcyclic behavior of silt soils. Seven cyclic triaxial tests were conducted, each with CSR = 0.18 and σ'_c = 90 kPa. Table 2.2 shows the void ratio (e) after normal consolidation and the number of loading cycles (N_{cyc}) to liquefy the specimens. The MD and MF tests were used to study liquefaction resistance and postliquefaction behavior, respectively. The coefficient of variation of the void ratio is 0.0125, and that of number of loading cycle is 0.1023. These small coefficients of variation were considered acceptable for a research quality testing program.

The liquefaction resistance of the tested silt is shown in Fig. 2.8 with two more cyclic tests under the CSR of 0.25 and 0.10. The testing showed that the specimen with CSR of 0.10 did not liquefy. The curve of CSR versus number of cycles is comparable to the liquefaction resistance of other silty soils (Boulanger et al. 1998; Guo and Prakash 1999).

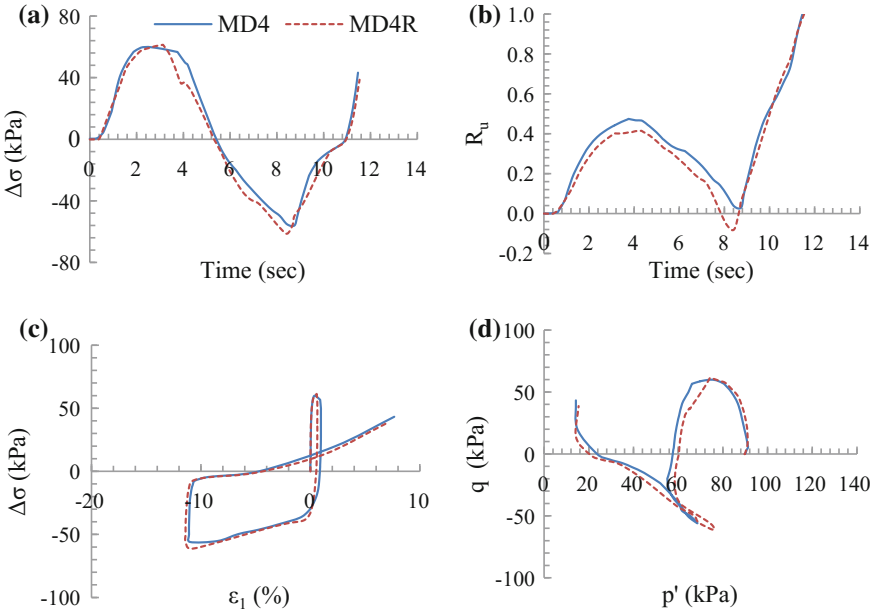

Fig. 2.7 Repeatability of cyclic testing with CSR of 0.35: **a** deviator stress versus time; **b** Ru versus time; **c** deviator stress versus axial strain; **d** q versus p′

Table 2.2 Statistics of cycles of loading to liquefy specimens with CSR = 0.18

Specimen Id	MD2	MD2R	MF1R1	MF1R2	MF2	MF3	MF4	Mean	Standard deviation	Coefficient of variation
e	0.661	0.681	0.660	0.669	0.657	0.663	0.659	0.664	0.008	0.0125
N_{cyc}	35.2	33.2	27.1	31.1	27.2	30.1	28.1	30.3	3.1	0.1023

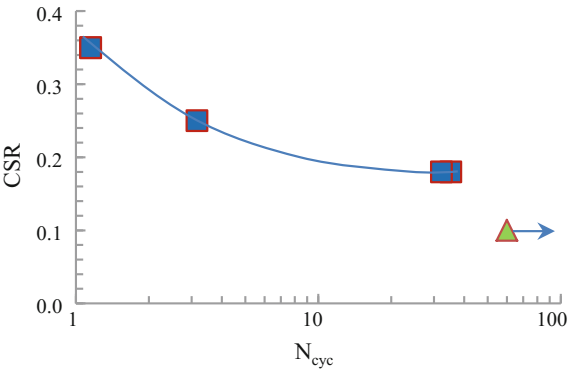

Fig. 2.8 Liquefaction resistance of the MRV silt normally consolidated to effective confining pressure of 90 kPa

2.4 Summary

This chapter presents a new slurry consolidation (or, deposition) approach to reconstitute low-plasticity silt specimens for laboratory triaxial testing. Specimen uniformity was verified by measuring the water content and particle size distribution in seven slices of the silt specimens. These measurements showed very little variation throughout the length of the specimens. The testing program was expedited with a special handling and moving technique to permit simultaneous specimen preparation and triaxial testing. The reliability of this technique was verified by confirming minimal disturbance of the specimen during movement. To further verify the validity this approach, tests were repeated for both static and cyclic triaxial conditions, and the results compared. The differences in the testing results of replicated specimens using identical testing parameters were minimal. Thus, this new approach can be used to reconstitute specimens of low-plasticity silt.

References

Boulanger, R. W., Meyers, M. W., Mejia, L. H., & Idriss, I. M. (1998). Behavior of a fine-grained soil during the Loma Prieta earthquake. *Canadian Geotechnical Journal, 35,* 146–158.

Brandon, T. L., Rose, A. T., & Duncan, J. M. (2006). Drained and undrained strength interpretation for low-plasticity silts. *Journal of Geotechnical and Geoenvironmental Engineering, 132*(2), 250–257.

Guo, T., & Prakash, S. (1999). Liquefaction of silts and silt-clay mixtures. *Journal of Geotechnical and Geoenvironmental Engineering, 132*(6), 716–735.

Wang, S., Luna, R., & Stephenson, R. W. (2011). A slurry consolidation approach to reconstitute low-plasticity silt specimens for laboratory triaxial testing. *Geotechnical Testing Journal, 34* (4), 288–296.

Chapter 3
Monotonic Shear Behavior of Low-plasticity Silt and Its Change with Soil Plasticity

This chapter reports monotonic shear behavior of MRV silt using triaxial compression testing and its change with soil plasticity, as presented in Wang and Luna (2012) and Wang et al. (2017). In particular, the unique behavior of this silt compared to classical behaviors of sand and clay is studied. A reasonable failure criterion to calculate the effective friction angle (Φ') of the low-plasticity silt is recommended, and the effects of overconsolidation ratio (OCR) and effective consolidation pressure (σ'_c) on the stress-strain behavior are evaluated. Finally, this chapter presents the variation of monotonic shear behavior of low-plasticity fine-grained soil against plasticity index.

3.1 Testing Program

The MRV silt, whose index properties are shown in Table 1.1, was studied for investigating monotonic shear behavior of low-plasticity silt. To evaluate the effect of plasticity index on shear behavior of the silt, sodium bentonite was added to form different soil mixtures, whose index properties were also listed in Table 3.1. Although the integral number is required for Atterberg limits, according to ASTM D 4318 (2005), the decimal points are remained for showing the small difference in the values of Atterberg limits of different soil mixtures. The liquid limits based on Casagrande and fall cone test methods are compared in Fig. 3.1, and all data points fall within the shaded area, suggesting the validity of determination of the liquid limits. The variations of Atterberg limits of the soil mixtures with added sodium bentonite contents were shown in Fig. 3.1. With an increase in added bentonite content, there is an increase in liquid limits determined by Casagrande and fall cone test methods, but the increase in plastic limit is less significant. The PI, as expected, increased with the added bentonite content.

Mineralogy of the MRV silt and the sodium bentonite were investigated, and the investigation results are shown in Table 3.2. The MRV silt contained quartz

S. Wang, *Monotonic, Cyclic and Postcyclic Shear Behavior of Low-plasticity Silt*,
https://doi.org/10.1007/978-981-10-7083-9_3

Table 3.1 Index properties of the MRV silt-bentonite mixtures

Index property	Added bentonite content			
	0%	2.5%	5.0%	7.5%
Clay content (%)	14.5	16.6	18.8	20.9
Specific gravity	2.71	2.70	2.68	2.67
$w_{L\ Casagrande}$	28.1	28.9	32.7	36.9
$w_{L\ Fall\ Cone}$	29.9	30.1	35.0	38.8
w_P	22.3	22.7	23.3	23.4
PI	5.8	6.2	9.4	13.5
C_c	0.089	0.128	0.199	–
C_r	0.009	0.010	0.016	–

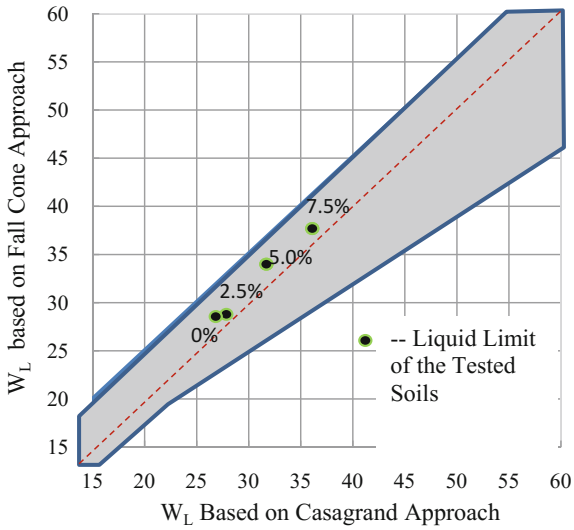

Fig. 3.1 Relationship between liquid limits determined by Casagrande and fall cone approaches

Table 3.2 Mineralogy of MRV silt and sodium bentonite

MRV silt	Montmorillonite	Quartz	Dolomite	Adularia	Muscovite	Phlogopite
Percent	2.2	51.5	22.0	19.2	3.8	1.3
Sodium Bentonite	Montorillonite	Rectorite	Anorthite	Barytocalcite	Gypsum	
Percent	64.0	11.1	11.3	10.5	0.5	

(51.5%), dolomite (22.0%), adularia (19.2%), montmorillonite (2.2%), muscovite (3.8%) and phlogopite (1.3%). The bentonite had minerals of montorillonite (64.0%), rectorite (11.1%), anorthite (11.3%), barytocalcite (10.5%), quartz (2.6%), gypsum (0.5%). Thus, the clay minerals in weight were 2.2% of MRV silt and 64.0% of the bentonite.

Static triaxial compression tests were carried out in a Humboldt triaxial system with various OCRs and effective consolidation pressures (Tables 3.3 and 3.4). The specimens were saturated with back pressures until the B value of at least 0.98 and 0.95, respectively for the MRV silt and its mixtures with bentonite. To avoid the development of cavitation due to negative excess pore water pressure during the shearing of overconsolidated specimens, back pressures greater than that producing a target B value were supplied. After saturation, the specimens were consolidated at required overconsolidation ratios and effective consolidation pressures (σ'_c). The overconsolidation ratios were achieved by consolidating the specimens to preconsolidation pressure ($\sigma'_p = \sigma'_c \times OCR$) and rebounding them to effective consolidation pressure (σ'_c). Due to the limited capacity of the testing equipment, only a normally consolidated test was conducted on the specimen with an effective consolidation pressure of 129 kPa.

For equalizing pore water pressure throughout the soil specimens during shearing, suitable strain rates needed to be determined for static shearing. Except for the specimens with PIs of 9.4 and 13.5 in Table 3.4, the strain rates for shearing were determined according to the 50% of primary consolidation time (t_{50}) following ASTM standard D 4767-04 (2004). Table 3.5 shows the variation of hydraulic conductivity of the MRV silt-bentonite mixture with added bentonite, which was calculated from isotropic consolidation tests. The hydraulic conductivity reduced significantly when the bentonite content increased from 0 to 2.5%, and to a lesser extent with further increase in bentonite content. For PIs of 9.4 and 13.5, the

Table 3.3 Static shearing tests on MRV silt

Test ID	σ_{BP} at B = 0.95 (kPa)	σ_{BP} at end of saturation (kPa)	B at end of saturation	σ'_p (kPa)	σ'_c (kPa)	OCR	e	u at critical state (kPa)	$\Delta\sigma$ at critical state kPa	A_f
MS1	241.3	289.6	0.985	–	50.0	1	0.700	300.6	85.0	0.13
MS2	217.2	241.3	0.980	–	90.0	1	0.679	269.2	144.0	0.19
MS3	217.2	241.3	0.981	–	129.0	1	0.652	299.4	154.8	0.38
MS4	241.3	337.8	0.994	102.4	51.2	2	0.665	337.3	113.7	0.00
MS5	193.1	265.4	0.991	180.0	90.0	2	0.653	263.6	198.9	−0.01
MS6	241.3	337.8	0.997	200.0	50.0	4	0.647	306.3	191.0	−0.16
MS7	265.6	362.0	0.991	364.8	91.2	4	0.612	287.2	370.3	−0.20
MS8	265.4	360.6	0.980	400.0	50.0	8	0.648	284.6	296.5	−0.26
MS9	248.2	386.1	1.000	720.0	90.0	8	0.591	255.6	513	−0.25

σ_{BP}—back pressure; e—void ratio of specimen after it was rebounded to effective; σ'_c—consolidation pressure; A_f—ratio of excess pore water pressure to deviator stress at the critical state

Table 3.4 Triaxial compression tests on MRV silt-bentonite mixtures

Test ID	PI	σ_{BP} (kPa)	B	σ'_c (kPa)	OCR	e	q (kPa)	S_u (kPa)	S_u/σ'_c
MSB1	6.0	455.1	0.985	90.0	1	0.653	61.4	30.7	0.341
MSB2	6.2	313.0	1.000	50.0	1	0.721	34.1	17.1	0.341
MSB3	6.2	386.4	0.983	90.0	1	0.649	62.5	31.3	0.347
MSB4	6.2	458.5	0.977	243.0	1	0.609	163.8	81.9	0.337
MSB5	6.2	386.1	1.000	90.0	8	0.559	347.0	173.5	1.928
MSB6	9.4	482.3	1.000	50.0	1	0.745	35.4	17.7	0.354
MSB7	9.4	506.8	0.994	90.0	1	0.628	55.4	27.7	0.308
MSB8	9.4	482.2	0.966	90.0	8	0.506	272.7	136.4	1.515
MSB9	13.5	530.9	0.975	49.4	1	0.783	29.9	15.0	0.303

Table 3.5 Hydraulic conductivity of MRV silt and silt-bentonite mixture

	Natural MRV silt	With 2.5% bentonite	With 5% bentonite
Hydraulic conductivity (m/s)	5.74×10^{-9}	1.09×10^{-9}	4.94×10^{-10}

shearing strain rate 0.005%/minute was used based on their consolidation and permeability characteristics. Lefebvre et al. (1989) stated that the variation of undrained shear strength against various strain rates ranged from 7 to 14%, with an average of 10% for destructured or structured clays. Therefore, it is believed that the effect of strain rate on undrained shear behavior was minimal in this current study.

3.2 Monotonic Shear Behavior of Low-plasticity Silt

3.2.1 Stress-Strain Behavior of Low-plasticity Silt

Figure 3.2 shows the deviator stress and excess pore water pressure response of the MRV silt specimens. Although the shearing of specimens with OCR = 1 was stopped at 20% axial strain, the specimens could be expected to reach critical state at the axial strain of about 25%. Shown in slightly overconsolidated specimens MS4 and MS5 (OCR = 2), there were no big increases in the deviator stress after the axial strain was larger than 20%. The deviator stresses ($\Delta\sigma$) and excess pore water pressures (u_e) of normally consolidated specimens at the critical state were estimated by extrapolation for the later analysis (Table 3.3). Figure 3.2a indicates that all overconsolidated specimens with OCR equal to or larger than 2 showed continuous dilation behaviors (strain-hardening), but the normally consolidated specimens had a slight strain-softening stage after the initial peak deviator stress. After the slight strain-softening stage, the higher deviator stress built up and the normally consolidated specimens showed strain-hardening behavior. Under higher

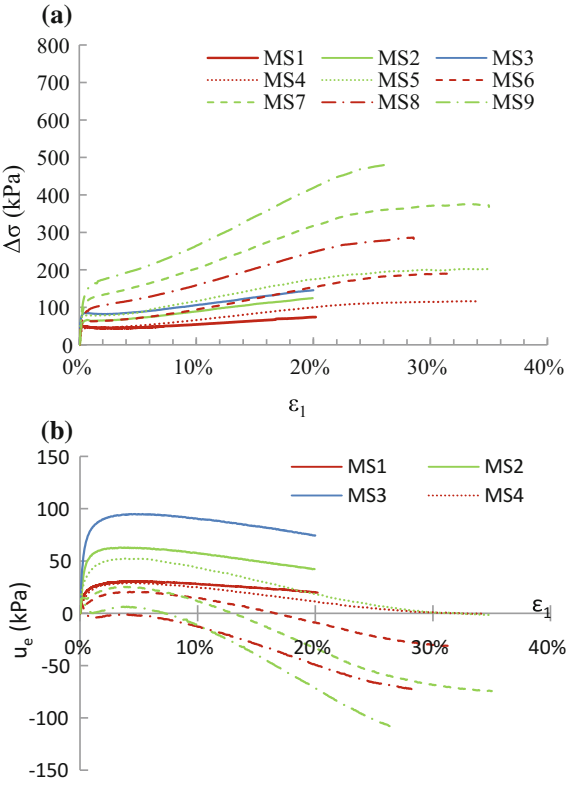

Fig. 3.2 Static testing results of MRV silt: **a** deviator stress versus axial strain, **b** excess pore water pressure versus axial strain

OCRs, the dilation behavior became more obvious for specimens with identical effective consolidation pressures. This was also indicated by the A_f value in Table 3.3. As the OCR increased, the A_f value decreased.

No unique critical state was observed among the different tested silt specimens. Classic sand specimens with different void ratios reach the unique critical state through different stress-strain paths under identical effective consolidation pressure, as do clay specimens with different OCRs. Hence, the silt tested here showed stress-strain behavior different from that of either sand or clay. This behavior was also demonstrated by the curves of excess pore water pressure against axial strain (Fig. 3.2b). No unique excess pore water pressure state existed.

3.2.2 *Effective Friction Angle*

The effective friction angle (ϕ') can be obtained based on various failure criteria. Possible failure criteria are maximum deviator stress ($(\sigma_1 - \sigma_3)_{max}$), maximum principal stress ratio ($(\sigma'_1/\sigma'_3)max$), maximum excess pore water pressure ($u_{e,\ max}$),

reaching K_f line, limiting strain, or excess pore water pressure of 0 ($u_e = 0$) (Brandon et al. 2006). The friction angle of the low-plasticity MRV silt tested here was calculated using all these failure criteria (Fig. 3.3). Because the silt just showed a little dilation behavior under normal consolidation, the excess pore water pressure did not reach zero. Thus, the Mohr circles in the Fig. 3.3e are based on overconsolidated specimens only. The failure criteria of $(\sigma_1 - \sigma_3)_{max}$, $(\sigma'_1/\sigma'_3)_{max}$, and 15% limiting strain yielded relatively constant friction angles for the MRV silt. Conversely, the friction angles based on $u_{e,\ max}$, $u_e = 0$, and reaching K_f line are widely scattered. Two criteria in particular, $(\sigma'_1/\sigma'_3)_{max}$ and 15% limiting strain, both yielded friction angles of approximately 35°. However, the friction angle was about 32° based on the criterion of $(\sigma_1 - \sigma_2)_{max,}$ which was obtained at the point of large strain, under which an earth structure would fail. Thus, the $(\sigma_1 - \sigma_2)_{max}$ is not appropriate criterion for calculation of the friction angle of the MRV silt. Brandon et al. (2006) did a similar research work for the normally consolidated Yazoo silt (nonplastic) and LMZD silt (PI = 4) and presented that all of the previously mentioned failures criteria except the $u_{e,max}$ can result in the friction angle within a narrow range for the two silts.

It should be noted that the friction angles of the MRV silt were obtained from both normally consolidated and overconsolidated specimens. There were two or

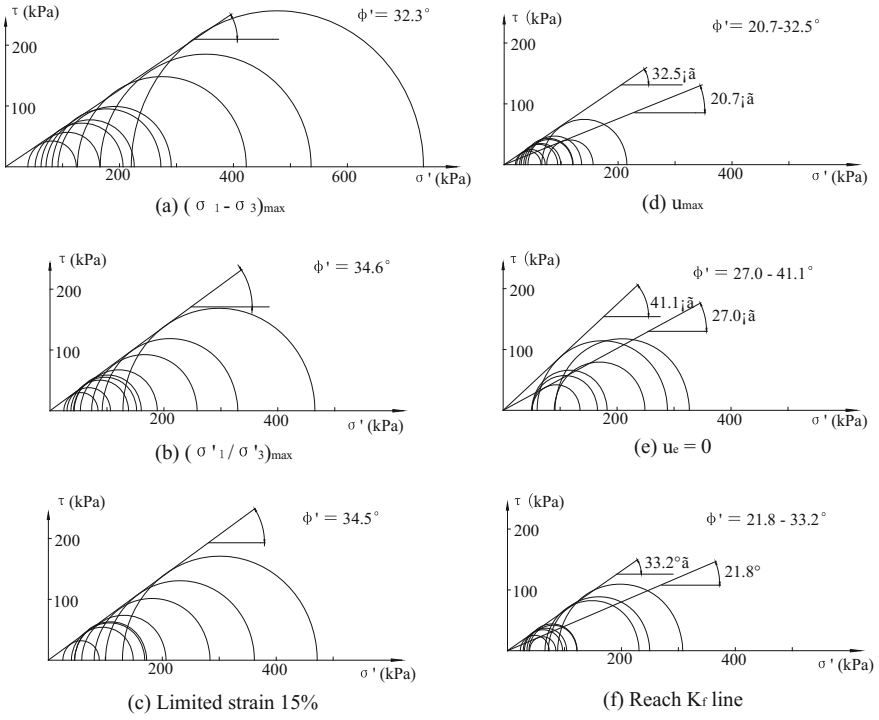

Fig. 3.3 Friction angle based on various failure criteria

three Mohr circles for each OCR in Fig. 3.3. Holtz et al. (2011) refer to a difference in the friction angle among the clays with different OCRs due to the stress history. However, the low-plasticity silt has less memory of stress history due to less mineral than clay. Figure 3.3 indicates that all Mohr circles can be best-fitted using one straight line in the $\tau - \sigma'$ space based on the failure criteria $(\sigma_1 - \sigma_3)_{max}$, $(\sigma'_1/\sigma'_3)_{max}$, and limiting strain 15%. Therefore, the OCR did not influence the friction angle obviously using these failure criteria. This kind of finding was also found by Izadi (2006) for the Collinsville silt from the same region with the tested MRV silt. Izadi (2006) presented that there was no any noticeable effect of the overconsolidation ratio on the magnitude of the friction angle.

To analyze the influence of the failure criterion on the calculated friction angle of low plasticity silt, this work was combined with the results reported by Brandon et al. (2006) and Izadi (2006). Figure 3.4 shows that the failure criteria of $(\sigma'_1/\sigma'_3)_{max}$, 15% limiting strain, and reaching K_f lines yielded a higher friction angle than other criteria. The friction angle is lowest based on the criterion of $u_{e,max}$ because full strength in terms of effective stress had not been mobilized. Although Brandon et al. (2006) concluded that any of the failure criteria except the u_{max} could be used to evaluate the friction angle of low-plastic, dilative silts, the criteria of $u_e = 0$ and reaching K_f line were also not available for the MRV silt tested here, because it did not dilate enough to induce negative excess pore water pressure and large ranges of stress paths touched the K_f line in the stress space, respectively. The criteria of 15% limiting strain and $(\sigma'_1/\sigma'_3)_{max}$ always gave a consistent estimation of friction angle. For the MRV silt tested here, the maximum σ'_1/σ'_3 appeared at around 10% axial strain. However, the axial strain at the maximum σ'_1/σ'_3 is probably larger than 15% for other low-plasticity silt. Thus, it was recommended that a 15% limiting strain be best criterion to calculate the effective friction angle of low-plasticity silt.

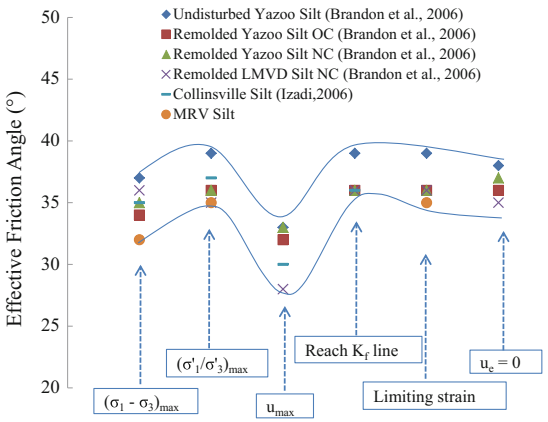

Fig. 3.4 Variation in friction angles based on various failure criteria

3.2.3 Critical State

The stress paths of all static tests were plotted in the Cambridge stress space (Fig. 3.5a, $p' = (\sigma'_1 + 2\sigma'_3)/3$; $q = \sigma_1 - \sigma_3$). All stress paths rose along one line (K_f line) after the phase transformation points were reached. The phase transformation point was designated as the state at which the reversal from contractive to dilative behavior occurred (Ishihara et al. 1975). A failure line (K_f line) was plotted with M of about 1.4 in the stress space; therefore, the friction angle was computed to be 38.4° using $\sin \Phi' = 3M/(6+M)$, which was larger than those using other failure criteria stated previously. Actually, the failure criterion of reaching K_f line is the similar with the method based on the M value in the calculation mechanism, because the criterion of reaching K_f line get data from stress space. The reasons for why the friction angles based on these two methods were so different included: there was a big range of stress path touching the K_f line and so it was difficult to determine data points to calculate σ'_1 and σ'_3 for plotting Mohr circles; the failure line in stress space was plotted subjectively and potential error may exist. Additionally, the M value gave unconservative results due to higher friction angle compare to other criteria. Thus, it was not a good way to calculate friction angle based on the M value.

To study the stress paths more closely, Fig. 3.5b was enlarged to focus on the early stage of stress paths. The OCRs were marked for each stress path from 1 to 8. In general, the stress path indicated that the silt specimens became more dilative, as the OCR increased. Further investigation identified the following phenomenon: Specimens with an OCR of 1 or 2 showed initial contraction followed by continuous dilation behavior; with an OCR of 4, the specimen at an effective consolidation pressure of 50 kPa showed behavior similar to that of specimens with an OCR of 1 or 2. But at an effective consolidation pressure of 90 kPa, the specimen with an OCR of 4 showed continuous dilation, as did the specimens under an OCR of 8. Thus, the specimen with higher effective consolidation pressure dilated more when the OCR was equal to 4. The result was opposite to the classical behavior of soil. Normally, with increasing effective consolidation pressure, soil specimens tend to contract. Yamamuro and Lade (1998) also observed this opposite behavior in silty sand. They noted that the specimen with an effective consolidation pressure of 25 kPa showed static liquefaction. As the pressure increased, the silty sand became more stable (i.e., more dilated). Thus, the low-plasticity silt tested here showed a behavior different from that observed in typical sands and clays.

This book also investigates the critical state in the e-ln p' space. One critical state line was obtained for the tested silt in Fig. 3.6. Because the void ratio (e) kept constant under the undrained shearing condition, the data points in the e-ln p' space can only move horizontally. Figure 3.6 indicates that all data points moved right to the critical state from the initial state due to the development of excess pore water pressure; therefore, all specimens at the ending of shearing showed dilation behavior compared to the state at the beginning of shearing, although the normally consolidated and slightly overconsolidated specimens had initial contraction at the

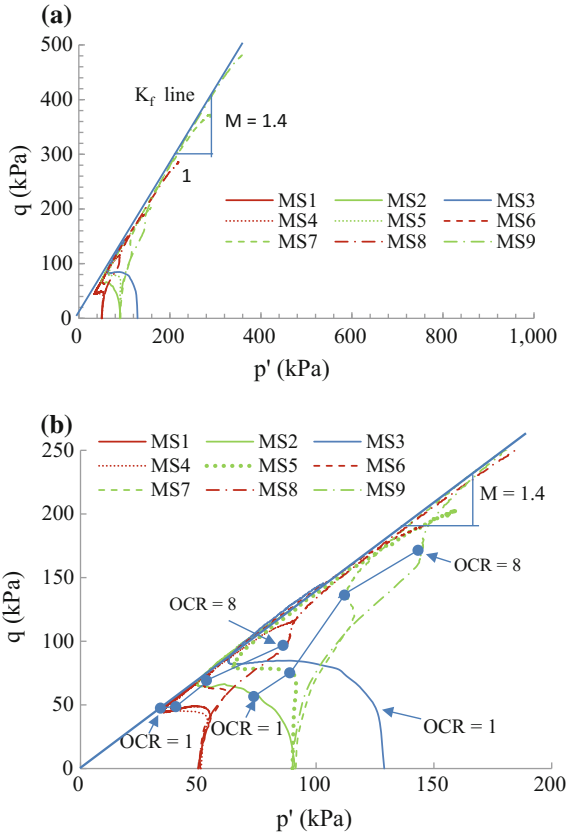

Fig. 3.5 Stress path in Cambridge space: **a** full range of data; **b** expanded inset from Fig. 3.9 (a)

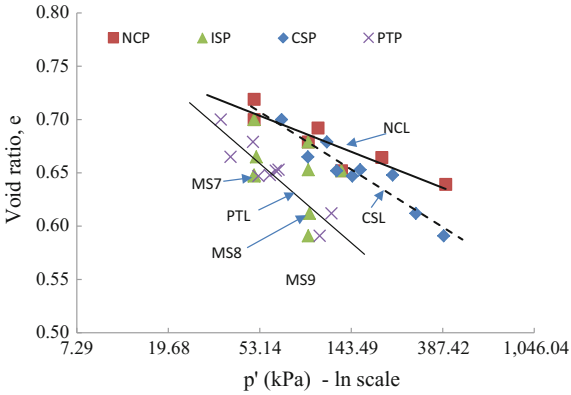

Fig. 3.6 Critical state diagram obtained from consolidated undrained tests (NCP—Normal Consolidation Point; ISP—Initial State Point; CSP—Critical State Point; PTP—Phase Transformation Point)

early stage of shearing in Fig. 3.5. This behavior was in agreement with the findings in the stress space, since all stress paths rose along the critical state line in the stress space after the phase transformation stage. The critical state line was not parallel to normal consolidation line. As noted by Boulanger and Idriss (2006), if the normal consolidation and critical state lines are not parallel, the silt behaves like a sand. Thus, the silt tested here had sand-like behavior. However, the work of Boulanger and Idriss does not address the effect of OCR on silt behavior. As noted in the next section, the OCR played a significant role in the normalized behavior of the tested silt, as it did in that of clay, so that the silt did not behave exactly like a sand.

From the initial state to the critical state, the general dilation behavior was found in the critical state diagram. However, as mentioned above, specimens with an OCR of 1 or 2 initially contracted, and then dilated. To identify the initial dilation or contraction in the e-ln p′ space, a phase transformation line was also plotted in the Fig. 3.6. Only data points of MS7, MS8, and MS9 are located left of the phase transformation line. Under undrained shearing condition, there is no change in the void ratio, so that the data points in the e-ln p′ space can only move horizontally. Due to the development of higher negative excess pore water pressure compared to other specimens, the highly overconsolidated specimens MS7, MS8, and MS9 dilated from the initial state to phase transformation state. Except for these three specimens, all showed contraction behavior from initial state to phase transformation state.

3.3 Normalized Behavior of Low-plasticity Silt

The deviator stress of some clays can be normalized by effective consolidation pressure (Ladd and Foott 1974; Ladd et al. 1977). Fleming and Duncan (1990) demonstrated that the undrained strength of low-plasticity Alaskan silts can also be normalized with relatively small variations. The small variations in the normalized values for identical OCRs were believed to result from sample preparation and reconsolidation effects.

Figure 3.7 shows the normalized curves of deviator stress, excess pore water pressure and stress path of the MRV silt tested here. With higher OCR, the normalized deviator stress was higher, and more negative normalized excess pore pressure was generated. In the normalized stress space (Fig. 3.7c), there was stronger dilation with higher OCR, except for the specimen MS1 with a σ'_c of 50 kPa and a OCR of 1, which had stress path close to the specimens with OCR of 2 before the PTP. Therefore, the OCR played a significant role in the normalized stress-strain behavior. Furthermore, under the same OCR, normalized behaviors were different for different effective consolidation pressures (σ'_c). When the OCR was equal to 1 or 8, the normalized deviator stress decreased with increasing effective consolidation pressure. On the other hand, when the OCR was 4, the normalized deviator stress increased with increasing effective consolidation pressure. Specimens with an OCR of 2 had intermediate behaviors, as indicated by

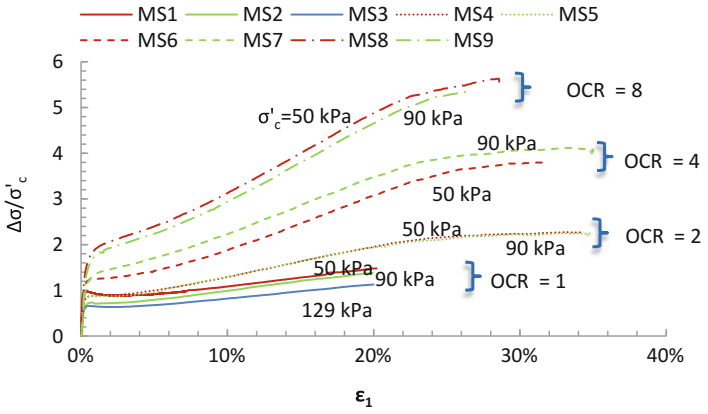

(a) Normalized Deviator Stress

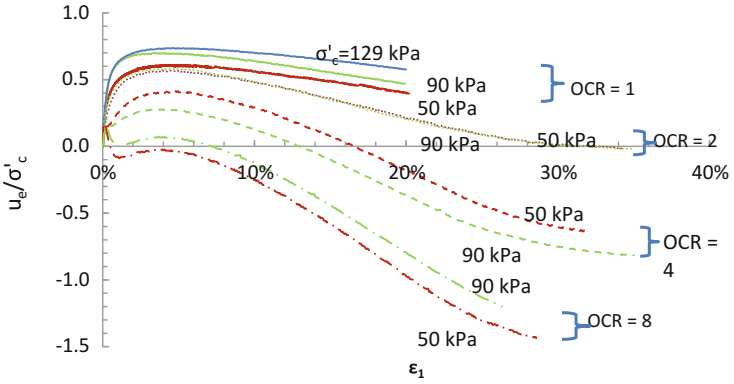

(b) Normalized Excess Pore Water Pressure

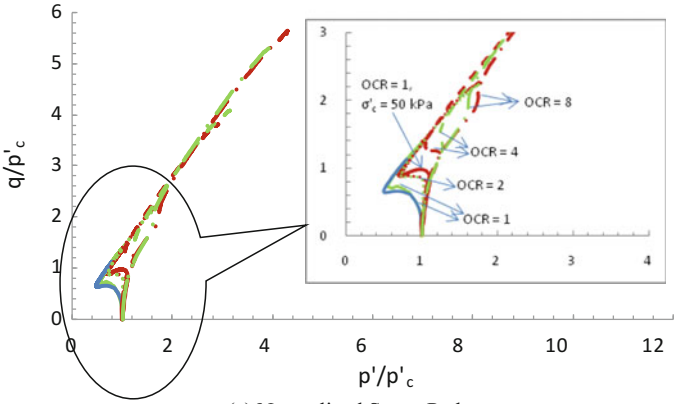

(c) Normalized Stress Path

Fig. 3.7 Normalized behaviors of MRV silt

closely matching curves of normalized deviator stress and excess pore water pressure against axial strain.

The stress-strain behavior appears not to be normalized by effective consolidation pressure. However, the variations of normalized stress-strain behavior induced by the effective consolidation pressure were much lower than those by the OCR. These small variations were caused in part by inevitable variations in procedures from one test to another. Thus, the MRV silt tested here can be said to have normalized behavior. Similarly, the excess pore water pressure could also be normalized by effective consolidation pressure.

Based on many tests of six clays, Ladd et al. (1977) developed the following equation to consider effect of OCR on the normalized shear strength of clay:

$$\frac{(S_u/\sigma'_C)_{(OC)}}{(S_u/\sigma'_C)_{(NC)}} = OCR^m \tag{3.1}$$

where, S_u is undrained shear strength, and σ'_c is effective consolidation pressure. In the equation, the m value is normally equal to 0.80, but this value varies from 0.75 to 0.85 based on the OCR. A higher OCR is probably associated with a higher value of m.

Furthermore, Ladd (1991) presented the following equation to calculate the S_u/σ'_c.

$$\frac{S_u}{\sigma'_c} = S \times OCR^m \tag{3.2}$$

where, S is 0.22 and 0.25, respective for clay and silt; m is 0.80 for both clay and silt.

This work studied the effect of OCR on the normalized shear strength of low-plasticity silt under isotropic consolidation, by combining the test results reported by Fleming and Duncan (1990), Yasuhara et al. (2003), and Izadi (2006). The undrained shear strength was determined as one-half of the deviator stress at an axial strain of 15%, as done by Fleming and Duncan (1990). Fleming and Duncan (1990) gave a narrow range of S_u/σ'_c for Alaskan Silt. The middle value of the narrow range of S_u/σ'_c was selected here. Izadi (2006) showed normalized deviator stress curves of Collinsville silt for two different initial void ratios (0.65 and 0.79) due to specimen preparation. With an examination, the deviator stress cannot be normalized by effective consolidation pressure for all specimens with initial void ratios of 0.65, partially because of cavitation during shearing. Thus, only the S_u/σ'_c was calculated for the specimens with initial void ratio of 0.79 under various OCRs. The Keuper Marl silt studied by Yasuhara et al. (2003) had a plasticity index of 19.7 and a liquid limit of 38.6, which was classified as a lean clay (CL) using the Unified Soil Classification System. However, the silt fraction was nearly 70% based on grain size distribution curve and thought to be low-plasticity silt (Izadi 2006). Thus, the Keuper Marl silt was included here. Table 3.6 lists the S_u/σ'_c for the silts at different OCRs. As OCR increased, the S_u/σ'_c increased in Fig. 3.8a.

Table 3.6 S_u/σ'_c of silts with various OCRs

Silt	PI	OCR				
		1	2	4	8	10
Alaskan	Close to A line in plasticity chart	0.925	1.775		2.925	
Keuper Marl	19.7	0.34	0.565	0.85		1.7
Collinsville	6	1.325	2.625	3.2		
MRV	6	0.566	0.820	1.332	1.951	

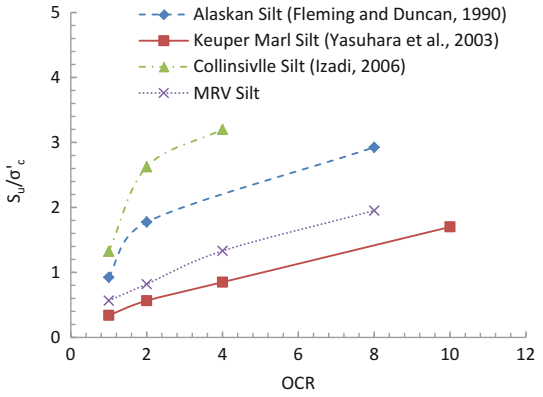

(a) S_u/σ'_c vs. OCR

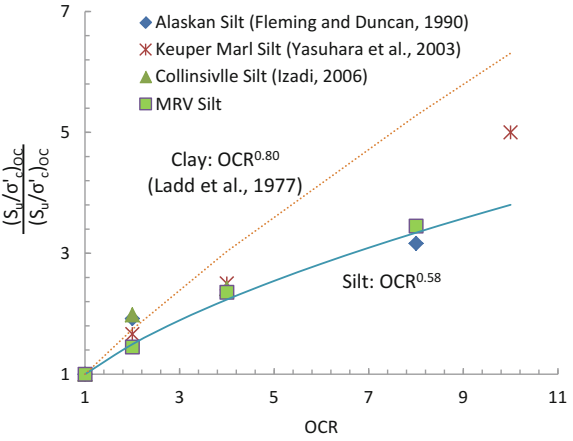

(b) $\dfrac{(S_u/\sigma'_c)_{OC}}{(S_u/\sigma'_c)_{NC}}$ vs. OCR

Fig. 3.8 Effect of OCR on the normalized shear strength

Different from clay, however, there was big difference in the variation of S_u/σ'_c with OCR among different silts; therefore, it is impossible to relate S_u/σ'_c to OCR using Eq. (3.2) for slits. As did by Ladd et al. (1977), the ratio of normalized shear strength of overconsolidated specimens to that of normally consolidated specimens $((S_u/\sigma'_c)_{OC}/(S_u/\sigma'_c)_{NC})$ was calculated. Figure 3.8b indicates that there was no big difference in the normalized shear strength ratio $(S_u/\sigma'_c)_{OC}/(S_u/\sigma'_c)_{NC}$ among different silts. Thus, there is no big effect of plasticity index on the normalized shear strength ratio for the low-plasticity silt.

The data points in Fig. 3.8 can be fitted with Eq. (3.1), with a value of m equal to almost 0.58 rather than 0.80, except the data point with the OCR of 10. A bigger m value is required for that data point, as does clay require for the high OCR value (Ladd et al. 1977). As is possible with clayey soil, the equation permits convenient prediction of the undrained shear strength of overconsolidated silty soil using the known shear strength of normally consolidated specimen. Figure 3.8b also plots the curve used to demonstrate the effect of OCR on the normalized shear strength ratio of clay. The curves for the clay is above the curve for the silt, indicating that the OCR affects the normalized shear strength ratio of the silt less than it does that of the clay. The m value is probably related to the plasticity of the silt. This hypothesis is supported by the fact that low-plasticity silts behave like an intermediate soil. The m value for the silts was determined based on limited data available for four kinds of low-plasticity silt. Additional research data could add to verify the validity of m = 0.58 for low-plasticity silt.

Figure 3.9 plots the curve of principal stress ratio (σ'_1/σ'_3) against axial strain. The maximum values of σ'_1/σ'_3 are located in a narrow zone of 3.45–3.77, which explains why the failure criterion of $(\sigma'_1/\sigma'_3)_{max}$ can yield a relatively constant friction angle. Thus, stress-strain behavior can be normalized using effective confining stress during the shearing.

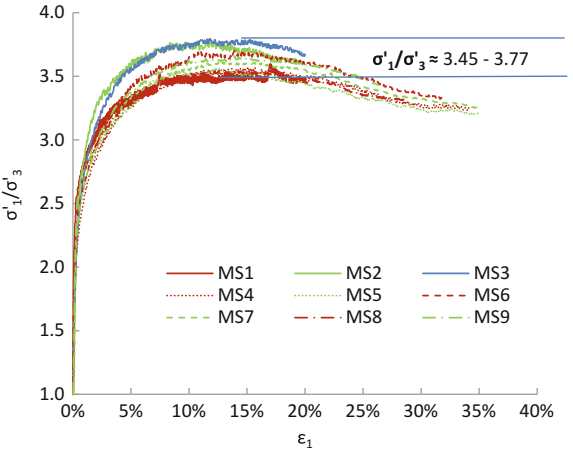

Fig. 3.9 σ'_1/σ_3 versus ε_1 of MRV silt

3.4 Effect of Plasticity Index on Silt Behavior

No definitive criteria is available to identify whether low-plasticity fine-grained soil behaves sand-like or clay-like. Although Boulanger and Idriss (2006) presented that the fine-grained soil with a PI from 3 to 6 can behave like an intermediate material, not enough laboratory data can confirm this. Particularly, as mentioned earlier, the Italian silt-clay mixtures with PIs of 11 and 13 even have transitional behavior. Thus, the research presented herein characterizes the effect of PI on shear strength behavior of low-plasticity silt and identifies a clear behavior threshold.

3.4.1 Stress-Strain Behavior of Silt-Bentonite Mixture

For convenience in the subsequent discussions, some terms related to the stress-strain behavior are defined herein and presented in Fig. 3.10 (q—deviator stress, = $\sigma'_1 - \sigma'_3$; ε_1—axial strain; σ'_1—maximum effective principal stress, σ'_3—minimum effective principal stress). Yield stress is the initial peak deviator stress, and the quasi-steady state is the point with the lowest deviator stress after yield stress. The critical state is considered reached when the deviator stress remains constant with an increase in axial strain. The excess pore water pressure at this point may not be at a constant value. This is partly due to the placement of the pore water pressure transducer being outside the specimen, which delays or introduces a lag-time of the pressure readings. One half of the deviator stress at the critical state is defined as undrained shear strength (S_u).

Figures 3.11 [$p' = (\sigma'_1 + 2\sigma'_3)/3$] shows stress-strain curves for consolidated undrained triaxial tests for normally consolidated soil mixtures (PI = 5.8, 6.2, 9.4, and 13.5) to a σ'_c of 50 kPa. The soil mixtures with IPs greater than 5.8 show a lower yield stress than the natural silt (PI = 5.8). This phenomenon was also shown in normally consolidated soil mixtures to a σ'_c of 90 kPa shown in Fig. 3.12. Most

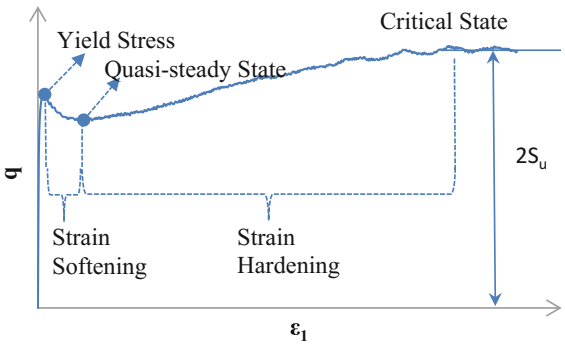

Fig. 3.10 Terminology on undrained shear behavior of MRV silt

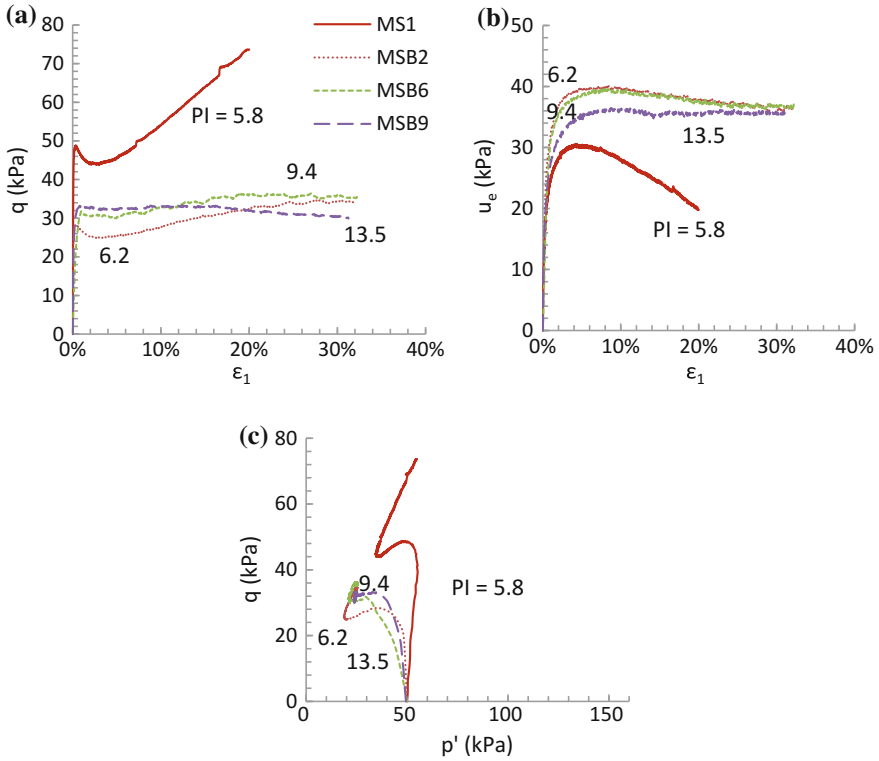

Fig. 3.11 Monotonic shear behavior of normally consolidated (σ'_c = 50 kPa) MRV silt and its mixtures with bentonite: **a** $\Delta\sigma$ versus ε_1; **b** u_e versus ε_1; **c** q versus p′

specimens (except PI = 13.5) had a slightly quasi-steady state after the yield stress. After the quasi-steady state, the specimens had strain-hardening behavior until the critical state at the large deformation was reached. With lower PI, the strain hardening was more evident (i.e. difference in deviator stress was larger between quasi-steady state and critical state) in Figs. 3.11a and 3.12a. The specimen with a PI of 13.5 had almost a constant deviator stress after yield stress. Shown in Figs. 3.11b and 3.12b, the natural MRV silt with a PI of 5.8 had a drop of excess pore water pressure after yield stress, indicating that there was stronger dilation behavior. However, there were no big differences in shape of the curves of deviator stress versus axial strain, excess pore water pressure versus axial strain, and stress path among the specimens with PIs of 6.0, 6.2, 9.4, and 13.5.

Figure 3.13 shows undrained shear behavior of the overconsolidated MRV silt and its mixtures with bentonite at σ'_c = 90 kPa and OCR = 8. Those three specimens with added bentonite (PI = 5.8, 6.2, and 9.4) resulted in a similar behavior. There was no quasi-steady state because the deviator stress kept increasing until critical state regardless of a sharp reduction in the slope of the curve of the deviator

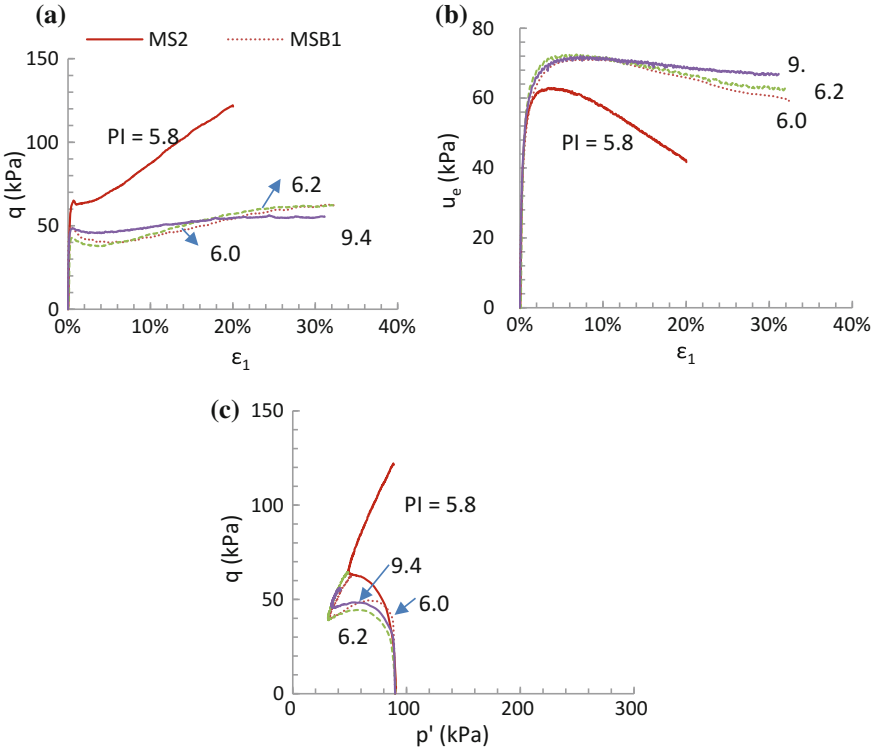

Fig. 3.12 Monotonic shear behavior of normally consolidated (σ'_c = 90 kPa) MRV silt and its mixtures with bentonite: **a** $\Delta\sigma$ versus ε_1; **b** u_e versus ε_1; **c** q versus p′

stress-strain (Fig. 3.13a). There was a development of negative excess pore water pressure (Fig. 3.13b), associated with the highly dilative behavior compared to the normally consolidated soils (Fig. 3.13b).

With a further investigation of excess pore water pressure response under high overconsolidation ratio (Fig. 3.13b), it was surprisingly interesting to note that the curves of excess pore water pressures versus axial strain of all soils with OCR = 8 had two peaks. One occurred at the axial strain of about 0.2% and the other at the axial strain close to 5%. To the authors' knowledge, this excess pore water pressure response was never observed in other soils. Normally, the highly overconsolidated soil has only one peak value of excess pore water pressure (i.e., the positive excess pore water pressure develops initially and then drops to negative pore water pressure). The reason why the tested MRV silt mixtures had the two peaks on the curves of excess pore water pressure versus axial strain will be discussed later.

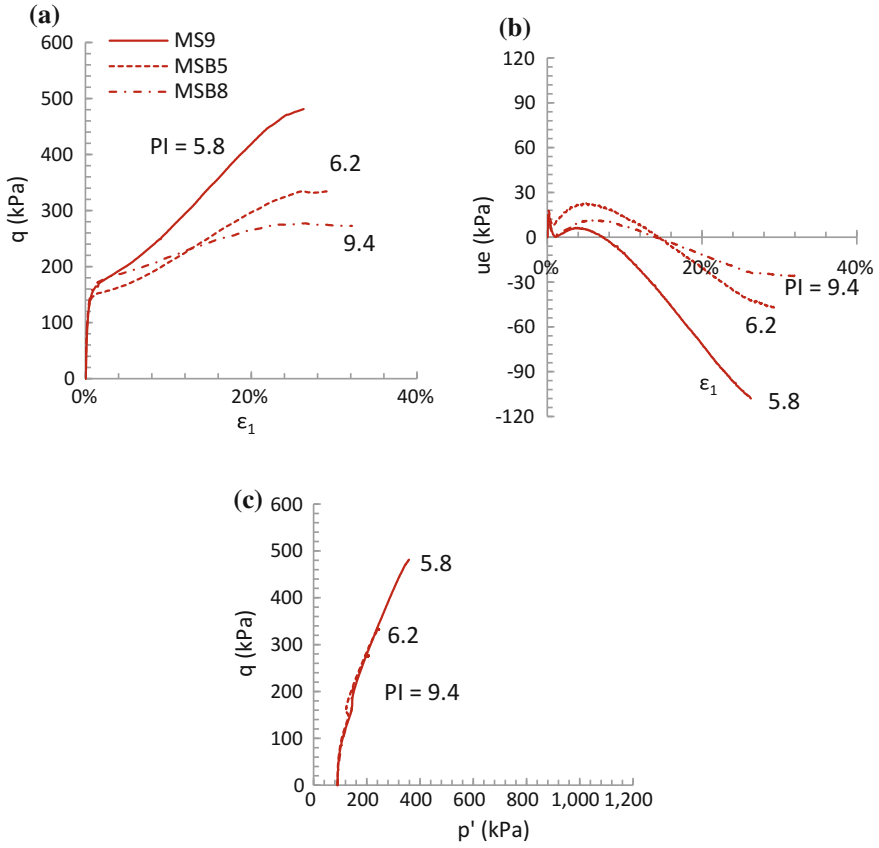

Fig. 3.13 Monotonic shear behavior of overconsolidated (σ'_c = 90 kPa and OCR = 8) MRV silt and its mixtures with bentonite: **a** $\Delta\sigma$ versus ε_1; **b** u_e versus ε_1; **c** q versus p′

3.4.2 *Undrained Shear Strength*

The undrained shear strengths for all normally consolidated specimens at various effective consolidation pressures were listed in Table 3.4. For the natural MRV silt specimens with PI of 5.8, the normalized shear strength (S_u/σ'_c) decreased with an increase in σ'_c from 50 to 129 kPa. Typical normally consolidated clays have a constant S_u/σ'_c ratio. However, there is a reduction in the S_u/σ'_c for the low plasticity natural MRV silt. Also shown in Fig. 3.14, the soil-bentonite mixtures had a slight reduction in normalized shear strengths when the PI increases from 6.2 to 13.5.

For undisturbed clays, researchers presented several relationships between the normalized shear strength with index properties (Skempton 1957; Worth and Houlsby 1985; Jamiolkowski et al. 1985; Mesri 1989). The relationships based on triaxial compression tests were also plotted in Fig. 3.14. The S_u/σ'_c of the MRV

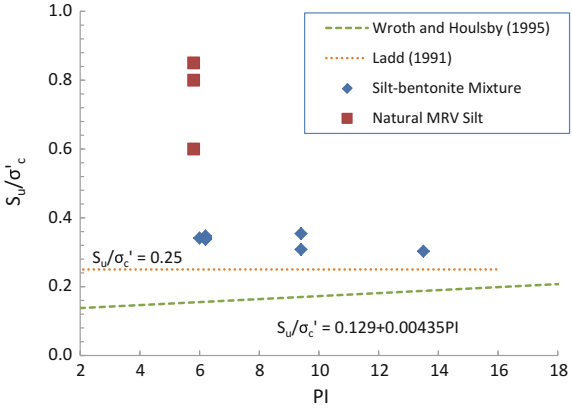

Fig. 3.14 Variation of normalized shear strength against plasticity index

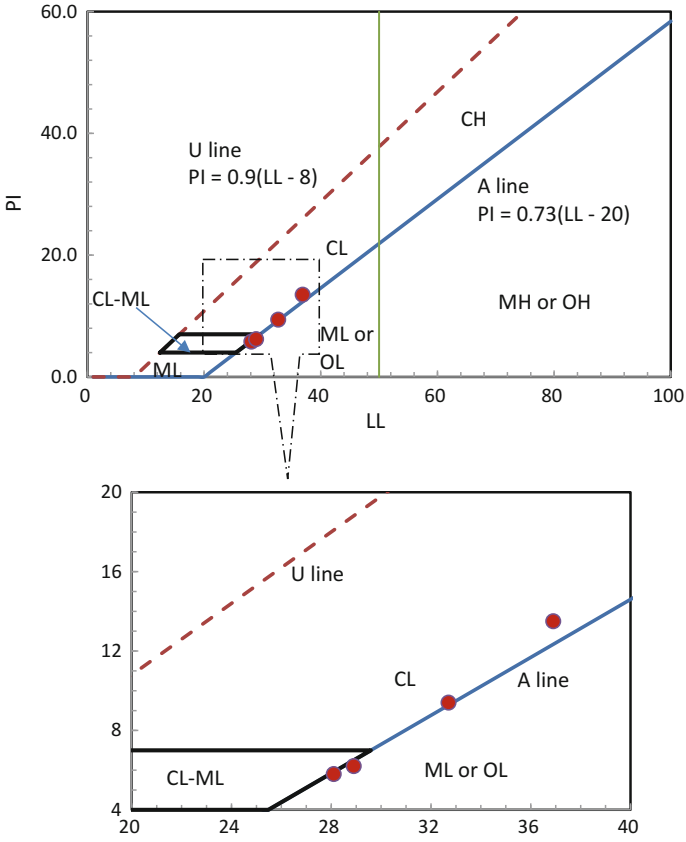

Fig. 3.15 Soil types of the MRV silt and its mixtures with bentonite using atterberg limit chart

silt-bentonite mixture was greater than the predicted value based on Ladd's equation for the low range of PI tested, especially at PI of 5.8. The higher S_u/σ'_c ratio was also observed in the test results on Alaskan silt by Fleming and Duncan (1990). The equation proposed by Wroth and Houlsby (1985) suggests that the S_u/σ'_c be in proportional to PI. Compared to current study, the S_u/σ'_c showed an opposite trend for the natural MRV silt.

3.5 Discussion

As stated earlier, the silt-bentonite mixtures changed from a relatively high strain-hardening behavior to a more plastic stress-strain behavior as the plasticity index increased from 5.8 to 13.5. A threshold PI = 6.0 was identified to distinguish the behavior from sand-like to clay-like. With a PI less than 6.0, the soil behaves like an intermediate material or sand because the natural MRV silt with a PI of 5.8 have both sand-like and clay-like behavior. Thus, the findings in the natural MRV silt and its mixtures with bentonite follow the criteria proposed by Boulanger and Idriss (2006).

Additionally, the soil behavior could be quickly identified using the plasticity chart. Figure 3.15 shows the plasticity chart with data points for the MRV silt and its mixtures. The data points from left to right show Atterberg limits of the soil mixtures with added bentonite contents of 0, 2.5, 5.0, and 7.5%, respectively. The soil mixture with added bentonite content 7.5% has a plasticity index of 13.5 and is classified as CL, so it showed plastic stress-strain behavior, as discussed previously. The other three data points almost lie on the A line so the soil mixtures can behave like both sands and clays. The natural MRV silt with a PI of 5.8 behaves like an intermediate material. Although the soil mixtures with PIs 6.2 and 9.4 were considered to behave more like clays, they also have slightly sand-like behavior because they have quasi-steady states (Figs. 3.11 and 3.12) regardless of no quasi-steady state line in Fig. 3.13.

To explain highly dilative behavior of the MRV silt from a microscopic level (Fig. 3.16), the MRV silt particles were found sub-angular to angular, and even very angular through a scanning electron microscope. The surface of the silt particles was also found rough. These features tend to contribute to a dilative behavior of this material. The previously stated interesting excess pore water pressure response during monotonic shearing of the specimens under an OCR of 8 could be related to the MRV silt particle characteristics. The soil specimens were found dilated twice possibly due to the angular shape of the silt particles. The clay minerals (montmorillonite) were only 2.2% of MRV silt in weight. When the bentonite (montmorillonite) having clay minerals of 64.0% added, the surface of the silt particle may be coated with clay minerals, which reduces the particle roughness. Hence, the friction on the particle surface was reduced and the dilation of the soil mixture became weaker at higher IPs within the tested range.

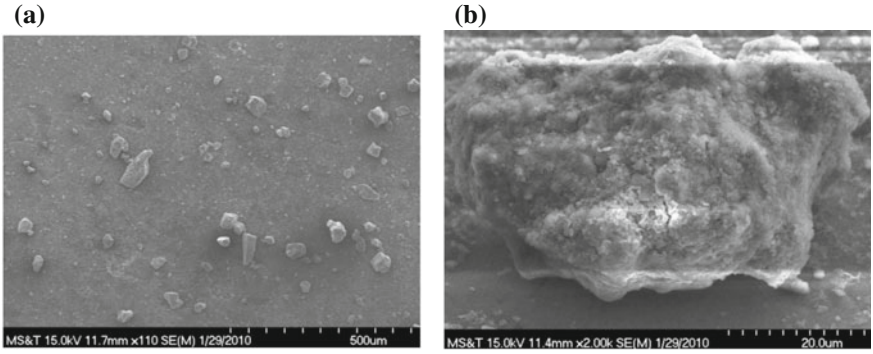

Fig. 3.16 Particle investigation for MRV silt: **a** overview, **b** surface roughness

3.6 Summary

The MRV silt tested here had no unique critical state among specimens with different OCRs. With an OCR of 1 or 2 initially contracted, and then dilated. With an OCR of 8, the silt dilated continuously. All these specimens (OCR = 1, 2, and 8) had a normal behavior, i.e., less dilation with higher effective consolidation pressure. For an OCR of 4, however, the specimens showed opposite behavior, i.e., higher dilation with higher effective consolidation pressure.

A critical state line was obtained in and the e-ln p′ space. The critical state line was not parallel to the normal consolidation curve. According to Boulanger and Idriss (2006), the silt behaves sand-like. However, in this work, the OCR did play a significant role in the stress-strain behavior of the silt, as it does in that of clay. These findings indicated that the silt had a unique behavior, and thus that it behavior was more complex than previously thought.

The failure criteria of u_{max}, u = 0, and reaching K_f line were not available to calculate friction angle of the silt tested here. This work suggested that limiting strain is the criterion best used to calculate the friction angle, because of more consistence of friction angle and more rationality for the low-plasticity silt.

The stress-strain behavior of the MRV silt can be normalized by effective consolidation pressure and effective confining pressure. As the OCR increased, the shear strength normalized by effective consolidation pressure increased. The m value of 0.58 was used to estimate the overconsolidated shear strength for low-plasticity silt using Eq. (3.1) when the normally consolidated shear strength was known. Although this value should be verified with more testing data, it provides a means to relate the shear strength of low plasticity silt to its OCR. However, the Eq. (3.2) cannot be used to relate the S_u/σ'_c to OCR, because there is big difference in the curve of S_u/σ'_c vs OCR among different silts.

The highly dilative behavior of the MRV silt was reduced significantly with a slight increase of PI from 5.8 to 6.0 by adding bentonite (2.5%). With an increase in plasticity index, the silt tends to lose the quasi-steady state and changes to more

plastic behavior. The soil mixture with a PI of 13.5 had plastic behavior and no increase in deviator stress after the yield stress. The overconsolidated condition influences the friction angle of the MRV silt-bentonite mixtures with PIs greater than 6.2, because the soil mixtures tend to retain the stress history (memory) like in clays. The soil mixtures with a PI greater than 6.2 had CSLs but no PTLs. The CSLs are almost parallel to the NCLs as it is common in clay-like behavior.

The normalized shear strength (S_u/σ'_c) of the MRV silt was significantly reduced with added bentonite. Compared to the value predicted with Ladd's equation, the silt-bentonite mixtures S_u/σ'_c was much higher. The may be due to the highly dilative behavior induced by the MRV silt particle features: angular silt particle and rough particle surface.

It may be concluded that the critical PI was about 6 to differentiate clay-like soil and intermediate soil for the subject silt. The findings in the natural MRV silt and its mixtures with bentonite follows the criteria presented by Boulanger and Idriss (2006) to identify soil behavior, and the plasticity chart also helps identify the testing behavior of the MRV silt and its mixtures with bentonite. It is worth emphasizing that the little change of plasticity index of the soil from 5.8 to 6.2 due to the addition of bentonite was difficult to be achieved in the laboratory. Based on the authors' experience, the plasticity index is not an ideal parameter to identify the transformation of shear behavior of the MRV silt and future research is needed. It is suggested that the soil mineralogy, which was not determined in the current research, be quantified for identifying the transformation of soil behavior.

References

ASTM. (2004). *Standard test method for consolidated undrained triaxial compression test for cohesive soils* (pp. D4767–4). West Conshohocken, PA.

ASTM. (2005). *Standard test methods for liquid limit, plastic limit, and plasticity index of soils* (pp. D 4318–05). West Conshohocken, PA.

Boulanger, R. W., & Idriss, I. M. (2006). Liquefaction susceptibility criteria for silts and clays. *Journal of Geotechnical and Geoenvironmental Engineering, ASCE, 132*(11), 1413–1426.

Brandon, T. L., Rose, A. T., & Duncan, J. M. (2006). Drained and undrained strength interpretation for low-plasticity silts. *Journal of Geotechnical and Geoenvironmental Engineering, 132*(2), 250–257.

Fleming, L. N., & Duncan, J. M. (1990). Stress-deformation characteristics of alaskan silt. *Journal of Geotechnical Engineering, 116*(3), 377–393.

Holtz, R. D., Kovacs, W. D., & Sheahan, T. C. (2011). *An introduction to geotechnical engineering*. Englewood Cliffs, NJ: Prentice-Hall, Inc.

Ishihara, K., Tatsuoka, F., & Yasuda, S. (1975). Undrained deformation and liquefaction of sand under cyclic stresses. *Soil and Foundations, 15*(1), 29–44.

Izadi, A. (2006). *Static behavior of silts*. MS Thesis, University of Missouri-Rolla, Missouri.

Jamiolkowski, M., Ladd, C. C., Germaine, J. T., Lancellotta, R. (1985). New developments in field and laboratory testing of soils. In *Proceedings of 11th International Conference on Soil Mechanics and Foundation Engineering* (Vol. 1, pp. 57–153). San Francisco, California.

Ladd, C. C. (1991). Stability evaluation during staged construction. *Journal of Geotechnical Engineering, 117*(4), 540–615.

Ladd, C. C., & Foott, R. (1974). New design procedure for stability of soft clays. *Journal of the Geotechnical Engineering Division, 100*(GT7), 763–786.

Ladd, C. C., Foott, R., Ishihara, K., Schlosser, F., & Poulos, H. G. (1977). Stress-deformation and strength characteristics. *Proceedings of the Ninth International Conference on Soil Mechanics and Foundation Engineering, Japanese Society of Soil Mechanics and Foundation Engineering, 2,* 421–494.

Lefebvre, G. S., Leboeuf, D., & Demers, B. (1989). Stability threshold for cyclic loading of saturated clay. *Canadian Geotechnical Journal, 26*(1), 122–131.

Mesri, G. (1989). A Re-evaluation of Su(mob) $\approx 0.22\sigma$'p Using Laboratory Shear Soils. *Canadian Geotechnical Journal, 26*(1), 301–309.

Skempton, A. W. (1957). Discussion of 'Planning and Design of New Hong Kong Airport. *Proceeding, Institution of Civil Engineers, 7,* 305–307.

Wang, S., & Luna, R. (2012). Monotonic behavior of Mississippi River Valley silt in triaxial compression. *Journal of Geotechnical and Geoenvironmental Engineering, 138*(4), 516–525.

Wang, S., Luna, R., & Yang, J. (2017). Effect of plasticity on shear behavior of low-plasticity fine-grained soil. *Journal of Materials in Civil Engineering, 29*(3), 1–7.

Worth, C. P., & Houlsby, G. T. (1985). Soil Mechanics—Property characteristics of normally consolidated clays. In *ASCE Research Conference on Shear Strength of Cohesive Soil*, Boulder (pp. 711–726). Colorado.

Yamamuro, J., & Lade, P. V. (1998). Steady-State Concepts and Static Liquefaction of Silty Sand. *Journal of Geotechnical and Geoenvironmental Engineering, 124*(9), 868–877.

Yasuhara, K., Murakami, S., Song, B. W., Yokokawa, S., & Hyde, A. F. L. (2003). Postcyclic degradation of strength and stiffness for low plasticity silt. *Journal of Geotechnical and Geoenvironmental Engineering, 129*(8), 756–769.

Chapter 4
Liquefaction Characteristics of Low-plasticity Fine-Grained Soil

This chapter investigates, the liquefaction characteristics of low-plasticity silt with various overconsolidation ratios, effective consolidation pressures and plasticity indexes. Especially, plasticity index is adopted as an important influence factor to evaluate soil behavior. With a point of view from engineering practice, an investigation is done in this chapter with collecting laboratory data presented by other scholars to evaluate the effect of plasticity on liquefaction resistance of low-plasticity fine-grained soils, after cyclic behavior of the MRV silt is studied using cyclic triaxial tests.

4.1 Testing Program

Liquefaction resistance of the MRV silt and its mixtures with bentonite was studied by conducting cyclic triaxial tests on specimens reconstituted using the slurry consolidation approach. The specimens were prepared in a split vacuum mold on a special experimental setup and then moved to the triaxial platen. Before back pressure was supplied for saturation, a high vacuum less than effective consolidation pressure was connected to the top and bottom ends of the specimens to remove air bubbles in the specimen. Saturation was achieved by supplying high back pressure. The back pressure was increased till the Skempton B value kept constant and was at least 0.94. All specimens were normally consolidated to effective consolidation pressure (σ'_c) of 90 kPa, with no initial shear stress. Cyclic triaxial tests were conducted with deviator stress controlled ($\Delta\sigma_{max} = 2 \times CSR \times \sigma'_c$). The frequency of symmetrically cyclic stress with a sine function was 0.1 Hz. Thus, the cyclic strength from this work needs to be adjusted to that with a frequency of 1 Hz, which is normally dominant in earthquake loading, when used for engineering practice. Boulanger and Idriss (2007) stated that cyclic strengths increase about 9% per log cycle of loading rate. Table 4.1 lists the testing results to of the MRV silt and its mixtures with bentonite.

S. Wang, *Monotonic, Cyclic and Postcyclic Shear Behavior of Low-plasticity Silt*,
https://doi.org/10.1007/978-981-10-7083-9_4

Table 4.1 Triaxial tests on the MRV silt and its mixtures with bentonite

Test ID	PI	σ'_c (kPa)	Void ratio (e)	Cyclic shearing		
				CSR	R_u	N_{cyc}
MS2	5.8	90.0	0.669			
MD2		91.1	0.661	0.18	1	35.2
MD3		91.2	0.670	0.25	1	3.2
MD4		90.8	0.676	0.35	1	1.2
MF1R2		89.9	0.669	0.18	1	31.1
MF4		90.3	0.659	0.18	1	29.1
MF5		90.2	0.655	0.18	1	33.2
MSB3	6.2	90.0	0.665			
MFB4		91.2	0.658	0.18	0.92	160
MFB5		90.4	0.675	0.18	0.86	89.2
MFB6		90.6	0.660	0.35	0.78	1.1
MSB7	9.4	90.0	0.688			
MFB7		91.2	0.690	0.18	0.82	407
MFB8		91.3	0.678	0.25	0.64	12.1
MFB9		91.3	0.685	0.35	0.55	1.2

Note In the Test ID, the M, S, D and B represents MRV silt, static test, dynamic test, and bentonite added, respectively. The F in "MF" indicates that the specimen experienced full liquefaction (R_u = 1.0 and axial strain of 9%). However, in the "MFB", the F indicates that there was 9% axial strain induced by cyclic loading. U_{rc} is reconsolidation level, and e′ is void ratio after reconsolidation

4.2 Cyclic Behavior of Low-plasticity Silt

4.2.1 Effect of Initial Consolidation Conditions

Figure 4.1 presents the variation of excess pore pressure ratio and cyclic axial strain (ε_{cyc}) with number of loading cycles (N_{cyc}) for specimens MD4 (OCR = 1), MLO2 (OCR = 2), MLO3 (OCR = 3) and MLO5 (OCR = 4) with a CSR of 0.35 and σ'_c of 90 kPa. Figure 4.1a shows that excess pore pressure developed in the specimens increased with increasing loading cycles. Specimens MD4, MLO2, MLO3 and MLO5 generated a R_u of 1 at loading cycles of 1.2, 5.1, 12.1 and 22.1, respectively. Thus, as OCR increased, the rate at which excess pore pressure built-up became slower and more loading cycles were required for the generation of R_u = 1.0. As indicated in Fig. 4.1a, more loading cycles were required to develop large cyclic axial strain.

Figure 4.2a, b present the cyclic shear strength (for R_u = 1.0) for MRV silt at different OCRs. Figure 4.2a shows the increase in cyclic shear strength with increasing OCR. Similar findings have been reported by other investigators such as Puri (1984), Sandoval_Shannon (1989), and Izadi (2008). To assess the cyclic shear strength of MRV silt, the CSRs for 10, 15, 20, 25 and 30 loading cycles of the MRV silt

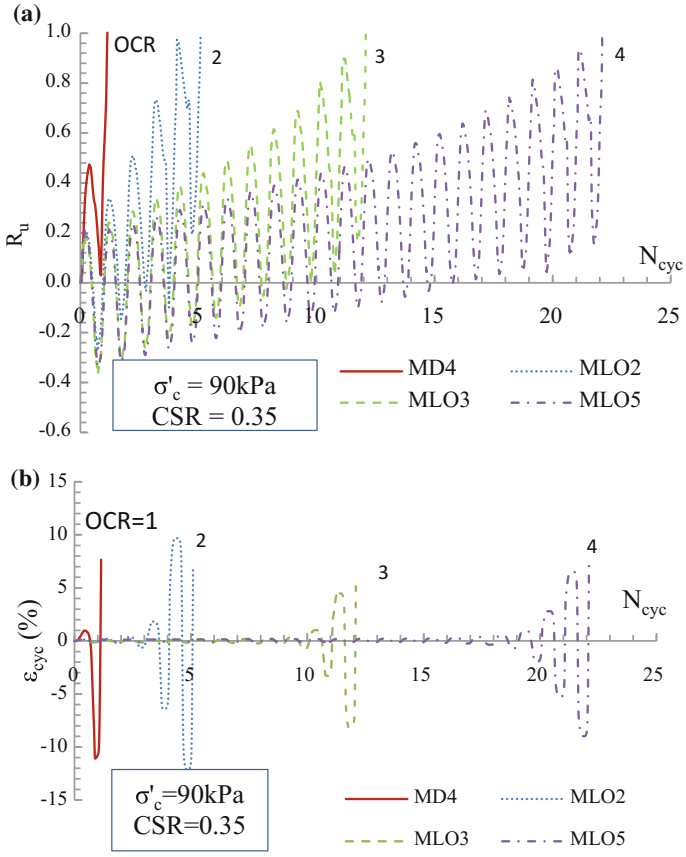

Fig. 4.1 Cyclic triaxial behaviors of MRV silt specimens at various initial overconsolidation ratios: **a** R_u versus N_{cyc}, **b** ε_{cyc} versus N_{cyc}

specimens at various OCRs were determined based on Fig. 4.2a, and they were normalized (with respect to the CSR of the normally-consolidated MRV silt). The plots of the variation of the normalized CSR with OCR, presented in Fig. 4.2b, show a substantial reduction in the rate of increase in $CSR_{OCR}/CSR_{OCR=1}$ with higher OCRs.

Figure 4.3 presents the cyclic triaxial behavior of normally-consolidated MRV silt during cyclic loading for various mean effective consolidation pressures. Figure 4.3a shows that the cyclic shear strength of MRV silt decreased with an increase in mean effective consolidation pressure. Increases in σ'_c, led to a reduction in the number of loading cycles required to attain $R_u = 1.0$. Similar findings have been reported by Moriwaki et al. (1982), Hynes and Olsen (1999), Bray and Sancio (2006) and Izadi (2008). As shown in Fig. 4.3b, more loading cycles were required to develop large cyclic axial strain. However, there was no constant relationship between cyclic axial strain at the end of cyclic loading and effective consolidation pressure.

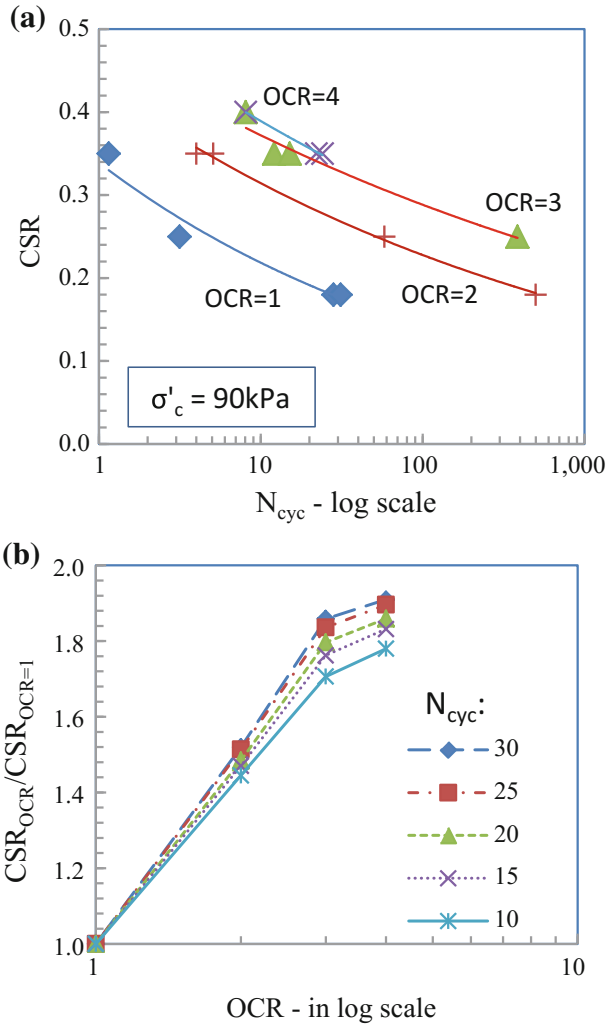

Fig. 4.2 Cyclic shear strength of MRV silt at various initial overconsolidation ratios: **a** CSR versus N_{cyc}, **b** $CSR_{OCR}/CSR_{OCR=1}$ versus OCR

4.2.2 Effect of Plasticity

As presented in Wang et al. (2016), all specimens were normally consolidated to effective consolidation pressure (σ'_c) of 90 kPa, with no initial shear stress. The void ratio (e) for each specimen after consolidation is given in Table 4.1. Cyclic triaxial tests were conducted with deviator stress controlled. The cyclic stress ratios (CSRs) are listed in Table 4.1. The frequency of symmetrical cyclic stress with a sine function was 0.1 Hz. For conducting postcyclic shearing, the cyclic loading

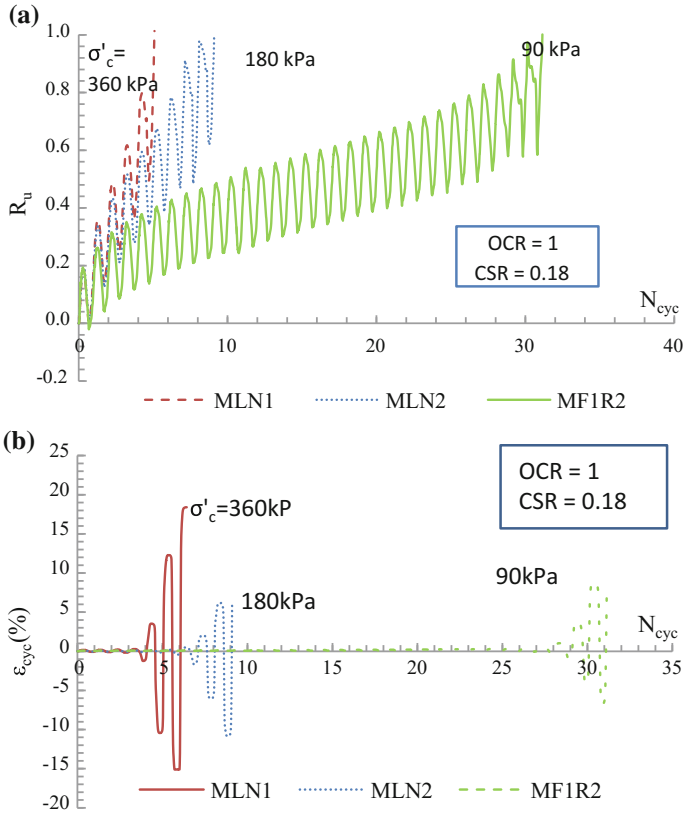

Fig. 4.3 Cyclic triaxial behaviors of the normally-consolidated MRV silt specimens with various mean effective consolidation pressures: **a** R_u versus N_{cyc}, **b** ε_{cyc} versus N_{cyc}

was ended till a 9% single-amplitude axial strain reached for each specimen. After cyclic loading, the deviator stress was slowly reduced to zero for each test, resulting in a slight change of axial strain. Table 4.1 lists the tests to investigate the cyclic strength of the tested MRV silt and its mixtures with bentonite. Totally, there are 12 cyclic triaxial tests.

Figure 4.4 shows the excess pore pressure response of MRV silt and its mixtures with bentonite under different CSRs. Each specimen had a positive cyclic strain of about 9.0% at the end of cyclic loading. As shown in Fig. 4.4a, the excess pore pressure build-up was less quickly with a higher plasticity index. Moreover, the natural MRV silt with a PI of 5.8 produced a R_u of 1.0 at the end of cyclic loading with a CSR of 0.18, but the specimens with PIs of 6.2 and 9.4 only developed a R_u of 0.92 and 0.82, respectively. Thus, the specimen with a higher plasticity index had a lower excess pore pressure ratio at the end of cyclic loading. The similar phenomenon was found for the specimens with other CSRs, as shown in Fig. 4.4b, c. The reasons was that the soil mixture with higher plasticity index had higher

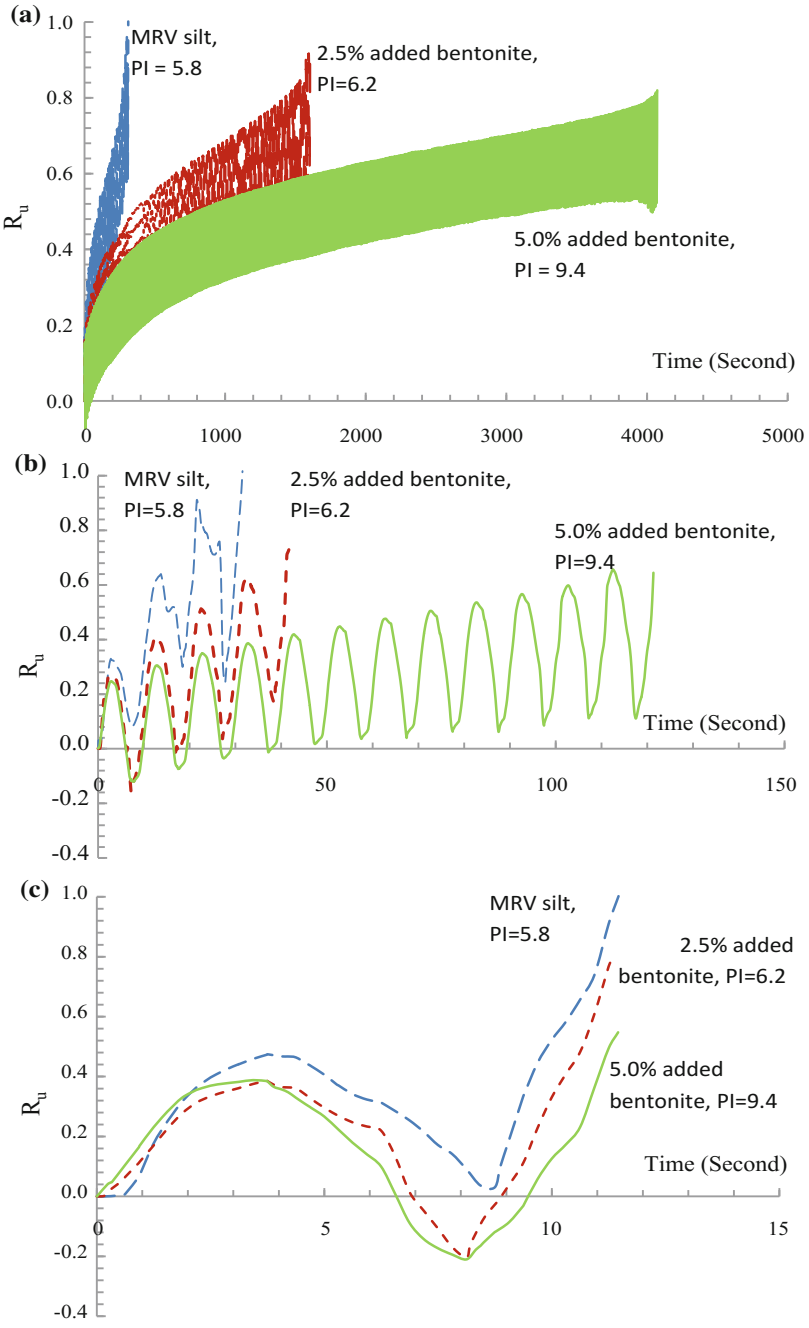

Fig. 4.4 Cyclic shear behavior of the MRV silt and its mixtures with bentonite at different CSRs: **a** 0.18, **b** 0.25, **c** 0.35

Table 4.2 Collection of laboratory data of cyclic tests on low-plasticity fine-grained soils

Soil material	Soil type	LL	PI	Fines content (%)	Spec. prep.	Test type	f (Hz)	σ'_c or σ'_{v0} (kPa)	e	Cyclic failure criteria	Number of tests	CSR	References
Adapazari soil	ML, CL	Close to A line, PI < 12		>35	UD	CTX	1	40	0.75–1.00	S.A.ε = 3%	10	0.24–0.59	Bray and Sancio (2006)
								50			16	0.28–0.595	
		Close to A line, PI = 12–18						40			6	0.275–0.595	
								50			16	0.276–0.487	
Loessial soil	ML	34	10	93–98	UD	CTX	1	69	0.738–0.818	D.A. ε = 5%	8	0.137–0.481	Puri (1984)
								103	0.734–0.799		8	0.139–0.475	
								138	0.734–0.799		8	0.145–0.481	
Laterite tailing	CL	34	12	100	UD	CDSS	0.1	100	1.324–1.451	γ = 3.75%	5	0.112–0.245	Wijewickreme et al. (2005)
Copper-gold tailing	ML	27	0	8.5–97.0				100	0.556		4	0.13–0.25	
Copper-gold-zinc tailing	ML	19	2	62.7–100.0				100–352	0.493–1.180		20	0.107–0.137	
		21	1	97.6				100, 250	0.840–0.870		3	0.115–0.19	
Clayey silt	ML		0	16.50	UD	CTX	0.2	150	0.640–0.647	D.A. ε = 5%	3	0.25–0.4	Wijewickreme and Sanin (2010)
		22	5	51				2	0.474–0.482		2	0.3–0.35	
		32	8	88				300	0.543–0.558		3	0.2–0.3	
		34	9	74				200	0.650–0.657		2	0.65–0.657	
		30	6.5	100				200	0.597–0.603		2	0.597–0.603	
Fraser river delta silt	ML	30.4	4	90	UD	CDSS	0.1	84.9–200	0.855–0.985	γ = 3.75%	11	0.1–0.29	El Hosri et al. (1984)
Mississippi river valley silt	ML	30	6		SC	CTX	0.1	35–105	0.751–0.824	D.A. ε = 5%	13	0.3–0.45	Izadi (2008)

(continued)

Table 4.2 (continued)

Soil material	Soil type	LL	PI	Fines content (%)	Spec. prep.	Test type	f (Hz)	σ'_c or σ'_{v0} (kPa)	e	Cyclic failure criteria	Number of tests	CSR	References
Fraser river delta silt	ML	30.4	4	90	SC	CDSS	0.1	97.3–103	0.843–0.866		4	0.1–0.14	El Hosri et al. (1984)
Quartz rock powder	ML		0	~94.5	SC			95.9–99.7	0.790–0.788		4	0.12	
Lime-stone power	ML	24	6	~88	SC	CTX	0.1	100	0.600	D.A. ε = 5%	7	0.109–0.221	Hyde et al. (2006)
Mississippi river valley silt	ML	28.1	5.8	94.5	SC	CTX	0.1	90	0.665–0.682	D.A. ε = 5%	7	0.18–0.35	Wang (2011)
		28.9	6.2	94.6					0.629–0.677		4	0.18–0.35	
	CL	32.7	9.4	94.8					0.685–0.690		3	0.18–0.35	

Note UD—undisturbed sampling; SC—slurry consolidation; CTX—cyclic triaxial test; CDSS—cyclic direct simple shear test; D.A.ε—double axial strain; S. A. ε—single axial strain; γ—shear strain; f—frequency; σ'_c—effective consolidation pressure for cyclic triaxial tests; σ'_{v0}—vertical overburden pressure for cyclic simple shear tests; e—void ratio after consolidation; N—number of loading cycles at the cyclic failure; Raw CSR—cyclic stress ratio before correction; CSR—cyclic stress ratio after being normalized

compressibility and so less excess pore pressure develops by cyclic loading in undrained condition.

It is noteworthy that the frequency of cyclic tests for all soils with various PIs was 0.1 Hz. As shown in Fig. 4.5, the permeability of the soil decreased sharply with an added bentonite content of 2.5%. As a result, the transmission of pore pressure from the specimen inside to the pore pressure transducer required more time with higher PI; therefore, the pore pressure transducer, which was located outside the specimens, provided less accurate pore pressure readings for the soil with higher PI. The additional time required for the transition of pore pressure from the specimen to the transducer location could explain, in part, why the excess pore pressure measured by the transducer at the end of cyclic loading was lower with a higher CSR, as shown in Fig. 4.4. With a lower CSR, the build-up of excess pore pressure was slower, so there was more time to transmit pore pressure from the specimen inside to the transducer during cyclic loading. Accurate measurements of pore pressure require that a miniature pore pressure transducer be placed in the specimen to measure pore pressure during dynamic loading (Murthy et al. 2007).

As shown in Fig. 4.6, the failure mode of the MRV silt with a PI of 6 was initial liquefaction under cyclic loading, because large axial strain developed when the excess pore pressure ratio was close to 1.0. Only with 1–2 loading cycles of large deformation, the axial strain and R_u reached 9.0% and 1.0, respectively. However, the specimens with bentonite added did not reach excess pore pressure ratio of 1.0 after several loading cycles with large deformation, especially for the MRV silt with added bentonite content of 5.0%. Thus, the soil mixtures with PIs of 6 and 10 showed cyclic softening rather than initial liquefaction. This finding comes close to supporting suggestion of Boulanger and Idriss (2006) that soil with a PI of at least 7 can be thought to have clay-like behavior. For MRV silt tested here, the critical PI can be thought to be 6, which is slightly lower than the value presented by Boulanger and Idriss (2006).

Cyclic failure was defined using the criterion of double-amplitude axial strain ($\varepsilon_{cyc,\ DA}$) of 5.0% in this study (Seed et al. 1983; Guo and Prakash 1999). Figure 4.7 shows the curves of CSR versus number of loading cycles (N_{cyc}). Generally, at a CSR lower than 0.35, the number of loading cycles required to induce a double-amplitude axial strain of 5.0% increased with an increase in PI from 6 to 10.

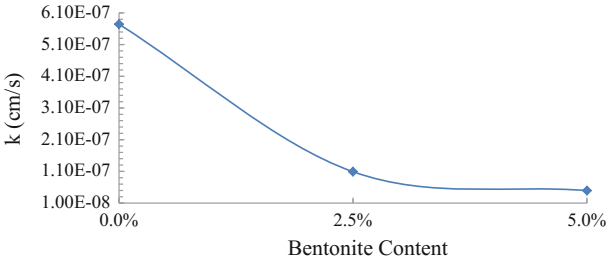

Fig. 4.5 Variation of permeability with bentonite content

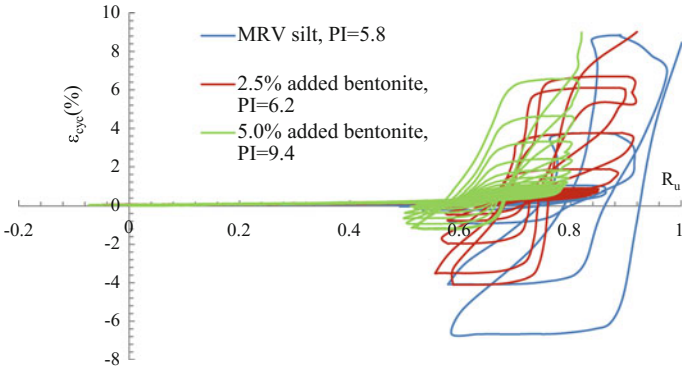

Fig. 4.6 Cyclic axial strain versus excess pore pressure ratio for different soils with a CSR of 0.18
Note Positive value of ε_{cyc} indicates that the specimen is under compression, negative value of that indicates that the specimen is under extension

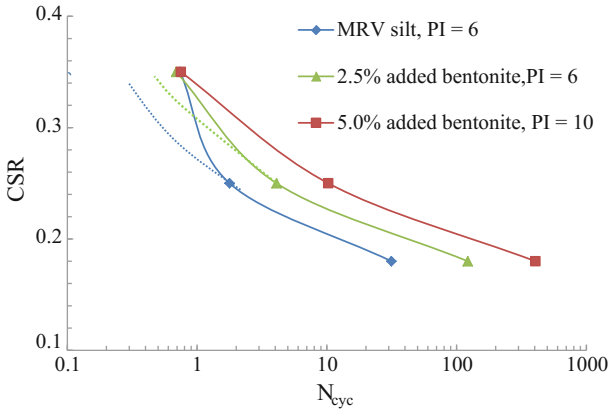

Fig. 4.7 Variation in liquefaction resistance with PI of the MRV silt/bentonite mixtures

This agrees with the finding by Guo and Prakash (1999), who examined the silt testing data by El Hosri et al. (1984). They presented that the liquefaction resistance increases with a decrease in PI in the low range, while the opposite is true in the high range of PI. The PI at the lowest liquefaction resistance is around 4. When the CSR was equal 0.35, there was no significant difference in the number of loading cycles required for cyclic failure of MRV silt regardless of PI, as shown in Fig. 4.7. With the CSR ranged from 0.25 to 0.35, the curves of CSR versus the number of loading cycle for the soil with bentonite added were expected to be like the dashed lines in Fig. 4.7. The non-ideal cyclic shear strength curves at high CSR were probably related to the transmission of pore pressure in specimens with high PIs.

4.3 Reexamination of Laboratory Data

4.3.1 Collection of Laboratory Data

Table 4.2 summarizes the laboratory data from some researchers, who conducted cyclic triaxial (CTX) or cyclic direct simple shear (CDSS) tests to evaluate liquefaction resistance of low-plasticity fine-grained soils under different testing conditions. Table 4.2 only lists the testing data when the cyclic failure was defined using double axial strain of 5%, shear strain of 3.75%, or single axial strain of 3%. They were considered to yield comparable testing results (Boulanger et al. 1998; Bray and Sancio 2006; Beroya et al. 2009). Cyclic failure defined by initial liquefaction ($R_u = 1$) can produce different results. For example, Puri (1984) found for loessial soils (PI = 10) that the 5 and 10% double amplitude axial strains developed before initial liquefaction, but the 20% double amplitude axial strain happened after that. Thus, to avoid the confusion from the criteria to define cyclic failure, the laboratory data of soils showing initial liquefaction were not considered here. In Table 4.2, the CSR is the cyclic stress ratio, defined as $\Delta\sigma/2\sigma'_c$ or $\tau/2\sigma'_{v0}$ ($\Delta\sigma$-deviator stress; effective consolidation pressure for cyclic triaxial tests; τ—shear stress; σ'_{v0}—vertical overburden pressure for cyclic simple shear tests) in the cyclic triaxial test and cyclic DSS test, respectively.

Besides the plasticity index, the factors influencing liquefaction resistance may include the following: shear mode, specimen preparation method, loading frequency, effective confining pressure, density, initial shear stress, and overconsolidation ratio, among others. To consider the effect of plasticity index on liquefaction resistance based on laboratory data, the cyclic strength of soils having different testing conditions needs to be normalized to that with the same testing conditions.

(1) Shear mode: CTX or CDSS tests are commonly conducted to investigate liquefaction resistance of soils. The stress path during the CDSS tests better simulates cyclic rotation of principal stresses during earthquake loading [97]. Seed [98] used the term C_r to relate CDSS and CTX testing results as $CSR_{CDSS} = C_r \times CSR_{CTX}$. Boulanger et al. (1998) recommended using $C_r = 0.7$ for several fine-grained soils under normal consolidation. Bray and Sancio (2006) suggested a C_r value of 0.8 for Adapazari silt. Hence, the use of a C_r value of 0.7–0.8 for fine-grained soils appears to be reasonable. In the current paper, a C_r of 0.75 was used to normalize CSR values obtained from CTX tests to equivalent CSR values based on CDSS tests.

(2) Specimen preparation: Laboratory tests can be performed on undisturbed specimens or specimens reconstituted using techniques such as slurry consolidation and moist tamping, among others. Bradshaw and Baxter (2007) reported that there is consensus that the specimens reconstituted by slurry consolidation (or deposition) approach have the most representative fabric for fluvial soils. Therefore, the slurry consolidation approach is best option to reconstitute specimens for laboratory tests, if undisturbed soil specimens are not available. Thus, the laboratory data in Table 4.2 were collected only from tests on

undisturbed specimens and reconstituted specimens prepared using slurry consolidation approach.

(3) Effective confining pressure: The cyclic strength normally increases with a decrease in effective confining pressure (Izadi 2008; Bray and Sancio 2006; Hynes and Olsen 1999; Riemer et al. 2008; Sağlam and Bakir 2014). Based on Hynes and Olsen (1999) and Bray and Sancio (2006), the factor of $K_\sigma = \left(\sigma'_{V0}/P_a\right)^{f-1}$ can be used to adjust the cyclic strength to that at effective confining pressure of 100 kPa (1 atm). The cyclic stress ratio (CSR) obtained from cyclic test at any effective confining pressure is multiplied with the K_σ to get the CSR at effective confining pressure of 100 kPa. The f values are about 0.8, 0.7 and 0.6, respectively for relatively loose, medium dense and dense or slightly overconsolidated deposits. Bray and Sancio (2006) found that the curve from the equation with f = 0.7 fitted well with laboratory data points of fine-grained soils in Adapazari, Turkey. In this study, the effect of effective confining pressure on cyclic strength was considered using the Hynes and Olsen's equation with f = 0.7.

(4) Density: The decrease in void ratio induces an increase in cyclic strength. Guo and Prakash (1999) assumed the CSR was inversely proportional to the void ratio. No other definitive equation has been presented to consider the effect of void ratio on the liquefaction resistance of low-plasticity fine-grained soil. Thus, in this study, the CSR for liquefaction evaluation was also considered to be inversely proportional to the void ratio, following the recommendation of Guo and Prakash (1999). For showing the effect of density on cyclic strength, it is best to normalize results by relative density. However, the maximum and minimum void ratios used for determining relative densities were not available for majority of studies in Table 4.2. Thus, all CSRs were converted to those at the void ratio of 0.600. As shown in the later, this chosen void ratio does not influence the conclusions which will be drawn in this study.

(5) Initial shear stress: Hyde et al. (2006) found that cyclic strength reduced with an increase in initial shear stress ratio for stress reversal; but for stress nonreversal, the cyclic strength reduced with an increase in the ratio up to 0.50–0.60 and kept increasing when the ratio exceeds 0.50–0.60. This book only considers level ground conditions where there is no effect of initial shear stress, and so the CTX tests with no initial shear stress were considered.

(6) Overconsolidation ratio: Puri (1984), Sandoval_Shannon (1989) and Izadi (2008) found that the increase of OCR increased the liquefaction resistance (cyclic strength) of the low-plasticity silt. The current work only collected the data from normally consolidated tests, since the data obtained from tests on overconsolidated specimens were very limited.

(7) Loading frequency: The increase in loading rate causes increase in the cyclic resistance of the silt (Sağlam and Bakir 2014). The CSRs were adjusted to be 1 Hz to more representative of earthquake loading and were normalized to include the effect of the strain rate using an average of 9% increase in CSR per

log cycle increase in rate, following the recommendation of Boulanger and Idriss (2007).

Table 4.2 collects testing data of the undisturbed specimens (Puri 1984; Bray and Sancio 2006; Wijewickreme and Sanin 2010; El Hosri et al. 1984; Wijewickreme et al. 2005) and the specimens reconstituted using slurry consolidation approach (Izadi 2008; Hyde et al. 2006; Khalili and Wijewickreme 2008; El Hosri et al. 1984). The PIs are in the ranges of 0–18 and 0–9.4, respectively for the undisturbed and reconstituted specimens. Because of too much testing data, Table 4.2 does not list them but only includes the range of each data range if available. As an example, Table 4.3 is given to show the raw CSRs and the CSRs after being normalized for the MRV silt.

4.3.2 *Variation of Liquefaction Resistance with Plasticity Index*

The cyclic stress ratios after being normalized were obtained and plotted with number of cycle (N_{cyc}) in Fig. 4.8. Some issues need to be explained here. There were no big differences in the curves of CSR versus N_{cyc} for the MRV silt and its mixtures with various percentage of kaolinite tested by Izadi (2008), because they had the same plasticity index of 6 regardless of different percentages of kaolinite. Thus, only one curve of CSR versus N_{cyc} was produced to fit all data points of the MRV silt and its mixtures (Izadi 2008). For the Adapazari soils investigated by Bray and Sancio (2006), there were two ranges of plasticity index: PI < 12 and 12 < PI < 18. To plot the curve of CSR versus plasticity index, the specific values need to be selected. The figure showing the Atterberg limits of the Adapazari soils by Bray and Sancio (2006) was reexamined. For PI < 12, the range was separated into two small ranges. The PI in the low range may be represented by 0, and in the high range the PI is scattered but relatively concentrates around 10. Thus, the range of PI < 12 was represented by two points of PI = 0 and 10. For the range of 12 < PI < 18, an average value of 15 was used.

Figure 4.8 indicates that the curves (dash) of CSR versus N_{cyc} for undisturbed soils are generally higher than those (solid) for reconstituted soils using slurry consolidation approach. Looking more closely, however, it can be found that the CSR for undisturbed soils were higher than that for reconstituted soils even at the same PI and N_{cyc}. This can be seen clearly in Fig. 4.9, which shows the values of CSRs required to induce cyclic failure at 30 loading cycles versus plasticity index. The cyclic shear strength of a natural deposit is often referred to an earthquake with a moment magnitude, $M_w = 7.5$, which is represented by 30 equivalent uniform loading cycles, N_{cyc} (Boulanger and Idriss 2007). As shown in Fig. 4.9, the undisturbed specimens have higher CSR than the reconstituted ones at the same PI.

Table 4.3 A study example including the raw CSRs and the CSRs after being normalized

Soil material	Soil type	LL	PI	Fines content (%)	Spec. prep.	Test type	f (Hz)	σ'_c or σ'_{v0} (kPa)	e	Cyclic failure criteria	N	Raw CSR	CSR	References
Mississippi river valley silt	ML	28.1	5.8	94.5	SC	TX	0.1	90	0.682	D.A. ε = 5%	0.78	0.35	0.315	Wang (2011)
								90	0.676		0.75	0.35	0.312	
								90	0.680		1.78	0.25	0.224	
								90	0.681		32.77	0.18	0.162	
								90	0.661		30.2	0.18	0.157	
								90	0.669		25.2	0.18	0.159	
								90	0.665		29.7	0.18	0.158	
		28.9	6.2	94.6				90	0.660		158	0.18	0.157	
								90	0.677		121	0.18	0.161	
								90	0.648		4.1	0.25	0.214	
								90	0.629		0.7	0.35	0.291	
	CL	32.7	9.4	94.8				90	0.690		405.2	0.18	0.164	
								90	0.688		10.3	0.25	0.227	
								90	0.685		0.8	0.35	0.316	

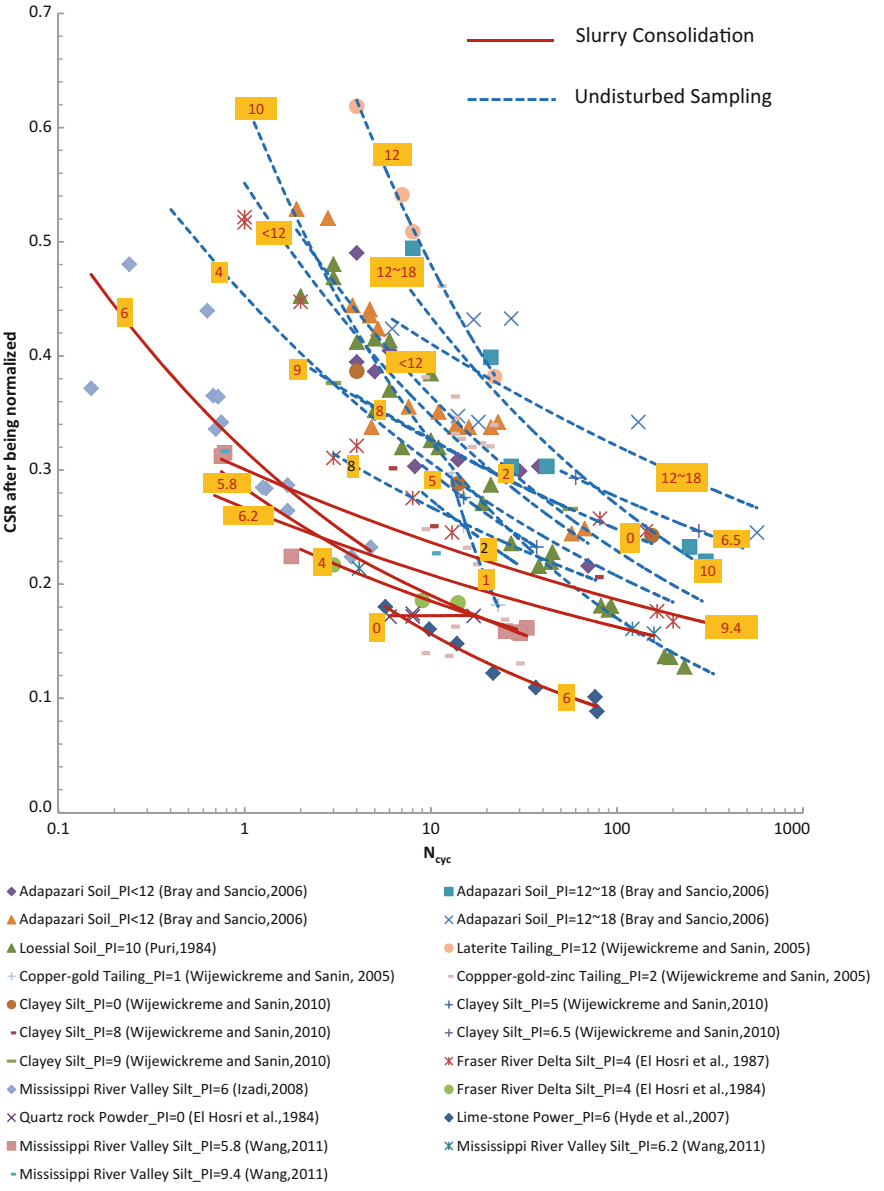

Fig. 4.8 Summary of relationships between CSR after being normalized and number of loading cycles of low-plasticity fine-grained soils (The numbers on the curves represent the values of plasticity index)

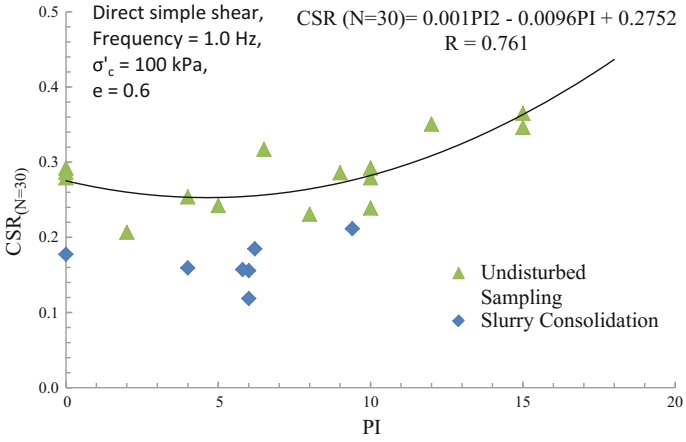

Fig. 4.9 Variation of $CSR_{(N=30)}$ with plasticity index for undisturbed and reconstituted specimens of low-plasticity fine-grained soils

Thus, although the specimen reconstituted using slurry consolidation approach best indicates soil fabric of undisturbed sample of low-plasticity soil (Bradshaw and Baxter 2007), the current study based on lots of laboratory data shows that the tests on soil specimens reconstituted using slurring consolidation approach still underestimate liquefaction resistance. Because of this, from here on, the study focuses on the undisturbed specimen results.

The data points of the undisturbed specimens were best-fitted using a parabola (the fitting accuracy R = 0.761). The effect of plasticity index on the CSR can be represented by the following equation:

$$CSR_{(N=30)} = 0.0010PI^2 - 0.0096PI + 0.2752 \tag{4.1}$$

When the PI is 4.8, the $CSR_{(N=15)}$ reaches the lowest value. With an increase in the PI up to 4.8, the $CSR_{(N=30)}$ decreases. With a further increase in the PI value larger than 4.8, the $CSR_{(N=30)}$ increases. When the CSR is normalized to other void ratios rather than 0.6, the best-fitted curves of $CSR_{(N=30)}$ versus PI were plotted in Fig. 4.10. It can be found that the PIs for lowest $CSRs_{(N=30)}$ are 4.8, 4.8, 4.6, 3.8 and 4.6, respectively when the void ratios used to normalize CSRs are 0.5, 0.6, 0.7, 0.8 and 0.9. Thus, low-plasticity fine-grained soil has lowest liquefaction resistance when its PI is about 4 $\sim$ 5. The above finding obtained from a comprehensive investigation using the collection of the extensive laboratory data happened to be similar to that by Guo and Prakash (1999) and Gratchev et al. (2006) who reported that the plasticity index for the minimum CSR was also about 4.

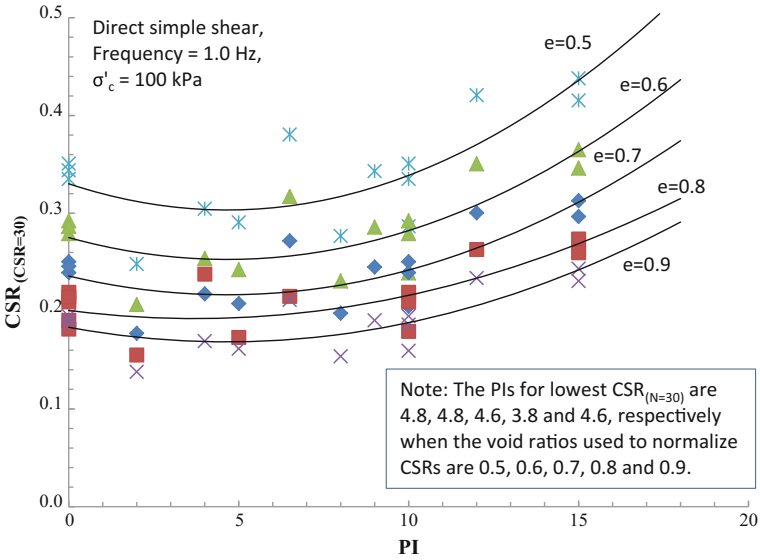

Fig. 4.10 Variation of $CSR_{(N=30)}$ with plasticity index for undisturbed specimens of low-plasticity fine-grained soils with different void ratios used for normalizing CSR data

4.3.3 Potential Application

For the claylike fine-grained soil with a plasticity index larger than 7 (reduced to 5, if CL-ML), Boulanger and Idriss (2007) presented Eq. (4.2) to evaluate liquefaction resistance, based on the finding that the cyclic strength can be expressed as a ratio of the soil's undrained shear strength (S_u).

$$CRR_M = C_{2D}\left(\frac{\tau_{cyc}}{S_u}\right)_{M=7.5}\frac{S_u}{\sigma'_{vc}}MSFK_\alpha \tag{4.2}$$

where, CRR_M is the cyclic resistance ratio at an earthquake with a magnitude of M; C_{2D} is a correction for two-dimensional versus one-dimensional cyclic loading; $(\tau_{cyc}/S_u)_{M=7.5}$ (or $(\tau_{cyc}/S_u)_{N=30}$) is the ratio of cyclic shear stress (τ_{cyc}) to S_u for 30 equivalent uniform cycles representative of an M_w = 7.5 earthquake; MSF is the magnitude scaling factor to approximately account for the correlation between earthquake magnitude and number of equivalent uniform loading cycles; K_α is the initial shear stress ratio correction factor. For specific number of loading cycles to evaluate liquefaction initiation, cyclic resistance ratio (CRR) is used instead in this section.

Although $\left(\tau_{cyc}/S_u\right)_{M=7.5} = 0.83$ was used for the claylike materials by Boulanger and Idriss (2007), they suggested that the continued compilation of laboratory test data can lead to future refinement. Actually, with a further

investigation by Boulanger and Idriss (2007), the natural silt (ML) has a lower $\left(\tau_{cyc}/S_u\right)_{M=7.5}$ than natural clays (CL & CH). The difference in $\left(\tau_{cyc}/S_u\right)_{M=7.5}$ between them was about 0.1. As stated by Boulanger and Idriss (2007), the available data was not sufficient to define the effect of the plasticity index, age, soil type, OCR, and test type on the value of τ_{cyc}/S_u at that time, therefore, the $\left(\tau_{cyc}/S_u\right)_{M=7.5}= 0.83$ was used in their work.

Until now, there has not been available chart to consider the effect of plasticity index on cyclic resistance ratio of low-plasticity fine-grained soils for engineering application. Equation (4.1) was presented based on extensive laboratory data of undisturbed specimens. It may be used to consider the effect of plasticity index when estimating the CRR for liquefaction resistance in engineering application.

Equation (4.1) is based on the fine-grained soils under the conditions of OCR = 1, σ'_v = 100 kPa and e = 0.6. Although some researchers found that cyclic resistance ratio increased with an increase in OCR (Puri 1984; Izadi 2008; Sandoval_Shannon 1989; Sağlam and Bakir 2014), no definitive relationship has been presented to consider the effect of OCR on the CSR. Thus, it will be impossible to predict the CRR of overconsolidated soils directly using Eq. (4.1). Equation (4.2) has been used by Boulanger and Idriss (2007) to do an evaluation of liquefaction resistance for Carrefour Shopping Center in Turkey during the 1999 Kocaeli earthquake. Therefore, it is recommended that the liquefaction evaluation be done using Eq. (4.2) with a consideration of the effect of plasticity index on liquefaction resistance shown in Eq. (4.1).

Following the recommendations of Boulanger and Idriss (2007), the low-plasticity fine-grained soils were divided into the claylike and sandlike soils to evaluate their liquefaction resistance. For the claylike fine-grained soil with a plasticity index larger than 7 (reduced to 5, if CL-ML), Boulanger and Idriss (2007) presented the following equation:

$$CRR_{M=7.5} = 0.18C_{2D}OCR^{0.8}K_{\alpha} \tag{4.3}$$

based on Eq. (4.2) to calculate the $CRR_{M=7.5}$ by considering the effect of OCR on the monotonic undrained shear strength with $S_u/\sigma'_{vc} = S \times OCR^m$(S = 0.22 and m = 0.8) and adopting $\left(\tau_{cyc}/S_u\right)_{M=7.5}= 0.83$. It is noted that the effect of effective confining pressure on CRR can be included in the S_u/σ'_{vc}.

To consider the effect of plasticity index, a coefficient of correction K_{PI} for claylike materials is proposed in this study and added into the equation as follows.

$$CRR_{M=7.5} = 0.18C_{2D}OCR^{0.8}K_{\alpha}K_{PI} \tag{4.4}$$

Because Eq. (4.3) was deduced by Boulanger and Idriss (2007) based on the natural silt (ML) and natural clays (CL & CH) with the PI values in the range of 10–27, the central value equal to 18.5 in the range was used to formulate the correction factor K_{PI} as follows.

$$K_{PI} = \frac{CRR}{CRR_{PI=18.5}} = \frac{0.0010PI^2 - 0.0096PI + 0.2752}{0.4399}$$

$$= 0.0023PI^2 - 0.0218PI + 0.6256 \quad - \quad \text{Claylike materials} \tag{4.5}$$

where, the $CRR_{PI=18.5}$ is the cyclic resistance ratio at the PI of 18.5 in Eq. (4.1). One of benefits of Eq. (4.5) is that the effect of void ratio on K_{PI} can be removed, because both the numerator (CRR) and the denominator ($CRR_{PI=18.5}$) in the equation should be multiplied by the same coefficient considering the effect of void ratio on CRR. Thus, Equation (4.5) can be used for any testing conditions. The equation was plotted in Fig. 4.11, the K_{PI} increases with an increase PI for claylike material with a PI higher than 7 (reduced to 5, if ML-CL). Since Eq. (4.1) was obtained based on the data of low-plasticity soil specimens with PI equal to 18 at maximum, it is required that Eq. (4.5) should only be used for the soil materials with PIs no greater than 18 to determine K_{PI} for considering the effect of plasticity index on cyclic strength.

For sandlike materials with PI up to 7 (reduced to 5, if ML-CL), the ratio of maximum CRR to minimum CRR at 30 loading cycles was calculated to be 1.02, according to Eq. (4.1). Thus, the effect of the PI up to 7 (reduced to 5, if ML-CL) on cyclic strength is slight and ignored when the frameworks of existing standard penetration test (SPT) and cone penetration test (CPT) is used for liquefaction evaluation. This is a little different with the suggestion by Ishihara (1993) for sandy soils, who stated that the plasticity index indicated little influence on liquefaction resistance at the plasticity index less than 10.

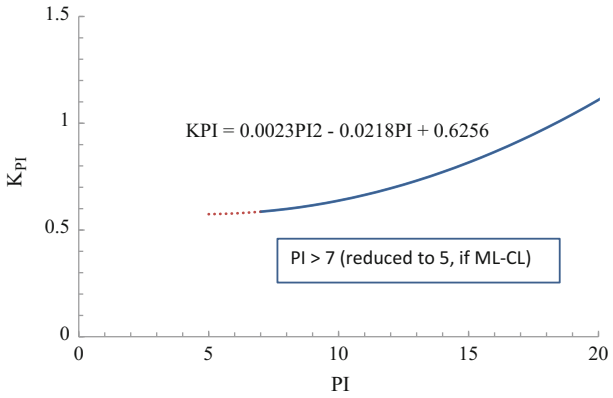

Fig. 4.11 Variation of K_{PI} against PI for claylike materials

4.4 Summary

The cyclic shear behavior of the MRV silt and its mixtures was first investigated. The liquefaction resistance increased as increase in overconsolidation ratio and decrease in effective consolidation stress. The MRV silt with bentonite added displayed cyclic softening behavior rather than initial flow liquefaction. With higher bentonite content more loading cycles were required to induce cyclic failure.

With a collection of extensive laboratory data, the CSRs obtained from different cyclic tests were corrected to the same testing conditions, and then the variation of CSR against number of loading cycles was plotted for different plasticity indexes. It was shown that the liquefaction resistance of the specimens reconstituted using slurry consolidation approach was lower than that of the undisturbed specimens. An equation was presented to show the effect of plasticity index on the liquefaction resistance of the low-plasticity fine-grained soils based on the laboratory data. The liquefaction resistance decreased with an increase in plasticity index less than 4–5 regardless of void ratio of test specimens. Beyond 4–5, it increased with a further increase in plasticity index.

Following the approach of Boulanger and Idriss (2007), the low-plasticity fine-grained soils were divided into the two types: claylike and sandlike materials. For the claylike materials with PI of 7–18 (change to 5–18, if ML-CL), the effect of plasticity index on cyclic stress ratio shown in Eq. (4.1) was combined with Eq. (4.3) for liquefaction evaluation. A correction factor K_{PI} was proposed to consider the effect of plasticity on liquefaction resistance. For sand-like materials with PI of 0–7 (changed to 0–5, if ML-CL), the frameworks of existing standard penetration test (SPT) and cone penetration test (CPT) based on liquefaction correlations can be used without considering the effect of plasticity index on cyclic strength, since the change of liquefaction resistance is slight when PI is up to 7 (reduced to 5, if ML-CL).

The proposed approach considers the effect of plasticity index on cyclic stress ratio was not verified, because no testing data are available to do that. However, so far, this idea is presented for a reasonable communication.

References

Beroya, M. A. A., Aydin, A., & Katzenbach, R. (2009). Insight into the effects of clay mineralogy on the cyclic behavior of silt-clay mixtures. *Engineering Geology, 106,* 154–162.

Boulanger, R. W., & Idriss, I. M. (2006). Liquefaction susceptibility criteria for silts and clays. *Journal of Geotechnical and Geoenvironmental Engineering, ASCE, 132*(11), 1413–1426.

Boulanger, R. W., & Idriss, I. M. (2007). Evaluation of cyclic softening in silts and clays. *Journal of Geotechnical and Geoenvironmental Engineering, 133*(6), 641–652.

Boulanger, R. W., Meyers, M. W., Mejia, L. H., & Idriss, I. M. (1998). Behavior of a fine-grained soil during the Loma Prieta earthquake. *Canadian Geotechnical Journal, 35,* 146–158.

Bradshaw, A. S., & Baxter, C. D. P. (2007). Sample preparation of silts for liquefaction testing. *Geotechnical Testing Journal, 30*(4), 1–9.

Bray, J. D., & Sancio, R. B. (2006). Assessment of the liquefaction susceptibility of fine-grained soils. *Journal of geotechnical and geoenvironmental engineering, 132*(9), 1165–1177.

El Hosri, M. S., Biarez, J., & Hicher, P. Y. (1984). Liquefaction characteristics of silty clay. In *Proceedings of the Eighth World Conference on Earthquake Engineering*. San Francisco, CA.

Gratchev, I. B., Sassa, K., & Fukuoka, H. (2006). How reliable is the plasticity index for estimating the liquefaction potential of clayey sands? *Journal of Geotechnical and Geoenvironmental Engineering, 132*(1), 124–127.

Guo, T., & Prakash, S. (1999). Liquefaction of silts and silt-clay mixtures. *Journal of Geotechnical and Geoenvironmental Engineering, 132*(6), 716–735.

Hyde, A. F. L., Higuchi, T., & Yasuhara, K. (2006). Liquefaction, cyclic mobility, and failure of silt. *Journal of Geotechnical and Geoenvironmental Engineering, 132*(6), 716–735.

Hynes, M. E., & Olsen, R. S. (1999). Influence of confining stress on liquefaction resistance. In *Proceeding of International Workshop on Physics and Mechanism of Soil Liquefaction* (pp. 145–152). Rotterdam, The Netherlands: Balkema.

Ishihara, K. (1993). Liquefaction and flow failure during earthquakes. *Geotechnique, 43*(3), 351–415.

Izadi, A. (2008). Liquefaction and post-liquefaction behavior of low plasticity silts using cyclic triaxial tests. *Ph. D. Dissertation*. Rolla, MO: Missouri University of Science and Technology.

Khalili, A., & Wijewickreme, D. (2008). New slurry displacement method for reconstitution of highly gap-graded specimens for laboratory element testing. *Geotechnical Testing Journal, 31*(5), 1–9.

Moriwaki, Y., Akky, M. R., Ebeling, R., Idriss, I. M., Ladd, R. S. (1982). Cyclic strength and properties of tailing slimes. In *Specialty Conference on Dynamic Stability of Tailings Dams* (Preprint 82–539). Reston, VA: ASCE.

Murthy, T. G., Loukidis, D., Carraro, J. A. H., et al. (2007). Undrained monotonic response of clean and silty sands. *Geotechnique, 57*(3), 273–288.

Puri, V. K. (1984). Liquefaction behavior and dynamic properties of loessial (silty) soils. *Ph. D. Disseratation*. Rolla, MO: University of Missouri.

Riemer, M., Moriwaki, Y., Obermeyer, J. (2008). Effect of high confining stresses on static and cyclic strengths of mine tailing materials. In *Geotechnical Earthquake Engineering and Soil Dynamics IV*. Geotechnical Special Publication, 181 (10 pg).

Sağlam, S., & Bakir, B. S. (2014). Cyclic response of saturated silts. *Soil Dynamics and Earthquake Engineering, 61–62,* 164–175.

Sandoval_Shannon, J. A. (1989). Liquefaction and settlement characteristics of silt soils. *Ph. D. Disseratation*. Rolla, Missouri, US: University of Missouri.

Seed, H. B., Idriss, I. M., & Arango, I. (1983). Evaluation of liquefaction potential using field performance data. *Journal of Geotechnical Engineering, 109*(3), 458–482.

Wang, S. (2011). Postcyclic Behavior of Low-plasticity Silt. *Ph.D. Dissertation*. Missouri University of Science and Technology, Rolla, MO, US.

Wang, S., Onyejekwe, S., & Yang, J. (2016). Reexamination of effect of plasticity on liquefaction resistance of low-plasticity fine-grained soils and its potential application. *Acta Geotechnica, 11*(5), 1209–1216.

Wijewickreme, D., & Sanin, M. (2010). Postcyclic reconsolidation strains in low-plastic fraser river silt due to dissipation of excess pore-water pressures. *Journal of Geotechnical and Geoenvironmental Engineering, 136*(10), 1347–1357.

Wijewickreme, D., Sanin, M.V., & Greenaway, G.R. (2005). Cyclic Shear Response of Fine-grained Mine Tailings. *Canadian Geotechnical Journal, 42*, 1408–1421.

Chapter 5
Postcyclic Compressibility of Low-plasticity Silt

This chapter investigates effect of cyclic loading on compressibility of low-plasticity silt. It reports the results of a laboratory investigation into the pre- and post-liquefaction consolidation characteristics of MRV silt, in which the permeability and its variation with soil plasticity are also evaluated. It should be noted that voids within the soil specimen are redistributed due to cyclic loading, and the specimen becomes less uniform (Amini and Trandafir 2008). Thus, the compressibility of the whole specimen rather than a portion of the specimen is compared with before and after liquefaction conditions.

5.1 Testing Program

Specimens (target dimensions: 71 mm diameter by 142 mm height) were prepared for triaxial tests using a slurry consolidation approach described in detail in Chap. 2. Each specimen was normally consolidated to an effective consolidation pressure (σ'_c) of 90 kPa. Specimens were tested under undrained conditions. Cyclic loading was applied until the desired excess pore pressure ratio (R_u) was attained. The R_u is the ratio of excess pore pressure (u_e) to effective consolidation pressure. For this study, the MRV silt is considered to have liquefied when $R_u = 1.0$. Cyclic loading, which was set by following a sine function, was applied at a frequency of 0.1 Hz rather than the predominant frequency for earthquake loading which is usually in the range of 1–5 Hz (Izadi 2008; Kramer 1996). The predominant frequency range (1–5 Hz) is too high for laboratory tests on low-plasticity silt. When cyclic loading is applied to low-plasticity silt in this frequency range, there is usually insufficient time for the transmission of the excess pore pressure from within the specimens to the pore pressure transducer. Taking cognizance of this fact, lower frequencies are generally used for low-permeability soils; 0.1 Hz in this case. Lefebvre and LeBoeuf (1987) and Boulanger et al. (1998) evaluated results from cyclic tests conducted at lower frequencies (<1 Hz) and recommended that whenever lower frequencies are

S. Wang, *Monotonic, Cyclic and Postcyclic Shear Behavior of Low-plasticity Silt*,
https://doi.org/10.1007/978-981-10-7083-9_5

used in the laboratory evaluation of resistance to liquefaction, the cyclic stress ratios (CSRs) be adjusted accordingly. The CSR is defined as the ratio of half the maximum deviator stress ($\Delta\sigma_{max}$) to the effective consolidation pressure. Considering that cyclic strength has been found to increase at about 9% per log cycle of the loading rate (Boulanger and Idriss 2007), the CSRs investigated in this study were 0.35, 0.25, 0.18 and 0.10. When the MRV silt specimens were liquefied, a single-amplitude axial strain was induced. In addition, for investigating effect of plasticity on postcyclic compressibility, the MRV silt-bentonite mixtures with added bentonite content of 2.5% and 5.0% were loaded cyclically. A 9% single amplitude axial strain was also generated for each specimen.

For studying the reconsolidation characteristics of MRV silt, after cyclic loading, a period of about 10 min was allowed for equilibrium of excess pore pressure within the specimen. During this period, excess pore pressure decreased by 5–10 kPa and the effective confining pressure (σ'_3) correspondingly increased by 5–10 kPa. Hence, at the start of reconsolidation, excess pore pressure was 80–85 kPa while the effective consolidation pressure (σ'_3) was 90 kPa before cyclic loading. Correspondingly, effective confining pressure (σ'_3) increased from a range of 5–10 kPa to 90 kPa during reconsolidation. Then, the drainage valves were opened to allow excess pore pressure to dissipate and the time rate of dissipation of excess pore pressure was recorded. To determine post-liquefaction compression and recompression indices, after effective confining pressure (σ'_3) attained a value of 90 kPa due to dissipation of excess pore pressure, extra consolidation pressure was incrementally applied on the specimen. Each increment of the pressure was 90 kPa. The pressure was added until the consolidation was finished on the specimen under the last effective consolidation pressure (Wang and Luna 2014).

5.2 Permeability

The permeability of MRV silt pre- and post-liquefaction was investigated to evaluate the effect of liquefaction on permeability. Permeability was determined using the expression (presented in Eq. 5.1) proposed by Terzaghi (1925) as cited in Holtz et al. (2011):

$$k = \frac{a_v \rho_w g c_v}{1 + e_0} \tag{5.1}$$

where, a_v is the coefficient of compressibility; ρ_w is the density of water; g is the acceleration of gravity; c_v is the coefficient of consolidation, and e_o is the initial void ratio. Permeability was evaluated for both pre- and post-liquefaction at an effective confining pressure (σ'_c) of 90 kPa. Admittedly, this expression was developed for one-dimensional (1-D) compression. However, specimens were consolidated under isotropic pressure and drainage was mostly 1-D. The permeability of pre-liquefaction MRV silt determined from 1-D oedometer consolidation

test was 8.603×10^{-7} cm/s while it was 5.83×10^{-7} cm/s under isotropic compression condition. Thus, as both values are within the same order of magnitude, the permeability of MRV silt determined from both the isotropic triaxial test and the 1-D oedometer test can be considered to be approximately equal. The authors did not investigate this difference any further. Notwithstanding the fact of the small difference in permeability values of MRV silt determined from the isotropic triaxial test and the 1-D oedometer test, the values determined from isotropic compression tests should be used with caution. It should be noted that these values were determined for the sole purpose of comparison of the pre- and post-liquefaction permeability of MRV silt specimens.

The pre-liquefaction permeability (k) and post-liquefaction permeability (k′) from seven tests run at CSRs of 0.18, 0.25 and 0.35 were determined and evaluated. Although various CSRs were adopted, the CSR had no effect on postcyclic behavior, as presented by Wang (2011). The results of the evaluation are presented in Fig. 5.1. The average of pre- and post-liquefaction permeability was 5.83×10^{-7} and 5.50×10^{-7} cm/s, respectively. Permeability essentially remained constant, indicating that cyclic loading had no significant effect on the permeability characteristics of the MRV silt. Figure 5.1 presents a plot of permeability before and after liquefaction. Figure 5.1 indicates that the variation (or spread of the data) of pre-liquefaction permeability (k) was more than that of post-liquefaction permeability (k′). The difference between the maximum permeability and the minimum permeability was greater for pre-liquefaction ($\Delta k = 2.85$ 10^{-7} cm/sec) than that for post-liquefaction ($\Delta k' = 0.88 \times 10^{-7}$ cm/sec). The smaller variation of k′ indicates a smaller change in the soil fabric or porosity among specimens after liquefaction. The application of cyclic loading on the specimens, leading up to liquefaction ($R_u = 1$), resulted in the rearrangement of the soil grains into similar micro-structural state and consequently led to similar permeability for the different specimens.

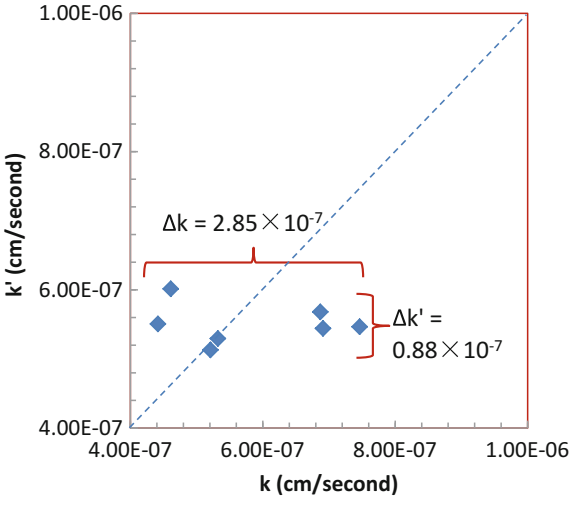

Fig. 5.1 Permeability of MRV silt before and after liquefaction

5.3 Compression and Recompression Indices

The normal consolidation line (NCL) during isotropic consolidation was used to show compressibility characteristics of the pre-liquefaction silt. The compressibility characteristics of the pre-liquefaction silt were presented in terms of the normal consolidation line (NCL) during isotropic consolidation. The plot of the void ratio, e-log σ'_3 relationship for pre- and post-liquefaction MRV silt is presented in Fig. 5.2. The pre-liquefaction compression index (C_c) and recompression index (C_r) was 0.0896 and 0.0090, respectively. In contrast, the slopes ($= -de/d\log\sigma'_3$) of the reconsolidation lines, being nearly parallel to the NCL, ranged from 0.0502 to 0.0604, much closer to C_c than C_r. Similar findings have been reported for silt and non-plastic silty materials by Thevanayagam et al. (2001) (for artificial soil mixtures of a sand and non-plastic silt) and Hyde et al. (2007) (for a powdered limestone [silt-sized particles = 69.2%, PI = 6]). It can be concluded that for sands and low-plasticity silts the post-liquefaction reconsolidation line tends towards being parallel to the compression line than the recompression line. However, as indicated by Yasuhara and Andersen (1991), Hyodo et al. (1994) and Hyde et al. (1997), the reconsolidation lines of clays and plastic silts are nearly parallel to their recompression lines. Thus, cyclic loading has more effect on the fabric change of low-plasticity soils than on that of high-plasticity soils.

The comparison of the compression and recompression indices of post- and pre-liquefaction MRV silt is presented in Fig. 5.3. In Fig. 5.3, the post-liquefaction compression and recompression indices are indicated by dashed lines. The data points in the reconsolidation stage (σ'_3 = 10–90 kPa) aligned well with the data points in the normal compression stage (σ'_3 = 90–360 kPa). This suggests that reconsolidation process is actually a process of compression rather than recompression. The post-liquefaction compression index (C'_c) and recompression index (C'_r) was 0.0589 and 0.0071, which were lower than the pre-liquefaction compression index (C_c) and recompression index (C_r), respectively. Therefore, whereas

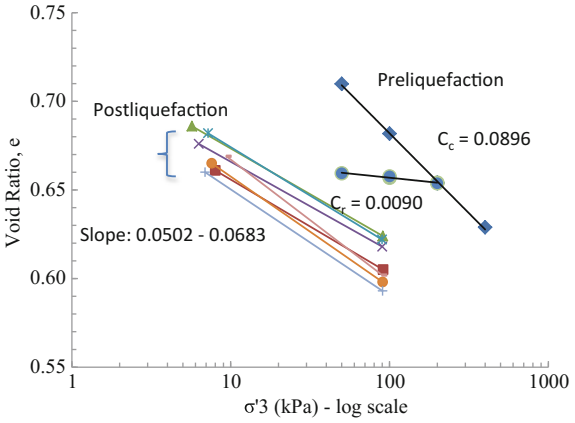

Fig. 5.2 Reconsolidation curves of MRV silt after full liquefaction

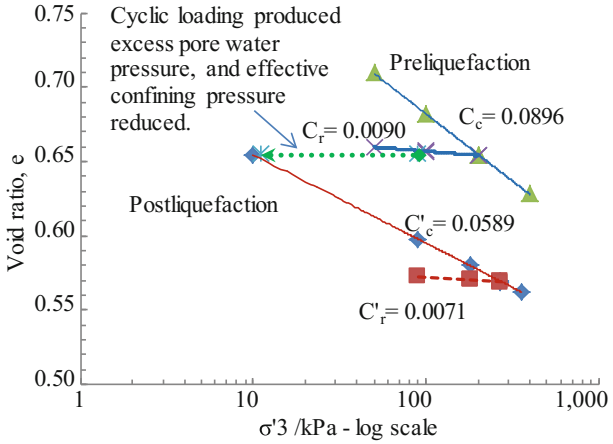

Fig. 5.3 Compression and recompression indices before and after liquefaction

the compressibility of MRV silt was improved (decreased) due to the liquefaction, its magnitude remained significant. The change in compressibility was mainly related to changes to the soil structure (fabric), besides grain size distribution and density. As presented in Fig. 5.4, the volumetric strain (4%) due to reconsolidation after liquefaction was low, indicating that the density did not change substantially. Thus, the small change in compressibility indicates that there was unsubstantial change in the soil structure.

5.4 Magnitude of Compressibility After Liquefaction

Liquefaction induces some settlement on soil mass, especially where there is an applied deviator stress, such as under foundations or on slopes. The volumetric strain or settlement induced by cyclic loading on the specimens was investigated for post-liquefaction consolidation tests. The results of this investigation are presented in Fig. 5.4 and Table 5.1. The axial displacement trajectories of a select specimen (MF1R2) show a maximum 9.8% strain (when R_u = 1.0) and an associated volumetric strain after liquefaction for this same specimen is also shown in Fig. 5.4. The summary of the volumetric strain induced on the liquefied specimens is presented in Table 5.2. Essentially, the contribution of the post-liquefaction compression (4%) is quite significant to ground settlement and it should be added to the deformations that will induce distress to the structure. The reconsolidation of typical silt in the New Madrid seismic zone may cause significant settlement after an earthquake event. When compared to the cyclic mobility threshold criteria of 3% single axial strain (Boulanger et al. 1998), the impact of the compression that occurs after liquefaction can be considered significant.

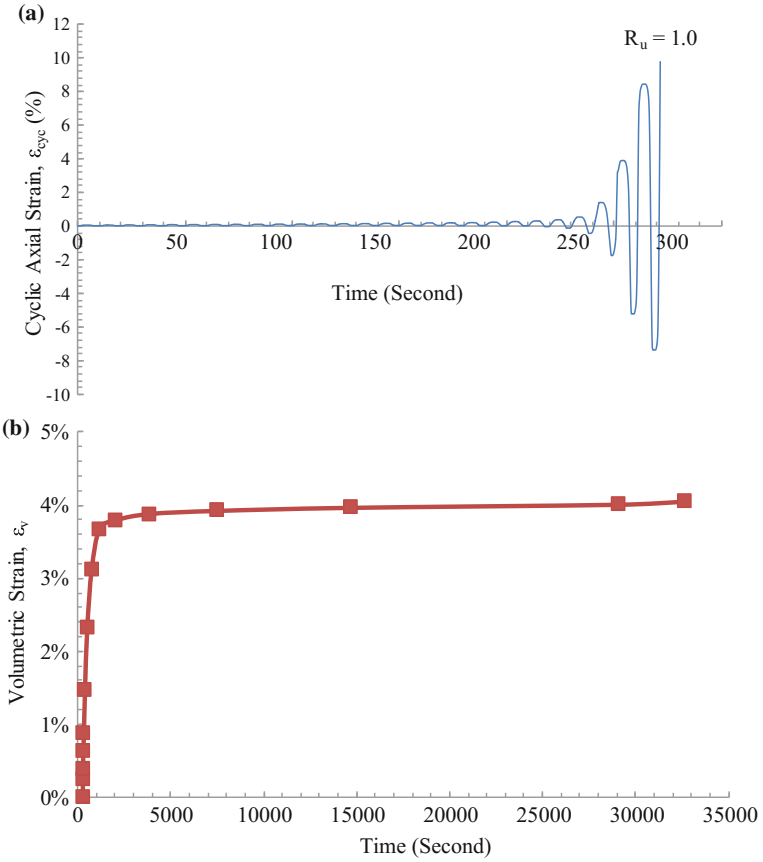

Fig. 5.4 Time history of axial strain to achieve $R_u = 1$ during cyclic loading and volumetric strain after liquefaction for selected specimen MF1R1: **a** axial strain versus time, **b** volumetric strain versus time

Table 5.1 Axial strain ($R_u = 1$) and volumetric strain after liquefaction

Test ID	CSR	ε_{cyc} (%)	ε_v (%)
MD2R	0.18	11.2	3.68
MD4	0.35	11.1	3.57
MD4R	0.35	11.4	3.45
MF1	<0.18	11.7	4.02
MF1R1	0.18	9.8	4.04
MF1R2	0.18	8.9	4.01

Table 5.2 Postcyclic consolidation parameters of MRV silt and its mixtures with bentonite

Item	Bentonite content		
	0%	2.5%	5.0%
PI	5.8	6.2	9.4
k′ (cm/s)	6×10^{-7}	9×10^{-8}	4×10^{-8}
C'_c	0.059	0.072	0.116

5.5 Effect of Plasticity on Postcyclic Compressibility

Figure 5.5 (σ'_m—mean effective stress) shows the reconsolidation curves of MRV silt with added bentonite. Taking the natural silt as an example (Fig. 5.5a), the ratio of compression index (C_c) to slope of reconsolidation is equal to 1.62 in average, and the ratio of slope of reconsolidation to recompression index (C_r) is equal to 6.14. Thus, the slope of reconsolidation is closer to the C_c, and the reconsolidation lines have similar slopes to their respective compression lines. As in the case of the natural MRV silt, the reconsolidation curves for the soil mixtures of MRV silt and bentonite have similar slopes to their compression lines than to their recompression lines. Thus, MRV silt and its mixture with bentonite were remolded during cyclic loading and behaved more like freshly deposited soils.

Table 5.2 shows the postcyclic permeability (k′) and compression index (C'_c). As shown in Fig. 5.6, they were each divided by precyclic permeability (k) and precyclic compression index (C_c) to obtain the permeability and compression index ratios (k′/k and C'_c/C_c), which show the changes in permeability and compressibility, respectively, due to cyclic loading. Figure 5.6 indicates that the k′/k and C'_c/C_c were lower than 1.0; therefore, the permeability and compressibility of the soils were reduced due to cyclic loading. Further, the reductions in permeability and compressibility of the soil mixtures of MRV silt and bentonite were greater than those of the natural MRV silt. As indicated in Fig. 5.6a, the reduction of permeability and compressibility due to reconsolidation after cyclic loading was not a big difference between the soil mixtures with bentonite contents added of 2.5% and 5.0%. For showing the effect of PI on reduction of permeability and compressibility, the values of Atterberg limits with tenths were used to plot the change of reduction of permeability and compressibility with the PI in Fig. 5.6b. With small change in PI around 6, the k′/k and C'_c/C_c decreased sharply. However, they did not change significantly with higher PI.

5.6 Summary

The liquefaction resistance and postcyclic reconsolidation characteristics of MRV silt were investigated using cyclic triaxial compression tests. MRV silt (PI = 5.8) reached liquefaction ($R_u = 1$), and a relationship of CSR versus N_{cyc} was reported.

Liquefaction had no significant effect on the magnitude of permeability. However, cyclic loading appears to remold the specimens. Compared to pre-liquefaction specimens, the permeability of post-liquefaction specimens showed less scatter; they fell within a narrow range.

The reconsolidation process of post-liquefaction specimens was similar to a process of compression rather than recompression. Compared to the pre-liquefaction compression and recompression indices, MRV silt became less compressible in reconsolidation. However, the degree of the compressibility of the

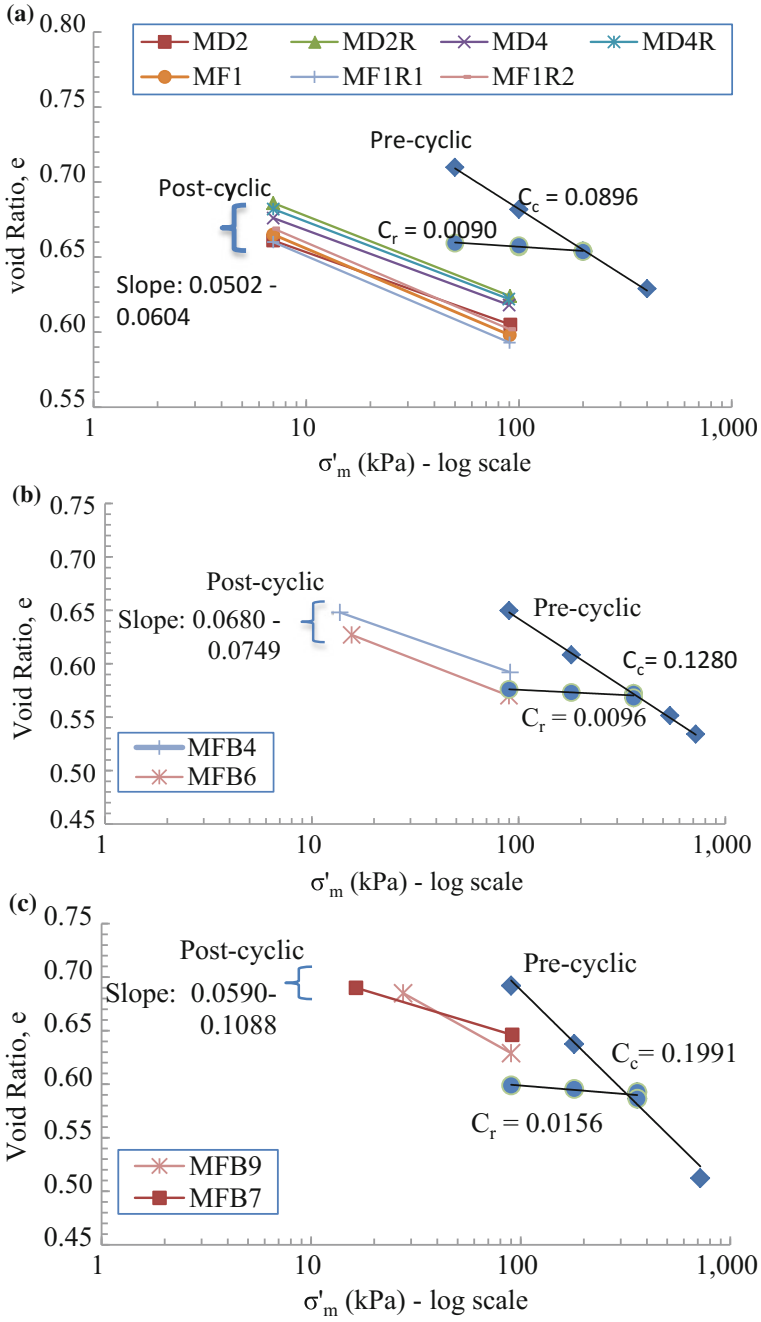

Fig. 5.5 Reconsolidation curves of MRV silt and its mixture with bentonite: **a** 0% added bentonite, **b** 2.5% added bentonite, **c** 5.0% added bentonite

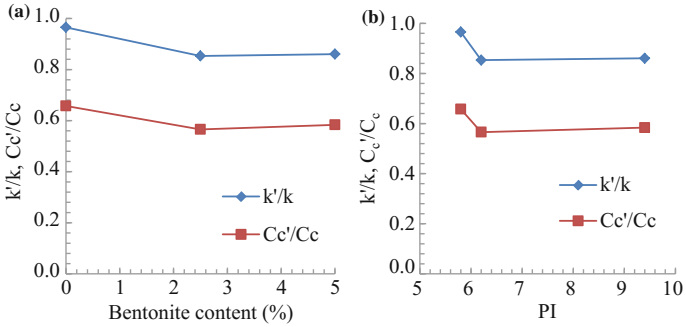

Fig. 5.6 Variation of normalized permeability and compression index with bentonite content and PI of the MRV silt/bentonite mixtures: **a** k′/k, C'_c/C_c versus bentonite content, **b** k′/k, C'_c/C_c versus PI

specimens remained significant. Due to the excess pore pressure generated by liquefaction, the specimen produced significant volumetric strain of about 4%.

The post-liquefaction reconsolidation characteristics of MRV silt indicate that the performance of infrastructure supported on the silt, from the compressibility point of review, remains a concern. MRV silt studied herein was obtained near the NMSZ and it is evident that a high risk of damage related to earthquakes M > 7.0 continues in this seismic zone (Elnashai et al. 2009). Hence, transport infrastructure, including embankments, within the NMSZ may perform poorly due to liquefaction during an earthquake and reconsolidation after the earthquake.

The MRV silt and its mixture with bentonite had reconsolidation curves with similar slopes to their compression lines than to their recompression lines. Thus, due to cyclic loading, the postcyclic MRV silt/bentonite mixtures behaved more like freshly deposited soils after they were remolded. However, cyclic loading reduced permeability and compressibility, because the specimens became denser after reconsolidation. With bentonite added, the cyclic loading induced reductions in the permeability and compressibility of the soil mixtures when other testing conditions were the same. Thus, the soil mixture with bentonite had more "memory" of its previous stress history and was less easily remolded. Nevertheless, there was no apparent effect of PI on the changes in permeability and compressibility due to cyclic loading based on the available test data.

References

Amini, Z. A., & Trandafir, A. C. (2008). Post-liquefaction shear behavior of Bonneville Silty-Sand. In *Geotechnical earthquake engineering and soil dynamics*. Geotechnical Special Publication, ASCE, No. 181.

Boulanger, R. W., & Idriss, I. M. (2007). Evaluation of cyclic softening in silts and clays. *Journal of Geotechnical and Geoenvironmental Engineering, 133*(6), 641–652.

Boulanger, R. W., Meyers, M. W., Mejia, L. H., & Idriss, I. M. (1998). Behavior of a fine-grained soil during the Loma Prieta earthquake. *Canadian Geotechnical Journal, 35,* 146–158.

Elnashai, A.S., Jefferson, T., Fiedrich, F., Cleveland L.J., & Gress, T. (2009). *Impact of New Madrid Seismic Zone earthquakes on the Central USA* (MAE Center Report No. 09-03) Mid-America Earthquake Center, University of Illinois, Urbana, Illinois, USA.

Holtz, R. D., Kovacs, W. D., & Sheahan, T. C. (2011). *An introduction to geotechnical engineering*. Englewood Cliffs, NJ: Prentice-Hall, Inc.

Hyde, A. F. L., Higuchi, T., & Yasuhara, T. (2007). Postcyclic recompression, stiffness, and consolidated cyclic strength of silt. *Journal of Geotechnical and Geoenvironmental Engineering, 133*(4), 416–423.

Hyde, A. F. L., Marto, A., & Yasuhara, K. (1997). Volumetric compression of periodically loaded silt. In *Proceeding of International Symp. on Deformation and Progressive Failure in Geomechanics*, Pergamon, London, 629–634.

Hyodo, M., Yamamoto, Y., & Sugiyama, M. (1994). Undrained cyclic shear behavior of normally consolidated clay subjected to initial static shear stress. *Soils and Foundations, 34*(4), 1–11.

Izadi, A. (2008). Liquefaction and post-liquefaction behavior of low plasticity silts using cyclic triaxial tests. *Ph.D. Dissertation*, Missouri University of Science and Technology, Rolla, MO, US.

Kramer, S. L. (1996). *Geotechnical earthquake engineering*. New Jersey: Prentice Hall.

Lefebvre, G., & LeBoeuf, D. (1987). Rate effects and cyclic loading of sensitive clays. *Journal of Geotechnical Engineering, 113*(5), 476–489.

Terzaghi, K. (1925). Erdbaumechanik auf Bodenphysikalischer Grundlage, Franz Deuticke, Leipzip und Wein.

Thevanayagam, S., Martin, G. R., Shenthan, T., & Liang, J. (2001). Post-liquefaction pore pressure dissipation and densification in silty soils. *Proceedings of 4th International Conference on Recent Advances in Geotechnical Earthquake Engineering and Soil Dynamics*. San Diego, CA.

Wang, S. (2011). Postcyclic behavior of low-plasticity silt. *Ph.D. Dissertation*. Missouri University of Science and Technology, Rolla, MO, US.

Wang S., Luna, R. (2014). Compressibility characteristics of low-plasticity silt before and after liquefaction. *Journal of Materials in Civil Engineering, 26*(6), 040140141-1 ~ 6.

Yasuhara, K., & Andersen, K. H. (1991). Recompression of normally consolidated clay after cyclic loading. *Soils and Foundations, 31*(1), 83–94.

Chapter 6
Postcyclic Shear Behavior of Low-plasticity Silt

This chapter reports postcyclic shear behavior characteristics of the MRV silt, both reconsolidated and not reconsolidated. The variation of postcyclic shear behavior of the silt with initial consolidation condition is addressed, and its postcyclic undrained monotonic shear strength is investigated for engineering applications. Additionally, the effects of plasticity and reconsolidation level on postcyclic shearing behavior are studied. The findings from the current research can advance the understanding of postcyclic undrained monotonic behavior of low-plasticity silt.

6.1 Testing Procedure

Cyclic triaxial tests of the MRV silt were carried out on specimens reconstituted using the slurry consolidation approach. The cyclic triaxial tests were conducted using an automatic pneumatic soil triaxial system. The specimens were prepared in a split vacuum mold on a special experimental setup and then moved to the triaxial platen. To assure the removal of any air bubbles and full saturation of the silt materials, approximately 45 kPa of vacuum ($<\sigma'_c$) was applied at the top and bottom of each specimen before back pressure was applied. Following the provisions of ASTM D4767-04 (2004), back pressure was increased until the Skempton B value remained constant and was at least 0.95 for each specimen. To evaluate the effect of σ'_c on postcyclic undrained monotonic shear behavior, the specimens were normally-consolidated under mean effective consolidation pressures of 90, 180 and 360 kPa. To evaluate the effect of initial OCR on postcyclic undrained monotonic shear behavior, overconsolidation was achieved by reducing σ'_c from OCR $\times$ 90 to 90 kPa. The initial OCRs investigated included 1, 2, 3 and 4. These low OCRs were adopted, because low OCRs silts develop liquefaction and cyclic mobility more easily than high OCRs silts. All specimens were consolidated istropically and no initial shear stress was applied.

S. Wang, *Monotonic, Cyclic and Postcyclic Shear Behavior of Low-plasticity Silt*,
https://doi.org/10.1007/978-981-10-7083-9_6

After consolidation, each specimen was subjected to deviator stress-controlled cyclic loading, as presented in Wang et al. (2015a, b, 2016). The cyclic stress ratios (CSRs) investigated from 0.18 to 0.40, for the two series of tests are presented in Table 6.1. The frequency of loading of the symmetrical cyclic stress was 0.1 Hz. The cyclic deviator stress was set following a sine function. Cyclic loading was stopped when the excess pore pressure ratio reached 1.0 ($R_u = 1.0$). The state of $R_u = 1.0$ has historically been referred to as "initial liquefaction" or "cyclic mobility". If the soil state is located on the right of critical state line (CSL) before cyclic loading, initial liquefaction is called when $R_u = 1.0$ due to cyclic loading; otherwise, cyclic mobility is called when $R_u = 1.0$ due to cyclic loading. The R_u here is defined on the basis of the transient excess pore pressure induced by cyclic loading. It should be noted that due to excess pore pressure equilibrium after cyclic loading, R_u may decrease and be slightly less than 1. After cyclic loading, the specimens were first subjected to two types of postcyclic procedures: (a) Fourteen specimens were fully reconsolidated, by opening the drainage valves on the triaxial chamber to enable complete dissipation of excess pore pressure; and (b) Four specimens were not reconsolidated, but were allowed to stand for a period of 5 min to achieve equilibrium of excess pore pressure.

Following the postcyclic processing of the specimens, the drainage valves were closed, and each specimen was then subjected to strain-controlled postcyclic undrained monotonic triaxial compression at a strain rate determined according to the time required for 50% reconsolidation after cyclic loading following the provisions of ASTM D4767-04 (2004). For purposes of clarity, particularly in the figures, the following symbology was used: "Recon" means the specimen(s) were reconsolidated after cyclic loading; "No_recon" means the specimen(s) were not reconsolidated after cyclic loading; and "No_cyc" means the specimen(s) were not previously subjected to cyclic loading.

To study effect of plasticity on postcyclic shear behavior, sodium bentonite was added to the MRV silt, and the properties of the soil mixtures can be found in Tables 3.1 and 3.2. The soil mixture specimens were loaded cyclically by single-amplitude axial strains of 9% which were equal to that of the MRV silt specimens when liquefied. Then, similarly with the MRV silt specimens, postcyclic shearing was conducted after the MRV silt-bentonite mixture specimens were reconsolidated or not. Table 6.2 lists the triaxial tests on the MRV silt and its mixtures with bentonite.

Additionally, to study effect of reconsolidation level on postcyclic shear behavior, the specimens were reconsolidated to various degrees ($U_r = 0$, 30, 60 and 100%) after the specimens were liquefied. The process of reconsolidation was monitored until the desired degree of reconsolidation is attained. The corresponding reconsolidation time for the various degrees of reconsolidation were determined by monitoring the full reconsolidation of several specimens, as indicated in Fig. 6.1. Then, the postcyclic undrained compression was conducted by displacement-controlled shearing. The deformation rate was computed according to the time required for 50% reconsolidation according to the ASTM standard D4767. The postcyclic triaxial test results are summarized in Table 6.3. The main testing procedures are indicated via stress paths in Fig. 6.2.

Table 6.1 Summary of triaxial tests on MRV silt specimens

Test ID	σ'_c (kPa)	OCR	e	D_r (%)	CSR	N_{liq}	e′	D'_r (%)	ε_v (%)	$S_{u,m}$ (kPa)	ψ
Reconsolidated after cyclic loading											
MD3	90	1	0.68	79.1	0.25	3.2	–	–	–	–	–
MD4	90	1	0.676	79.5	0.35	1.2	0.618	84.4	3.44	226	−0.028
MF1R1	90	1	0.66	80.8	0.18	28.2	0.593	86.6	4.05	223	−0.053
MF1R2	90	1	0.669	80.1	0.18	31.1	0.602	85.8	4.01	218	−0.044
MLO1	90	2	0.641	82.4	0.18	500	–	–	–	–	
MLO2	90	2	0.647	81.9	0.35	5.1	0.588	87.0	3.57	385	−0.058
MLO4	90	2	0.637	82.8	0.25	58.1	0.576	88.0	3.67	400	−0.070
MLO3	90	3	0.636	82.9	0.35	12.1	0.592	86.6	2.69	–	
MLO6	90	3	0.625	83.8	0.25	386.2	0.581	87.6	2.75	467	−0.065
MLO7	90	3	0.622	84.1	0.4	8.1	0.574	88.2	2.99	507	−0.072
MLO5	90	4	0.615	84.7	0.35	22.1	0.572	88.4	2.69	536	−0.074
MLO8	90	4	0.611	85.0	0.4	8.1	0.577	87.9	2.16	535	−0.069
MLN2	180	1	0.646	82.0	0.18	9.1	0.58	87.7	3.98	–	–
MLN1	360	1	0.627	83.6	0.18	5.1	0.553	90.0	4.51	–	–
Not reconsolidated after cyclic loading											
MF4	90	1	0.659	80.9	0.18	28.1	0.659	80.9	–	48	0.005
MLO9	90	2	0.636	82.9	0.35	4	0.636	82.9	–	71	−0.018
MLO10	90	3	0.632	83.2	0.35	15.1	0.632	83.2	–	105	−0.022
MLO11	90	4	0.608	85.3	0.35	24.1	0.608	85.3	–	150	−0.046

Note D_r—relative density before cyclic loading; N_{1iq}—number of loading cycles required to induce liquefaction; e′—void ratio after reconsolidation; D'_r—relative density after reconsolidation; $S_{u,m}$—measured undrained shear strength of liquefied silt; ψ—state parameter computed based on CSL of postcyclic specimens

Table 6.2 Triaxial tests on the MRV silt and its mixtures with bentonite

Test ID	PI	σ'_c (kPa)	Void ratio, e	Cyclic shearing			Reconsolidation		(Postcyclic) shearing	Note
				CSR	R_u	N_{cyc}	U_{rc} (%)	e′	Strain rate (%/min)	
MS2	5.8	90.0	0.669						0.1	Static
MD2		91.1	0.661	0.18	1	35.2				Cyclic
MD3		91.2	0.670	0.25	1	3.2				
MD4		90.8	0.676	0.35	1	1.2				
MF1R2		89.9	0.669	0.18	1	31.1	100	0.602	0.1	Cyclic and postcyclic shearing
MF4		90.3	0.659	0.18	1	18.1	0	0.659	0.1	
MF5		90.2	0.655	0.18	1	45.2	NA	0.566	NA	Cyclic and recon.
MSB3	6.2	90.0	0.665						0.01	Static
MFB4		91.2	0.658	0.18	0.92	160	100	0.591	0.01	Cyclic and postcyclic shearing
MFB5		90.4	0.675	0.18	0.86	89.2	0	0.675	0.01	
MFB6		90.6	0.660	0.35	0.78	1.1	NA	0.569	NA	Cyclic and recon.
MFB7	9.4	90.0	0.688						0.004	Static
MFB7		91.2	0.690	0.18	0.82	407	100	0.646	0.004	Cyclic and postcyclic shearing
MFB8		91.3	0.678	0.25	0.64	12.1	0	0.678	0.004	
MFB9		91.3	0.685	0.35	0.55	1.2	NA	0.574	NA	Cyclic and recon.

Note U_{rc} is reconsolidation level, and e′ is void ratio after reconsolidation

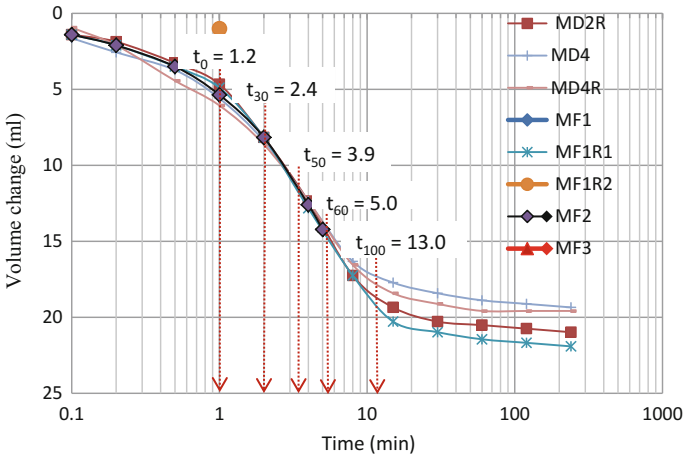

Fig. 6.1 Time required to reach various reconsolidation levels after liquefaction (e.g., t_{30} indicates time for 30% reconsolidation)

Table 6.3 Summary of all postliquefaction triaxial compression tests on normally consolidated MRV silt

Test ID	σ'_c (kPa)	e	CSR	ε_{cyc} (%)	U_r (%)	e′	ε_v (%)
MD2R	90.8	0.681	0.18	11.2	100	0.624	3.39
MD3	90.0	0.680	0.25	11.8	NA	NA	NA
MD4	90.0	0.676	0.35	11.1	100	0.618	3.46
MF1	90.6	0.665	<0.18	11.7	100	0.598	4.02
MF1R1	90.4	0.660	0.18	9.8	100	0.593	4.04
MF1R2	89.9	0.669	0.18	8.9	100	0.602	4.01
MF2	90.7	0.657	0.18	11.3	60	0.615	2.53
MF3	90.5	0.663	0.18	14.5	30	0.637	1.56
MF4	90.3	0.659	0.18	11.5	0	0.659	0.00

Note σ'_c—effective consolidation pressure, e—void ratio after consolidation, CSR—cyclic stress ratio, ε_{cyc}—cyclic axial strain, U_r—degree of reconsolidation, e′—void ratio after reconsolidation, ε_v—volumetric strain, NA—not available

6.2 Effect of CSR on Postliquefaction Shear Behavior

The effect of CSR on the postcyclic monotonic shear behavior of the MRV silt is addressed herein. As indicated in Tables 6.1 and 6.3, specimen MF1 with a CSR of less than 0.18 took 66.2 cycles of loading to liquefy; specimens MF1R1 and MF1R2, both with CSRs of 0.18, required an average of 29 cycles to liquefy; and specimen MD4 with a CSR of 0.35 required only one cycle to liquefy. All specimens induced identical excess pore pressures of about 90 kPa to achieve liquefaction. However, the development of cyclic axial strain (ε_{cyc}) at the end of cyclic

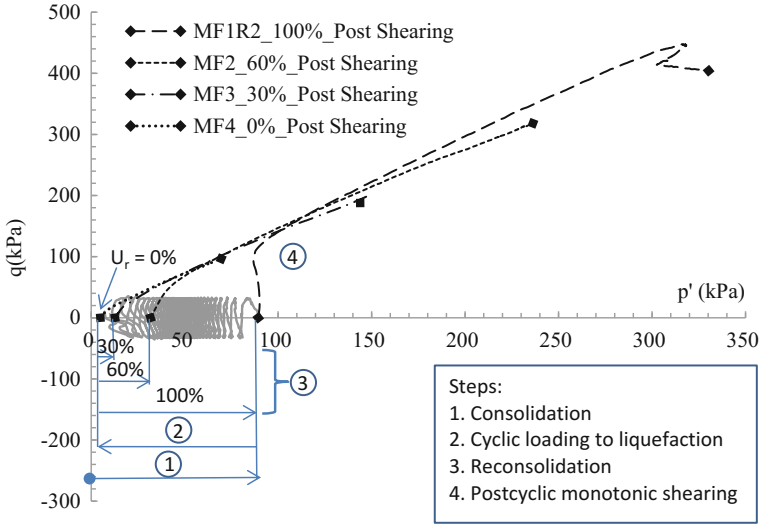

Fig. 6.2 Testing procedure shown as stress paths

loading varied slightly, and there was no obvious relationship between cyclic strain and CSR. Figure 6.3 shows the postcyclic behavior of all four specimens. For specimens with different CSRs, the results of postcyclic shear tests produced curves demonstrating that deviator stress, excess pore pressure, and stress path were similar among all specimens. Thus, the CSR has no significant effect on the postcyclic shearing behavior of MRV silt.

Table 6.3 also shows the volumetric strain due to the reconsolidation after full liquefaction. Specimen MD4 had a slightly smaller volumetric strain than others, but the difference was not large. This observation was similar to that of sand tested by Chern and Lin (1994). Chern and Lin (1994) carried out postcyclic consolidation tests on loose, clean sand and silty sand and found that the reconsolidation volumetric strain was related to the residual pore pressure ratio developed during cyclic loading, regardless of the cyclic stress ratio or the number of loading cycles.

6.3 Shear Behavior of Postcyclic Specimens with Reconsolidation

6.3.1 Postcyclic Undrained Monotonic Shear Behavior

After cyclic loading, some specimens were fully reconsolidated by dissipating the excess pore pressure. In the reconsolidation process, specimens were densified, resulting in the development of volumetric strain (ε_v). The relationship between volumetric strain and pre-cyclic loading void ratio (e) of specimens (Fig. 6.4),

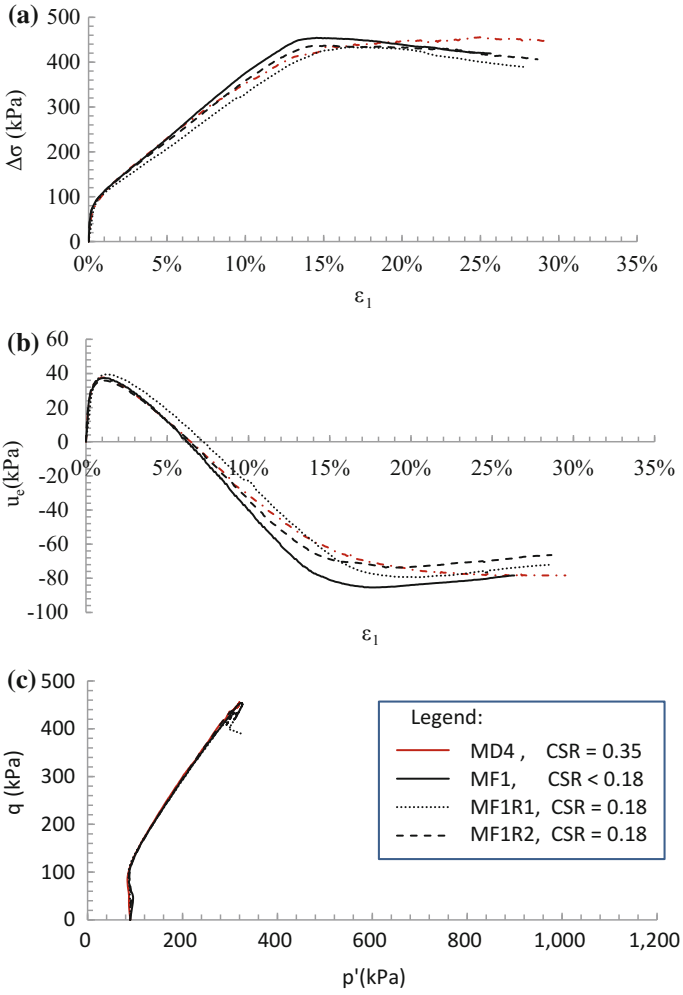

Fig. 6.3 Postliquefaction monotonic shear behavior of MRV silt with full reconsolidation with various CSRs: **a** $\Delta\sigma$ versus ε_1, **b** u_e versus ε_1, **c** q versus p′

shows a near linear correlation between ε_v and e. Volumetric strain increased with the increase in void ratio of specimens. The differences in void ratio were a result of the different previous stress histories of specimens before cyclic loading. As expected, a large volume change was recorded due to reconsolidation for specimens, which were in a less dense state before cyclic loading.

Figure 6.5 shows the monotonic shear behavior of all specimens reconsolidated after cyclic loading. The plots of deviator stress ($q = \sigma_1 - \sigma_3$) and excess pore pressure against axial strain (ε_a) (presented in Fig. 6.2a, b, respectively), were similar for all normally-consolidated specimens (OCR = 1) with different CSRs. Figure 6.5a shows no substantial difference in maximum deviator stress of

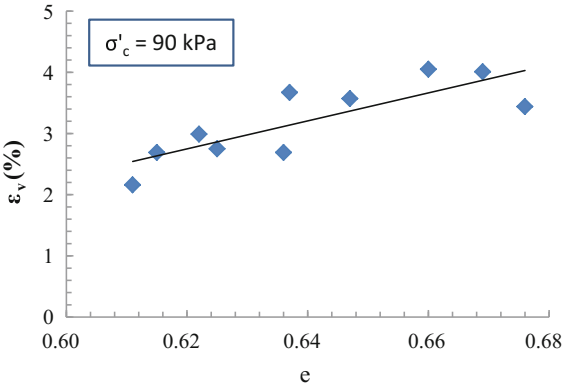

Fig. 6.4 Volumetric strain induced by reconsolidation after cyclic loading versus initial void ratio

specimens. There was a slight drop in deviator stress at larger axial strains for specimens MF1R1 and MF1R2 (CSRs = 0.18). Conversely, specimen MD4 (CSR = 0.35) showed no drop in deviator stress at larger axial strains, but also had a slightly higher (relative to other specimens) deviator stress at the end of tests. In Fig. 6.5b, the normally-consolidated specimens developed positive excess pore pressure (contraction tendency) initially, and then develop negative excess pore pressure (dilative tendency) when the axial strain exceeded about 6.5%. The dilative behavior can be explained using the state parameter (ψ), which is defined as the difference between the current void ratio and the void ratio at the same mean effective stress on the CSL (Been and Jefferies 1985). A negative ψ value is associated with dilative behavior; otherwise contractive behavior is shown in the soil. As shown in Fig. 6.5d, all data points of the reconsolidated specimens are on the left of the CSL, and so the values of ψ are negative and the specimens dilated. Figure 6.5b also shows the miniscule effect of CSR on excess pore pressure. Similar results were obtained for specimens with higher OCRs (2, 3, and 4), as shown in Figs. 6.5a, b. Thus, it can be concluded that CSR had no substantial effect on the postcyclic shear behavior of the MRV silt regardless of OCR, when liquefaction was induced. It should be noted that CSR will influence postcyclic undrained strength if liquefaction is not reached.

Figure 6.5c shows the stress paths for specimens reconsolidated after cyclic loading plotted on the Cambridge space, where mean principal effective stress, $p' = (\sigma'_1 + 2\sigma'_3)/3$, and deviator stress, $q = \sigma'_1 - \sigma'_3$. In Fig. 6.5c, all specimens with the same OCR had very similar effective stress paths (ESPs) at both the initial stages (start point at $p' = 90$ kPa) and the terminal stage (terminal points marked by squares, which indicates the end of monotonic loading), except those with OCR of 3, which had different terminal points. However, the differences in terminal points were small and considered to be within the limits of experimental error. A comparison of the total stress paths (slope = 1:3) and the ESPs, shows that all specimens contracted initially, resulting in the development of positive u_e and hence a reduction in p'. Subsequently, negative u_e developed after a short period of time, and the ESPs progressed almost along the failure line (i.e., K_f line) for MRV silt

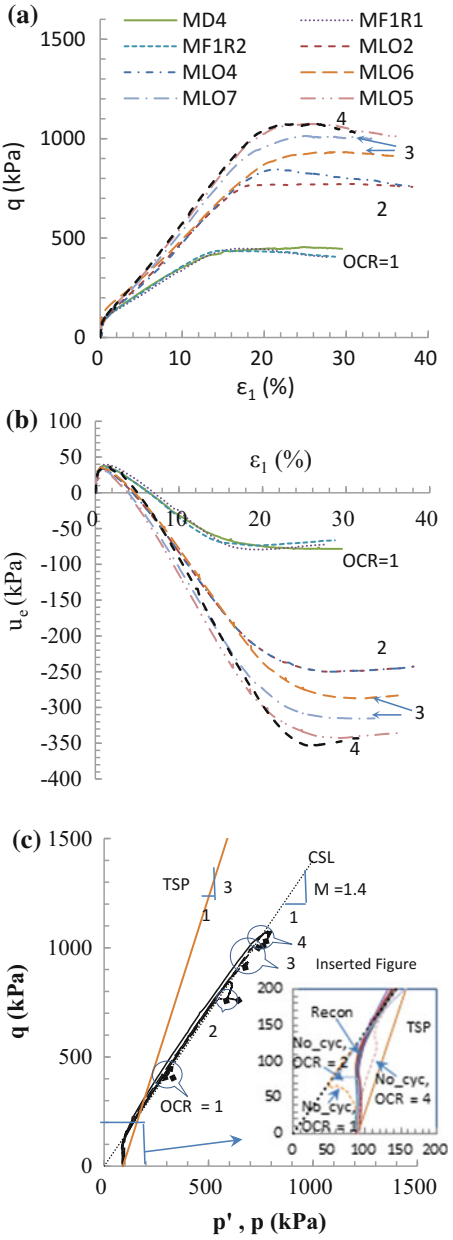

Fig. 6.5 Monotonic undrained shear behavior of the MRV silt specimens reconsolidated after cyclic loading: **a** q versus ε_1, **b** u_e versus ε_1, **c** q versus p′, p, **d** e versus p′ [$p' = (\sigma'_1 + 2\sigma'_3)/3$, $q = \sigma_1 - \sigma_3$]

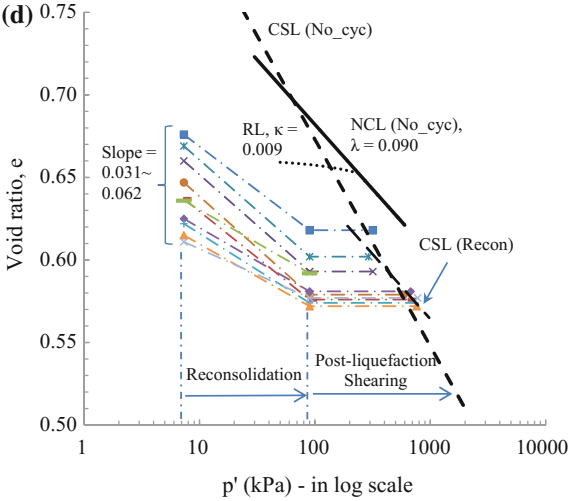

Fig. 6.5 (continued)

specimens not previously subjected to cyclic loading. The slope of the K_f line, M, of the MRV silt specimens not previously subjected to cyclic loading is 1.4 (see Chap. 3). Thus, the OCR of specimens had no effect on the ESP at the initial stages postcyclic shearing. This phenomenon of the reconsolidated specimens (represented by the symbol "Recon") was not observed for the specimens not previously subjected to cyclic loading (represented by the symbol "No_cyc"). The OCR had more influence on the stress paths of the specimens not previously subjected to cyclic loading. The ESPs of the specimens not previously subjected to cyclic loading presented in Chap. 3 and those of postcyclic loading specimens from this study are presented in the inserted figure in Fig. 6.5c. The figure does not show plots for OCR = 3 as that presented in Chap. 3 investigated the ESPs for specimens with OCRs of 1, 2, and 4 only. In contradistinction to postcyclic loading specimens, the specimens consolidated to different OCRs, not previously subjected to cyclic loading had different ESPs at the initial stages of shearing. For OCRs of 1 and 2, the postcyclic loading specimens had less positive excess pore pressure than the virgin specimens, and the postcyclic load specimens with OCRs of 1 and 2 contracted less than the virgin specimens. The opposite is true for the case with OCR of 4.

Figure 6.5d shows stress paths in *e-logp′* plane during both reconsolidation and postcyclic shearing. The critical state line (CSL) determined in Wang and Luna (2012) is also plotted in Fig. 6.2d. The slopes ($\Delta e/\Delta \log p'$) of the normal consolidation line (NCL, λ) and the recompression line (RL, κ), were determined as, 0.090 and 0.009, respectively. The slopes of the reconsolidation lines ranged from 0.031 to 0.062. Since the slopes of the reconsolidation process fall within the range of the NCL and RL slopes, the reconsolidation behavior was intermediate between recompression and virgin compression. The slope of reconsolidation line decreased with increase in the OCR. The average slopes of reconsolidation lines with OCR of

1, 2, 3 and 4 were 0.060, 0.058, 0.041 and 0.035, respectively. Thus, for the specimens with high OCR the reconsolidation process was more similar to recompression behavior. This is because the reconsolidated specimens with higher OCR are denser and it is also more difficult to remobilize their soil fabric. The end points of postcyclic shearing stress paths are located right of their respective start points in Fig. 6.5d. Thus, although the specimens contracted at the initial period of shearing, the specimens generally dilated. Owing to the fact that silt generally behaves somewhat like sand, the MRV silt CSL (slope of 0.125) is not parallel to its NCL (slope of 0.090) (see Chap. 3). The CSL of reconsolidated MRV silt (slope of 0.079) was different from that of MRV silt not previously subjected to cyclic loading although all stress path end points were located close to the CSL (see Fig. 6.5d). However, one should also consider that these CSLs were determined based on a best-fitted linear approach.

6.3.2 *Effect of OCR on Postcyclic Undrained Monotonic Shear Strength*

A summary of the postcyclic undrained shear strength of specimens is presented in Table 6.1. Undrained shear strength (S_u) is defined herein as one-half the deviator stress at critical state during shearing. The undrained monotonic shear strength of specimens not previously subjected to cyclic loading presented in Chap. 3 are adopted in this study for purposes of comparison. The comparison of undrained monotonic shear strength between reconsolidated postcyclic and the specimens not previously subjected to cyclic loading is presented in Fig. 6.6. Figure 6.6a shows the relationship between undrained monotonic shear strength and OCR, where strength increased with an increase of OCR for both the specimens reconsolidated after cyclic loading and those not subjected to cyclic loading. The undrained monotonic shear strengths of overconsolidated specimens ($S_{u,OC}$) for both pre- and postcyclic cases were normalized with respect to the undrained monotonic shear strengths of normally-consolidated specimen ($S_{u,NC}$) and their relationship with OCR is presented in Fig. 6.3b. Figure 6.3b also presents the pre-cyclic case (No_cyc) the data points of $S_{u,OC}/S_{u,NC}$ that have been be best-fitted using the following equation (Wang and Luna 2012):

$$S_{u,OC}/S_{u,NC}(\sigma'_c = 90\,\text{kPa}) = \text{OCR}^{0.58} \tag{6.1}$$

For the postcyclic case, the data points of $S_{u,OC}/S_{u,NC}$ can be best-fitted using the following equation:

$$S_{u,OC}/S_{u,NC}(\sigma'_c = 90\,\text{kPa}) = \text{OCR}^{0.68} \tag{6.2}$$

6.3.3 *Effect of σ'_c on Postcyclic Undrained Monotonic Shear Behavior*

Figure 6.7 presents the postcyclic shear behavior of normally-consolidated specimens reconsolidated after cyclic loading. Three different mean effective consolidation pressures (σ'_c = 90, 180 and 360 kPa) were investigated for the consolidation process. In Chap. 3, the normalized behavior of undrained monotonic shearing of MRV silt not previously subjected to cyclic loading (No_cyc) with OCRs of 1, 2, 4 and 8 was studied. This was done to investigate the possibility of normalizing the undrained monotonic shear behavior of specimens reconsolidated after cyclic loading with respect to mean effective consolidation pressure. The relationships of normalized deviator stress and normalized excess pore pressure with axial strain are presented in Fig. 6.7a, b, respectively. It is indicated that postcyclic shearing curves can also be normalized by the mean effective consolidation pressure.

As shown in Fig. 6.7a, the normalized deviator stress increased with increase in axial strain, unlike the case of undrained monotonic shear behavior of the specimens without previous cyclic loading. Normally-consolidated specimens of MRV silt not previously subjected to cyclic loading had a quasi-steady state during monotonic shearing (see Chap. 3). Figure 6.7a shows that during postcyclic

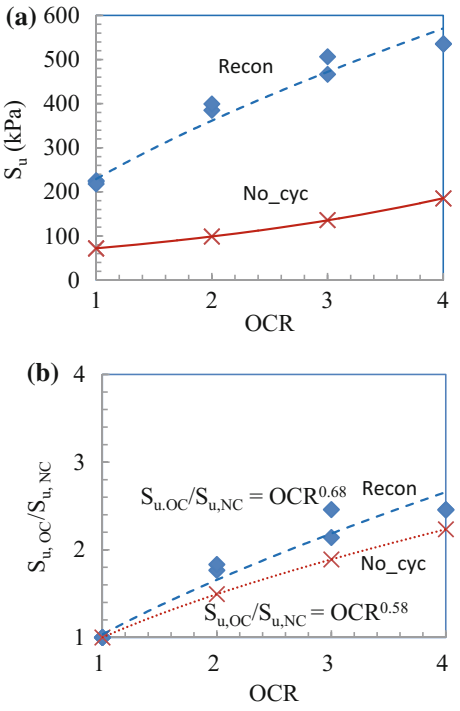

Fig. 6.6 Comparison of monotonic undrained shear strength of MRV silt specimens reconsolidated after cyclic loading with that of virgin MRV silt: **a** S_u versus OCR, **b** $S_{u,OC}/S_{u,NC}$ versus OCR

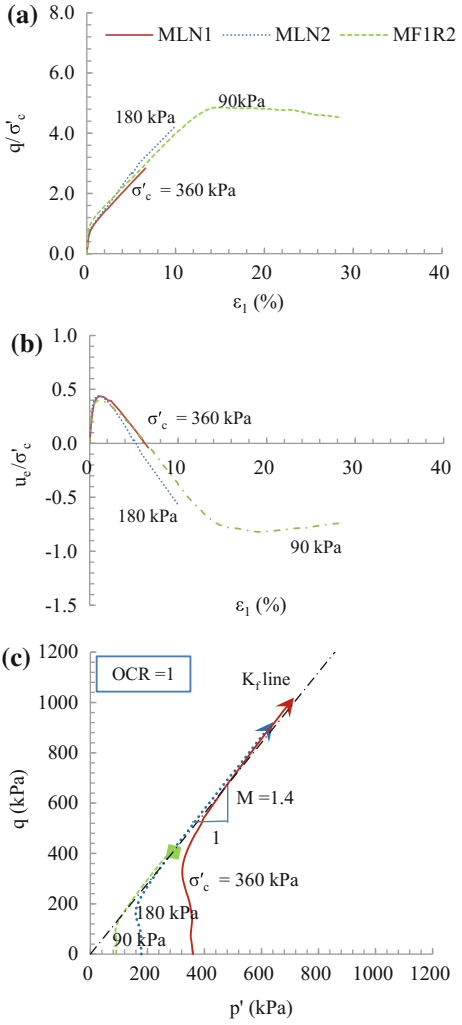

Fig. 6.7 Monotonic undrained shear behavior of the reconsolidated MRV silt specimens with different mean effective consolidation pressures: **a** q versus ε_1, **b** u_e versus ε_1, **c** q versus p′, p, **d** e versus p′ [$p' = (\sigma'_1 + 2\sigma'_3)/3$, $q = \sigma_1 - \sigma_3$]

undrained monotonic shearing at higher σ'_c, specimens had a higher deviator stress at identical ε_a. At the initial stages of postcyclic shearing, specimens contracted and produced positive excess pore pressure, the magnitude of which pressure was higher for reconsolidated specimens with a higher σ'_c (see Fig. 6.7b). At an axial strain of about 1%, the excess pore pressure reached its maximum positive value and started to decrease, and so the specimens became dilative. Due to the low capacity (4.9 kN) of the load cell for axial load, postcyclic shearing of specimens at σ'_c equal to 180 and 360 kPa had to be stopped before the specimens reached their critical state. The ESPs for specimens reconsolidated after cyclic loading are presented in Fig. 6.7c. These effective stress paths have their terminal points at the following magnitudes (MLN1, σ'_c = 360 kPa; MLN2, σ'_c = 180 kPa) whose

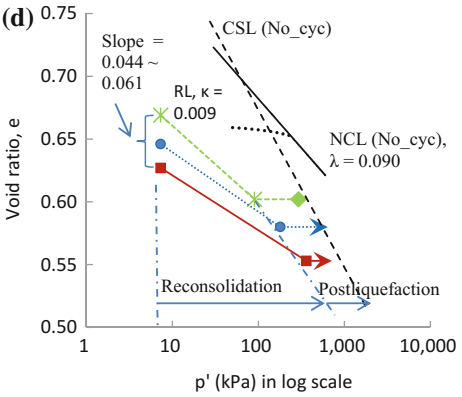

Fig. 6.7 (continued)

postcyclic shearing was terminated due to the capacity of load cell are marked by arrows. All normally-consolidated specimens would tend to contract slightly at the initial stages of shearing and then dilate subsequently along the K_f line.

Figure 6.7d shows the relationship between void ratio and p′. Since the normally-consolidated specimens (180 and 360 kPa) did not attain their respective critical states, it was impossible to evaluate whether their critical states are located close to the CSL of No_cyc specimens. The reconsolidation curve of normally consolidated specimen MF1R1 (σ'_c = 90 kPa), MLN2 (σ'_c = 180 kPa), and MLN1 (σ'_c = 360 kPa) has a slope of 0.061, 0.047, and 0.044. Thus, the reconsolidated process of normally consolidated specimen with higher initial effective consolidation pressure followed a recompression behavior, since it was denser.

6.4 Shear Behavior of Postcyclic Specimens without Reconsolidation

6.4.1 Postcyclic Undrained Monotonic Shear Behavior

Figure 6.8 shows monotonic shear behavior of all specimens not reconsolidated after cyclic loading. The relationship of the deviator stress against axial strain is presented in Fig. 6.8a. The deviator stress increased during shearing until critical state was reached. At the early stages of postcyclic shearing, effective confining pressure (σ'_3) was very low due to non-dissipation of excess pore pressure. Hence, the specimens not reconsolidated after cyclic loading dilated early and started to develop negative excess pore pressure at almost zero axial strain during the postcyclic monotonic shearing, as shown in Fig. 6.8b. This is in contradistinction to the excess pore pressure response of specimens reconsolidated after cyclic loading. A positive correlation between OCR and the deviator stress at failure of specimens

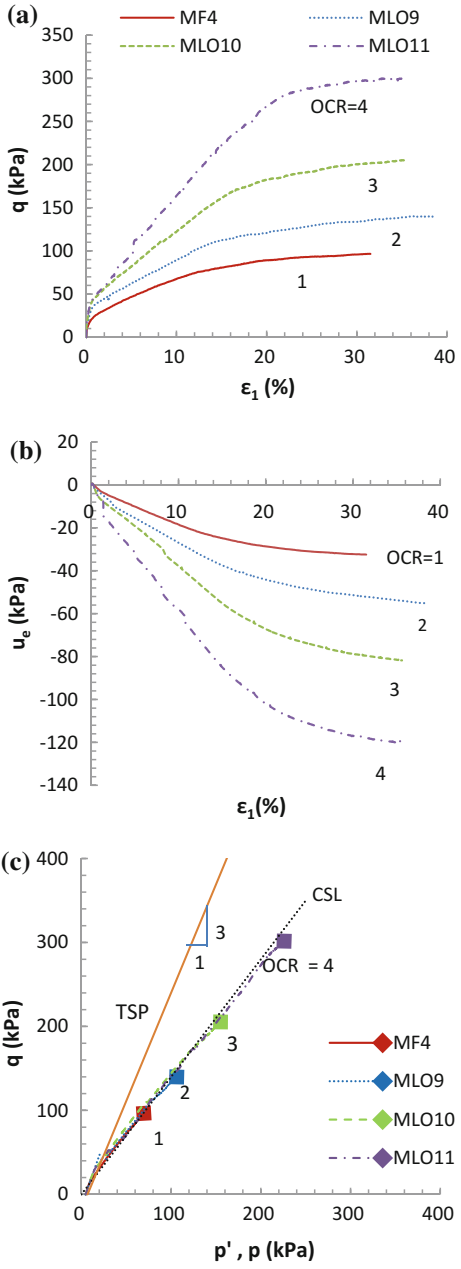

Fig. 6.8 Monotonic undrained shear behavior of postcyclic MRV silt specimens not reconsolidated: **a** q versus ε_1, **b** u_e versus ε_1, **c** q versus p′, p, **d** e versus p′ [$p' = (\sigma'_1 + 2\sigma'_3)/3$, $q = \sigma_1 - \sigma_3$]

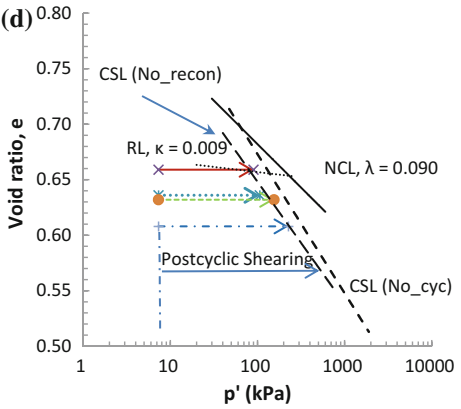

Fig. 6.8 (continued)

was indicated. Thus, the effect of densification of soil specimen due to overconsolidation before cyclic loading remained intact irrespective of cyclic loading. Specimens are thought to be significantly remolded by cyclic loading given R_u reached a value of 1.0 (Thevanayagam et al. 2001). Figure 6.8c shows stress paths of MRV silt specimens (initially consolidated to different OCRs) not reconsolidated after cyclic loading. All ESPs in Fig. 6.8d started at a low p′ (about 7 kPa). The specimens dilated early, resulting in negative σ'_c. The ESPs of specimens progressed very close to and along the K_f line.

Figure 6.8d shows stress paths in the *e-logp′* space during postcyclic shearing. Figure 6.8d shows that specimens tend to dilate; the stress paths moved towards the right but terminated before the CSL of the specimens not previously subjected to cyclic loading. Similar to the reconsolidated specimens, the CSL of the specimens not reconsolidated after cyclic loading (slope of 0.110) and that of the specimens not previously subjected to cyclic loading (slope of 0.125) are considered different.

6.4.2 *Effect of OCR on Postcyclic Undrained Monotonic Shear Strength*

The relationship between postcyclic undrained monotonic shear strength of the MRV silt not reconsolidated and OCR is presented in Fig. 6.9. Figure 6.9a shows that the curve of the specimens not reconsolidated was almost parallel to those of the specimens not previously subjected to cyclic loading. Also, for all OCRs, the postcyclic specimens without reconsolidation had lower undrained shear strength than the specimens not previously subjected to cyclic loading.

The effect of OCR on undrained shear strength for the postcyclic specimens without reconsolidated is presented in Fig. 6.9b. Data points obtained from Chap. 3 for the specimens not previously subjected to cyclic loading are also plotted in

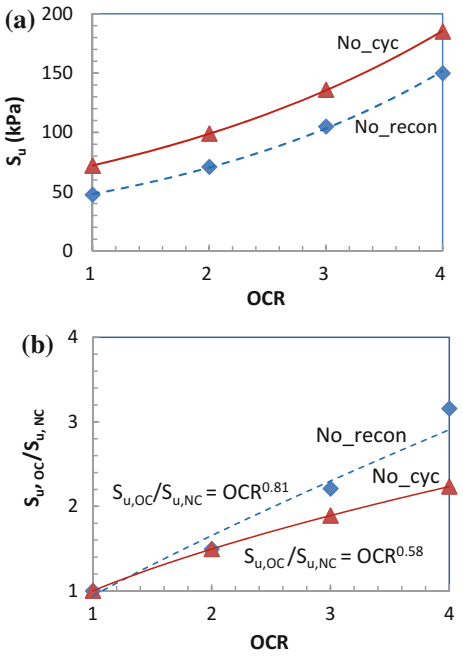

Fig. 6.9 Comparison of monotonic undrained shear strength of postcyclic MRV silt specimens not reconsolidated with that of silt specimens not previously subjected to cyclic loading: **a** S_u versus OCR, **b** $S_{u,OC}/S_{u,NC}$, (**b**) $S_{u,OC}/S_{u,NC}$ versus OCR

Fig. 6.9b. It is shown that the $S_{u,OC}/S_{u,NC}$ ratio increased with increase in OCR for both postcyclic specimens without reconsolidation and the specimens without previous cyclic loading. In contradistinction to the case of specimens reconsolidated after cyclic loading (see Fig. 6.6), the curve of $S_{u,OC}/S_{u,NC}$ against OCR for specimens without reconsolidation is much more (The difference in exponent of the equation is bigger) different from that of the specimens not previously subjected to cyclic loading. For postcyclic specimens without reconsolidation, the data points of $S_{u,OC}/S_{u,NC}$ can be best-fitted using the following equation:

$$S_{u,OC}/S_{u,NC}(\sigma'_c = 90\,\text{kPa}) = \text{OCR}^{0.81} \tag{6.3}$$

6.5 Change of Critical State Line Due to Cyclic Loading

To further understand the undrained shear behavior of postcyclic MRV silt, the state parameter (ψ) in critical state mechanics was computed based on CSL of postcyclic specimens as listed in Table 6.1. The undrained shear strength can be predicted as follows (Wood 1990; Wroth 1984):

$$S_u = M/2 \times p'_0 \times 10^{-\psi/\lambda} \tag{6.4}$$

where M is slope of failure line in q versus p′ space, p'_0 is the initial mean effective stress in postcyclic shearing, and λ is the slope of the CSL.

The undrained shear strength of postcyclic MRV silt was predicted using Eq. (6.4) and plotted against the measured values, shown in Fig. 6.10. The predicted undrained shear strength was computed for each reconsolidated condition (No_Recon and Recon) using the corresponding state parameters, ψ. Figure 6.10a used the CSL for the specimens not previously subjected to cyclic loading. Comparatively, Fig. 6.10b used the CSL for the postcyclic specimens. Thus, it is shown that Eq. (6.4) with λ of the CSL for the postcyclic specimens can be used to more effectively predict the postcyclic undrained shear strength of MRV silt.

In critical state soil mechanics, different soils are thought to have unique critical states and the same undrained shear strength at the large deformation regardless of the difference in initial fabric of the soil. The difference between the CSL of MRV silt not previously subjected to cyclic loading and that of MRV silt not reconsolidated after cyclic loading is probably attributable to the change in fabric due to cyclic loading. Similar findings have been presented in other studies. Vaid and Chern (1985), Seed (1987) and Stark and Mesri (1992) reported that the CSL may

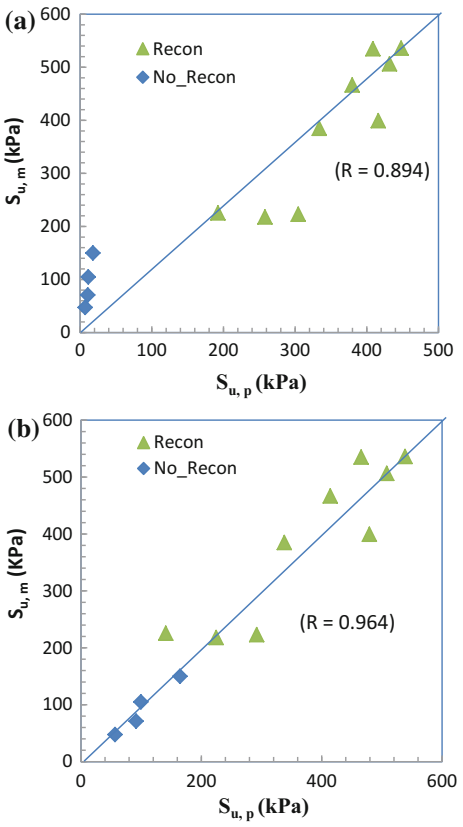

Fig. 6.10 Comparison between the predicted and measured undrained shear strength of MRV silt: **a** the predicted value based on the CSL of precyclic silt; **b** the predicted value based on the CSL of postcyclic silt

be influenced by shearing mode, effective confining pressure, and sample preparation method, all of which may change the arrangement of soil grains. Particularly, Nocilla et al. (2006) studied Italian silt with PIs of 11 and 13 and concluded that no unique NCL and CSL were found for the Italian silt because specimens prepared with slurries of different water content generated different fabrics.

6.6 Effect of Reconsolidation Level on Postcyclic Behavior

6.6.1 Undrained Shear Behavior

Figure 6.11 shows the postliquefaction monotonic behavior of MRV silt at various degrees of reconsolidation. At full reconsolidation, specimen MF1R2 contracted initially then dilated continuously (Fig. 6.11c). As indicated by the deviator stress-strain curve of the Fig. 6.11a, the deviator stress reached a peak value of about 437 kPa at an axial strain of 14%. The deviator stress drops slightly after continued axial strain. On the other hand, the other three specimens dilated continuously until they reached the critical state at the axial strain greater than 25%.

Figure 6.11b shows the excess pore pressure response. A higher degree of reconsolidation resulted in a higher initial effective confining pressure and a higher density at the beginning of postcyclic monotonic shearing. It is known that under constant effective confining pressure, soil with higher density dilates easier and earlier. Considering density, the effect of reconsolidation is a change of shear behavior from contraction to dilation. To the contrary, from the perspective of effective confining stress, reconsolidation leads to a change in shear behavior from dilation to contraction. However, as shown in Fig. 6.11b, because all specimens after liquefaction had a negative excess pore pressure at large deformation, it was thought that the change in effective confining stress due to reconsolidation was more pronounced. At large deformation, however, all specimens almost dilated along the same failure line (Fig. 6.11c), indicating that the degree of reconsolidation does not significantly change the slope of the failure line (or the effective friction angle).

6.6.2 Shear Strength and Stiffness

The shear strength and stiffness at small deformation are referred to as yield shear strength (S_y) and initial stiffness (E_i), respectively. The shear strength and stiffness at large deformation are referred to as undrained shear strength (S_u) and secant modulus (E_{sec}), respectively. The initial stiffness is the initial tangential modulus, which is in turn the slope of the curve of deviator stress versus axial strain at the axial strain of 0%. To get the yield shear strength, two tangential lines were plotted, as indicated in Fig. 6.12. The yield shear strength was half of the deviator stress at

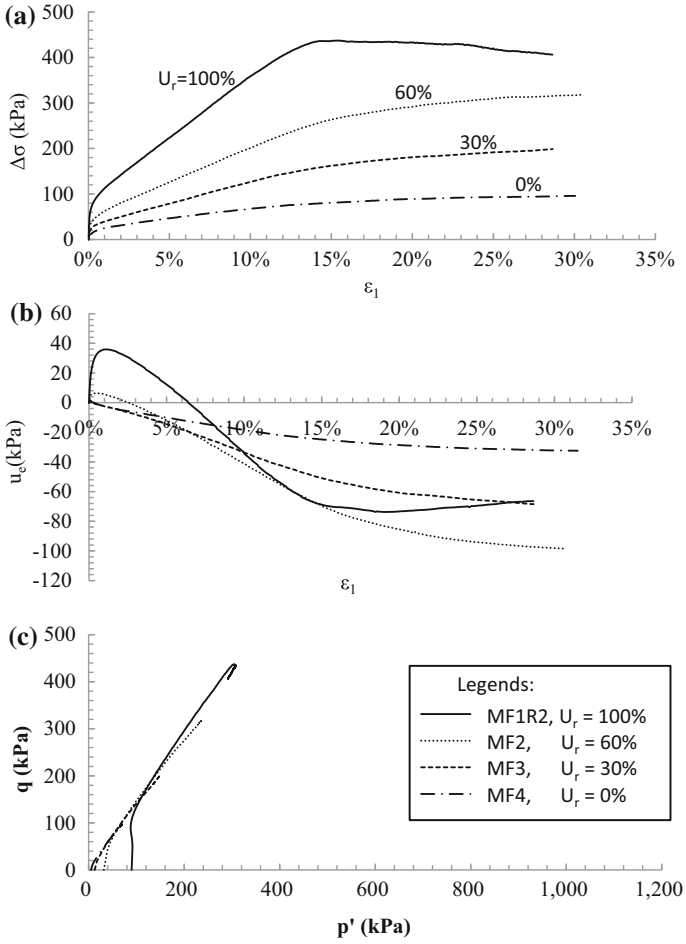

Fig. 6.11 Postliquefaction undrained shear behavior of MRV silt under various reconsolidation levels after full liquefaction: **a** $\Delta\sigma$ versus ε_1, **b** u_e versus ε_1, **c** q versus p′

an axial strain, in which those two tangential lines intersect (Wood 1990). The common definition of E_{sec}, namely of E_{s50}, was used to calculate this modulus at the intersection of 50% of the ultimate shear stress (Yasuhara et al. 2003).

Figure 6.13 shows the method by which initial stiffness (E_i) and yield shear strength (S_y) were determined. The ratios of initial stiffness and yield shear strength, each at various degree of reconsolidation, to those at zero degree of reconsolidation (i.e., $S_y/S_{y,\ Ur\ =\ 0\%}$, and $E_i/E_{i,\ Ur\ =\ 0\%}$). The initial stiffness and yield shear strength increased steadily with increase in the degree of reconsolidation. With full reconsolidation, yield shear strength and initial stiffness of the liquefied silt were 6.3 times the yield shear strength and 5.9 times the initial stiffness of unconsolidated liquefied silt, respectively. As shown in Fig. 6.14, the $E_{sec}/E_{sec,\ Ur\ =\ 0\%}$ increased as

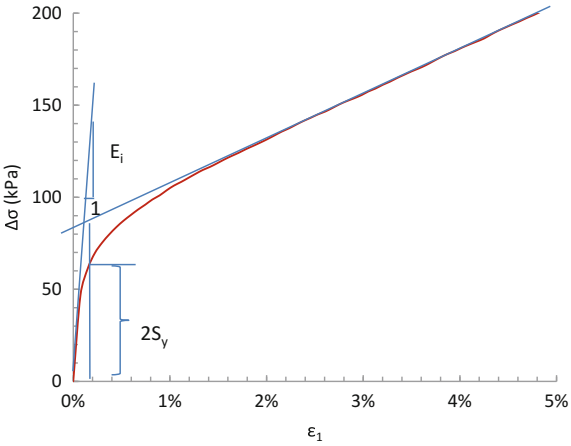

Fig. 6.12 Determination of yield shear strength and initial stiffness

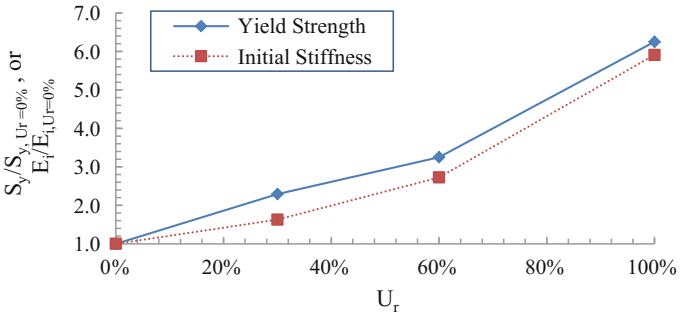

Fig. 6.13 Recovery of yield shear strength and initial stiffness with reconsolidation

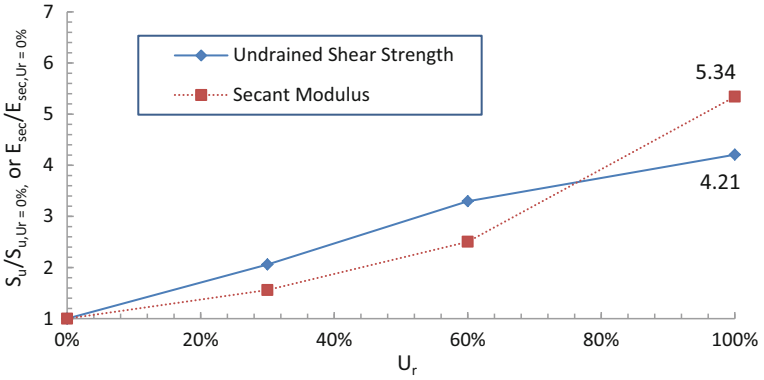

Fig. 6.14 Recovery of undrained shear strength and secant modulus with reconsolidation

reconsolidation level increased. The same was true of the $S_u/S_{u,\ Ur\ =\ 0\%}$; however, the increase was not as large as that at U_r = 100%. The undrained shear strength of fully reconsolidated liquefied silt was 4.2 times larger than that of unreconsolidated liquefied silt. The secant modulus of fully liquefied silt was 5.3 times larger than that of unreconsolidated liquefied silt.

6.6.3 *Apparent OCR*

OCR_{app} is defined as the ratio of initial effective consolidation pressure (σ'_c) before cyclic loading to effective confining pressure (σ'_3) at the beginning of postliquefaction shearing. It is induced by excess pore pressure during cyclic loading. Several researchers have used the term apparent overconsolidation ratio (OCR_{app}) to study postcyclic undrained shear strength (Soroush and Soltani-Jigheh 2009; Yasuhara et al. 2003; Ashour et al. 2009). This work computed OCRapp for MRV silt at various degrees of reconsolidation.

Figure 6.15 shows the effect of OCR_{app} on the normalized shear strength (S_u/σ'_3) of MRV silt. The undrained shear strength (S_u) was normalized by the effective confining pressure at the beginning of postcyclic shearing. The normalized shear strength ratio $[(S_u/\sigma'_3)_{OC}/(S_u/\sigma'_3)_{NC}]$ is defined as the ratio of the normalized shear strength of the overconsolidated specimen to that of the normally consolidated specimen. For purposes of comparison, data on the normalized shear strength ratio $[(S_u/\sigma'_c)_{OC}/(S_u/\sigma'_c)_{NC}]$ of MRV silt for static triaxial tests described in Chap. 3 are also included in Fig. 6.15. This comparison indicates no significant difference between the static and postcyclic monotonic test in the variation in the normalized shear strength ratio with the OCR and OCR_{app}. Thus, the OCR and OCR_{app} have the same effect on the increase in normalized shear strength ratio.

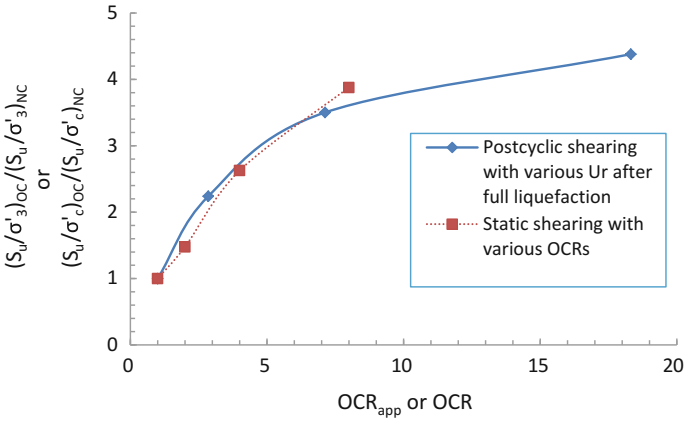

Fig. 6.15 Effect of OCR or OCR_{app} on the normalized undrained shear strength

With identical effective consolidation pressure, overconsolidation produces the same increase in undrained shear strength regardless of how the overconsolidation condition was developed. Actually, the OCR and OCR_{app} represented two different overconsolidation processes. The OCR was generated by reducing cell pressure while keeping pore pressure constant so that the effective consolidation pressure was reduced from the product of the OCR and σ'_c to σ'_c. Conversely, the OCR_{app} was generated by increasing pore pressure while keeping cell pressure constant to change effective consolidation pressure. In other words, the OCR and OCR_{app} just represented two different ways to induce overconsolidation, and they had the same effect on normalized shear strength ratio.

6.7 Effect of Plasticity on Postcyclic Shear Behavior

6.7.1 Stress-Strain Behavior

Postcyclic monotonic shearing was conducted on the specimens experiencing previous cyclic loading. The CSR for cyclic loading included 0.18, 0.25 and 0.35. However, as found previously, the CSR had no obvious effect on postcyclic shear behavior, which was governed by excess pore water pressure or cyclic strain produced by previous cyclic loading. Thus, the effect of CSR on the postcyclic shearing behavior was neglected here. Figure 6.16 shows the postcyclic shear behavior for the natural MRV silt. Compared to the static specimen MS2 ($R_u = 0$), the reconsolidated specimen MF1R2 after cyclic loading ($R_u = 1.0$ and $U_r = 100\%$) have an initial stiffness close to that of static specimen. However, due to reconsolidation, the specimen started to obtain much higher dilative behavior than static specimen at a small axial strain. Reversely, the unreconsolidated specimen MF4 after cyclic loading ($R_u = 1.0$ and $U_r = 0\%$) have a lower initial stiffness than the static specimen. The unreconsolidated specimen slowly recovered its undrained shear strength with an increase in axial strain. As shown in Fig. 6.16b, the stress path climbed along almost the same slope after phase transformation, indicating the effective friction angle was not influenced by cyclic loading. The reason was that the soil fabric (or microstructure) in the critical state tended to be the same between the specimens with and without cyclic loading.

Figure 6.17 shows the postcyclic shear behavior of MRV silt with added bentonite content of 2.5%. For comparison, it also shows curves for static test on the mixture (MSB3) with the same added bentonite content. Since the density of the specimens increased due to reconsolidation, the reconsolidated specimen (MFB4) showed more strain-hardening behavior than the static specimen (MSB3) (Fig. 6.17a) and dilated more (Fig. 6.17b). The reconsolidated specimen (MFB4) had significantly greater undrained shear strength at the critical state than the static specimen (MSB3). Conversely, the specimen without reconsolidation (MFB5) had undrained shear strength close to that of the static specimen (MSB3), although different cyclic strains were induced by cyclic loading.

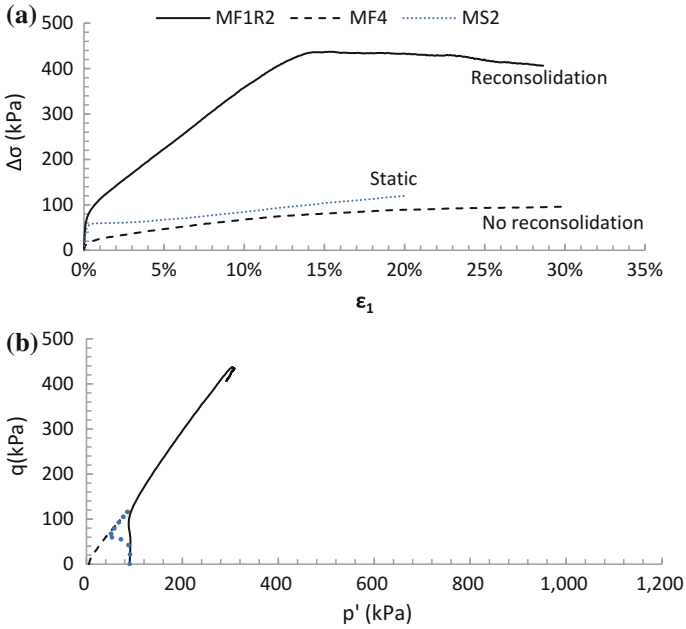

Fig. 6.16 Comparison of undrained stress-strain behavior of MRV silt with and without liquefaction: **a** $\Delta\sigma$ versus ε_1, **b** q versus p′

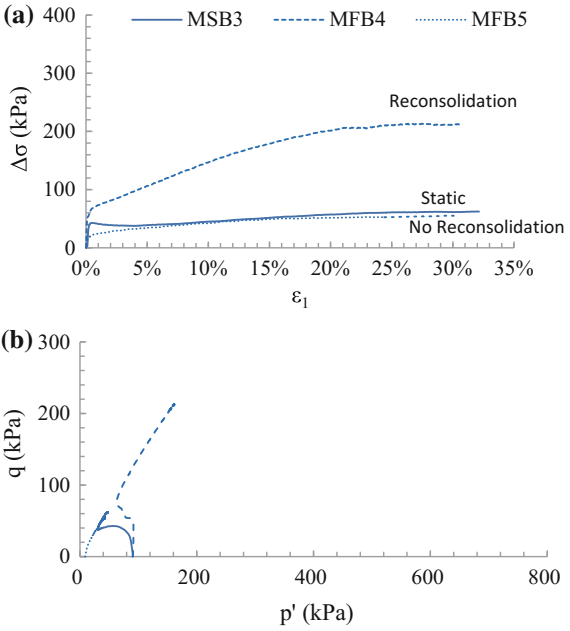

Fig. 6.17 Postcyclic shear behavior of MRV silt with 2.5% added bentonite: **a** $\Delta\sigma$ versus ε_1, **b** q versus p′

Figure 6.18 shows the postcyclic monotonic shear behavior of MRV silt with added bentonite content of 5.0%. Like MRV silt specimen with added bentonite content of 2.5%, the specimen with full reconsolidation (MFB7) showed more strain-hardening behavior and more dilative behavior than the specimen without previous cyclic loading (MSB7). On the other hand, the specimen without reconsolidation (MFB8) had lower initial stiffness than that with no previous cyclic loading (MSB7). At large deformation, the specimen without reconsolidation (MFB8) had a deviator stress versus axial strain curve close to that of the specimen without previous cyclic loading (MSB7), indicating that the soil shear strength was recovered at the large deformation because that soil fabric (or microstructure) was not changed significantly by cyclic loading.

6.7.2 *Shear Strength and Stiffness*

This section addresses the changes in undrained shear strength and initial stiffness due to cyclic loading. The effect of addition of bentonite on changes in the strength and stiffness due to cyclic loading was addressed. Figure 6.19 shows the variations

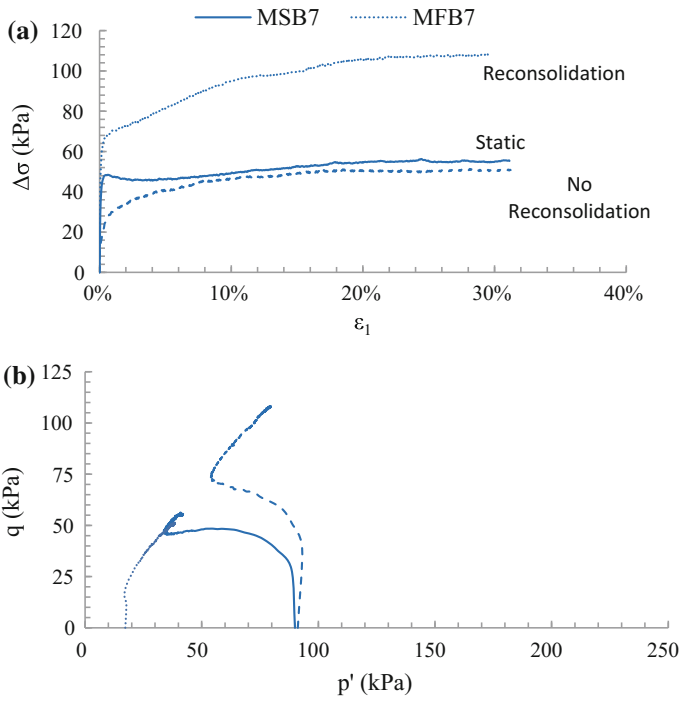

Fig. 6.18 Postcyclic behavior of the MRV silt with 5.0% added bentonite: **a** $\Delta\sigma$ versus ε_1, **b** q versus p′

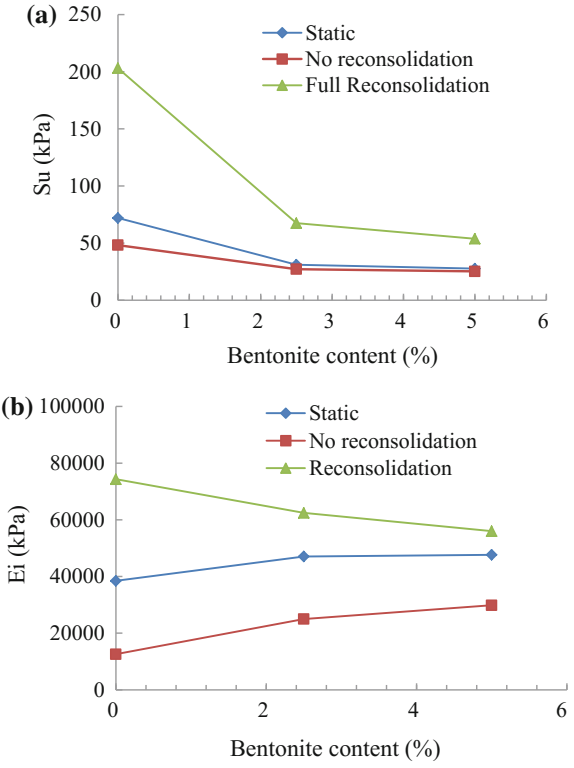

Fig. 6.19 Variations in undrained shear strength and initial stiffness of MRV silt/bentonite mixtures with bentonite content: **a** S_u versus bentonite content, **b** E_i versus bentonite content

with added bentonite content in the undrained shear strength and initial stiffness of the specimens for each case. The undrained shear strength decreased sharply with an increase in added bentonite content from 0 to 2.5% in all cases including static tests, and postcyclic tests after no reconsolidation and full reconsolidation. With a further increase in added bentonite content, the decrease in undrained shear strength became small; however, there were no consistent relationships between initial stiffness and added bentonite content for static tests, and postcyclic tests after no reconsolidation and full reconsolidation.

Undrained shear strength and initial stiffness were normalized by those of the static specimen without previous cyclic loading. Figure 6.20 shows the ratios of undrained shear strength and initial stiffness of the soil after no reconsolidation and full reconsolidation to those of the soil without previous cyclic loading ($S_{u,postcyclic}/S_{u,static}$ and $E_{i,postcyclic}/E_{i,static}$) for various added bentonite contents. With full reconsolidation, the strength ratio $S_{u,postcyclic}/S_{u,static}$ $E_{i,postcyclic}/E_{i,static}$) are larger than unity; therefore, the undrained shear strength and initial stiffness increased after reconsolidation. With an increase in added bentonite content, $S_{u,postcyclic}/S_{u,static}$ and $E_{i,postcyclic}/E_{i,static}$ decreased, and the decrease was larger when the added bentonite content increased from 0 to 2.5%. Without reconsolidation, the undrained shear strength decreased after cyclic loading. The strength

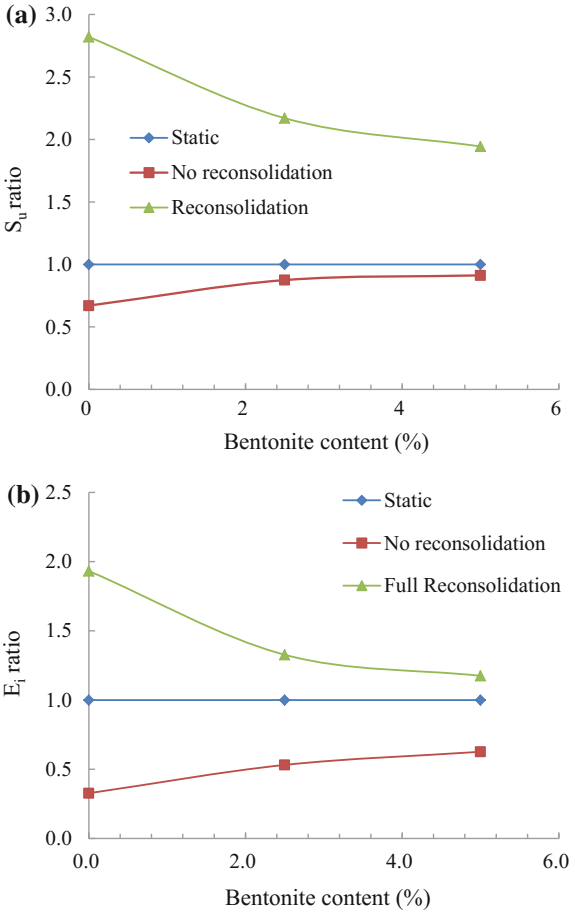

Fig. 6.20 Variations in undrained shear strength and initial stiffness ratios of MRV silt/bentonite mixtures with bentonite content: **a** S_u versus bentonite content, **b** E_i versus bentonite content

ratio $S_{u,postcyclic}/S_{u,static}$ came closer to unity with a higher added bentonite content. Thus, postcyclic undrained shear strength tended to be closer to precyclic undrained shear strength for soil with a higher added bentonite content probably because the undrained shear strength of MRV silt with bentonite added was less affected by cyclic loading. Although there was difference between the variation for $E_{i,postcyclic}/E_{i,static}$ and that for the $S_{u,postcyclic}/S_{u,static}$, the change in initial stiffness of the soil with added bentonite due to cyclic loading was less than that of natural MRV silt, especially for the soil with no reconsolidation. As noted previously, because more plastic soil is non-sensitive to be remolded during cyclic loading, postcyclic soil behaves more like soil without previous cyclic loading.

Figure 6.21 shows the changes of $S_{u,postcyclic}/S_{u,static}$ and $E_{i,postcyclic}/E_{i,static}$ with PI. Similarly with k′/k and C_c'/C_c, the changes of $S_{u,postcyclic}/S_{u,static}$ and $E_{i,postcyclic}/E_{i,static}$ were larger with added bentonite content increasing from 0 to 2.5% than those with added bentonite content increasing from 2.5 to 5.0%.

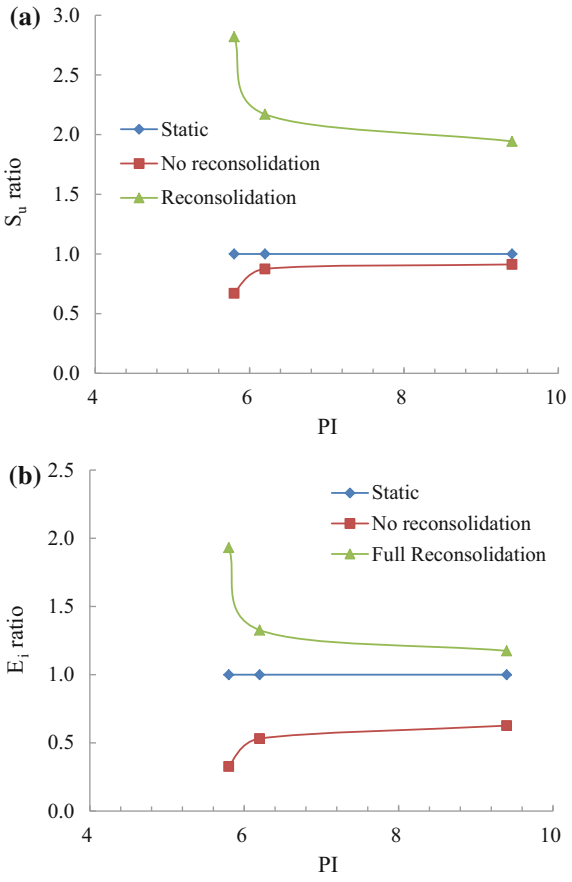

Fig. 6.21 Variations in undrained shear strength and initial stiffness ratios of MRV silt/bentonite mixtures with PI **a** S_u versus PI, **b** E_i versus PI

6.7.3 Discussion

The changes in undrained shear strength and initial stiffness of the low-plastic fine-grained soil after cyclic loading compared to those without previous cyclic loading became less evident with an increase in added bentonite content. This finding agrees with the statement by Robertson (2010), who indicated that non-plastic or low-plastic soils tend to be more susceptible to significant strength loss than more plastic soils. The difference may be attributable to the fact that that higher plasticity soils tend to be more compressible and therefore develop less excess pore water pressure and degrade less. The change of volumetric strain with PI can also explain this. As shown in Fig. 6.22, although cyclic loading was stopped at the same cyclic strain, the induced volumetric strain of the soil with higher PI due to full reconsolidation after cyclic loading was lower because of less excess pore pressured developed by cyclic loading. However, the opposite phenomenon was reported by Song et al. (2004), who conducted postcyclic shearing on non-plastic

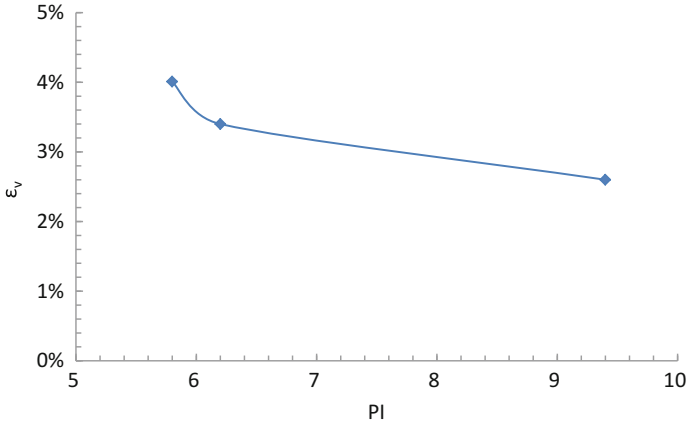

Fig. 6.22 Variation in volumetric strain with PI due to full reconsolidation after nearly identical axial strain (9%) induced by cyclic loading

specimens without reconsolidation. They indicated that stiffness tended to decrease less markedly in nonplastic silt with an increase in excess pore pressure ratio than in plastic Arakawa clay with a PI of 17.3. The frequency for all cyclic tests conducted by Song's group was 0.1 Hz, despite low permeability of the Arakawa clay compared to the nonplastic silt. Comparison of the reduction of stiffness between the soils with different PI (one nonplastic and the other 17.3) may be more interesting using the same level of cyclic strain. Song's group reported no volumetric strain measured, no further analysis of their results is possible.

For the studied materials in this study, the undrained shear strength and initial stiffness increased largely due to cyclic loading when the PI changed around 6.0, indicating that MRV silt's shear behavior changed significantly around PI of 6.0 due to addition of bentonite. If integer number was used for the PI, the PIs were 6 both for MRV silt with added bentonite contents of 0 and 2.5% (see Table 3.1). Thus, the PI is not an ideal index to evaluate the transformation of soil behavior due to addition of clay when the PI is around 6. This finding agrees with that of Beroya et al. (2009), who pointed out that the PI did not adequately encapsulate the effects of clay mineralogy on the soil behavior.

6.8 Summary

The effect of initial consolidation conditions on postcyclic undrained monotonic shear behavior of low-plasticity silt and its mixtures with sodium bentonite was studied by conducting triaxial tests on MRV silt. Two series of cases based on the postcyclic processing of specimens were investigated: (a) specimens were fully reconsolidated (by opening the drain valves) and (b) specimens were not

reconsolidated but were allowed to stand for five minutes for the equilibration of excess pore pressure within the specimen after cyclic loading. The following conclusions are drawn based on this study.

The CSR had no apparent effect on postcyclic undrained monotonic shear behavior of MRV silt with various OCRs. In contradistinction to the specimens not previously subjected to cyclic loading studied in Chap. 3 where stress state (OCR) had an effect on ESP, specimens reconsolidated after cyclic, consolidated to various OCRs, had almost the same ESPs at the early period of postcyclic undrained monotonic shearing. Thus, the stress state (OCR) did not influence the early period of ESP of the postcyclic specimens. With a higher OCR, the reconsolidation process followed a behavior more similar to recompression. The CSL of MRV silt was not substantially changed by cyclic loading followed by reconsolidation. The MRV silt with a higher OCR had higher postcyclic undrained monotonic shear strength, since the specimens became denser due to reconsolidation. The postcyclic shearing curves can be normalized by the mean effective consolidation pressure as those of the specimens not previously subjected to cyclic loading studied in Chap. 3, which indicates that the normalization characteristics were not removed by cyclic loading.

The specimens not reconsolidated after cyclic loading dilated early, resulting in negative excess pore pressure. Their stress paths climbed along the K_f line. The critical state line of the specimens not reconsolidated after cyclic loading was different from that of the specimens not previously subjected to cyclic loading. The undrained monotonic shear strength of MRV silt not reconsolidated after cyclic loading decreased compared to the specimen not previously subjected to cyclic loading, but did not approach zero.

The undrained shear strength of postcyclic MRV silt can be predicted based on Eq. (6.4) adopting the state parameter. However, the prediction will be better if the CSL change due to cyclic loading is considered. As other authors have found the CSL may not be unique for silts and can change due to cyclic loading when the R_u reaches a value of 1.0.

The shear strength and stiffness of MRV silt at both small and large deformation increased steadily with an increase in the degree of reconsolidation. For small deformations, yield strength always increased slightly more than initial stiffness with an increase in reconsolidation level. For large deformation, however, undrained shear strength and secant modulus increased significantly for low and high degrees of reconsolidation, respectively.

The normalized shear strength ratio increased with increasing OCR_{app}. The relationship of the normalized shear strength ratio to OCR_{app} after liquefaction was almost identical to that of normalized shear strength ratio to OCR for specimens not subjected to cyclic loading. The process of produce OCR and OCR_{app} represented two different ways to induce overconsolidation, and they had the same effect on normalized shear strength ratio.

The undrained shear strength increased due to reconsolidation after cyclic loading. With no reconsolidation, the initial stiffness of the soil was low compared to the specimen without previous loading due to high excess pore pressure induced

by cyclic loading. With an increase in added bentonite content, there was less reduction in undrained shear strength with no reconsolidation.

The cyclic and postcyclic shear behaviors of MRV silt-bentonite mixture changed significantly when the PI changed around 6. MRV silt with a PI < 6 behaved like sand (large deformation develops after liquefaction), and that with a PI > 6 behaved like clay (It shows cyclic softening). However, for engineering practice, it is difficult to catch the small difference in the plasticity index. The plasticity index seems to be not an ideal factor to identify the transformation of soil behavior. In future, the effects of clay mineralogy on the cyclic and postcyclic shear behavior of low-plasticity silt need to be investigated.

To better understand the postcyclic behavior of low-plasticity silt and reach a conclusion with general applicability, it is recommended that further research be conducted on other low-plasticity silts. It is also recommended that further research be conducted to study the change in soil fabric due to cyclic loading.

References

Ashour, M., Norris, G., & Nguyen, T. (2009). Assessment of the undrained response of sands under limited and complete liquefaction. *Journal of Geotechnical and Geoenvironmental Engineering, 135*(11), 1772–1776.

ASTM. (2004). Standard test method for consolidated undrained triaxial compression test for cohesive soils. D4767–4. West Conshohocken, PA.

Been, K., & Jefferies, M. G. (1985). A state parameter for sand. *Geotchnique, 35*(2), 99–112.

Beroya, M. A. A., Aydin, A., & Katzenbach, R. (2009). Insight into the effects of clay mineralogy on the cyclic behavior of silt-clay mixtures. *Engineering Geology, 106,* 154–162.

Chern, J. C., & Lin, C. C. (1994). Postcyclic consolidation behavior of loose sands. In *Proceeding of Settlement 94, Geotechnical Special Publication*, ASCE, No. 40.

Nocilla, A., Coop, M. R., & Colleselli, F. (2006). The mechanics of an Italian silt: An example of 'transitional' behavior. *Geotechnique, 56*(4), 261–271.

Robertson, P. K. (2010). Evaluation of flow liquefaction and liquefied strength using the cone penetration test. *Journal of Geotechnical and Geoenvironmental Engineering, 136*(6), 842–853.

Seed, H. B. (1987). Design problems in soil liquefaction. *Journal of Geotechnical Engineering, 113*(8), 827–845.

Song, B. W., Yasuhara, K., & Murakami, S. (2004). Direct simple shear testing for postcyclic degradation in stiffness of nonplastic silt. *Geotechnical Testing Journal, 27*(6), 1–7.

Soroush, A., & Soltani-Jigheh, H. (2009). Pre- and postcyclic behavior of mixed clayey soils. *Canadian Geotechnical Journal, 46,* 115–128.

Stark, T. D., & Mesri, G. (1992). Undrained shear strength of liquefied sands for stability analysis. *Journal of Geotechnical Engineering, 118*(11), 1727–1747.

Thevanayagam, S., Martin, G. R., Shenthan, T., & Liang, J. (2001). Post-liquefaction pore pressure dissipation and densification in silty soils. In *Proceedings of 4th International Conference on Recent Advances in Geotechnical Earthquake Engineering and Soil Dynamics*, San Diego, CA.

Vaid, Y. P., & Chern J. C. (1985). Cyclic and monotonic undrained response of saturated sands. In *Proceedings of Advances in the Art of Testing Soils under Cyclic Conditions*, New York, pp. 120–147.

Wang, S., & Luna, R. (2012). Monotonic behavior of Mississippi River Valley silt in triaxial compression. *Journal of Geotechnical and Geoenvironmental Engineering, 138*(4), 516–525.
Wang, S., Luna, R., & Onyejekwe, S. (2015a). Postliquefaction behavior of low-plasticity silt at various degrees of reconsolidation. *Soil Dynamics and Earthquake Engineering, 75,* 259–264.
Wang, S., Luna, R., & Onyejekwe, S. (2016). Effect of initial consolidation condition on post-liquefaction undrained monotonic shear behavior of Mississippi River Valley silt. *Journal of Geotechnical and Geoenvironmental Engineering, 142*(2), 04015075-1-11.
Wang, S., Luna, R., & Zhao, H. (2015b). Cyclic and postcyclic shear behavior of low-plasticity silt with varying clay content. *Soil Dynamics and Earthquake Engineering, 75,* 112–120.
Wood, D. M. (1990). *Soil behavior and critical state soil mechanics*. Cambridge University Press.
Wroth, C. P. (1984). The interpretation of in situ soil tests. *Géotechnique, 34*(4), 449–489.
Yasuhara, K., Murakami, S., Song, B. W., Yokokawa, S., & Hyde, A. F. L. (2003). Postcyclic degradation of strength and stiffness for low plasticity silt. *Journal of Geotechnical and Geoenvironmental Engineering, 129*(8), 756–769.

Chapter 7
Effect of Cyclic Loading Magnitude on Shear Behavior of Low-plasticity Silt

This chapter focuses on investigating effect of cyclic loading magnitude on shear behavior of low-plasticity silt. Various excess pore pressure ratios were reproduced at limited number of loading cycles, and then monotonic shear testing was carried out after full and no reconsolidation. The monotonic shear and reconsolidation volumetric behaviors after cyclic loading are examined. Comparatively, there are few studies on the determination of the threshold strain for postcyclic shear strength, especially for low-plasticity silt. This chapter also investigates cyclic loading induced threshold strain for postcyclic shear strength after reconsolidation of the reconstituted MRV silt specimens.

7.1 Experimental Program

The specimens were prepared in a split vacuum mold using the slurry consolidation approach and were saturated with the aid of vacuum and back-pressure. A B-value ($\Delta u/\Delta\sigma_c$) of at least 0.94 was reached for saturation of every specimen tested. In previous testing the silt produced significant dilation during shearing. Therefore, an additional backpressure of 100 kPa was applied to avoid cavitation. Some specimens were normally consolidated to an effective confining pressure of 90 kPa, and the others were overconsolidated with overconsolidation ratio (OCR) of 4 and σ'_c of 90 kPa. Following consolidation, all specimens were dynamically loaded by uniform cycles. For excess pore pressure uniformity in the specimen, the frequency of symmetrically cyclic stress with a sine function was 0.1 Hz, which was lower than dominant frequency in earthquake loading. The cyclic stress ratios (CSRs, i.e. ratio of deviator stress to twice effective confining pressure) are listed in Tables 7.1 and 7.2. When the different magnitudes of excess pore pressure ratio (i.e., R_u = 0.85, 0.70, or 0.35) were reached, cyclic loading was stopped and the deviator stress was slowly reset to zero. Figure 7.1 shows the stress paths for the two sets of tests (one

S. Wang, *Monotonic, Cyclic and Postcyclic Shear Behavior of Low-plasticity Silt*,
https://doi.org/10.1007/978-981-10-7083-9_7

with full reconsolidation and the other without reconsolidation) with the CSR set at 0.18. Notice that Fig. 7.1 includes the steps followed in the testing procedure.

As presented in Wang et al. (2013, 2014) the first set of specimens was dynamically loaded at various excess pore pressure ratios, then fully reconsolidated, and finally sheared monotonically in undrained conditions (see Fig. 7.1a). The second set of specimens was also dynamically loaded various excess pore pressure ratios, but they were not reconsolidated. Instead, undrained shearing took place once excess pore pressure reached equilibrium (see Fig. 7.1b). The test results are summarized in Tables 7.1 and 7.2, respectively. For a comparison, the fully liquefied specimens with full and no reconsolidation (MF1R1 and MF4) and static specimen without previous cyclic loading were also listed in the tables. For more details regarding the full experimental program see Wang (2011). The ratio of undrained shear strength of postcyclic specimens ($S_{u,post}$) with reconsolidation to that of virgin specimen ($S_{u,virgin}$) reported in Chap. 3 are presented in Table 7.1.

7.2 Effect of Excess Pore Pressure on Postcyclic Shear Behavior with Full Reconsolidation

7.2.1 Undrained Shear Behavior

Figure 7.2 shows deviator stress, excess pore pressure, and stress paths for the monotonic shearing after cyclic loading. At about 25% axial strain, all specimens except MF1R2 reached the critical state. The specimen MF1R2 reached the critical state at about 13% axial strain. Clearly, except for static specimen MS2, the specimen with greater excess pore pressure ratio had a larger deviator stress and developed more positive excess pore pressure (Fig. 7.2a, b). The stress paths in Fig. 7.2c indicate that all specimens initially contracted; however, the specimen with 100% liquefaction (MF1R2) contracted less than the other specimens. Specimens ML2 (R_u = 0.70) and ML3 (R_u = 0.35) had nearly identical curves of deviator stress and excess pore pressure versus axial strain. When excess pore pressure ratio was increased to 0.85, the deviator stress resistance increased and the excess pore pressure decreased further after the initial peak value (Fig. 7.2a, b). The phenomena can also be explained by axial strain induced by cyclic loading. Because the specimens with R_u = 0.35 and 0.70 had little axial strain (0.18 and 0.21%, respectively) induced by cyclic loading and had little change of soil skeleton or fabric, postcyclic reconsolidation produced little volume change (see Table 7.1). However, the specimen with R_u = 0.85 become much denser than the specimens with R_u = 0.35 and 0.70, thus, the specimen with R_u = 0.85 dilated more during postcyclic shearing, inducing a higher deviator stress and negative excess pore pressure.

Table 7.1 Summary of triaxial tests of MRV silt with full reconsolidation after various liquefaction levels

Test ID	OCR	Void ratio (e)	CSR	Dr	N_{cyc}	R_u	$u_{e,cyc}$ (kPa)	ε_{cyc} (%)	e′	D_r'	ε_v (%)	S_u (kPa)	$S_{u,post}/S_{u,virgin}$
MF1R2	1	0.669	0.18	31.14	31.1	1.00	89.9	8.46	0.602	0.858	*4.0*	205.05	2.82
ML1		0.653	0.18	26.18	26.2	0.85	76.9	0.84	0.621	0.842	*1.9*	105.38	1.46
MLO17		0.671	0.18		23.1			0.55				53.54	0.74
ML2		0.674	0.18	0.796	22.2	0.70	63.4	0.22	0.666	0.803	*0.5*	48.36	0.67
ML3		0.662	0.18	0.807	6.2	0.35	27.2	0.12	0.660	0.808	*0.1*	43.89	0.61
MS2		0.679	0	0.792	0	0	0	0	0.679	0.792	*0*	72.00	1
MLO5	4	0.615	0.35		22.1			7.15				536.02	2.89
MLO14		0.63	0.35		20.1			1.62				302.13	1.63
MLO16		0.616	0.35		17.1			0.87				236.44	1.28
MLO15		0.623	0.35		14.2			0.55				162.16	0.88
MLO13		0.62	0.35		12.1			0.22				166.18	0.90
MS7		0.612	0		0			0				185.15	1

Note e—void ratio; D_r—relative density; N_{cyc}—number of cycles of loading; ε_{cyc}—axial strain induced by cyclic loading; $u_{e,cyc}$—excess pore pressure induced by cyclic loading

Table 7.2 Summary of triaxial tests of MRV silt without reconsolidation after various liquefaction levels

Test ID	B-value	σ_c' (kPa)	e	D_r	N_{cyc}	ε_{cyc} (%)	R_u	$u_{e,cyc}$	u_e after equilibrium	σ_3' after equilibrium
MF4	0.94	90.3	0.660	0.808	28.14	11.5	1.00	90.3	85.1	5.2
ML4	0.93	90.5	0.643	0.823	25.17	0.95	0.85	76.9	72.9	17.6
ML5	0.93	91.1	0.645	0.821	18.12	0.23	0.70	63.4	58.1	33.0
ML6	0.94	90.7	0.667	0.802	4.01	0.19	0.35	27.21	23.7	67.0
MS2	0.98	90.0	0.679	0.792	0	0	0	0	0	90.0

Note e—void ratio; D_r—relative density; N_{cyc}—number of cycles of loading; ε_{cyc}—axial strain induced by cyclic loading; $u_{e,cyc}$—excess pore pressure induced by cyclic loading

7.2.2 Shear Strength and Stiffness at Small Deformation

This work studied the effect of limited excess pore pressure on strength and stiffness at small deformation, which are respectively called yield shear strength and initial stiffness. In Fig. 7.3, the values of yield shear strength and initial stiffness at any excess pore pressure ratio were normalized by the values with 0% liquefaction (i.e. without previous cyclic loading). The postcyclic yield shear strength increased with an increase in excess pore pressure ratio up to $R_u = 0.85$. Beyond that, there was a small reduction in the yield shear strength. The initial modulus increased with an increase in excess pore pressure ratio. When the excess pore pressure ratio was larger than 0.70, it increased less. With an increase in excess pore pressure ratio, the increase in initial stiffness of the MRV silt was larger than that in yield shear strength, suggesting that limited excess pore pressure with full reconsolidation has a greater impact on initial stiffness than on yield shear strength. The increase in initial modulus and yield shear strength was induced by the increase of soil density due to reconsolidation after liquefaction.

7.2.3 Shear Strength and Stiffness at Large Deformation

Undrained shear strength (S_u) is plotted against excess pore pressure ratio in Fig. 7.4. The undrained shear strengths of postcyclic specimens with $R_u = 0.35$ and 0.70 were only slightly lower than that of static specimen MS2, which had no previous cyclic loading. When the excess pore pressure ratio was 0.85, the undrained shear strength increased. The reason why the S_u of the specimens with R_u of 0.35 and 0.70 decreased compared to the static specimen MS2 probably included: the fabric of the soil was damaged during cyclic loading; the decrease in void ratio due to reconsolidation was not enough to increase the undrained shear strength; and small variations in testing results were caused in part by inevitable variations in procedures from one test to another. In Fig. 7.4, the volumetric strain (ε_v) due to reconsolidation is plotted against excess pore pressure ratio. When the

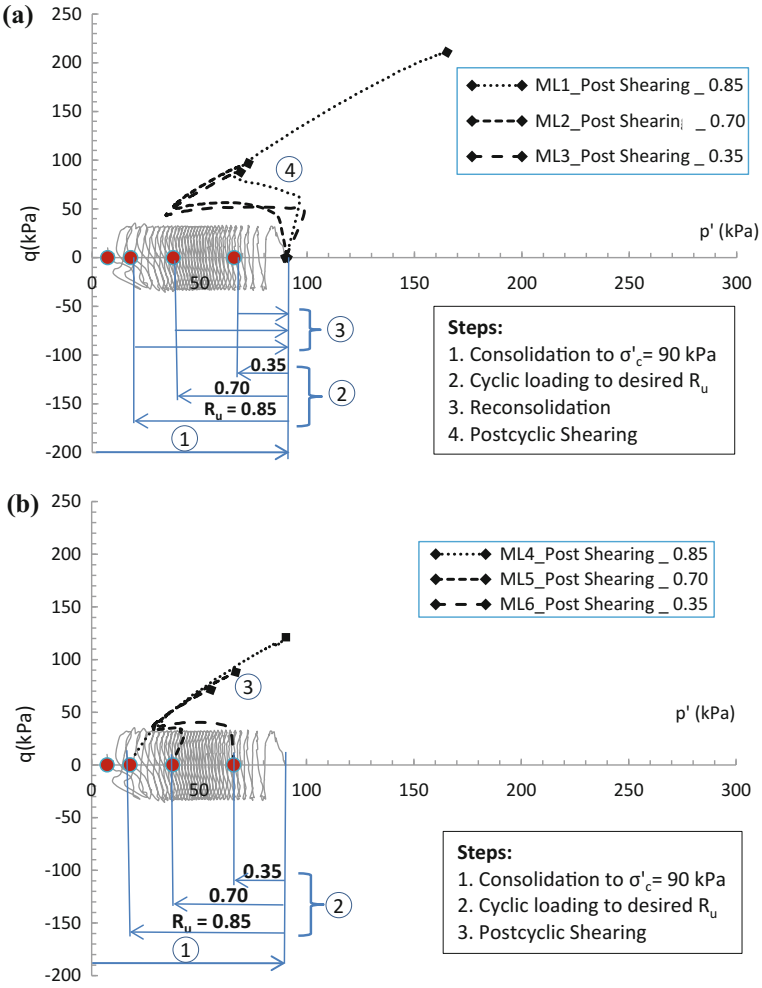

Fig. 7.1 Testing procedures via stress paths to study postcyclic behavior of MRV silt with limited excess pore pressure: (**a**) with full reconsolidation, (**b**) with no reconsolidation

excess pore pressure ratio was up to 0.70, the volumetric strain was small. Beyond that point, there was a larger volumetric strain due to reconsolidation. Together, Figs. 7.4 and 7.5 demonstrate that an excess pore pressure ratio of 0.70–0.80 is a prerequisite for significant volume reduction and thus for an increase in undrained shear strength due to reconsolidation after cyclic loading.

In Fig. 7.6, the secant modulus (E_{sec}) is plotted against excess pore pressure ratio. In contrast to the undrained shear strength, there was no apparent relationship between secant modulus and excess pore pressure ratio. The secant modulus was larger at excess pore water pressure ratios of 0.35 and 0.70 than other levels because the soil did not dilate significantly after deviator stress exceeded yield stress, at

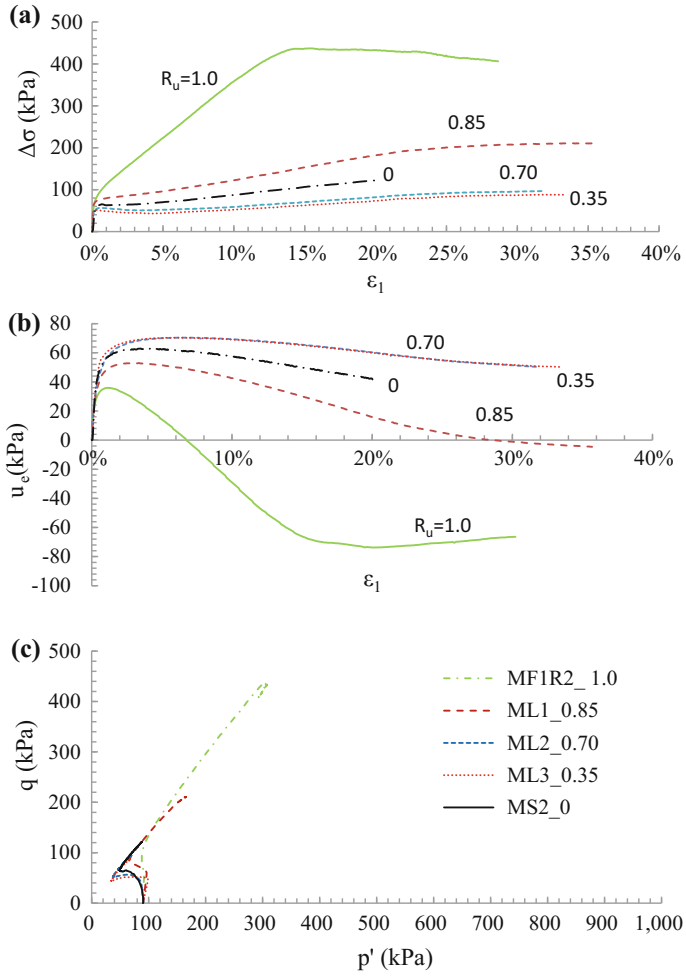

Fig. 7.2 Postcyclic shear behavior of MRV silt with full reconsolidation after various excess pore pressure ratios: (**a**) $\Delta\sigma$ versus ε_1, (**b**) $\Delta\sigma$ versus ε_1, (**c**) q versus p′ (the values after test ID are R_u)

which the slope of deviator stress-strain changes a lot. For example, Fig. 7.7 demonstrates this phenomenon by comparing ML1 and ML3. The $\Delta\sigma_{max}/2$ of the specimen ML3 occurred before yield stress; therefore, the secant modulus was almost equal to the initial stiffness. Thus, the small strain governs the deviator stress-strain behavior of the postcyclic specimens with excess pore pressure ratios of 0.35 or 0.70, but large strain governs that of the static specimen and postcyclic specimens with excess pore pressure ratios greater than 0.70.

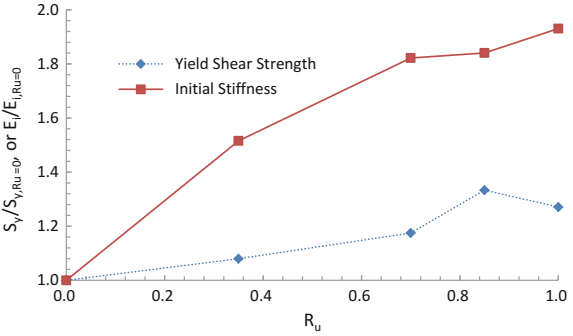

Fig. 7.3 Variation in yield shear strength and initial stiffness of MRV silt with full reconsolidation against increased excess pore pressure ratio

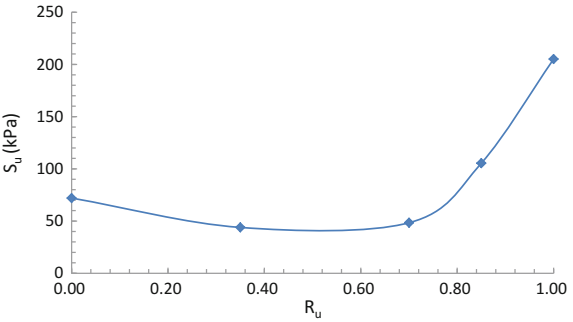

Fig. 7.4 Effect of excess pore pressure ratio on undrained shear strength of MRV silt with full reconsolidation

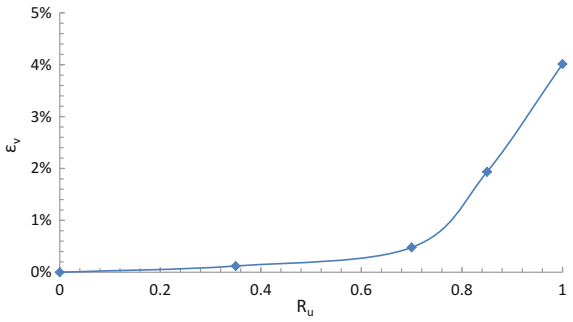

Fig. 7.5 Volumetric strain of MRV silt due to reconsolidation against excess pore pressure ratio

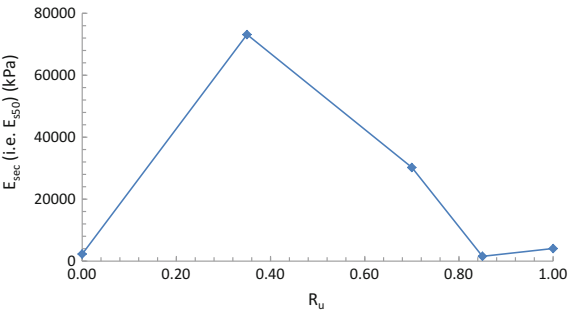

Fig. 7.6 Effect of excess pore pressure ratio on secant modulus (i.e. E_{s50}) of fully reconsolidated MRV silt

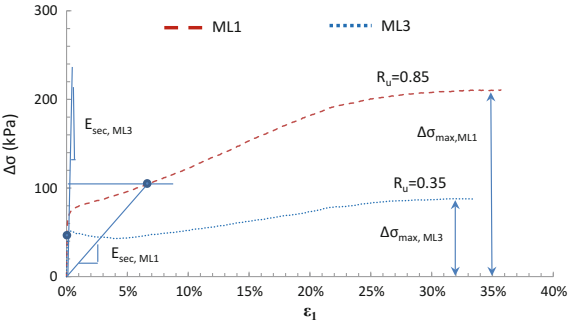

Fig. 7.7 Determination of secant modulus for specimens with two excess pore pressure ratios

7.3 Effect of Excess Pore Pressure on Postcyclic Shear Behavior—without Reconsolidation

7.3.1 Undrained Shear Behavior

Figure 7.8 shows the deviator stress and excess pore pressure versus axial strain, and stress paths starting at various levels of excess pore pressure ratio. As shown in Table 7.2, the effective confining pressure at the beginning of postcyclic monotonic compression was lower at higher excess pore pressure ratio. Specimens with lower effective confining pressure developed more negative excess pore pressure during postcyclic shearing and dilated earlier. As indicated in Fig. 7.8c, specimens MF4 and ML4 dilated initially, but the other specimens contracted initially, then dilated after the phase transformation point. There was no apparent relationship between the stress-strain curve at large strains and excess pore pressure ratio, although a lower deviator stress at identical axial strain was expected at higher R_u.

7.3.2 Shear Strength and Stiffness at Small Deformation

Figure 7.8a is enlarged in Fig. 7.9 to show more in detail the relationship between the deviator stress and axial strain at small deformation. Specimens ML5 (R_u = 0.70) and ML6 (R_u = 0.35) had a small drop in deviator stress beyond the yield stress, so they had quasi-steady states (as marked with dots in Fig. 7.9), as did static specimen MS2. Conversely, specimens ML4 (with an excess pore pressure ratio of 0.85) and MF4 (with an excess pore pressure ratio of 1.0) continued dilating until they reached critical state (Fig. 7.8). Yield shear strength and initial stiffness decreased significantly when the excess pore pressure ratio was larger than 0.7, as indicated in Fig. 7.10, which also compares these decreases by normalizing them with respect to yield shear strength and initial stiffness of MRV silt without previous cyclic loading (MS2). Yield shear strength decreased more with excess pore pressure ratio than did initial stiffness.

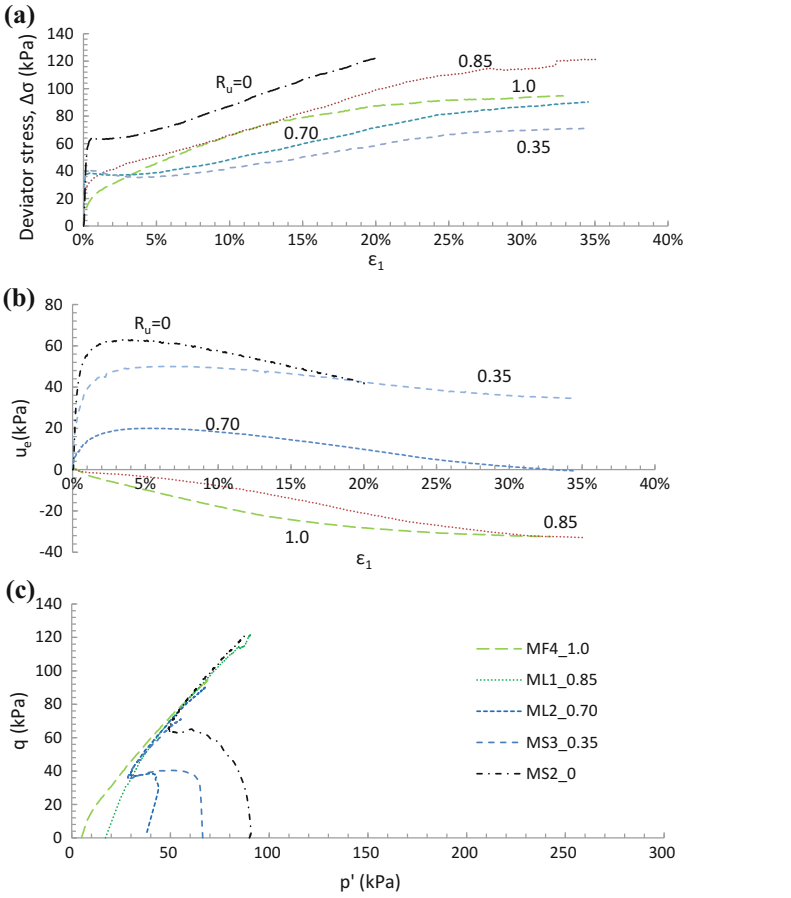

Fig. 7.8 Postcyclic behavior of MRV silt without reconsolidation after various excess pore pressure ratios: (**a**) $\Delta\sigma$ versus ε_1, (**b**) $\Delta\sigma$ versus ε_1, (**c**) q versus p′ (the values after test ID are R_u)

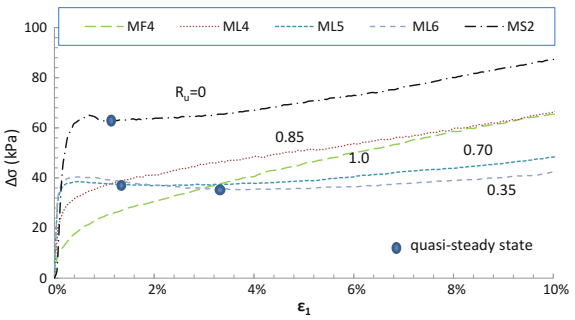

Fig. 7.9 Postcyclic behavior of MRV silt without reconsolidation after various excess pore pressure ratios at small deformation

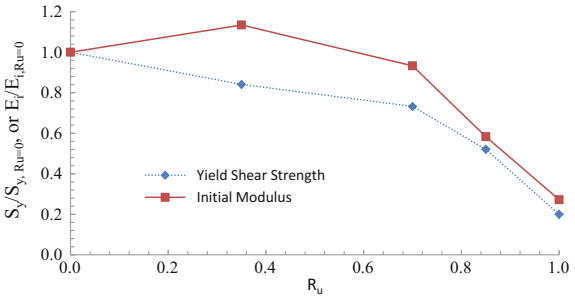

Fig. 7.10 Effect of various excess pore pressure ratio on normalized yield shear strength and initial stiffness of MRV silt without reconsolidation

Undrained shear strength was expected to increase as excess pore pressure ratio decreased because the fabric of the specimen with a lower excess pore pressure ratio was less affected by cyclic loading, and it had higher effective confining pressure. However, it was found that there was no apparent relationship between undrained shear strength and secant modulus against excess pore pressure ratio. Thus, no plots were shown for shear strength and stiffness at large deformation.

7.4 Threshold Strain for Postcyclic Shear Behavior

7.4.1 Stress-Strain Behavior

Specimens which had previously been subjected to cyclic loading were reconsolidated and then sheared monotonically under strain control. The stress-strain curves for the MRV silt specimens with OCRs of 1 and 4 are presented in Fig. 7.11. Figure 7.11 indicates that all specimens had a well-defined strain-hardening behavior in the initial stage and high initial stiffnesses. The critical state, at which the deviator stress did not change substantially, was reached at an axial strain in the range 25–30% for each specimen. As shown in Fig. 7.11a, for normally consolidated MRV silt, the deviator stress-strain curves for the specimens subjected to a residual axial strain (induced by previous cyclic loading) of $\leq 0.55\%$ were below that for virgin specimen without previous cyclic loading. The opposite was true for the specimens subjected to a residual axial strain of $\geq 0.84\%$. Similar results were found for specimens with an OCR of 4, as presented in Fig. 7.11b.

For both cases, there was no substantial difference in the variation of stress-strain curve with residual axial strain when the residual axial strain was $\leq 0.55\%$. As stated previously, the stress-strain curves of the virgin specimens plot above the curves of the specimens with residual axial strains of $\leq 0.55\%$. It should be reiterated, however, that the static triaxial tests were carried out in a test setup different from that used for postcyclic triaxial tests. The postcyclic monotonic triaxial tests were conducted on the same specimens used for cyclic loading but on a different (static) load frame. The cyclic triaxial chamber including the specimen was moved to the static load frame (placed by the GCTS loading frame) for the test. The static

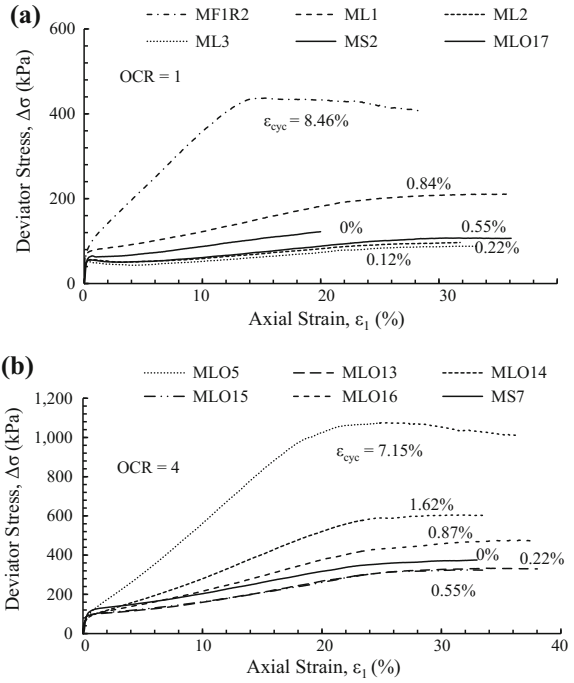

Fig. 7.11 Stress-strain behavior of the MRV silt: (**a**) OCR = 1, (**b**) OCR = 4

load frame was also used for the static consolidated undrained tests on virgin specimens. The difference in the stress-strain curve was expected and can be attributed to the different loading setup. Compared to the virgin specimen, the decrease in the undrained shear strength at low levels of axial strain is thought to be attributable, to some degree, to the testing system. This difference was consistently small and was not further investigated as it was found to have no noticeable effect on the test results. Hence, more emphasis will be on the increase rather than the decrease in undrained shear strength with residual axial strain.

7.4.2 Determination of Threshold Axial Strain

The effect of cyclic axial strain due to previous cyclic loading on postcyclic shear strength was investigated. The relationship between the shear strength ratio ($S_{u,post}$/$S_{u,virgin}$) and cyclic axial strain is presented in Fig. 7.12. As shown in this figure, the postcyclic shear strength was reduced slightly when cyclic axial strain was smaller than approximately 0.4%, but increased substantially when the cyclic axial strain exceeded 0.4%. The cyclic axial strain at which postcyclic shear strength starts increasing is defined as threshold cyclic axial strain. When cyclic axial strain exceeds this threshold value, soil fabric is mobilized substantially resulting in significant increases in soil density principally due to reconsolidation.

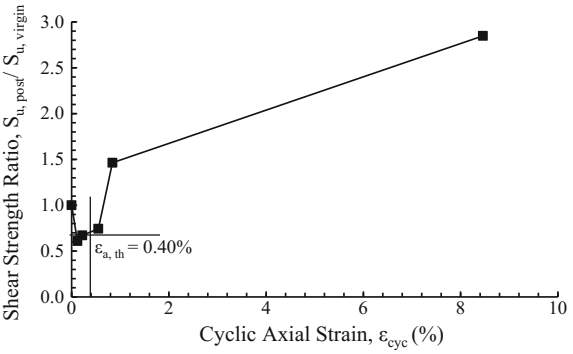

Fig. 7.12 Variation of postcyclic shear strength against cyclic axial strain for the normally consolidated MRV silt

Erken and Ulker (2007) presented a shear stress-controlled approach for determining yield cyclic shear strain, over which cyclic shear strain increases sharply during cyclic tests. As presented in Fig. 7.13, the mean effective stress (p′) decreased due to a build-up of excess pore pressure from the starting of cyclic loading. The increase in the cyclic shear strain was gradual initially but became rapid at the later stage. Two envelope lines, denoting approximately the positive limits of the cyclic shear strain (γ_{cyc}) versus p′ plot were drawn. The cyclic shear strain at the point of intersection of the boundary lines was defined as the yield cyclic shear strain by Erken and Ulker (2007). The yield cyclic axial strain was determined using the approach of Erken and Ulker (2007). Correspondingly, the cyclic axial strain ($\varepsilon_{a,c}$), rather than the γ_{cyc}, was used in this space. For example, as presented in Fig. 7.14, the yield cyclic axial strains for two cyclic triaxial tests with different OCRs and CSRs were determined to be 0.51 and 0.48%, respectively. It is pertinent to note that a large positive cyclic axial strain developed earlier than a large negative cyclic axial strain, although the latter seemed to start to develop at a higher mean effective stress (p′) than the former. The mean effective stress during the cyclic triaxial test increased due to negative excess pore pressure in extension. Thus, yield cyclic axial strain was determined as single amplitude in compression with positive axial strain rather than in extension with negative axial strain.

Although there is a difference in the values of the yield cyclic axial strain and the threshold cyclic axial strain, this difference is small. It is logical to consider the

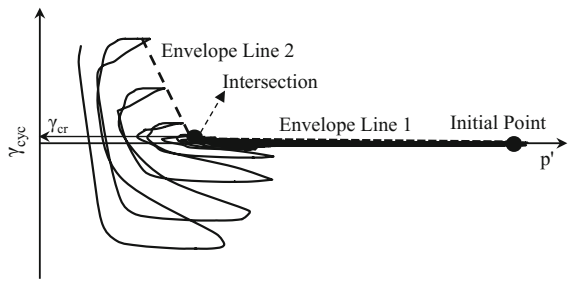

Fig. 7.13 Determination of critical yield shear strain

threshold cyclic axial strain as almost equal to the yield cyclic axial strain. When soil develops a yield cyclic axial strain, the cyclic axial strain starts to increase rapidly, resulting in substantial changes in the microstructure of the soil. This large change of microstructure leads to an equally large rearrangement of microstructure by way of reconsolidation. Consequently, there is a large increase in the postcyclic shear strength of the soil. To verify the validity of this hypothesis, a series of cyclic triaxial tests with OCR = 4 was conducted at different residual cyclic axial strains. The results of these tests, presented in Fig. 7.15, show that the threshold cyclic axial strain for OCR = 4 is also equal to 0.40%, which is close to the yield cyclic axial strain of 0.48% presented Fig. 7.14b.

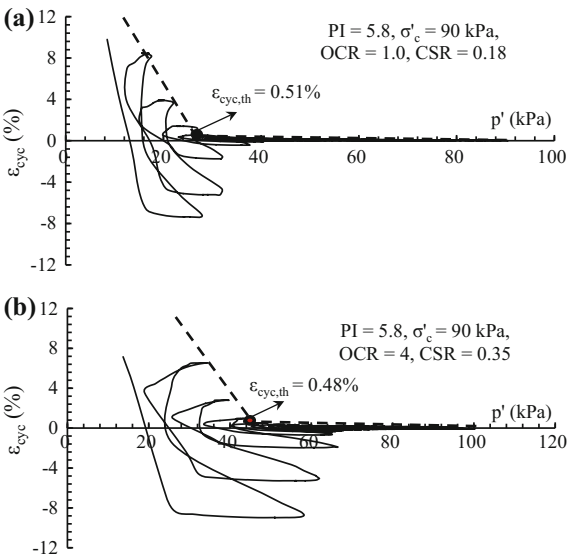

Fig. 7.14 Determination of yield cyclic axial strain for two cyclic triaxial tests of the MRV silt: (**a**) OCR = 1, (**b**) OCR = 4

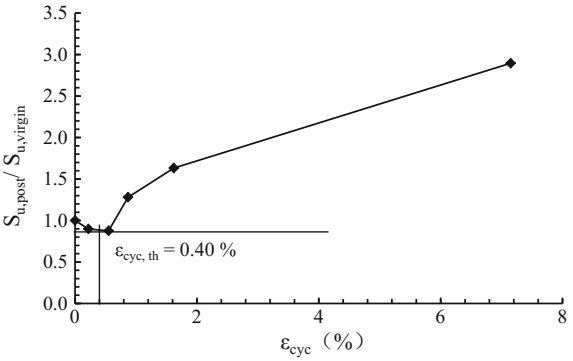

Fig. 7.15 Variation of postcyclic shear strength against cyclic axial strain for the MRV silt with OCR of 4

7.4.3 Influence Factors

Previous studies (Silver and Seed 1971; Dobry et al. 1982; Dyvik et al. 1984; Youd 1972) reveal that variations (including substantial variations) of void ratio (e) and confining stress have a negligible influence in the threshold strain for cyclic pore water pressure in sands. For clays, for the rather wide range of over-consolidation ratio (OCR) of 1 to 6 and corresponding e, Ohara and Matsuda (1988) obtained a threshold strain for cyclic pore water pressure of between 0.08 and 0.10% for kaolinite. For sand and sandy clay, Hsu and Vucetic (2004) found that although e, relative density (D_r) and confining stress substantially influence cyclic settlement and cyclic pore water pressure patterns and rates, they do not substantially influence the value of threshold strain for volume change and the build-up of pore pressure. For clayey soils, Hsu and Vucetic (2004, 2006) reported that the threshold shear strain for pore pressure accumulation and volume change increases with PI. However, there are no published studies on the influence factors of the threshold cyclic axial strain for low-plasticity silt.

The effects of CSR, OCR, effective consolidation pressure and PI on the threshold cyclic axial strain of the MRV silt were investigated. Various quantities of Sodium Bentonite were added to MRV silt to obtain specimens with different PIs. The PI and the other index properties of the MRV silt-bentonite mixtures investigated are presented in Table 7.3. The PI, OCR, and CSR for each specimen are presented in Table 7.4. As stated previously, since there is no substantial difference between yield cyclic axial strain and threshold cyclic axial strain, the threshold axial strain can be determined not only on the basis of a series of cyclic triaxial tests followed by postcyclic shearing, but also on one cyclic triaxial test according to the approach of Erken and Ulker (2007). In order to minimize testing time, the approach of Erken and Ulker (1995) was employed. The threshold cyclic axial strain was determined for each case with specific PI, OCR, and CSR, as presented in Table 7.4.

(1) Cyclic Stress Ratio (CSR)

The effect of CSR on postcyclic shear behavior was investigated in Chap. 5. No significant difference in the postcyclic shear behavior of specimens due to different CSRs was found, and it was concluded that postcyclic behavior was related to excess pore pressure ratio or residual cyclic strain rather than CSR. The effect of CSR on threshold cyclic axial strain for the MRV silt with an OCR of 1.0 and σ'_c of 90 kPa is presented in Fig. 7.16, which indicates that the threshold cyclic axial strain did not change substantially with CSR.

(2) Overconsolidation Ratio (OCR)

The variation of threshold cyclic axial strain with OCR is presented in Fig. 7.17. Figure 7.17 indicates that the OCR has no effect on threshold cyclic axial strain. Although a higher OCR can increase cyclic strength due to increase in soil density, as reported by Izadi (2008), the soil fabric was mobilized at similar threshold cyclic

Table 7.3 Index properties of the tested soils

Index property	Added bentonite content (%)			
	0	2.5	5.0	7.5
Clay content (%)	14.5	16.6	18.8	20.9
Specific gravity	2.71	2.70	2.68	2.67
Liquid limit (%)	28.1	28.9	32.7	36.9
Plastic limit (%)	22.3	22.7	23.3	23.4
PI	5.8	6.2	9.4	13.5
C_c	0.089	0.128	0.199	N/A
C_r	0.009	0.010	0.016	N/A

Note PI—plasticity index, C_c—compression index, C_r—recompression index

Table 7.4 List of cyclic triaxial tests

Specimen ID	PI	σ'_c (kPa)	OCR	CSR	$\varepsilon_{cyc,th}$ (%)
MF1R1	5.8	90	1	0.18	0.51
MD3	5.8		1	0.25	0.61
MD4	5.8		1	0.35	0.41
MLO2	5.8		2	0.35	0.40
MLO3	5.8		3	0.35	0.49
MLO4	5.8		2	0.25	0.59
MLO5	5.8		4	0.35	0.48
MLO6	5.8		3	0.25	0.39
MLO7	5.8		3	0.4	0.51
MFB1	6		1	0.25	0.72
MFB2	6.2		1	0.25	0.69
MFB3	6.2		1	0.18	0.61
MFB4	6.2		1	0.18	0.40
MFB5	6.2		1	0.18	0.41
MFB6	6.2		1	0.35	0.39
MFB7	9.4		1	0.18	0.38
MFB8	9.4		1	0.25	0.70
MFB9	9.4		1	0.35	0.42
MLN1	5.8	180	1	0.18	0.40
MLN2	5.8	360	1	0.18	0.20

Note PI—plasticity index, σ'_c—effective consolidation pressure, OCR—overconsolidation ratio, CSR—cyclic stress ratio, $\varepsilon_{cyc,th}$—threshold cyclic axial strain

axial strain for cyclic tests at different OCRs. A search of literature has so far yielded no other work on the effect of OCR on threshold cyclic axial strain of low-plasticity silt. However, Ohara and Matsuda (1988) conducted tests on kaolinite found that the threshold strain for cyclic pore water pressure did not vary with OCR within a range of 1–6.

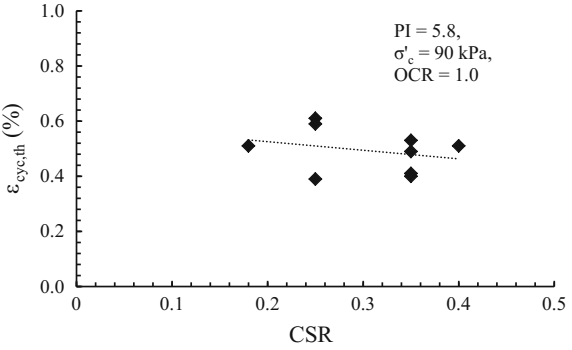

Fig. 7.16 Threshold cyclic axial strain versus CSR for the MRV silt

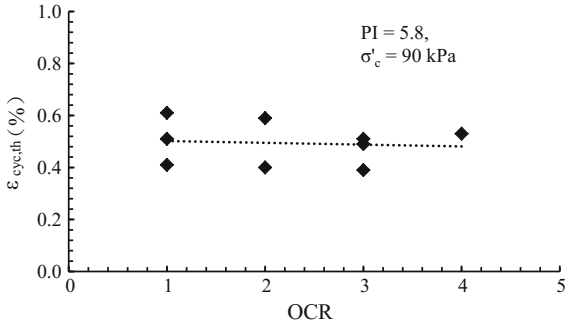

Fig. 7.17 Threshold cyclic axial strain versus OCR for the MRV silt

(3) Effective Consolidation Pressure

The variation of threshold cyclic axial strain for postcyclic shear strength with effective consolidation pressure for the MRV silt with an OCR of 1 is presented in Fig. 7.18. The threshold cyclic axial strain for postcyclic shear strength decreases linearly with effective consolidation pressure. As noted by Hsu and Vucetic (2004), although effective consolidation pressure substantially influence the cyclic settlement and cyclic pore water pressure patterns and rates, it does not substantially influence the value of threshold strain for volume change and build-up of pore pressure. Thus, the effective consolidation pressure has different effect on the threshold strain for postcyclic shear strength and that for volume change and build-up of pore pressure.

(4) Plasticity Index (PI)

Various quantities of bentonite were added to the MRV silt to create low-plasticity soil mixtures with PIs of 5.8–9.4. The relationship between threshold cyclic axial strain and PI is presented in Fig. 7.19. F`rom Fig. 7.19, in the narrow PI range (5.8–9.4), there was very little change in the threshold cyclic axial strain with respect to PI. However, as found in Chaps. 3 and 4, the static and cyclic shear

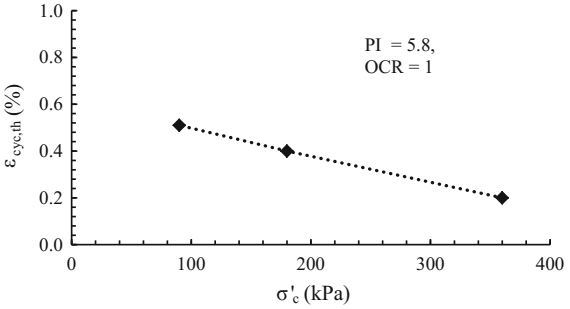

Fig. 7.18 Threshold cyclic axial strain versus effective consolidation pressure for the MRV silt

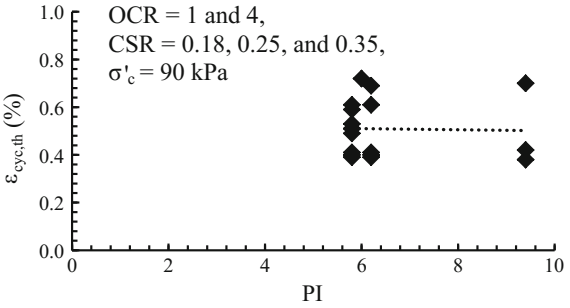

Fig. 7.19 Threshold cyclic axial strain versus plasticity index

behavior of the soil change substantially due to addition of bentonite. After a quasi-steady state, the MRV silt exhibits nearly continuous strain-hardening behavior until critical state under monotonic triaxial tests, but the MRV silt-bentonite mix exhibits plastic behavior. Correspondingly, while MRV silt is liquefiable under cyclic loading, the MRV silt-bentonite mix exhibits cyclic softening. Although the soil behavior changes substantially within the narrow range of PI, the threshold cyclic axial strain did not change substantially. Soil mixtures with higher plasticity indices are required for tests in future.

Vucetic (1994) found that the threshold shear strain for cyclic pore-water pressure increased with PI, as presented in Fig. 7.20. The axial strains for MRV silt and the MRV silt-bentonite mix were converted to shear strain by multiplying 0.75 as suggested by Bray and Sancio (2006) and the threshold shear strain for postcyclic shear strength are presented in Fig. 7.20. Figure 7.21 also presents data from Houston and Herrmann (1980), Lefebvre et al. (1989), Diaz-Rodriguez and Santamarina (2001) and Erken and Ulker (2007). The data were summarized in Table 7.5. The band and average line of threshold shear strain for postcyclic shear strength change are shown on Fig. 7.20. The band and average line show that the threshold shear strain for postcyclic shear strength increased with PI. The minimum threshold shear strain is about 0.1% and exists for non-plastic soil. From the average line, increases in the threshold shear strain are larger when PI is less than 50

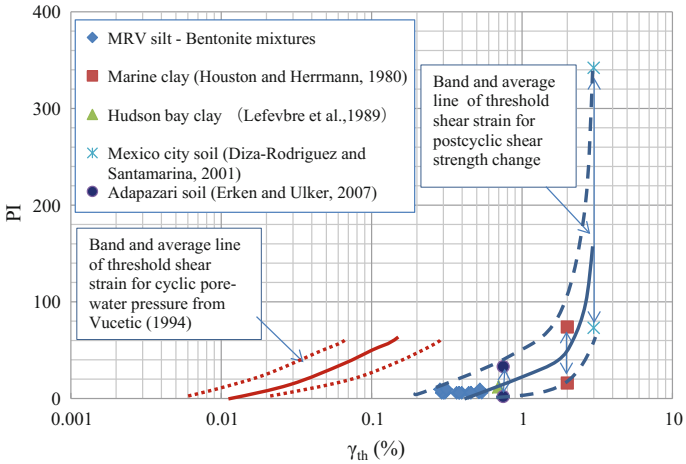

Fig. 7.20 The effect of plasticity index on threshold shear strain

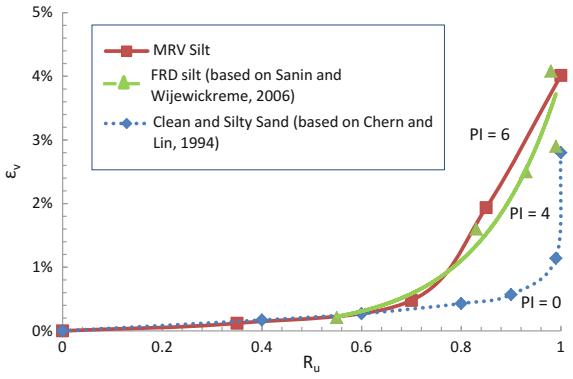

Fig. 7.21 Variation in volumetric strain with various excess pore pressure ratios in MRV silt and clean and silty sand

Table 7.5 Threshold shear strain for postcyclic shear strength of different soils

Soil name	PI	γ_{th} (%)	References
Mexico City soil	73–342	3	Diaz-Rodriguez and Santamarina (2001)
Hudson Bay	12	0.7	Lefebvre et al. (1989)
Adapazari soil	2–33	0.75	Erken and Ulker (2007)
Marine clay	16–74	2	Houston and Herrmann (1980)
MRV silt	5.8	0.35	This study
	6.0	0.52	
	6.2	0.35	
	9.4	0.38	

than when PI is greater than 50. When the PI is greater than 100, the threshold shear strain tends to become constant with a maximum of approximately 3%. For comparison, the average line for postcyclic shear strength change is almost parallel to that for cyclic pore-water pressure in the semi-log space.

7.5 Discussion

It was found that an excess pore pressure ratio greater than 0.70 is a prerequisite for an increase in postcyclic yield shear strength (S_y), initial stiffness (E_i) and undrained shear strength (S_u) due to full reconsolidation. A reasonable explanation for why these values increase significantly only when the R_u is greater than 0.70 is that the increase in soil density is insufficient to compensate for the reduction due to the weakened fabric during cyclic loading. As shown in Fig. 7.21, volumetric strain increased significantly when the excess pore pressure ratio was greater than 0.70. This finding for MRV silt was similar to the result for slightly overconsolidated Fraser River Delta (FRD) silt with a PI of 4.0 (Sanin and Wijewickreme 2006) but contradicts that for clean and silty sands (Chern and Lin 1994). Sanin and Wijewickreme (2006) stated that the specimens started to suffer to significant postcyclic volume strain for FRD silt when they had a R_u close to but less than 1.0. Chern and Lin (1994) presented that a R_u of 1.0 is a prerequisite to significant volume change due to reconsolidation in clean and silty sands. Thus, cyclic loading damages the fabric of MRV silt at lower excess pore pressure ratio than it does that of clean and silty sand.

This study of postcyclic strength and stiffness change due to cyclic loading and reconsolidation is beneficial not only for stability and deformation evaluation in earthquake engineering, but also as a means to develop guidelines for ground mitigation such as dynamic compaction and stone column installation in low-plasticity silts. The installation of remedial wick drains can help reconsolidate the ground and increase shear strength (Thevanayagam et al. 2001).

Several researchers have studied postcyclic undrained shear strength; these included Poulos et al. (1985), Seed (1987), Ishihara et al. (1990), Seed and Harder (1990), Thevanayagam et al. (1996), Olson and Stark (2002, 2003), Robertson (2010), and others. Generally, there are three approaches to predict the undrained shear strength of soil with previous cyclic loading: laboratory testing, in situ testing, and normalized strength (Kramer 1996). Each approach has its own advantages and limitations, and each yields somewhat different undrained shear strengths, indicated in Wang (2011). Thevanayagam et al. (1996) analyzed the postcyclic undrained shear strength of 24 sandy soils (including one sandy silt) and presented relationships for the lower bounds of undrained shear strength for clean sands and silty sands, shown in Fig. 7.22. The minimum void ratios for about 10 soils were also determined according to ASTM standard (D 1557), which was followed for the current research, as mentioned in previous section. The data of the MRV silt tested here were added to Fig. 7.22 and fall below SM lower bound. The undrained shear

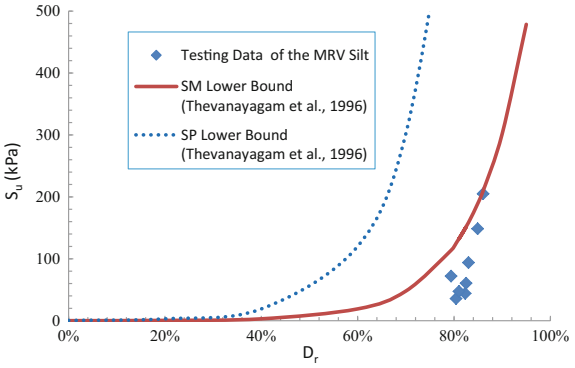

Fig. 7.22 Relationship between undrained shear strength and relative density

strength increased sharply with a small increase in relative density. This phenomenon presents a challenge to estimate the undrained shear strength, especially for in situ testing. It also requires that relative density be measured accurately; otherwise, the results will be inaccurate.

7.6 Summary

This chapter examined the effect of cyclic loading magnitude on monotonic shearing behavior of the MRV silt. The postcyclic shear tests on MRV silt reconstituted specimens were conducted with full and no reconsolidation after various levels of excess pore pressure ratio. Based on the above analysis, the following conclusion can be drawn for the soil tested and under the single initial effective stress and relative density.

With full reconsolidation, yield shear strength and initial stiffness generally increased with excess pore pressure ratio. Undrained shear strength increases significantly for a silt with a excess pore pressure ratio higher than 0.70 compared to virgin silt (i.e., silt without previous cyclic loading). Thus, an excess pore pressure ratio greater than 0.70 is a prerequisite for a significant increase in undrained shear strength.

Without reconsolidation, excess pore pressure ratio had no apparent effect on the reductions in undrained shear strength and secant modulus. However, the yield shear strength and initial stiffness were reduced with an increase in excess pore pressure ratio. These reductions were significant (about 80% for yield shear strength and about 76% for initial stiffness in maximum) when the excess pore pressure ratio was greater than 0.70.

Significant increase in the volumetric strain due to reconsolidation appeared at lower excess pore pressure ratio for low-plasticity silt than for clean and silty sand. This indicates that cyclic loading tends to modify or strain the fabric of the low-plasticity silts at lower excess pore pressure ratio than it does that of clean and silty sand with no plasticity.

When the specimen experienced a cyclic axial strain greater than 0.4% and was reconsolidated, the undrained shear strength increased with cyclic axial strain. The threshold cyclic axial strain for postcyclic shear strength increase was determined to be 0.4%. The yield cyclic axial strain equal to the strain at the intersection of two envelops in γ_{cyc} versus p′ space according to Erken and Ulker (2007) was not substantially different with the threshold cyclic axial strain. The approach of Erken and Ulker (2007) can be used for the determination of the threshold cyclic axial strain, so that a series of triaixal tests are not required, thereby reducing substantially the cost of testing. Threshold cyclic axial strain decreased with effective consolidation pressure, but it did not change substantially with CSR and OCR. The threshold cyclic axial strain did not change substantially with PI in a narrow range of 5.8–9.4. However, when threshold cyclic axial strain was converted to threshold shear strain, and data from other researchers were included in the analysis, it was found that the threshold shear strain increases substantially, especially with PI less than 50. The minimum and maximum values of the threshold shear strain were 0.1 and 3.0%, respectively.

The postcyclic undrained shear strength of MRV silt falls within the range for SM/ML reported by Thevanayagam et al. (1996). Due to the reconsolidation after cyclic loading, undrained shear strength increases significantly with an increase in relative density. The determination of accurate relative density is crucial to estimate undrained shear strength of MRV silt after cyclic loading, but continues to be a challenge for fine-grained soils.

The practical implications of the research presented herein are that in some low magnitude events where the number of cycles increased the pore water pressure to levels that do not trigger liquefaction (flow or cyclic) a reduction in strength and stiffness is still evident. A collapse or stability condition may not be experienced but a decrease in performance due to deformations may be evident when limited excess pore pressure ratio ($R_u < 1.0$) is induced. After reconsolidation the material tends to gain strength and stiffness.

References

Bray, J. D., & Sancio, R. B. (2006). Assessment of the liquefaction susceptibility of fine-grained soils. *Journal of Geotechnical and Geoenvironmental Engineering, 132*(9), 1165–1177.

Chern, J. C., & Lin, C. C. (1994). Post-cyclic consolidation behavior of loose sands. In *Proceeding of Settlement 94*, Geotechnical Special Publication, ASCE, No. 40.

Diaz-Rodriguez, J. A., & Santamarina, J. C. (2001). Mexico city soil behavior at different strains: Observations and physical interpretation. *Journal of Geotechnical and Geoenvironmental engineering, 127*(9), 783–789.

Dobry, R., Ladd, R. S., Yokel, F. Y., Chung, R. M., & Powell, D. (1982). Prediction of pore-water pressure buildup and liquefaction of sands during earthquakes by the cyclic strain method. In *NBS Building Science Series No. 138*, National Bureau of Standards, U.S. Dept. of Commerce, Washington, D.C., p. 150.

Dyvik, R., Dobry, R., Thomas, G. E., & Pierce, W. G. (1984). Influence of Consolidation Shear Stresses and Relative Density on Threshold Strain and Pore Pressure during Cyclic Straining of Saturated Sands. Miscellaneous Paper, GL-84-15, Dept. of the Army, U.S. Army Corps of Engineers, Washington, D.C., p. 74.

Erken, A., & Ulker, B. M. C. (2007). Effect of cyclic loading on monotonic shear strength of fine-grained soils. *Engineering Geology, 89,* 243–257.

Houston, W. N., & Herrmann, H. G. (1980). Undrained cyclic strength of marine soils. *Journal of Geotechnical and Geoenvironmental Engineering, 106*(6), 691–712.

Hsu, C. C., & Vucetic, M. (2004). Volumetric threshold shear strain for cyclic settlement. *Journal of Geotechnical and Geoenvironmental Engineering, 130*(1), 58–70.

Hsu, C. C., & Vucetic, M. (2006). Threshold shear strain for cyclic pore-water pressure in cohesive soils. *Journal of Geotechnical and Geoenvironmental Engineering, 132*(10), 1325–1335.

Ishihara, K., Yasuda, S., & Yoshida, Y. (1990). Liquefaction-induced flow failure and residual strength of silty sands. *Soils and Foundations, 30*(3), 69–80.

Izadi, A. (2008). Liquefaction and post-liquefaction behavior of low plasticity silts using cyclic triaxial tests. PhD Dissertation, Missouri University of Science and Technology, Rolla, MO, US.

Kramer, S. L. (1996). *Geotechnical earthquake engineering*. New Jersey: Prentice Hall.

Lefebvre, G. S., Leboeuf, D., & Demers, B. (1989). Stability threshold for cyclic loading of saturated clay. *Canadian Geotechnical Journal, 26*(1), 122–131.

Ohara, S., & Matsuda, H. (1988). 'Study on settlement of saturated clay layer induced by cyclic shear. *Soils and Foundations*, *28*(3), 103–113.

Olson, S. M., & Stark, T. D. (2002). Liquefied strength ratio from liquefaction flow failure case histories. *Canadian Geotechnical Journal, 39,* 629–647.

Olson, S. M., & Stark, T. D. (2003). Yield strength ratio and liquefaction analysis of slopes and embankments. *Journal of Geotechnical and Geoenvironmental Engineering, 129*(8), 727–737.

Poulos, S. J., Castro, G., & France, J. W. (1985). Liquefaction evaluation procedure. *Journal of Geotechnical Engineering, 111*(6), 772–792.

Robertson, P. K. (2010). Evaluation of flow liquefaction and liquefied strength using the cone penetration test. *Journal of Geotechnical and Geoenvironmental Engineering, 136*(6), 842–853.

Sanin, M. V., & Wijewickreme, D. (2006). Cyclic shear response of channel-fill Fraser River Delta Silt. *Soil Dynamics and Earthquake Engineering, 26,* 854–869.

Seed, H. B. (1987). Design problems in soil liquefaction. *Journal of Geotechnical Engineering, 113*(8), 827–845.

Seed, R. B., & Harder, L. F. (1990). SPT-based analysis of cyclic pore pressure generation and undrained residual strength. In *Proceedings of the H. Bolton Seed Memorial Symposium* (Vol. 2, pp. 351–376). Berkeley: University of California.

Silver, M. L., & Seed, H. B. (1971). Volume changes in sands during cyclic loading. *Journal of Soil Mechanics & Foundations Div ASCE, 97*(9), 1171–1182.

Thevanayagam, S., Martin, G. R., Shenthan, T., & Liang, J. (2001). Post-liquefaction pore pressure dissipation and densification in silty soils. In *Proceedings of 4th International Conference on Recent Advances in Geotechnical Earthquake Engineering and Soil Dynamics*, San Diego, CA.

Thevanayagam, S., Wang, C. C., & Ravishankar, K. (1996). Determination of Post-liquefaction Strength: Steady State vs Residual Strength. *Geotechnical Special Publication, 58*, 1210–1224.

Vucetic, M. (1994). Cyclic threshold shear strain in soils. *Journal of Geotechnical Engineering, 120*(12), 2208–2228.

Wang, S. (2011). Postcyclic behavior of low-plasticity silt. Ph.D. Dissertation. Missouri University of Science and Technology, Rolla, MO, US.

Wang, S., Luna, R., & Yang, J. (2013). Postcyclic behavior of low-plasticity silt with limited liquefaction. *Soil Dynamics and Earthquake Engineering, 54,* 39–46.

Wang, S., Onyejekwe, S., & Yang, J. (2014). Threshold strain for postcyclic shear strength change of Mississippi River Valley silt due to cyclic triaxial loading. *Journal of Testing and Evaluation, 42*(1), 69–77.

Youd, L. T. (1972). Compaction of sands by repeated shear straining. *Journal of Soil Mechanics and Foundations Division, 98*(7), 709–725.

Chapter 8
Reliquefaction Characteristics of Low-plasticity Silt

This chapter reports effect of previous cyclic shearing on liquefaction resistance of low-plasticity silt from the Mississippi River Valley. Some ground improvement techniques for promoting the liquefaction resistance of low-plasticity silts are proposed based on the research findings.

8.1 Testing Program

Test specimen was installed in the triaxial chamber for each test, after which the specimen was brought to full saturation (B-value > 0.95) by applying a combination of vacuum and backpressure. To get the specimens fully-saturated, a vacuum pressure of 45 kPa was applied for about 0.5 h, and then a high backpressure of about 400 kPa was applied in 25 kPa increments. Each increment of backpressure was applied for about 1 h. After backpressure saturation was complete (B-value > 0.95 saturation), specimens were normally consolidated with effective consolidation pressure (σ'_c) of about 90 kPa. The average water content of consolidated specimens was about 24.7 ± 0.5%, yielding a w_c/LL of 0.88 + 0.02. On completion of consolidation, cyclic loading was applied to the specimens. The cyclic loading was controlled with deviator stress (i.e., $\Delta\sigma$, which is equal to maximum effective stress σ'_1 minus minimum effective stress σ'_3). The cyclic deviator stress was set following the sine function. Cyclic loading was applied at a frequency of 0.1 Hz instead of the predominant frequency for earthquake loading which tends to be in the range of 1–5 Hz (Izadi 2008; Kramer 1996). The predominant frequency range is rather too high for laboratory tests on low-plasticity silt. When cyclic loading is applied to low-plasticity silt at this frequency range, there is usually insufficient time for the transmission of excess pore pressure (Δu) from the specimens to the pore pressure transducer. Taking this fact into consideration, a lower frequency (0.1 Hz in this case) is typically used. Since this study presents the effect of previous cyclic shearing on liquefaction resistance and as

S. Wang, *Monotonic, Cyclic and Postcyclic Shear Behavior of Low-plasticity Silt*,
https://doi.org/10.1007/978-981-10-7083-9_8

discussed in Chap. 7, excess pore pressure or residual cyclic strain is the key factor influencing postcyclic behavior of silt, the influence of load frequency on postcyclic behavior is not taken into consideration in this study.

Two types of tests were conducted in this study: (a) tests to determine the number of liquefaction tests required to substantially increase the liquefaction resistance of specimens; and (b) tests to evaluate the effect of the cyclically induced axial strain on liquefaction resistance. As presented in Wang et al. (2013), Cyclic loading was continuously applied until full liquefaction in the tests to determine the number of liquefaction tests required to substantially increase the liquefaction resistance. Full liquefaction was attained when the excess pore pressure ratio, R_u ($=\Delta u/\sigma'_c$) had a value of 1.0. After full liquefaction, the cyclically induced axial strain was held constant, while the deviator stress was set back to zero so that the specimen would be reconsolidated under isotropic consolidation pressure. The drainage valves were then opened and excess pore pressure was allowed to dissipate completely to achieve full reconsolidation. During this process, there was very small change in axial strain (less than 0.01%). This very small change in axial strain can be attributed to the high stiffness of the specimen. The specimen was in compression during the process. As presented later in this chapter, the specimen had none to very small axial strain in compression during the reliquefaction tests, especially for the first few loading cycles. After full reconsolidation was attained, repeated cyclic loading was applied on the reconsolidated specimens. This repeated cyclic loading was continuously applied until the specimens liquefied completely, and the reconsolidation was allowed again. This process of reliquefaction and reconsolidation was repeated until the specimen no longer liquefied. The excess pore pressures, axial strain of specimens, number of loading cycles required to liquefy specimens and void ratio change were recorded. The cyclic stress ratios investigated for different specimens included 0.20, 0.25, and 0.35. For each specimen, the CSRs remained constant for the duration of the cyclic loading.

The tests to evaluate the effect of the residual strain induced by cyclic loading on liquefaction resistance followed a procedure similar to that described above. However, while for the initial liquefaction test, specimens were not loaded until full liquefaction was attained (they were loaded to various excess pore pressure ratios, all less than 1), the reconsolidated specimens were loaded cyclically again until full liquefaction ($R_u = 1.0$). All cyclic tests for studying the effect of level of previous cyclic shearing on liquefaction resistance were conducted at a CSR of 0.25.

8.2 Testing Results

8.2.1 Excess Pore Pressure Response

During cyclic loading, excess pore pressure is developed in the specimens. As presented in Fig. 8.1 ($p' = \sigma'_1/3 + 2\sigma'_3/3$, $q = \sigma'_1 - \sigma'_3$), the excess pore pressure

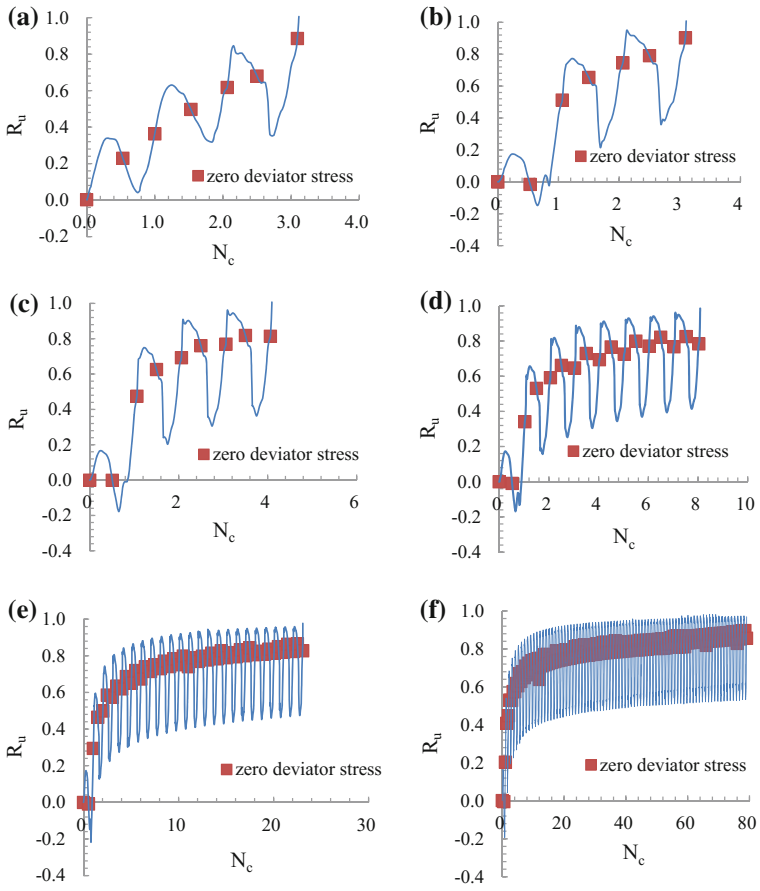

Fig. 8.1 Excess pore pressure ratios during different liquefaction tests for the specimen with a cyclic stress ratio of 0.25: **a** 1st, **b** 2nd, **c** 3rd, **d** 4th, **e** 5th, **f** 6th

ratio induced by cyclic loading increased until unity. However, under less than three liquefaction tests, the specimen just required about 3 loading cycles to liquefy the specimen. After the specimen was reconsolidated after the 2nd liquefaction test, the specimen required about 4 loading cycles to liquefy. With more liquefactions and reconsolidations, more loading cycles were required to attain liquefaction. As presented in Fig. 8.1f, the specimen required a large number of loading cycles to develop liquefaction after the 5th liquefaction test. Additionally, as presented in Fig. 8.1e, f, it is indicated that while excess pore pressure developed at a fast rate at the initial stage of cyclic loading, it increased very slightly at the later stages.

The different rates of development of excess pore pressure in the specimen in compression and in extension during cyclic loading were investigated using stress paths, as presented in Fig. 8.2. The changes of excess pore pressure and p′ were

identical in magnitude (with reference to the p′-q stress space). In the first loading cycle for each repeated liquefaction test in Fig. 8.2b−f, the excess pore pressure within half cycle of loading in extension was much higher than that within half cycle of loading in compression, with the excess pore pressure being negative in compression. However, as presented in Fig. 8.2a, the excess pore pressure with the half cycle in compression was positive and even higher than that within the half cycle in extension during the 1st liquefaction test. This excess pore pressure response indicates that the specimen became stiff in compression and exhibited dilative behavior inducing negative excess pore pressure after the specimen liquefied and was reconsolidated. In extension, however, the specimen still showed contractive behavior, developing positive excess pore pressure. The results presented in Figs. 8.1 and 8.2 are for specimens tested at a CSR of 0.25. Results for specimens tested at different CSRs had similar excess pore pressure response. This finding for the MRV silt agrees with that for sand with large previous strain studied by Ishihara and Okada (1978).

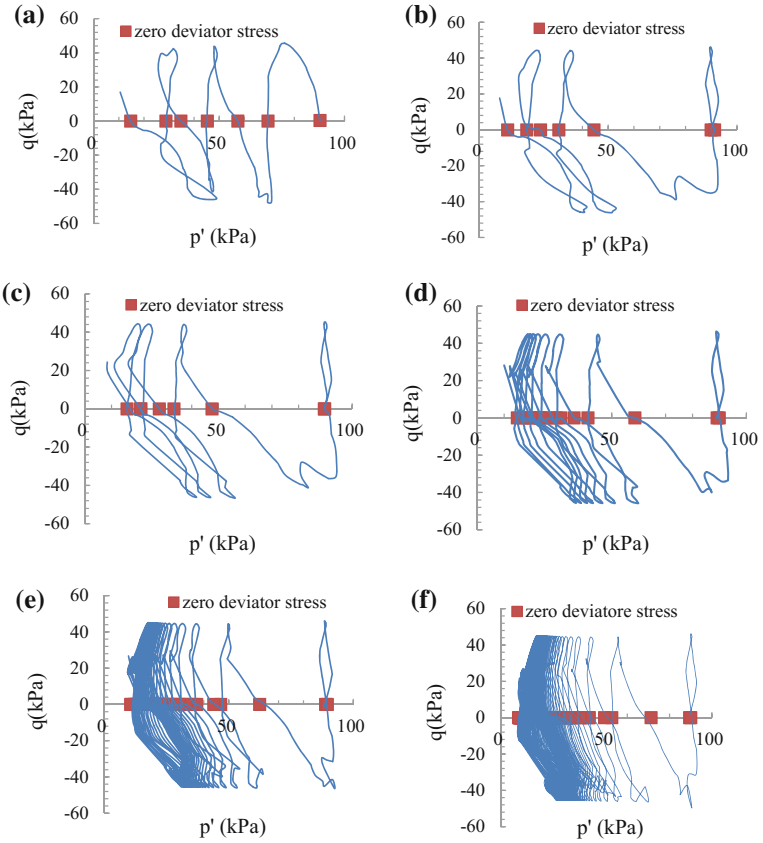

Fig. 8.2 Stress paths during different liquefaction tests for the specimen with a cyclic stress ratio of 0.25: **a** 1st, **b** 2nd, **c** 3rd, **d** 4th, **e** 5th, **f** 6th

8.2.2 *Axial Strain*

Analyses of Fig. 8.3 indicate that the double-amplitude axial strain increased with time for each cyclic loading. Further analyses of these curves show that a higher negative axial strain developed during the cyclic loading after the 1st liquefaction and reconsolidation cycle. This indicates that a higher axial strain developed in extension than in compression and that stiffness was higher in compression than in extension. This phenomenon is in agreement with excess pore pressure response stated in the last section. The higher stiffness in compression than in extension developed due to the reconsolidation after 1st cyclic loading. The reconsolidation was carried out under a cyclically induced axial strain.

The cyclically induced axial strains at liquefaction are presented in Table 8.1. Axial strains due to reconsolidation are also presented in Table 8.1. For the

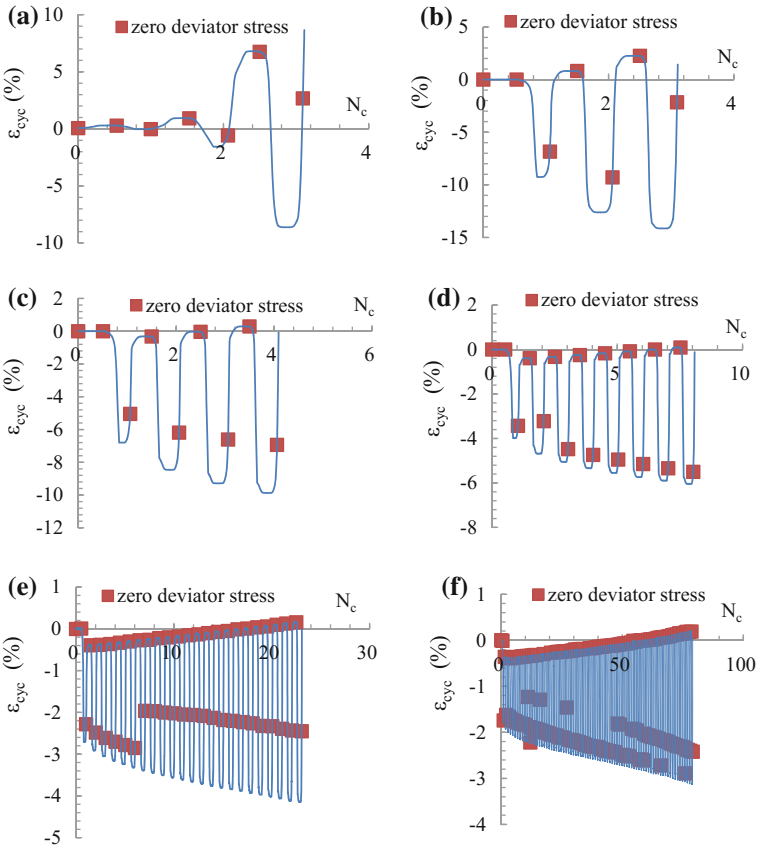

Fig. 8.3 Axial strain versus time during different liquefaction tests for the specimen with a cyclic stress ratio of 0.25: **a** 1st, **b** 2nd, **c** 3rd, **d** 4th, **e** 5th, **f** 6th

Table 8.1 Axial strain due to different liquefaction and reconsolidation tests

Test ID	CSR	Cyclically induced axial strain at liquefaction (%)					
		1st	2nd	3rd	4th	5th	6th
RL1	0.25	8.65	1.42	−0.08	−0.12	−0.01	0.07
RL2	0.35	5.60	−0.66	−0.62	−0.24	−0.18	−0.10
RL3	0.20	11.85	4.73	3.73	0.32	−0.75	−0.42
Test ID	CSR	Axial strain due to reconsolidation (%)					
		1st	2nd	3rd	4th	5th	6th
RL1	0.25	−0.16	−0.17	−0.10	−0.06	0	0
RL2	0.35	−0.29	−0.25	−0.12	−0.05	−0.04	−0.01
RL3	0.20	−0.31	−0.24	−0.21	−0.30	−0.14	0

specimen RL1 tested at a CSR of 0.25, there was a cyclically induced axial strain of 8.65% at the end of the 1st cyclic loading. The specimen achieved reconsolidation under this cyclically induced axial strain. Due to reconsolidation, specimen RL1 had an axial strain of −0.16%, implying that the specimen surprisingly dilated in the vertical direction. The recorded volumetric strain was positive, 3.72%. Thus, the specimen contracted in the horizontal direction. The dilation of specimen indicates that stiffness was very high in compression. The specimens tested at CSRs of 0.20 and 0.35 exhibited similar phenomenon.

8.2.3 Liquefaction Resistance

With reconsolidation after liquefaction, the liquefaction resistance changes, since the soil fabric and density changes. Figure 8.4 presents the relationship between liquefaction resistance, relative density and the number of liquefaction tests. The number of loading cycles (N_c) required to reach full liquefaction (R_u = 1.0) is the measure of liquefaction resistance. As presented in Fig. 8.4, the relative density of specimens increased with the number of liquefaction tests. At over six liquefaction tests, the relative density approached to 100%. Correspondingly, the specimen required many loading cycles to be liquefied.

With increase in the relative density, the specimen became denser and liquefaction resistance increased. However, there was no significant improvement in the liquefaction resistance with number of liquefaction tests at less than four liquefaction tests. At less than four liquefaction tests, there was even a decrease in liquefaction resistance for specimens tested at a CSR of 0.20. After being subjected to more than four liquefaction tests, the specimens had a significant increase in liquefaction resistance. This suggests that, notwithstanding the fact that the density of specimens kept increasing due to reconsolidation after liquefaction, the liquefaction resistance in the field will only increase after the ground has been subjected to more than four liquefaction-inducing earthquakes (of a similar frequency and

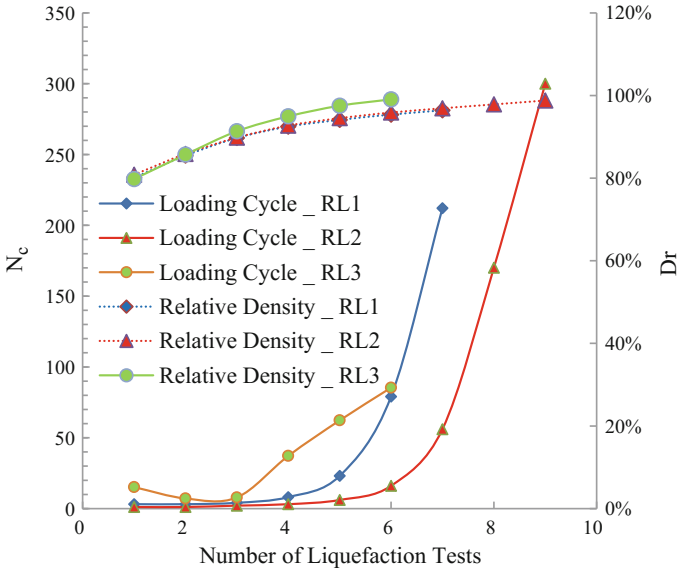

Fig. 8.4 Variation of liquefaction resistance and relative density against number of liquefaction tests

amplitude). The insignificant increase in liquefaction resistance after up to four liquefaction tests can be attributed to a weakening of the soil fabric regardless of the increase in soil density. At those few liquefaction tests (<4), the soil micro-structure becomes weak, and offers a lower liquefaction resistance. Liquefaction resistance only increased at more liquefaction tests (>4) when the soil became sufficiently densified to nullify the effect of weakening of the soil fabric.

8.2.4 Effect of the Level of Cyclically Induced Axial Strain

In the second type of tests (b), the cyclic loading was stopped at different levels of liquefaction. The plot of the cyclic number ratio against the excess pore pressure ratio induced by previous cyclic loading is presented in Fig. 8.5. The cyclic number ratio ($=N_{c,r\ (reloading)}/N_{c,v\ (virgin)}$) is the number of loading cycles to liquefy the specimens with various previous excess pore pressure ratios ($N_{c,r\ (reloading)}$) normalized with respect to the number of loading cycles to liquefy the specimens without previous cyclic loading ($N_{c,v\ (virgin)}$). Liquefaction resistance attained its peak at excess pore pressure ratio equal to 0.35.

The relationship between cyclic number ratio and cyclically induced axial strain is presented in Fig. 8.6. It is indicated that the liquefaction resistance increased significantly with a slight increase in previous cyclically induced axial strain

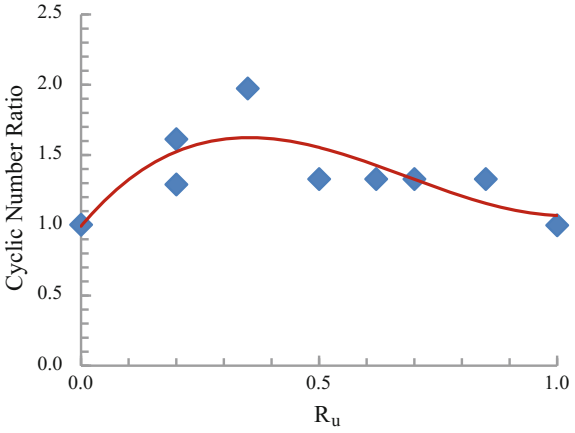

Fig. 8.5 Variation of cyclic number ratio against excess pore pressure ratio

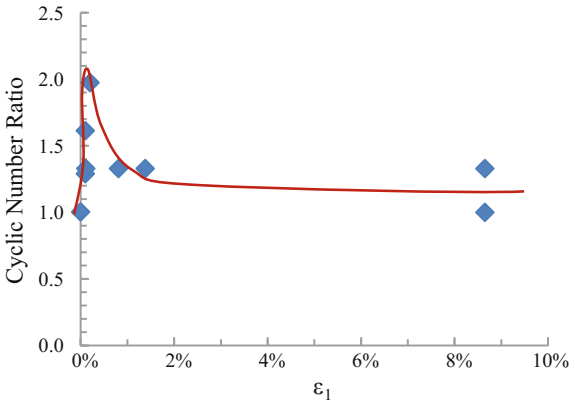

Fig. 8.6 Variation of cyclic number ratio against cyclically induced axial strain

ranging from 0 to 0.2%. This is in agreement with the findings of Finn et al. (1970). They attributed the increase of liquefaction resistance with small previous cyclically induced strain mainly to the interlocking of the particles in the original sand structure due to the elimination of small local instabilities at the contact points without any general structural rearrangement. The liquefaction resistance increased up to 0.2% previous cyclically induced axial strain and decreased significantly when the previous cyclically induced axial strain was increased from 0.2 to 1.35%. Further increase in previous cyclically induced axial strain led to no change in liquefaction resistance.

8.3 Discussion

The liquefaction resistance of MRV silt has been found to increase significantly only after experiencing a number of liquefaction tests (usually 4). Otherwise, there is usually no significant change in liquefaction resistance. The liquefaction resistance of MRV silt has also been found to increase significantly when the strain induced by previous cyclic loading is at about 0.2%. As reported in the previous sections, low-plasticity MRV silt does not gain a significant increase and can even experience a reduction in liquefaction resistance with few liquefaction tests. Thus, the repeated liquefaction needs to be evaluated, and the ground should be mitigated correspondingly.

With previous cyclic shearing inducing a previous cyclically induced axial strain of 0.2%, the reconsolidated soil required twice as many loading cycles as the virgin soil to liquefy. While after more than four liquefaction tests, the liquefaction resistance increased significantly. The rate of increase in liquefaction resistance with higher number of liquefaction tests was such that after seven liquefaction tests, the soil no longer liquefied with increasing number of liquefaction tests. Thus, inducing repeated liquefaction, though difficult to achieve in practical terms, could be a very effective way to mitigate the MRV silt ground to avoid liquefaction. While inducing a cyclically induced axial strain of 0.2% can be easily achieved in practical terms, it delivers a lower level of improvement to liquefaction resistance than inducing repeated liquefaction. Consequently, methods deployed to increase the liquefaction resistance of silts should be such that induces both previous cyclic loading and previous strain on the soil mass. However, the choice of the method of liquefaction mitigation for a soil mass will be dependent on the existing ground conditions and intensity of the earthquake anticipated. Ground improvement methods which can deliver impulse or vibratory loading on the surface or within the subsurface of a soil mass such as, dynamic compaction, vibroflotation, or blasting can induce both previous cyclic loading and previous strain on a soil mass and hence can be used to increase the liquefaction resistance of silts (Thevanayagam et al. 2001).

Both large-preshearing (repeated liquefaction) and small-preshearing can be effected by means of dynamic compaction, vibroflotation and blasting. However, because these proposed improvement techniques tend to induce large strains, it is rather difficult to achieve small-preshearing using them. Thus, the large-preshearing (repeated liquefaction) is more appropriate for improving the liquefaction resistance of soils. As the increase in liquefaction resistance is attributed to the increase in density due to reconsolidation, specific attention should be paid to the time required for reconsolidation. The time required for reconsolidation (the dissipation of the excess pore pressure developed during the ground improvement process) is site-specific and it is best determined in the field.

8.4 Summary

An experimental program was conducted to study the effect of previous cyclic shearing on liquefaction resistance of the low-plasticity MRV silt. The following conclusions were reached based on the tests and studies carried out during this experimental program.

The specimens in triaxial setup experienced much higher excess pore pressure in extension than in compression at the first half cycle of cyclic loading after the 1st liquefaction test. Correspondingly, there was a higher axial strain in extension than in compression, indicating that the specimens became stiffer in the direction in which the cyclically induced axial strain held constant before reconsolidation started.

In the range of one to four liquefaction tests, the liquefaction resistance of reconsolidated specimens was almost equal to and in some cases less than that of virgin specimens. Liquefaction resistance of specimens increased significantly as the relative density approached 100% after five or more liquefaction tests.

When a R_u of less than 1.0 was induced, the liquefaction resistance of the specimens increased compared to that of virgin specimens. The liquefaction resistance reached its peak when the value of the previous cyclic loading induced an excess pore pressure ratio of 0.35 or a cyclically induced axial strain of 0.2%.

The application of cyclic loading to induce a cyclically induced axial strain of 0.2% or more than four liquefaction tests can be an effective way to increase the liquefaction resistance of silt soils. However, specific soil conditions and the intensity of potential earthquakes need to be evaluated to determine the most appropriate method for increasing the resistance of the soil to liquefaction.

References

Finn, W. D., Bransby, P. L., & Pickering, D. J. (1970). Effect of strain history on liquefaction of sand. *Journal of Soil Mechanics and Foundations Division, 96*(SM6), 1917–1933.

Ishihara, K., & Okada, S. (1978). Effects of stress history on cyclic behavior of sand. *Soils and Foundations, 8*(4), 31–45.

Izadi, A. (2008). Liquefaction and post-liquefaction behavior of low plasticity silts using cyclic triaxial tests. *Ph. D. Dissertation*. Rolla, MO, US: Missouri University of Science and Technology.

Kramer, S. L. (1996). *Geotechnical earthquake engineering*. New Jersey: Prentice Hall.

Thevanayagam, S., Martin, G. R., Shenthan, T., Liang, J. (2001). Post-liquefaction pore pressure dissipation and densification in silty soils. In *Proceedings of 4th International Conference on Recent Advances in Geotechnical Earthquake Engineering and Soil Dynamics*. San Diego, CA.

Wang, S., Yang, J., & Onyejekwe, J. (2013). Effect of previous cyclic shearing on liquefaction resistance of Mississippi River Valley silt. *Journal of Materials in Civil Engineering, 25*(10), 1415–1423.